1994

Seismic modeling of structures with steel deck reinforced concrete diaphragms

Francisco Santiago Yeomans Reyna
Iowa State University

Order Number 9424279

Seismic modeling of structures with steel deck reinforced concrete diaphragms

Yeomans Reyna, Francisco Santiago, Ph.D.

Iowa State University, 1994

U·M·I
300 N. Zeeb Rd.
Ann Arbor, MI 48106

Seismic modeling of structures with steel deck reinforced concrete diaphragms

by

Francisco Santiago Yeomans Reyna

A Dissertation Submitted to the

Graduate Faculty in Partial Fulfillment of the

Requirements for the Degree of

DOCTOR OF PHILOSOPHY

Department: Civil and Construction Engineering
Major: Civil Engineering (Structural Engineering)

Approved:

Members of the Committee:

Signature was redacted for privacy.

Signature was redacted for privacy.

In Charge of Major Work

Signature was redacted for privacy.

For the Major Department

Signature was redacted for privacy.

For the Graduate College

Iowa State University
Ames, Iowa

1994

A MI PADRE

TABLE OF CONTENTS

1. INTRODUCTION

1.1 General Remarks

Many of today's steel frame structures are constructed with steel-deck-reinforced concrete (SDRC) floor systems, because of their advantages over more traditionally reinforced concrete slab systems. Approximately 100 million square feet of composite steel floor decks are built every year in the United States (77). A complete discussion of these advantages had been presented in many references (77,78,80,81,82) and thus only few of the most important advantages will be mentioned here. The cold-formed steel deck functions as a permanent formwork for the cast-in-place concrete and functions also as main positive reinforcement once the concrete has cured. Considerable economic benefit is obtained since this floor system eliminates formwork and temporary shoring. The open or closed cell of the deck allows easy access for utilities, and the rapidly installed steel deck provides a safe working platform for construction crews. Figure 1 shows a typical composite floor system.

Steel-deck-reinforced concrete floor systems are built by connecting cold-formed steel deck sections to the surrounding support beams that are usually made of steel. Typical fasteners used are screws, power driven pins, arc spot welds, headed shear studs, or other positive shear transfer devices. Seams between adjacent steel deck panels are fastened through welds, or screws. Additional reinforcing steel may be needed for negative or positive bending moments. To develop a composite action between the steel deck and concrete a shear transfer capacity must be assured. This transference is obtained by a combination of chemical bond, friction and mechanical interlocking of the shear transfer devices at the interface. Shear transfer devices are typically embossments, indentations, holes, and transverse wires attached to the steel deck.

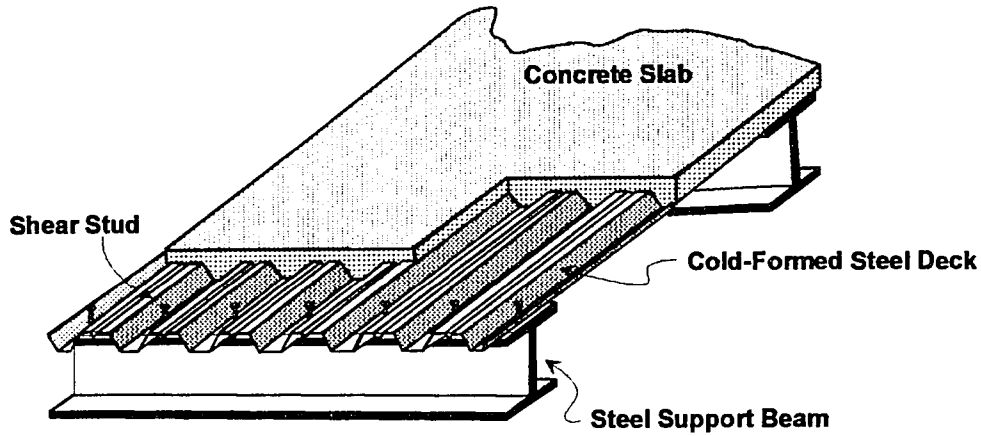

Figure 1. Typical steel-deck-reinforced concrete slab (modified from Reference 78)

1.2 Brief SDRC Historical Work

Floor slabs can be subjected to gravity loads as well as lateral loads generated from earthquake and/or wind forces. Gravity loads produce out-of-plane bending behavior on the floor slabs and lateral loads produce in-plane behavior of the slab. Buildings subjected to lateral loads must have floors and roofs capable of transferring in-plane shear forces from one wall to another. These floors are termed as diaphragms and are typically made of hollow-core planks, reinforced concrete, composite steel-deck-reinforced slabs, or timber. The function of the diaphragm is to brace a structure against lateral forces, such as wind or earthquake loads, and to transmit these forces to the other resisting elements of the structure. Figure 2 illustrates a schematic of a typical frame-wall structure.

The out-of-plane behavior of floor slabs has been extensively studied and a reliable prediction of their bending capacity can be achieved. Related to steel deck floor slabs, In the 1950s research started leading to the acceptance of the steel deck as a tensile reinforcement (79). In 1967 a research project was initiated at Iowa State university under the sponsorship of the American Iron and Steel Institute (AISI). The research objective was to develop a unified design method and standard test procedure for using the cold-formed steel deck as tensile reinforcement for concrete slabs (80,81,82). In the late 1960s additional research on the gravity load-carrying capacity of composite steel deck started at West Virginia University (83). During the last decade, additional studies on the same subject have been conducted (21,22,23,24,84,85,89). Most of that research stemmed from work at Iowa State University (ISU), and led to the development of a national set of standards (25,26).

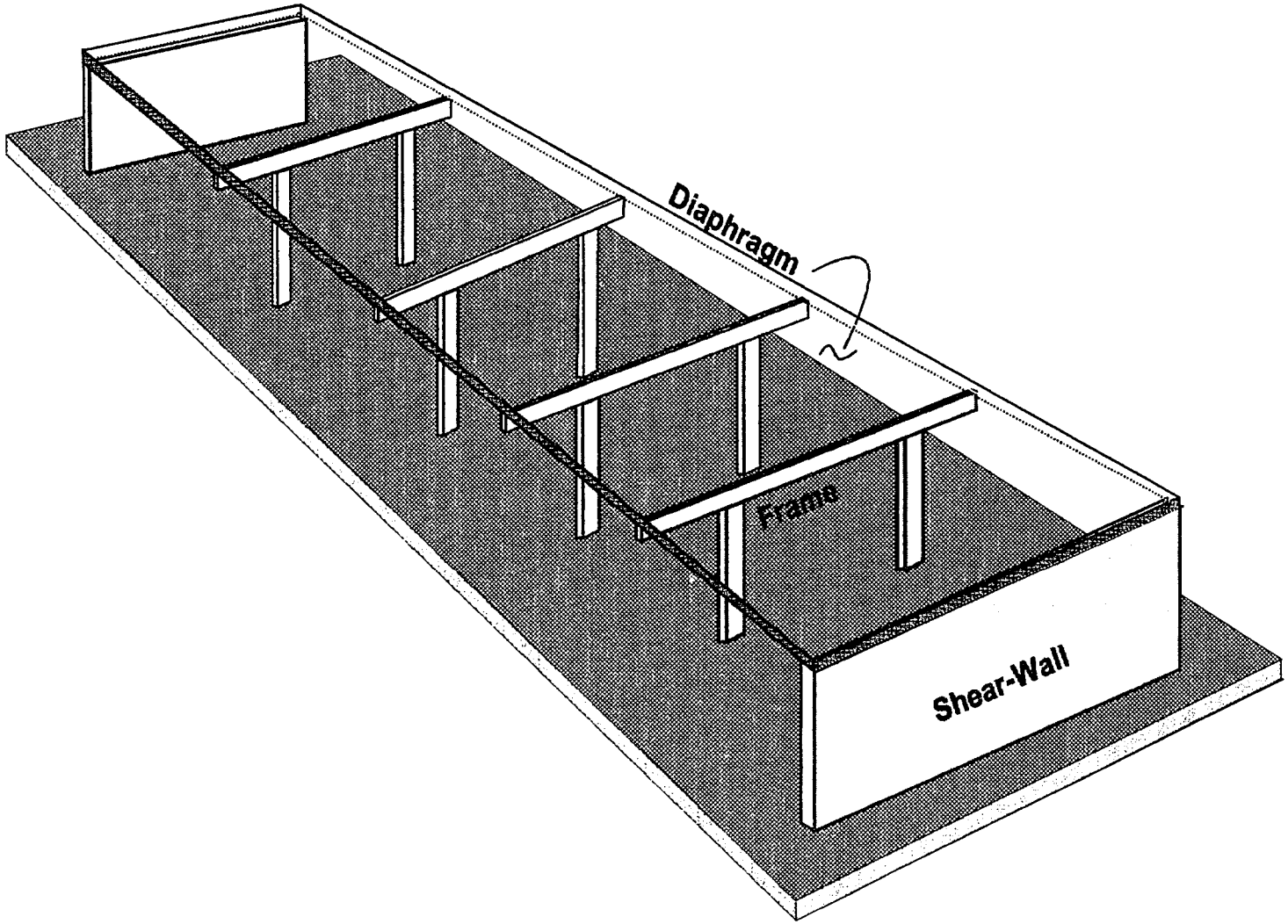

Figure 2. Frame-wall structure schematic

1.3 Problem Statement

The in-plane behavior of diaphragms has not been completely understood. Experimental and analytical research on floor diaphragms under seismic loads has been scarce. The lack of information on the behavioral characteristics of these elements has guided the current design practice to use simple assumptions such as rigid behavior or in the best case elastic response. Experience from past earthquakes, such as the 1985 Mexico City earthquake (20) has shown the severity of damage caused by the shaking. The damage attached by many structures shows that the seismic loads can be large enough to cause inelastic behavior of members and connections. Figure 3 shows a concrete structure damaged by the Mexican earthquake.

The seismic analysis of concrete structures requires analytical models with adequate prediction capability on strength, stiffness and ductility under cyclic loading. The current state of the art on mathematical modeling of reinforced concrete behavior permits accurate predictions of hysteretic response in flexure (8,9,67). These models can be constructed using bending analysis for a defined geometry and material properties and following a set of rules. Inelastic deformations as consequences of seismic response are not limited to flexure; tests of large-scale specimens indicated that inelastic shear deformation effects can form up to 50% of the hinging region deformation (45). Inelastic shear effects are more pronounced on shear walls. During the last 10 years, only few attempts were made to propose hysteretic shear models (45,67), but those models were limited in scope due to lack of sufficient experimental data. A hysteretic shear model for reinforced concrete elements was developed by Ozcebe & Saatciouglu (45); the model consists of an envelope curve and set of rules for unloading and reloading branches of the hysteretic relationship. The proposed model was limited to members subjected to

Figure 3. Collapsed reinforced-concrete structure after 1985 Mexico City earthquake

combined shear force and bending moment reversals, with a shear force capacity higher than that of flexural capacity. Additionally, the model was limited to the range of displacements where strength decay is not observed.

The assumption of rigid floor diaphragms is generally used for simplicity on the analysis and due also to a lack of understanding of the in-plane behavior of floor systems. The rigid diaphragm assumption has been questioned since early 1960s by Blume et al. (69). More recent research on that subject showed that there is an important effect on the dynamic response of many structures due to flexible diaphragm behavior (33,37,39,42,55, 70,72). Floor flexibility effects have been found to be more pronounced on L- or Y-shaped buildings, and for long rectangular buildings with a dual-bracing system (frames and shear walls).

Most of the mentioned studies on diaphragm flexibility were carried out based on elastic behavior assumption, that is, neglecting any possible deterioration of the floor system due to cracking, yielding, etc. The changing flexibility of a diaphragm system due to cracking is expected to affect not only the distribution of lateral forces on the resisting systems (frames, shear walls), but also the dynamic characteristics of the structure due to local vibration modes of the diaphragm system. In early 1990s Kunnath et al. (32,33,34) reported a study on seismic response of reinforced concrete buildings with inelastic floor diaphragms. In this work an analytical procedure was stated to help in the inelastic analysis of building systems with inelastic in-plane floor flexibility, but due to the lack of data on the hysteretic shear characteristics of slab panels the same shear spring proposed for walls is used for slabs.

The work presented in this document focused on the development of an inelastic hysteretic model for steel-deck-concrete diaphragm and the required structural modeling to incorporate the inelastic diaphragm effect.

1.4 Objective of Research

1.4.1 Objective of overall project

During the last decade a research program on diaphragms had been developed at ISU as part of the US-Japan coordinated program for masonry building research. Each category of this program is conducted under the supervision of the Technical Coordinating Committee for Masonry Research (TCCMAR). The TCCMAR committee was organized to function under the auspices of the Panel of Wind and Seismic Effects of the US-Japan Cooperative Program in Natural Resources (UJNR). The research undertaken for the overall project at Iowa State University is related to two categories of TCCMAR program. Category 5, entitled "Diaphragms," and Category 2, entitled "Force-Displacement and Strain Math Models." As result of this program a hysteretic model for shear response of hollow-core plank diaphragms was developed (28,38).

The original steel-deck-reinforced concrete diaphragm research project at ISU (Phases I and II) had as objective the investigation of behavioral and strength characteristics of SDRC floor diaphragms. The research work was divided in three areas: First, experimental investigation of failure modes by introducing the effect of various system parameters. Second, development of analytical predictive methods for diaphragm strength and stiffness. Third, development of design recommendations for SDRC diaphragms.

A new phase on the SDRC diaphragm research program had been added. This phase had as a main objective the determination of a hysteretic shear model for SDRC diaphragms subjected to in-plane loads. To accomplish the objective the work in this new phase had been divided in three sections. First section consisted of determination of the hysteretic model based on regression analysis of the experimental data. Second section

covered analytical determination of the envelope curve considering the nonlinearity of concrete and steel deck as well as considering the interface between both materials. Third section consisted of dynamic inelastic analysis of a typical wall-frame structure with long rectangular plan.

1.4.2 Objective and scope of this study

The main objective of this work was to investigate analytically the nonlinear inelastic behavior of steel-deck-reinforced concrete diaphragms subjected to seismic loads. The specific objective was the development of a hysteretic model with nonlinear, inelastic, degrading and pinching capabilities to predict the in-plane shear response of steel-deck-reinforced concrete slabs under earthquake loads, and the modeling of structures incorporating the diaphragm action. To satisfy these objectives, the following tasks were defined:

- √ Perform literature review of previous hysteretic models used on concrete and steel structures, as well as literature review on modeling of floor systems.
- √ Accomplish a literature review on structural member macro-modeling focused in degrading type elements.
- √ Development of a hysteretic model for SDRC diaphragms that include the following expressions:
    1. Envelope curve equation
    2. Pinch force expression
    3. Loop stiffness equations
    4. Cyclic loop equation
    5. Strength and stiffness degradation
    6. Hysteresis rules

- √ Establishment of an analytical procedure to obtain the pre-peak envelope curve of steel-deck-reinforced concrete diaphragm under monotonic in-plane load
- √ Definition of a procedure for macro modeling of diaphragms on regular structures, as well as development of the diaphragm stiffness matrix
- √ Development of a computer program for the inelastic dynamic matrix analysis of wall-frame structures under earthquake motion

2. REVIEW OF PREVIOUS RESEARCH

2.1 General

To study the inelastic response of a system, a mathematical model of restoring force characteristics must be set up. A complete description of the behavioral characteristics of a structure throughout the elastic and plastic ranges requires two types of mathematical modelling: First, modelling of the force-deformation relationship under stress reversal, called "hysteresis model"; and Second, modelling of the distribution of stiffness along the member, called "member model."

A hysteretic model predicts the force-displacement relation for a system using stiffness and strength information. The model is defined by its envelope or skeleton curve, and by its hysteresis curve or loop. The skeleton curve is the line joining the peak points in the force-deflection curve for a progressive sequence of loading and unloading. The hysteresis curve or loop is the curve defined under load reversals.

A member model describes the distribution of stiffness along its length. Inelastic deformations are distributed differently in steel and concrete members. Steel members under bending shows concentrated inelastic deformation under severe stress forming plastic hinges. A typical member model in this case is one with an elastic center portion and plastic hinges at the ends. For reinforced concrete flexural elements, inelastic deformation does not concentrate in a particular section, but rather spreads through the member. In this case, a rule to distribute this plasticity must be set.

Usually, the hysteretic effect is associated with a specific location in the element (hysteretic model level) that is called concentrated plasticity section (32). After defining the concentrated plasticity on specific sections of a member, distribution rules are applied (member model level).

2.2 Hysteretic Models

2.2.1 Basic characteristics

The development or selection of a hysteretic model might be accomplished by looking for specific characteristics. In 1979, Riddell and Newmark (4) stated some of the most desirable model characteristics. These features can be summarized as follows:

- Reality: model parameters must be directly associated with known physical characteristics.
- Accuracy: the model response should compare favorably with measured results.
- Simplicity: the prediction should be completed with the simplest method possible.
- Consistency: the relationship between a response variable and any specific parameter should be consistent.

Many hysteretic models have been developed in the past. Each successive model has improved upon the first effort in some way. Specifically, the hysteretic characteristics of a reinforced or prestressed concrete models have become more refined. These characteristics have been stated by Otani (5), Sozen (6), and Wakabayashi (3) as follows:

- The stiffness must change with the cracking of the concrete and the yielding of longitudinal reinforcement.
- The loading stiffness in the second cycle is lower than that in the first cycle.
- The average peak-to-peak stiffness decreases with the increase of the maximum displacement amplitude.
- The load-deflection curve for any cycle can be represented ideally by a series of linear segments with characteristic slopes. These slopes are the initial slope, fully cracked section slope, slope after yielding, and the return slope.
- There is a tendency for a very low incremental stiffness near the origin followed by a stiffening region (pinching effect).

- The hysteresis loops for reinforced concrete elements under flexure are spindle-shaped, with some pinching due to shear effect. Ductility and energy dissipation capacity are large, and degradation of strength due to repetition of loading is small.
- The hysteretic behavior of reinforced concrete members failing in shear shows a drastic strength deterioration after maximum carrying capacity is reached; loops showed a pinching shape, and a small energy dissipation capacity.

A classification of the hysteretic models in three families was presented by Wakabayashi (3). The first family is termed masing-type family and is characterized by having hysteresis curves geometrically similar to its envelope curves. Some examples of this family are the bilinear model, trilinear model, and Jennings model (7). The next is called degrading-type family. This type allows for the effect of stiffness degradation caused by load reversals in inelastic ranges. Many models of this type have been proposed such as Clough model (8), Takeda model (9), Sina model (10), Q-Hyst model (10), etc. The third is the slip-type family. This family is often used to represent bolt connection in a steel structure, bracing members with significant buckling effect, and reinforced concrete members with shear distortion as dominating behavior. Some examples of this type are the double bilinear model (11), and Iwan model (12). Figure 4 shows some examples of hysteretic models. Since models of the third family have been also published as degrading type because of common characteristics, only discussion related with the two previous models will be presented.

2.2.2 Masing-type models

The most popular model of the masing-type family is the bilinear hysteretic model (3). An example is showed in Figure 4. This model is positive bilinear or negative bilinear if the slope of the second line is positive or negative, respectively. The elasto-plastic model is a special case defined for zero slope of the second branch. The common point

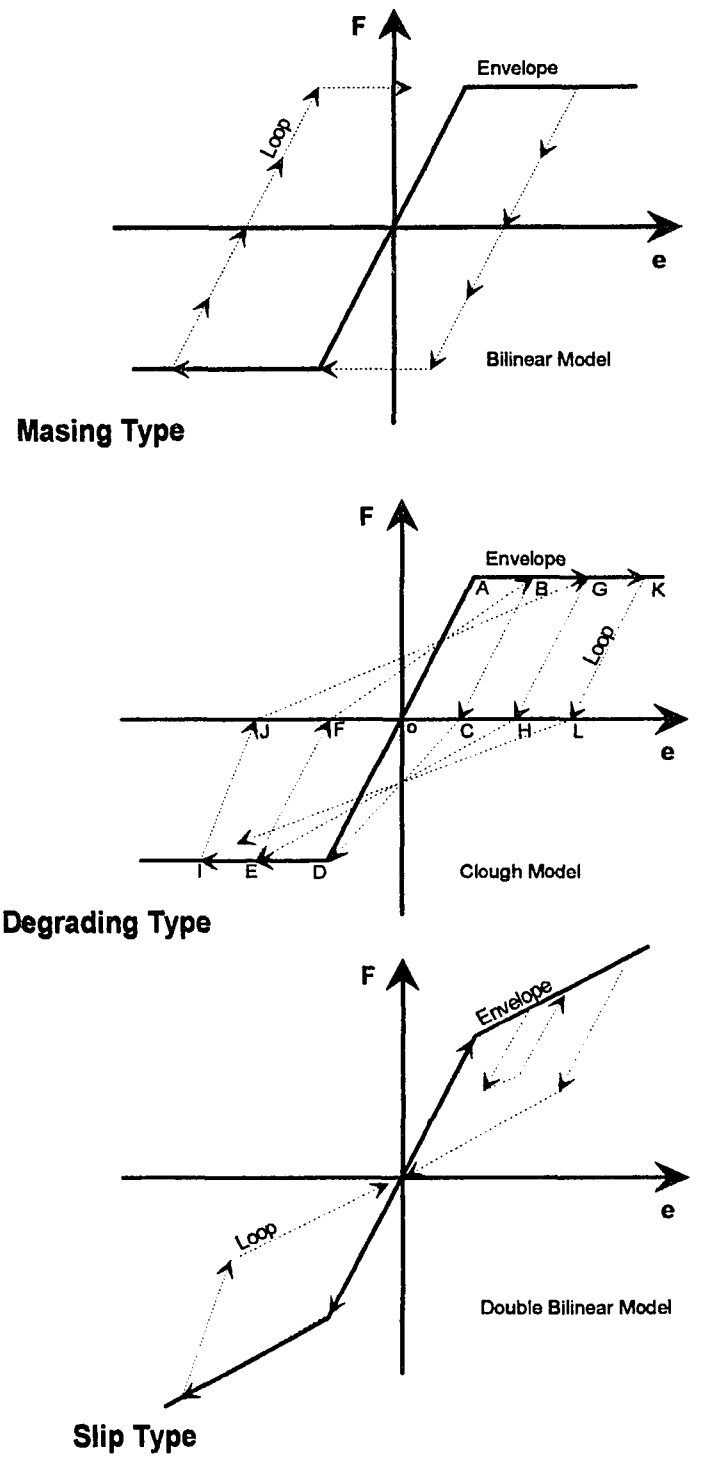

Figure 4. Examples of hysteretic models

between the two straight lines forming the skeleton curve is generally assumed as the yield point. This model is often used to predict the force-displacement characteristics of a steel frame. For simplicity, this model is sometimes used for reinforced concrete systems, but in general this model provides only a rough estimate.

The trilinear model (3) for this family has no degradation characteristics. The skeleton curve is formed with three lines, with Points A and B corresponding to the cracking and yielding points respectively (see Figure 5). Only few rules are necessary to define this model. Essentially, Line CD is parallel to and twice as long as Line OA, and Line DE is parallel to and twice as long as Line AB. This model is sometimes used for composite steel and reinforced concrete systems, but the trilinear model with degradation properties is preferred.

The Jennings model (7) was developed in the eariy 1960s. This model use closed formed mathematical formulas with smooth rounded curves that are general enough to describe the behavior of systems ranging from linear to elasto-plastic. The skeleton curve uses a formula similar to that first proposed by Ramberg and Osgood (13) to describe relations between stress and strain. Curve ABC (see Figure 5) is obtained by inverting Line OA and extending it in such a way that the coordinates of ABC are twice those of OA. This model has been widely used on steel elements, since can represent the Bauschinger effect and the effect of gradual yielding. One main disadvantage is the complexity of the hysteretic rules, because the force in the skeleton equation as well as in the loop equations is not explicitly expressed as function of displacement.

2.2.3 Degrading type models

Clough and Johnston (8) in 1966 proposed a degrading bilinear model, improving the elasto-plastic model by accounting for the stiffness degradation observed during the

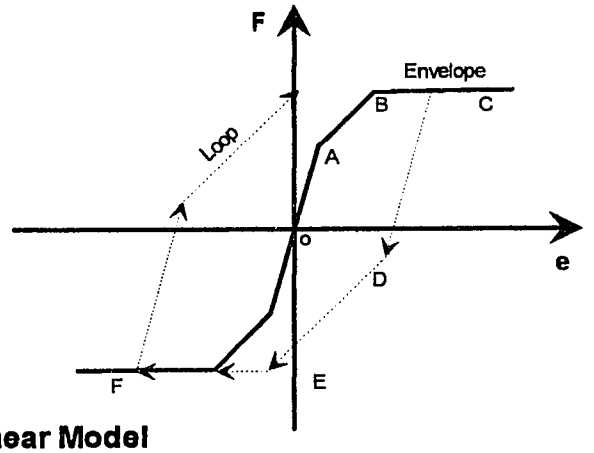

Trilinear Model

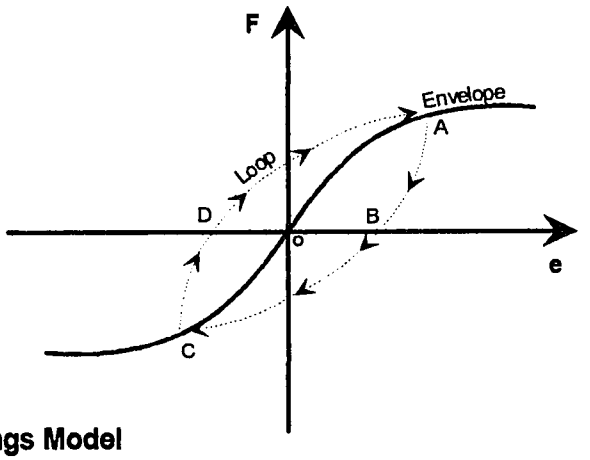

Jennings Model

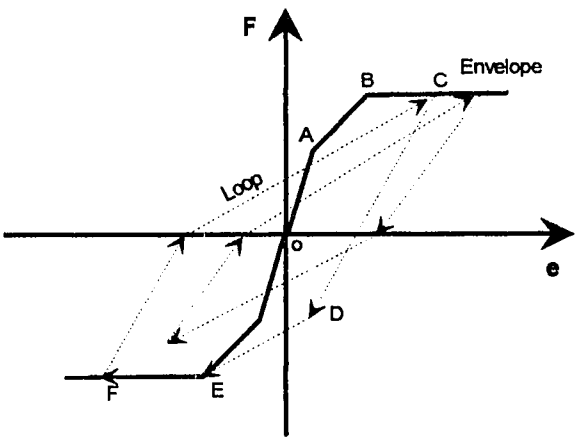

Takeda Model

Figure 5. Trilinear, Jennings and Takeda models

cyclic loading of reinforced concrete components. Some of the rules defining the model are as follows (see Figure 4): Line OA is parallel to BC and Line OD is parallel to Line EF. From Point C the stiffness changes, heading toward the yield Point D. From Point F the slope changes and the line proceed to Point B, closing the cycle. The Clough model was the first major step in differentiating steel member models from concrete member models by considering degradation in the loading stiffness, but the model lacks in modeling degradation of the unloading stiffness, pinching effect, and strength deterioration.

Takeda, Sozen, and Nielsen (9), in 1970, proposed one of the most popular degrading models, called "Takeda" model (see Figure 5). This is a tri-linear degrading type model used generally to model flexural behavior of concrete elements. Series of 16 rules are stated to develop force-displacement relationships; many of them for low-amplitude cycles contained between large amplitude cycles previously reached. These rules determine different stiffness characteristics for reinforced concrete elements at different load levels as cracking, yielding, unloading, and reloading in successive cycles. Eventhough this model is a real improvement over Clough model, it is still lacking in modelling the pinching effect and strength deterioration. After the Takeda model, other less complicated models were developed by different researchers.

Otani (15) in 1975, proposed a modified version of Takeda model to represent the stiffness variation of a joint spring in conjunction with a flexural spring. The skeleton curve used was bilinear with the yield as a break point in the envelope. This model had fewer rules than those of Takeda model since the cracking point was not recognized; therefore, all the rules related to cracking points were eliminated. In 1979 The Q-Hyst model developed by Saiidi and Sozen (10) was presented as a modified version of the bilinear hysteresis model. The objective of this model was to provide a very simple hysteretic model with reduced loop area (energy dissipated) and softened hysteresis loops specially

for unloading and load reversal stages. Only four rules define the model thus making it easy to use. As the Otani and simple bilinear models, the Q-Hyst model does not provide energy dissipation unless the system yields, therefore, an unreal condition is given when these models are applied to reinforced concrete elements subjected to displacements lower than yield displacement.

Another model originating from theTakeda model is the Sina model developed by Saiidi and Sozen (10). This model considers pinching effect and is still simpler than Takeda model because only eleven rules are needed. The skeleton curve consists of three sections, cracking, yielding, and ultimate stage, therefore is more accurate than Otani model which does not consider cracking stage. This is one of the best models used to reproduce the behavior of concrete elements under bending, because it needs only few rules to be described and considers pinching action.

In the late 1980s, Ewing, Kariotis, and El-Mustapha (16,41), developed a hysteretic model named EKEH model. It has nonlinear, inelastic, degrading and pinching capabilities as is shown in Figure 6. This model was specifically designed to predict the nonlinear, hysteretic behavior of reinforced masonry cantilever shear walls. Later research done at Iowa State University by Meyer (14), and Tremel (19) showed that the same model can be used on precast prestressed hollow-core diaphragms. The skeleton curve consisted of a second order function and two linear segments. Key parameters for the envelope were the initial stiffness, peak strength, deformation at peak strength, and post-peak degradation factor.

In 1988 as part of a research made at Iowa State University by Porter and Yeomans (28,38), a hysteretic model for hollow-core plank cantilever guided diaphragm was developed (see Figure 6). The main characteristics of this model were: inelastic, nonlinear, with pinching and degrading capabilities. The model is intended to be used in

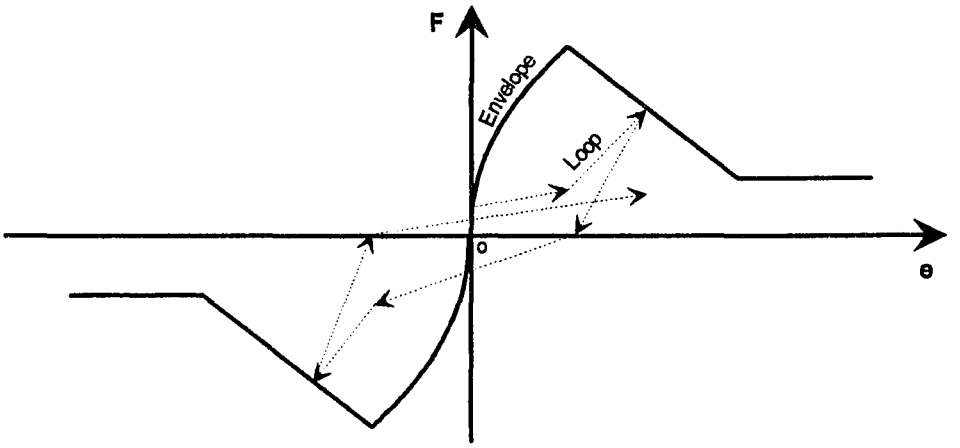

EKEH Model

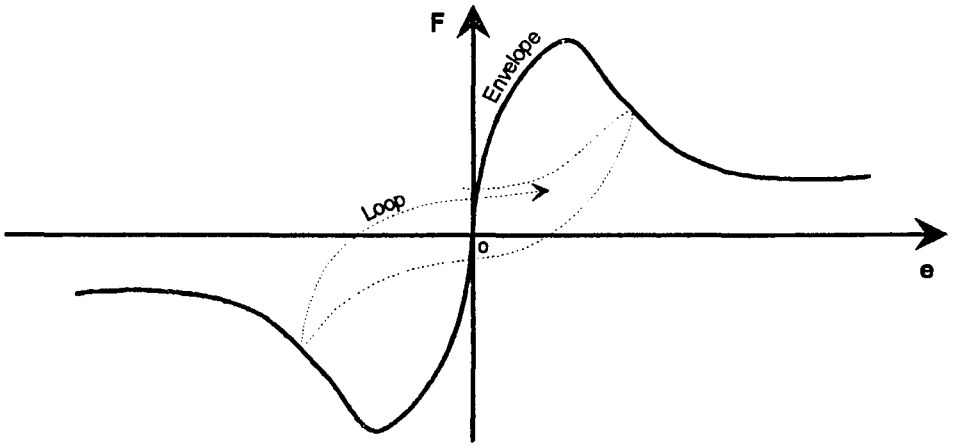

Hollow-Core Plank Model

Figure 6. EKEH, and Hollow-Core Plank models

diaphragms with shear as predominant type of failure. The model consists of a primary shear force-displacement envelope curve for a cantilever guided diaphragm, and unloading and reloading branches under cyclic loading. Since continuous expressions were used to define the envelope and the cyclic loops, only few rules are needed to define the hysteresis. Modifications to the element model level are needed to be used for continuous diaphragm systems. Only the stabilized behavior is intended to be modeled.

A series of 37 masonry shear wall tests was used in 1989 by Soroushian, Obaseki and Choi (27) in the developing of a hysteretic model for masonry shear walls. The model accounts for the deteriorating nature of this type of material, and differentiate characteristics of walls with shear or flexural modes of failure. Statistical regression analysis was used in the development of the model, which is defined by nine coefficients.

In 1989, Ozcebe and Saatciouglu (45) proposed a hysteretic model for shear response of reinforced concrete members. The model consists of a primary curve defined by shear force-shear displacement relationship under monothonic loading. The second part is formed by unloading and reloading loops, established through a statistical analysis of experimental data. Since the experimental observations are based in test specimens designed to yield in flexure before shear failure, the proposed model is limited to structural elements that yield in flexure before shear failure. It is also limited to the deformation range where strength decay is not observed.

2.2.4 Hysteresis model summary

Many hysteretic models have been developed over time. Each successive model has improved upon the first effort in some way. For concrete systems, definition of skeleton curve and cyclic loop have become more refined (2,5,6).

The simplest case of skeleton curve is found in the bilinear model, where only two straight lines connected at yield point define the envelope curve. Improvement on envelope definition is acquired by using trilinear models, which are defined by a series of three straight lines connected at cracking and yielding points. An unreal condition (linear elastic behavior) is given when these models are applied to concrete elements subjected to displacements lower than that corresponding to the first break point. This problem is avoided in some models that use continuous equations to define the skeleton curve (16, 27,28).

Most of the models have cyclic loops defined by straight lines. Early models such as bilinear and trilinear from Masing family, used straight lines parallel to the envelope curve to describe the cyclic loops. Such models when applied to concrete elements resulted in overestimated cyclic dissipated energy (area inside loop), and in unreal cyclic force-displacement behavior. Later, improvements were obtained in the energy prediction by including stiffness degradation and pinching effect. Lately, a series of models has been developed defining the hysteresis loops by continuous nonlinear equations (27,28,44). This approach usually reproduces accurate cyclic paths, but increases the complexity of the solution.

Models discussed here might be grouped in three sections: First, those developed to model elements with flexural type failure such a Bilinear (3), Jennings (7), Clough (8), Takeda (9), Q-Hyst (10), Sina (10), etc. Second, models developed to reproduce behavior of elements with shear type failure, e.g., EKEH model(16,41), hollow-core plank diaphragm model (28,38), etc. Third, models developed to simulate both behaviors, flexure and shear, such as that proposed by Soroushian (27). A careful selection of the model has to consider the expected type of failure, to accurately reproduce the actual behavior. An alternate procedure is to use two hysteretic models together, one for each type of failure,

and coupling their effect through a flexibility approach at the member model level (54).

Finally, the actual tendency in the hysteretic model development suggests the following procedures to obtain their components. Envelope curve, might be obtained by using results derived directly from laboratory tests, or, by using empirical expressions obtained from regression analysis of experimental data, or, if it is possible, from the principles of applied mechanics. For cyclic loops, the actual trend suggests the uses of empirical expressions (43,90).

2.3 Member Models

Modelling of elements in structural analysis might be approached through micro- or macro-modelling. Micro modelling uses mainly the finite element method (FEM). Additionally, other micro-modelling techniques can be used, such as the fiber or filament model, which has been used in the analysis of single components. Finite element analysis (FEA) can be used effectively as long as the dynamic analysis remains in the linear behavior. However, as soon as the analysis transforms to inelastic stage, FEA is no longer effective because of its huge demand on computational needs.

Macro-modelling approach, offer an attractive option not only in computational savings but also in model flexibility. It has capability to model almost any type of behavior by using the overall response pattern through simplified extensions from micro-level. Most of the analytical schemes used actually are based on macro-modelling approaches (34,41,42,49,54). Member modeling as part of the macro-modelling scheme, is in charge of the stiffness distribution throughout the element.

Penzien (57) in 1960, stated the first attempts to study the seismic response of multistory buildings by using shear-beam approach for beam and columns. All the elements on a specific level were substituted by a single nonlinear (elasto-plastic) spring.

This approach is called also shear-frame analysis, and is only valid when rotational displacements of the floor system are negligible. Obviously, this approach failed in presence of shear walls.

In 1965 Clough et al. (58) stated the first proposal of the beam model. A two-component formulation was introduced, wherein each element is substituted by two fictitious members in parallel. One is an elastic member that introduces strain hardening, and the other is an ideal elastoplastic element that introduces yielding (see Figure 7). Later, in 1968, Aoyama and Sugano (59) extended the approach proposed by Clough to a multi-component representation (see Figure 7) based in a non-degrading trilinear hysteresis. Under this approach, the member is substituted by three fictitious elements working in parallel. One of the elements is a linear elastic member, and the other two are elastic elements but with elasto-plastic springs at different ends. The main problem with the multi-component approach from Clough and Aoyama et al. is: First, deflection curve for each fictitious element does not coincide each other except for ends. Second, both formulations were presented for non-degrading systems; therefore their application to reinforced concrete was really limited.

Next, Gilberson (60) in 1969, presented a different type of formulation with the one-component model. Under this approach, the member is substituted by an elastic element and two rigid-inelastic rotational springs concentrated at two member ends (see Figure 7). End springs were introduced to consider inelastic and hysteretic effects. The inelastic moment-rotation relationship of the spring was determined assuming the inflection point at the center of the member. The author maintained that the one component model was more versatile than the multi-component approach because it can treat any load-deformation relation. Later, in 1976, Takizawa (50,51) showed that by some mathematical

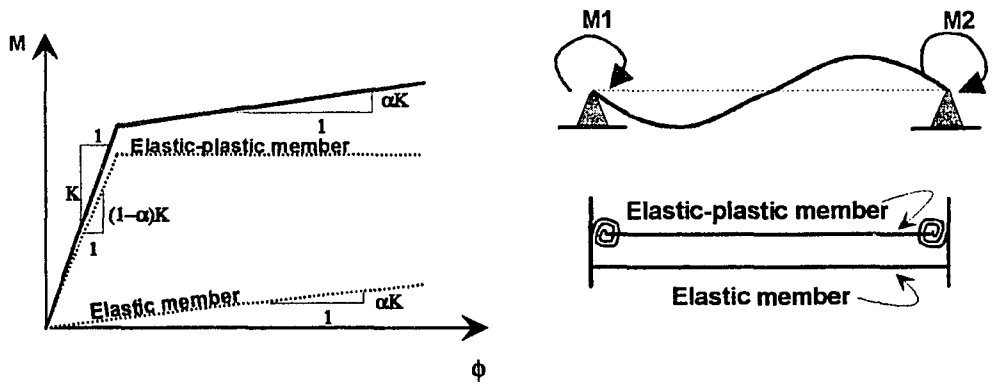

Two-Component Model

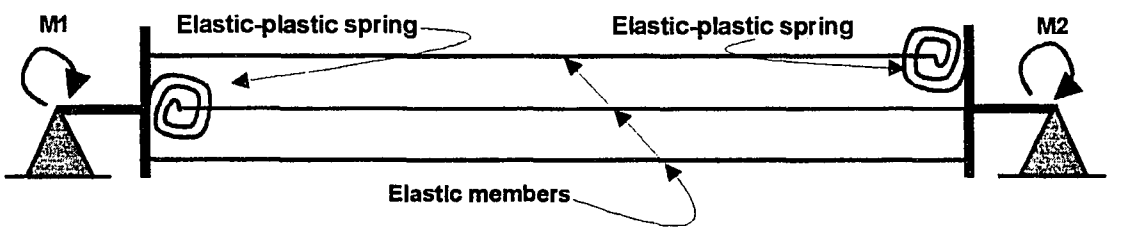

Multi-Component Model

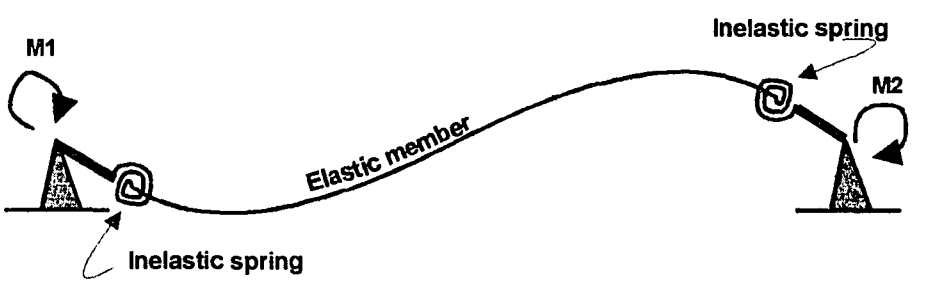

One-Component Model

Figure 7. One, two, and multi-component models (modified from reference 62)

manipulation, the multi-component formulations of Clough and Aoyama allows similar versatility as does Gilberson approach.

As long as the concentrated inelasticity remain close to the ends of the member, and the contraflexure point stays close to the center of the element, Gilberson formulation seems to be the easier approach. Steel frame members under flexure follow usually that behavior, that is the reason of the widely use of one-component model for steel members (61). For the case of concrete elements, the inelasticity is not restricted to the end of the element, but it is spread through the member length (see Figure 8). To overcome the problem presented by concrete elements, variations of the one-component model have been suggested.

Consideration to the distribution of plasticity along the element was introduced by Takizawa (50,51) and Otani (15,66). In 1976, Takizawa proposed a model with a parabolic distribution of flexibility along the reinforced concrete member. This parabola was defined according with the flexural stiffness at the element ends based in moment-

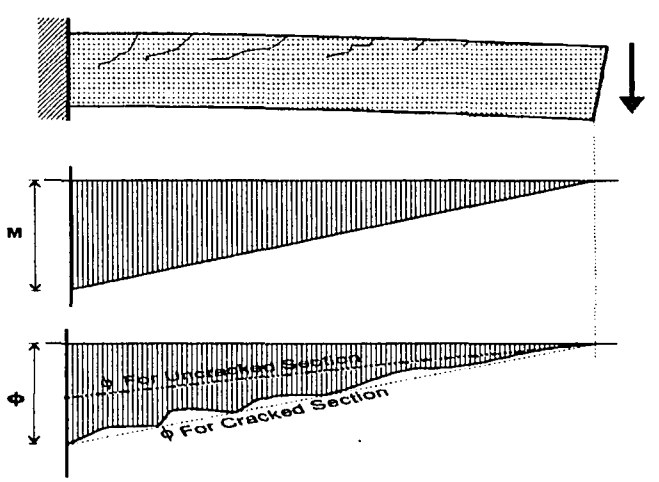

Figure 8. Distribution of curvature along the concrete beam (modified from reference 6)

curvature relationship, and by assuming elastic stiffness at the inflection point. Otani proposed a rigidity distribution formulation based in a combination of two cantilevers with time-varying span length. Properties of each cantilever were associated with those from a unit length cantilever.

In the late 1970s, Saiidi and Sozen (53) proposed a distributed plasticity model for reinforced concrete beams. Under their approach the flexibility is distributed associating elastic rigidity at the inflection point, cracking and yielding effects are also considered in the distribution rule. The moment-rotation relationship is determined assuming that the inflection point is fixed at the middle of the member.

During the 1980s, several models had been developed which adopt new variations of previous schemes. Among the most important are the work by Roufaiel and Meyer (68) which consider the finite size of the plastic regions at the ends of the member. A modified Takeda hysteresis model (bilinear type) is suggested; therefore no cracking effects are included. Ewing et al. (16) presented a computer program for analysis of masonry structures. This program can work with eleven different hysteretic models, one of them seeming adequate for reinforced concrete (R/C) elements, but with no capabilities for non-symmetric envelopes.

In 1990, studies at SUNY/Buffalo by Kunnath et al. (32) led to the development of an analytical model for inelastic response of R/C structures. The main features of their development included: First, distribution of flexibility model allowing variation for the contraflexure point. Second, new hysteretic model (three-parameter model) with stiffness degradation, strength deterioration, and pinching capabilities. Third, use of non-symmetric envelope curve that distinguishes cracking and yield effect. Fourth, separation of shear and flexure effect in walls, allowing them to be modified independently. Later, the same approach was applied to concrete structures with flexible diaphragms (33). The main

drawback was the lack of diaphragm hysteretic information; therefore diaphragms were assumed with same characteristics as those from shear walls.

Different approaches to analyze inelastic behavior of reinforced concrete members has been developed. Among the most used are the filament or layering model, and the multiple spring model. The multiple spring model was proposed by Takayanagi (67). The concrete member is substituted by a series of flexural springs; each spring has a uniform flexural rigidity changing according with the hysteresis model associated with it. Another very efficient approach, is the filament or layering model. Under this model the cross section of a member is divided into a number of filaments or layers, with each layer having associated material behavioral characteristics depending in the current state of stress-strain. Resultant forces for a cross section are obtained by integrating the filament contributions. This approach has been successfully used in the determination of skeleton curves for flexural elements such as beams, shear wall and even slabs (42), also shear envelopes had been determined by this procedure by combining it with the compression field theory (45).

2.4 Structural Analysis Considering Diaphragms

2.4.1 General

A common practice in the analysis of structures is to assume the floor system as perfectly rigid. This assumption, although acceptable for many structures, is not realistic for certain building configurations, and has been questioned as early as 1961 by Blume (69). Experience and research in the subject, had been shown that for frame-wall structures built with stiff shear walls and flexible frames, and buildings with long and

narrow floor plans, the influence of flexible diaphragms on the seismic response is of importance (33,37,39,42,70,72).

2.4.2 Review of previous work

Early 1980s, Ewing et al. (30) stated a methodology for inelastic analysis of wood diaphragms on masonry structures. An inelastic hysteretic model for wood diaphragms was used. The diaphragm response and its effect on the out-of-plane motion of unreinforced masonry walls were investigated. For the analysis, the diaphragm was idealized as a deep shear beam and was divided into several shear segments with hysteretic characteristics, resulting in a model formed by a series of masses and springs. The analysis proposed did not consider the flexural stiffness of diaphragms, the lateral stiffness of interior frames, and the flexibility of exterior shear walls (see Figure 9).

In 1982, an experimental and analytical study on the inelastic effect of reinforced concrete slabs under in-plane loads was reported by Nakashima, Huang, and Lu (39,71). Two scale models of a portion of a floor system were tested to examine the in-plane characteristics. Key parameters considered in the experimental testing includes stiffness, strength, and effect of gravity loads. An origin-oriented hysteretic model was developed, therefore, no pinching effect was included. Comparison between diaphragms with and without gravity load showed approximately the same behavior, crack pattern, failure mode, and stiffness degradation were practically the same, and a difference no greater than 15% was found in the ultimate load.

In 1984, Jain and Jennings (70) proposed a method to analyze single- and double-story buildings considering the flexibility of the system due to shear and bending. The floors of the multistory building with end-walls were modeled as equivalent, distributed bending beams while the shear walls were treated as bending beams and interior frames

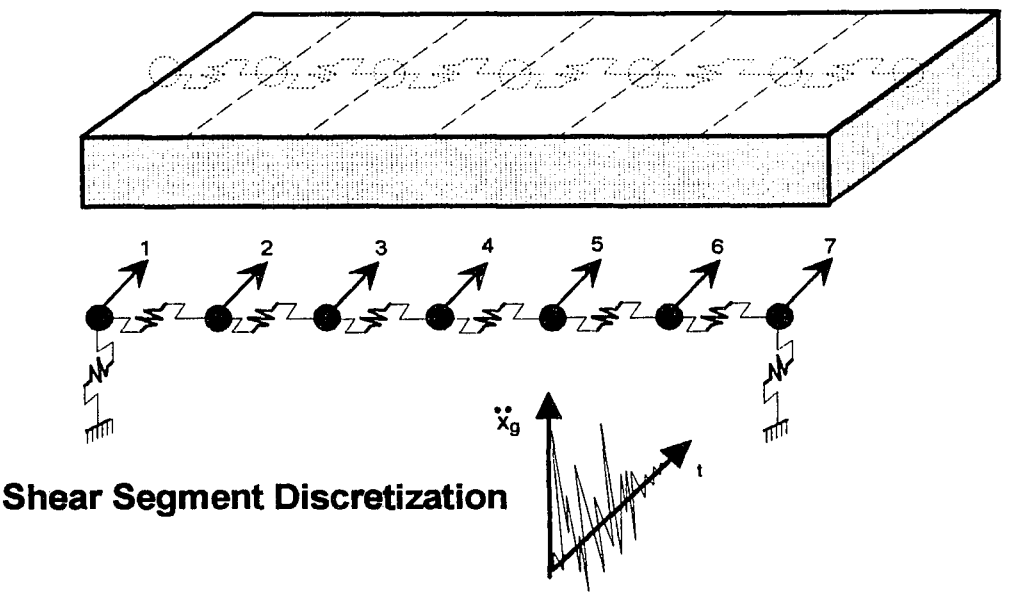

Shear Segment Discretization

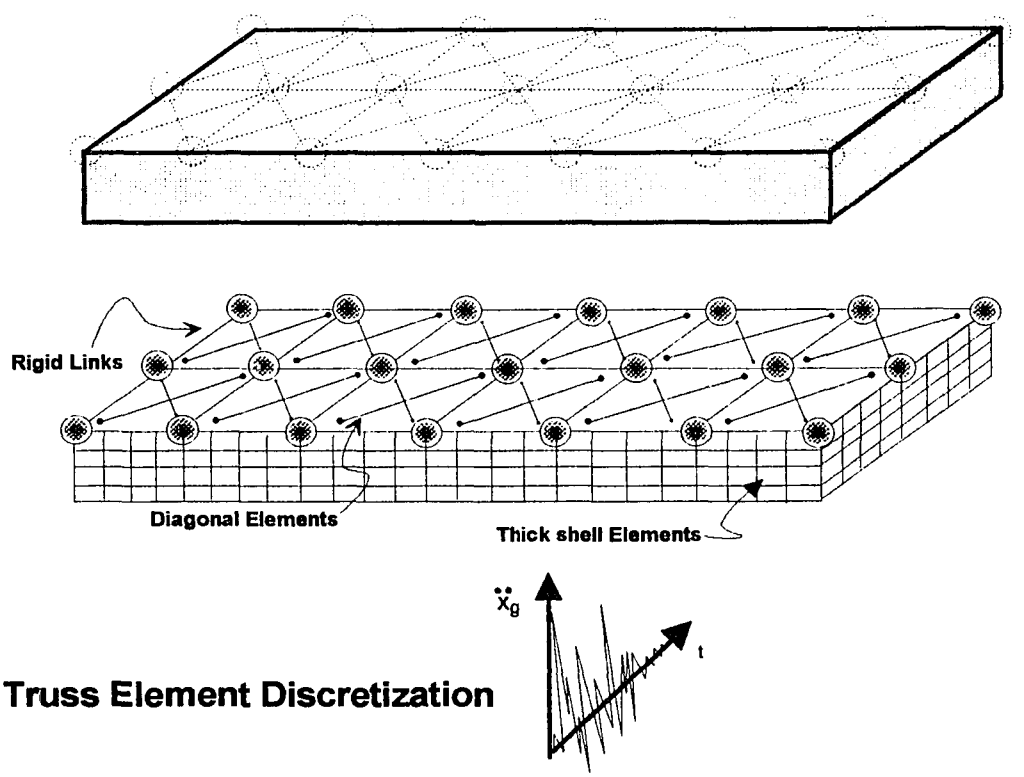

Truss Element Discretization

Figure 9. Diaphragm models

were considered as shear beams. The procedure assumes elastic behavior, and neglects shear stiffness of diaphragms; therefore, direct application of such procedure on degrading composite diaphragms is limited.

In 1984, Button et al. (72) presented a study describing the influence of diaphragm flexibility in the seismic response of a variety of buildings. A computer program COMBAT was used to model the in-plane effects of diaphragms, under elastic behavior. Main conclusion was that neglecting floor flexibility is a potential error in the non-conservative side.

Reinhorn et al. (37,42) in late 1980s, developed a computer program (IDARC2) for the inelastic modeling of reinforced concrete building structures with flexible floor diaphragms. The slab elements are modeled as deep beams with two in-plane degrees of freedom (dof) per node (lateral displacement in the in-plane direction and rotational deformation in the orthogonal direction). Main effects modeled in diaphragms are bending and in-plane shear. The in-plane shear is modeled by an inelastic spring that is connected in series to the flexural spring. Due to the lack of information on the hysteresis characteristics of the shear behavior of slab panels, the same shear spring characteristics used for shear walls was used for diaphragms.

A finite element approach to consider diaphragm flexibility has been used also by many authors. Celebi et al. (31) in 1989, reported a 3D finite element analysis of the West Valley College Gymnasium in Saratoga, CA., results were compared with records obtained from the same structure during the 1984 Morgan Hill earthquake. The model used beam elements for shear walls and columns, and in-plane stress elements for the plywood diaphragm. Since only linear analysis was achieved, degrading effects of the model were globally considered with 5% viscous damping.

Saffarini et al. (36) in 1992, reported a comparison on the response of 37 structures modeled with and without floor flexibility. Diaphragms were modeled with eight node elastic shell elements. The finite element analysis was used as reference, and measures of error in neglecting floor flexibility were evaluated. As part of their conclusions, errors were reported to be function of ratio between the in-plane floor stiffness and the stiffness of the lateral load-resisting system.

In 1992, Tena-Colunga (35) reported a discrete linear-elastic, multi-degree-of-freedom dynamic model for the analysis of unreinforced masonry structures with flexible diaphragms. The model considers rotations of shear walls in the global degree of freedom through static condensation. Diaphragms are represented as elastic shear springs, with stiffness evaluated considering in-plane shear and bending. Since contribution of the supporting floor system to the diaphragm stiffness is not included, the value used for the diaphragm stiffness is a lower bound.

Hart et al. (73,74) in 1992 reported an analytical work in the feasibility of using an elastic analysis with SAP90 to quantify the inelastic behavior of masonry structures. The structures considered were the TMS shopping Center (74), and the DPC Gymnasium(73); both structures built with flexible steel-deck diaphragms and masonry shear walls. In this study the inelasticity of masonry walls was included through an iterative procedure where the updating stiffness was obtained from the ACI (63) formula for the effective moment of inertia. Steel-deck diaphragms were considered behaving as linear elastic truss elements, with axial stiffness determined from the shear characteristics of the floor panels. Figure 9 shows a schematic of diaphragm modeled with equivalent truss elements.

2.4.3 Summary of diaphragm models

Rigid behavior is a common assumption in floor modeling. Such assumption was questioned in the early 1960s by Blume (69). From that time, different approaches to diaphragm modeling have been reported (30,31,35,37,42,70,72,73,74). A first classification might be to consider the model level, that is, micro- and macro-modelling. Micro-modelling uses mainly the finite element approach, but also fiber or layer models are included in this level. Macro-modelling includes all the "member-type" elements such as beam element, shear wall element, etc.

Micro-modelling has been used in floor modeling, as long as linear behavior is used (31,36). Inelastic modeling of diaphragms at micro-model level has been restricted to analyze independent floor segments.

Macro-modelling of floor elements has been used under two main approaches: First, floor elements idealized as shear segments (30,35,73,74). Second, floor elements idealized as deep beam segments with shear and bending characteristics (37,39,42,70, 71, 72). Neglecting the flexural behavior of reinforced concrete diaphragms might lead to erroneous results, because the two failure types can be triggered depending in a series of factors such as in-plane shear stress level, etc. (75).

Model of floor elements has been limited, most of them under linear elastic assumptions. Only few attempts to model inelastic characteristics of diaphragms had been reported, some for plywood diaphragms (30), and others for reinforced concrete diaphragms (37,39,42,71). Only one inelastic model with flexural and shear capabilities has been reported for reinforced concrete diaphragms (42). Since there was no experimental data for R/C diaphragms under shear failure, the model assumed for the floor system the same shear characteristics than for R/C shear walls (42).

Steel-deck-reinforced concrete elements are close in behavior to reinforced concrete elements. Obviously, a main difference occurs from the way in that the steel reinforcement is attached or bonded to concrete. Since there is no previous research reported for SDRC diaphragms, and due to the similarities between SDRC and R/C elements, this research will rely in all previous R/C diaphragm research.

3. ANALYTICAL INVESTIGATION ON HYSTERETIC MODEL FOR SDRC DIAPHRAGMS

3.1 Introduction

Steel-deck-reinforced concrete diaphragms may be classified as reinforced concrete elements with an extra component due to the interface between concrete and steel deck. Main characteristics of reinforced concrete hysteretic models such as degrading and pinching effects are also characteristics of SDRC models. Accordingly, SDRC hysteresis may be classified as a degrading type model.

Most of the previous diaphragm work has been devoted to simulate the diaphragm behavior as rigid, or, in the best of the cases, as linear elastic (35,70,72,73,74). Few intents have been made in the prediction of the behavior of reinforced concrete diaphragms through hysteretic models. Nakashima et al. (39,71) in 1982 proposed an origin-oriented hysteretic model for reinforced concrete diaphragms, therefore the model neglected pinching effects. Up to date, one of the most complete models for reinforced concrete diaphragms was proposed by Reinhorn et al. (37,42) in late 1980s. This model considers the diaphragm as formed by two rotational springs at the member end (flexural effects) and a shear spring. A plasticity distributed rule is used to consider the spread of cracking due to bending through the element. Shear effects were assumed since there was no available experimental data for reinforced concrete diaphagms. Steel-deck diaphragms have been modeled as linear elastic elements (73,74) only. No hysteretic model on SDRC diaphragms has been reported.

As part of this work, a hysteretic model for SDRC diaphragms is developed. This model is defined by its envelope or skeleton curve, and by its hysteresis curve or loop.

The following sections describe the equations and assumptions necessary for the development of the envelope and hysteresis curves required for the hysteretic model.

3.2 Envelope Curve Development

The two components of a hysteretic model are the envelope or skeleton curve and the hysteresis curve or loops. The envelope curve is defined by the line joining the peak points in the force-deflection curve for a progressive sequence of loading and unloading. For degrading materials, the force associated with the first time the displacement extends into a new and larger amplitude is called virgin load and will be reduced under subsequent cycles with the same amplitude until a stabilization occurs. Correspondingly, two types of envelope curves may be considered, virgin and stabilized envelopes. The virgin envelope is an upper bound and the stabilized envelope is a lower bound in the force-displacement behavior (see Figure 10).

The envelope curve may be described by using any of the following three methods or procedures (32):

- Experimental data method
- Statistical or empirical method
- Analytical method

The experimental data method assumes linear variation between consecutive force-displacement data points. Figure 10 shows an example of this method. The statistical or empirical procedure is based on applying statistical analyses to the experimental data. Usually a regression analysis and goodness of fit processes are used. Finally, the analytical method consist in the development of the envelope curve based on equilibrium and compatibility considerations.

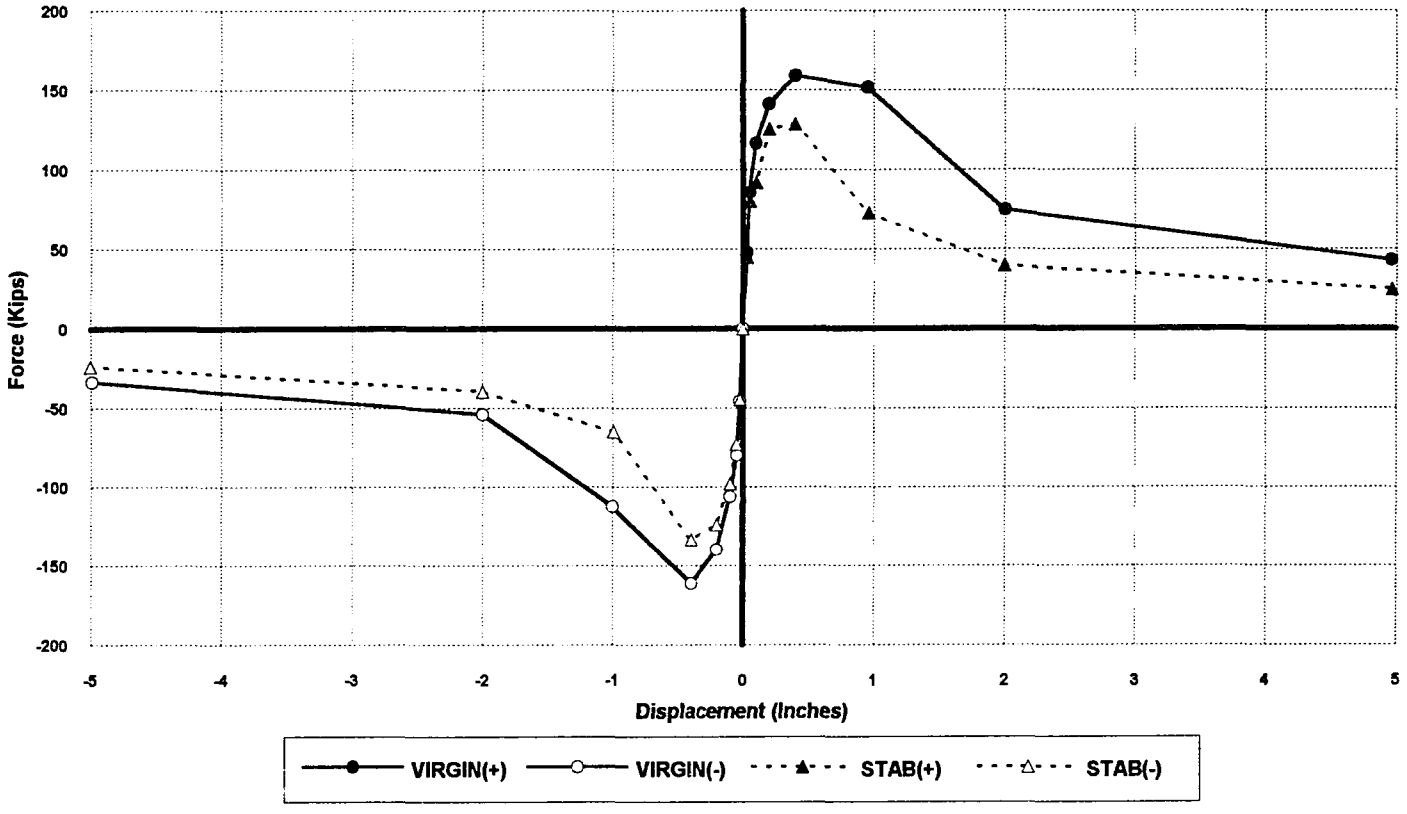

Figure 10. Virgin and stabilized envelopes for diaphragm 10

This work includes the determination of the envelope curve by the statistical and analytical methods. Application of the experimental data method is straightforward and does not need any extra explanation.

3.3 Statistical Method

3.3.1 General

The idea of using fitted expressions on experimental data to describe a hysteretic model has been used widely, especially by Japanese researchers (43,44,50,51,90). The complex behavior of concrete and its dependability in considering factors such as component arrangement, strength, etc., made the selection of this method an easy choice. The statistical approach has been widely used in the model description process because usually yields better indicators of element behavior than analytical predictions based many times in rough and approximate assumptions (32).

To define the envelope curve for SDRC diaphragms using the empirical or statistical method, experimental data obtained from testing 32 full-scale specimens was used. The experimental program consisted of two phases: First, a series of nine diaphragm tests (Phase I) was performed at ISU by Porter and Greimann (78). Later, an additional twenty-three diaphragm tests (Phase II) were also performed at ISU by Porter and Easterling (89). Numerous SDRC diaphragm parameters were varied and tested. Key parameters included steel-deck type, fastener type and number, concrete thickness, diaphragm depth-to-span ratio, loading, and framing member size. More detailed description of the experimental program is found in Appendix A.

3.3.2 Input data

The envelope data used in this work was obtained from 32 tests. Data was classified as positive or negative, and as virgin or stabilized. A graphical representation of these characteristics is shown in Figure 10. For a given envelope in the positive (1st quadrant) or negative (3rd quadrant) region, the data was again classified as being in the pre-peak region or post-peak region. At least 32 force-displacement data-points were available for envelope analysis on each of the 32 tests (more points were usually recorded in the experimental test). Each diaphragm test data was divided in 8 blocks or sections according to the described classification. Therefore, any pre-peak section had five data points (including the origin), and each post-peak section has four data points. There is one exception in the arrangement of data coresponding to Test 1. Diaphragm Test 1 was used mainly as a pilot specimen to check the supporting frame behavior and was subjected to monothonic load, therefore there was no stabilized data to consider.

A first step in any data analysis is often a graphical study of the characteristics of the data sample. A graphical representation of envelope virgin force-displacement data points for all 32 tests is shown in Figure 11. From this plot the following conclusions may be stated:

- The general path of force-displacement behavior is nonlinear
- For small displacements a linear assumption should be investigated
- The scatter of the points increases around the peak load

3.3.3 Test for normality

The next step in the analysis of data was the identification of the probability density function (pdf) that described the random component of the independent variable (shear force). This step is important since hypothesis testing and regression analysis are based

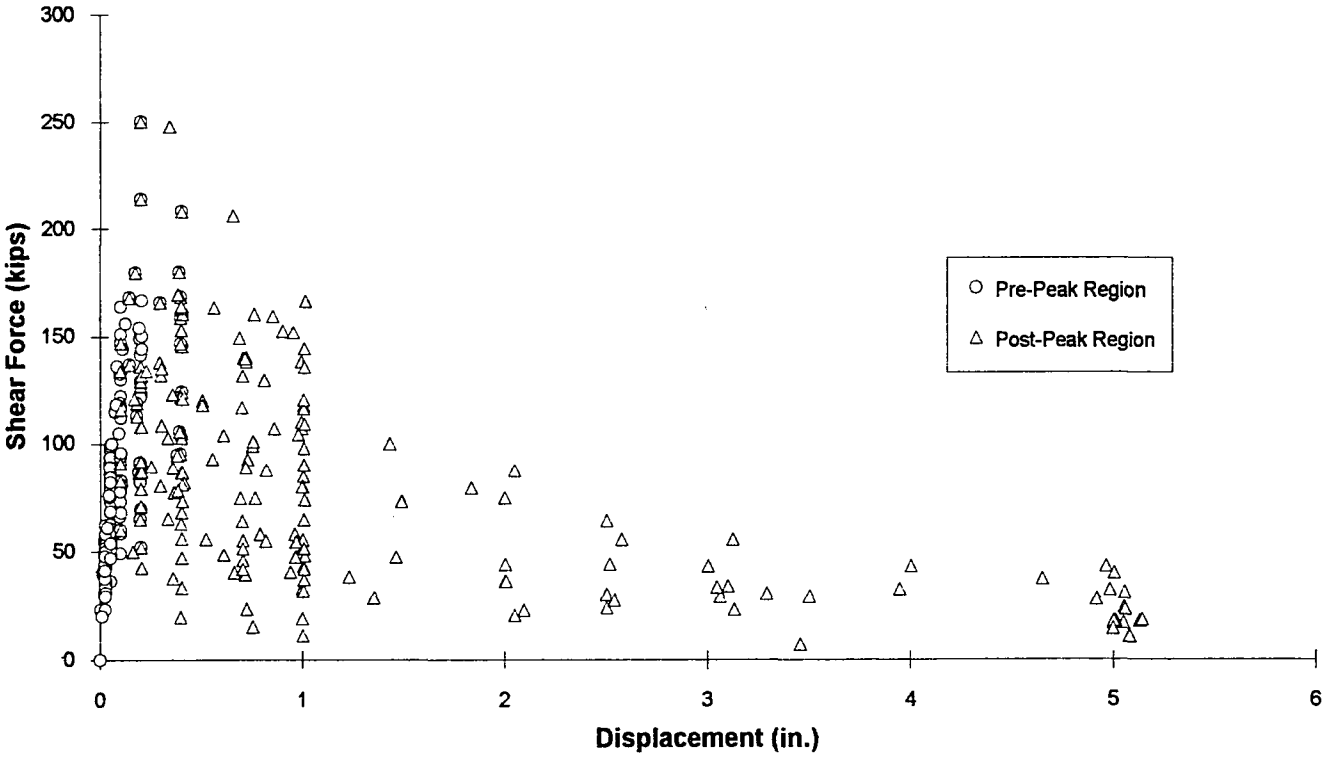

Figure 11. Positive virgin envelope data points (diaphragms 1-32)

on the assumption that the pdf is known. Additionally, the least squares method assumes that the errors (that is, the differences between predicted and measured values) are normally distributed. An exact procedure for testing for normality does not exist (91). However, the force values could be separated into groups having similar values of displacements and each group may be analyzed as an univariate problem. Usually a chi-square test for goodness-of-fit, or Kolmogorov-Smirnov tests are used to test for normality (26,91,92). Since the Kolmogorov-Smirnov test is generally suggested when the sample is small (91), and because there is no measure of small or large sample for these tests, both methods were used in this work in testing for normality.

To test the hypothesis that the force follows a normal distribution, the chi-square test was based on a comparison of the observed frequencies of the force in the sample with the frequencies expected with the normal distribution. The test statistic used, was a function of the observed and expected frequencies. A region of rejection in a chi-square distribution was defined according to a specific level of significance. If the computed estimate of the test statistic were outside the region of rejection there was no statistical basis for rejecting the null hypothesis. Next, a description of the process used is presented:

First, the virgin envelope force data was grouped according to the displacements used during experimental testing (Split-Sample method). As mentioned in Appendix A, Section A4, each test except diaphragm 1 was subjected to a series of selected displacements of ±0.025 in., ±0.05 in., ±0.100 in., ±0.200 in., ±0.400 in., ±1.000 in., ±2.500 in., and ±5.000 in. Second, for each group the next series of steps were followed:

- Evaluate: sample mean (μ_s), standard deviation (σ_s) and frequencies versus force range.
- formulate the null (H_o) and the alternative (H_a) hypotheses:

H_0 : Shear forces at this displacement follow a normal distribution with a mean and standard deviation of μ_s and σ_s, respectively.

H_a : Shear forces at this displacement are not normally distributed with parameters μ_s and σ_s.

- Evaluate the test statistic χ_c^2 as function of the observed and expected frequencies as follows:

$$\chi_c^2 = \sum_{i=1}^{k} \frac{(O_i - E_i)^2}{E_i} \qquad [3\text{-}1]$$

where:

χ_c^2: is the computed value of the test statistic having a χ^2 distribution

O_i: is the observed frequency in cell i

E_i: is the expected frequency in cell i

k: number of cells or categories into which the data was divided.

- Select the level of significance α. Usually if the decision is not considered critical, a value of 5% may be used because of convention.
- Define the region of rejection. The rejection region is defined using a chi-square distribution with k-3 degrees of freedom, and by selecting the significance level α
- If the estimate of test statistic χ_c^2 falls outside of the rejection region, H_o is accepted. If the estimate falls in the rejection region, H_a is accepted.

The Kolmogorov-Smirnov procedure tests the same null and alternate hypotheses as does the chi-square test evaluation. The test statistic "D" is given by the maximum absolute difference between the values of cumulative distributions of the force sample and the normal probability distribution function. Critical values defining the inner edge of the

rejection region are usually available only for limited values of significance level, critical values used in this work were obtained from Appendix A of Reference 91.

A general purpose statistical package (STATISTICA) developed by StatSoft (93) was used in the analysis procedure. Specific details of the output are given in the following tables. Table 1 shows the computations for the positive envelope shear forces at +0.025 in. displacement. Figure 12 shows a frequency histogram for virgin positive forces at 0.025 in. Table 2 shows a summary of the results obtained by applying the Kolmogorov-Smirnov and Chi-square tests to all the virgin data. Based on results shown in Table 2, the null hypothesis statement of "envelope data values come from a population with normal distribution" can not be rejected.

3.3.4 Least squares method assumptions

The purpose of this sub-section is to select an empirical model to fit the experimental envelope data. A series of 11 different models is used to select a model to fit the data. First, least squares criterion is used to select the "best" model for each specific diaphragm test. Hereinafter, a reliability criteria is established to select the model that best fits all diaphragm tests.

The Least squares method defines error as the difference between the predicted and experimental values and assumes the following about the errors:

- independent of each other.
- have zero mean.
- have constant variance across all values of displacement.
- are normally distributed.

For this work, independence of errors is assumed. The implications of the last three assumptions can be seen in Figure 13, where the independent shear force variable

Table 1. Chi-square and Kolmogorov-Smirnov tests for positive envelope force at 0.025 in. displacement

Boundary	Observed Frequency O_i	Percent Observed	Cum. % Observed $Cum\ O_i$	Expected Frequency E_i	Percent Expected	Cum. % Expected $Cum\ E_i$	$\frac{(O_i - E_i)^2}{E_i}$	$\frac{\lvert Cum\ O_i - Cum\ E_i \rvert}{100}$ D
≤28.89	6	8.9552	8.9552	5.4964	8.2037	8.2037	0.0461	0.0075
32.78	6	8.9552	17.9105	4.9955	7.4560	15.6597	0.2020	0.0225
36.67	5	7.4627	25.3731	7.3162	10.9196	26.5793	0.7333	0.0121
40.56	7	10.4478	35.8209	9.2697	13.8353	40.4146	0.5557	0.0459[a]
44.44	13	19.4030	55.2239	10.1608	15.1653	55.5799	0.7933	0.0036
48.33	9	13.4328	68.6567	9.6354	14.3813	69.9612	0.0419	0.0130
52.22	9	13.4328	82.0896	7.9049	11.7984	81.7596	0.1517	0.0033
56.11	6	8.9552	91.0448	5.6106	8.3740	90.1335	0.0270	0.0091
+∞	6	8.9552	100.000	6.6105	9.8665	100.000	0.0564	0.0000
							$\chi^2 = \Sigma$	$= 2.6075$[b]

[a] $D = 0.0459$ (test statistic for Kolmogorv-Smirnov test), is compared with $D_c = 0.1662$, $D < D_c$ then accept H_o

[b] $\chi^2 = 2.6075$ (test statistic for chi-square test), the critical value is $\chi_c^2 = 12.596$ (for 6 dof, and $\alpha = 5\%$) then accept H_o

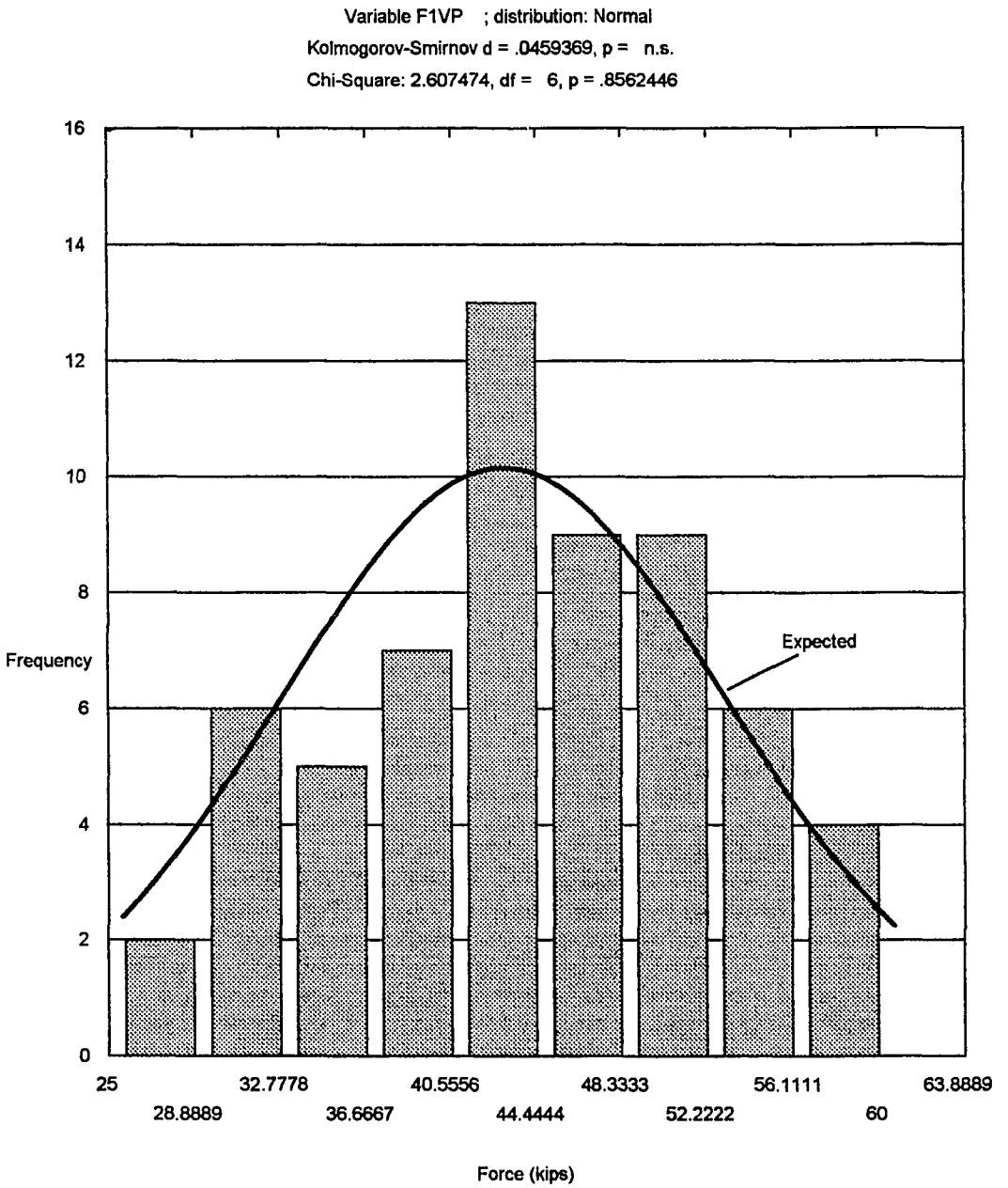

Figure 12. Frequency histogram for positive envelope force at 0.025 in. displacement

Table 2. Kolmogorov-Smirnov and Chi-square test results for virgin envelope forces

		Kolmogorov-Smirnov Test		chi-square Test		
Associated Displ.(in.)	Envelope Type	D	D_α [a]	χ^2	χ_c^2 [b]	p_{value}
0.025	Virgin +	0.0459	0.1662	2.6075	12.5960	0.8562
0.050	Virgin +	0.0671	0.1662	7.3787	14.0700	0.3906
0.100	Virgin +	0.0629	0.1662	10.1604	15.5120	0.2540
0.200	Virgin +	0.0597	0.1662	7.9910	14.0700	0.3334
0.400	Virgin +	0.0449	0.1662	9.2206	16.9250	0.4172
1.000	Virgin +	0.1042	0.1662	13.3432	18.3110	0.2052
2.500	Virgin +	0.0547	0.1662	3.5186	7.8170	0.3184
5.000	Virgin +	0.1109	0.1700	8.3814	11.0730	0.1365
-0.025	Virgin -	0.0407	0.1327	8.5602	12.5960	0.2000
-0.050	Virgin -	0.0540	0.1327	12.6346	22.3670	0.4764
-0.100	Virgin -	0.0670	0.1327	12.7893	14.0700	0.0775
-0.200	Virgin -	0.0659	0.1327	10.3220	16.9250	0.3251
-0.400	Virgin -	0.3940	0.1327	10.2603	16.9250	0.3299
-1.000	Virgin -	0.1038	0.1327	20.0009	22.3670	0.0953
-2.500	Virgin -	0.0458	0.1943	5.8799	14.0700	0.5538
-5.000	Virgin -	0.1102	0.2027	5.6666	12.5960	0.4615

[a] $D_\alpha = \frac{1.36}{\sqrt{N}}$, for $\alpha = 0.05$, and N = number of forces

[b] Evaluated for $\alpha = 0.05$, and υ dof, $\upsilon = \kappa - 3$, κ = number of categories

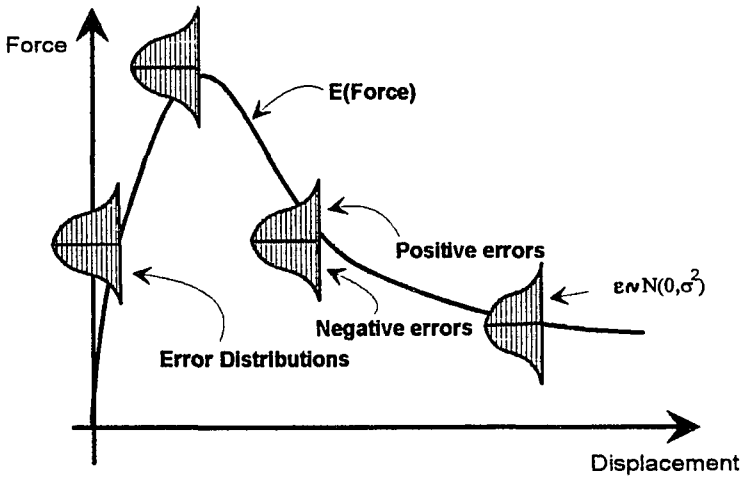

Figure 13. Error assumptions with the least squares method

is shown following a normal distribution with mean given by the envelope curve and constant variance through all the curve. Hypothesis of normality for the envelope data can not be rejected according to the results from the previous section. However, the hypothesis of constant variation may not be valid, since large dispersion or data scattering was observed close to the peak load (see Figure 11).

An analysis of the envelope data was made using the Split-Sample method described before. The objective was to identify the pattern followed by the variance of the envelope data for different displacements. Results of such analysis are presented as a plot of the standard deviation versus displacement for all the envelope data points (Figure 14). Figure 14 shows that: First, the variance of the data is not constant through all displacements, especially for pre-peak displacements, but seems to be proportional to the force level. Second, for large displacements, variance values are approximately constant.

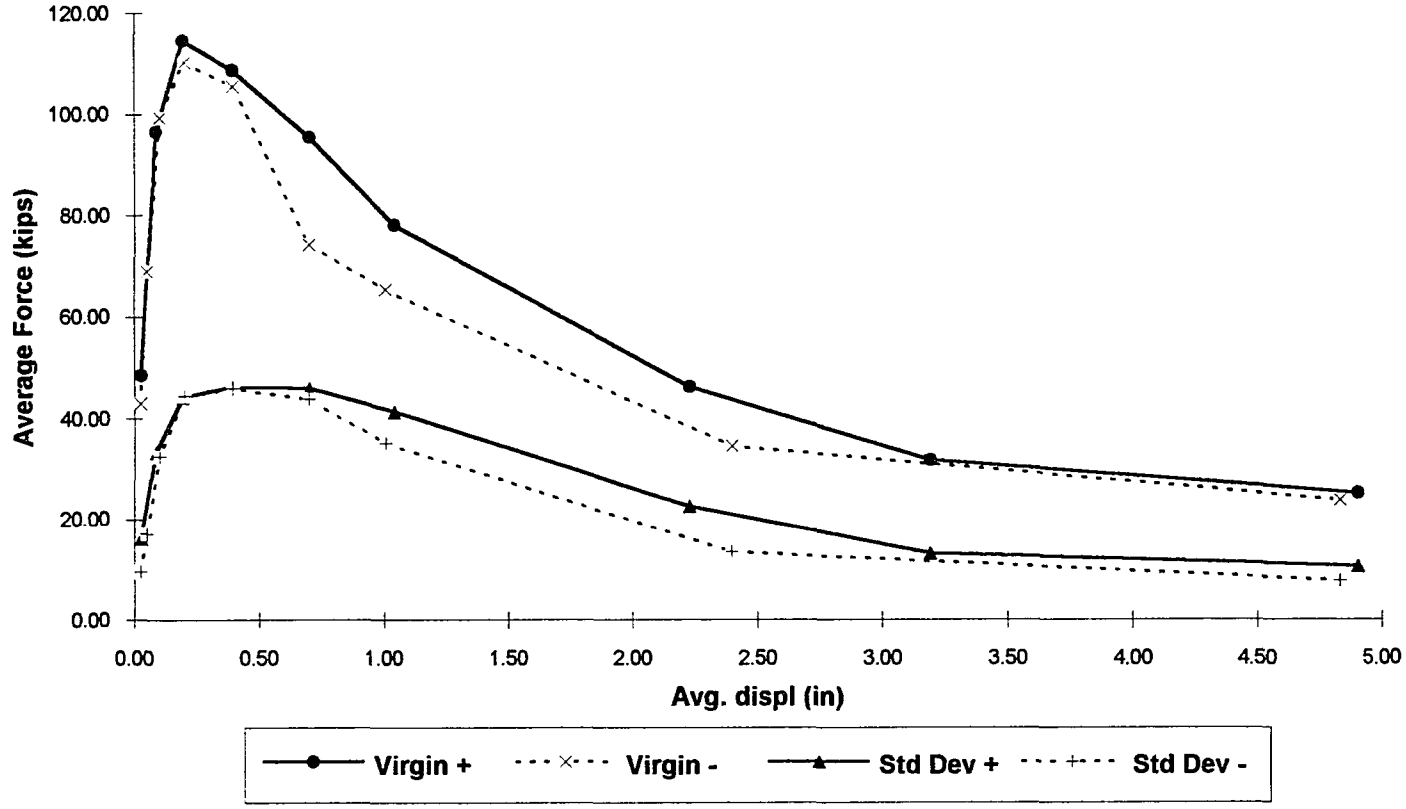

Figure 14. Standard deviation of virgin envelope data

Variance varying proportionally to force level may be explained according to the type of failure observed in diaphragms. Diagonal tension and shear transfer mechanism failures (see Appendix A for a description of failure types) are a function of the concrete tension stress and bond stresses, respectively, which are highly variable in nature. Once the peak load and failure type are reached, diaphragms start to degrade in strength with increased cyclic displacements until a strength plateau is reached. Such stable region is a result mainly of the more uniform steel deck response since at this displacement level the concrete is mostly cracked for diagonal tension mode of failure or the shear interface has lost most of its transfer capacity for shear transfer mechanism.

Constant variance may not be a real assumption, specially for pre-peak displacements; therefore, some kind of variance stabilization technique should be considered. However, some authors (91,94) are not too rigid in the full validation of the general assumptions. For example, Mendenhall et al. state: "In actual practice, the assumptions need not hold exactly in order for least squares estimators and test statistics to posses the measures of reliability that is expected from a regression analysis." Accordingly, for this work a compromise was made to continue with the regression analysis. First, a selection of the best model among a series of provided models was made according to the least squares method, but neglecting any effect due to heterogeneous scatter. The scattering of data may result in nonconstant variance or heteroscedasticity. Since the pool of models was used with the same scattered data, the effect of neglecting such a condition was reduced. Second, once the best model from the pool was selected, a consideration of the heteroscedasticity of the data were made to get more reliable regression coefficients.

3.3.5 Regression analysis

3.3.5.1 Basic considerations A pool of eleven different models will be considered to select the "best model" according to the least squares criteria. Those models were selected based on: First, their plot may fit the envelope data point pattern and other sets of data related to cyclic loops. Second, they are of common use according to different authors (91,92,94,95). See Table 3 for a description of models.

To fit models from Table 3 to the experimental data, the least squares method for linear regression models was used. Note that from a statistical point of view, a linear model has all their coefficients (a, b) appearing linearly; therefore, Models 1,4,7,9 from Table 3 are linear. Nonlinear models have at least one of the derivatives of y with respect to a and b coefficients as a function of at least one of a and b coefficients(95). Therefore, in applying least squares to those nonlinear models a previous linearization has to be made. For example Model 2 is linearized by applying logarithms to both sides of the equation. A problem may be generated when this type of linearization is applied. The error minimization process is made in the log y versus x space and not at the y vs x space; therefore, the sum of the squares of the errors may not be a minimum in the y domain even though they are in the log y space. In spite of this consideration, transformations usually provide reasonable estimates in the x-y space (91).

3.3.5.2 Goodness of fit To evaluate the reliability of the regression models, an estimate or index has to be used. Among the most used indices are : the correlation coefficient (R), the standard error of the estimate (S_e), the mean absolute error (MAE), etc.

Table 3. Identification of regression models

Model Number	Model Name	$y = f(x)$
1	Linear	$y = a + bx$
2	Exponential	$y = e^{(a+bx)}$
3	Reciprocal - y	$y = \frac{1}{a+bx}$
4	Reciprocal - x	$y = a + \frac{b}{x}$
5	Double reciprocal	$y = \frac{1}{a+\frac{b}{x}}$
6	Reciprocal exponential	$y = \frac{1}{1+e^{(a+bx)}}$
7	Logarithmic - x	$y = a + b\ln(x)$
8	Multiplicative	$y = a\,x^{b}$
9	Square root x	$y = a + b\sqrt{x}$
10	Square root y	$y = (a+bx)^2$
11	S curve	$y = e^{\left(a+\frac{b}{x}\right)}$

The correlation coefficient is an index of the degree of linear association between two random variables. The standard error of the estimate measures the standard deviation of the errors. The standard error S_e, is usually preferred to the correlation coefficient because its magnitude is an indicator of the error and has the same units as the criterion variable. The standard error of the estimate is given by:

$$S_e = \sqrt{\left[\frac{1}{\nu}\sum_{i=1}^{n}\left(\hat{Y}_i - Y_i\right)^2\right]} \qquad [3\text{-}2]$$

where:

S_e: standard error of estimate

υ: degrees of freedom = n-2

n: number of observations

$\hat{Y}_i$: ith predicted value

Y_i: ith measured value

The mean absolute error (MAE) is another index of regression reliability. MAE measures the average deviation from the fitted line. MAE may be defined also as the mean of the absolute value of the residuals. The MAE has the same units as the criterion variable and its magnitude is an indicator of the error. Since MAE is evaluated with the total number of observations, the MAE is less sensitive to small samples than the standard error of the estimate. The mean absolute error is given by:

$$MAE = \frac{\sum_{i=1}^{n}\left|\hat{Y}_i - Y_i\right|}{n} \qquad [3\text{-}3]$$

Because the number of observations per test was relatively small, the mean absolute value was preferred as the statistic to be used to select the "best model" using the least squares criteria.

The regression analysis was applied using dimensionless independent and dependent variables. The dimensionless parameters were defined as follows:

$$x = \frac{e}{e_p} \quad [3\text{-}4]$$

$$y = \frac{F}{F_p} \quad [3\text{-}5]$$

where:

x: Independent dimensionless parameter

y: Dependent dimensionless parameter

e: Displacement

e_p: Peak displacement

F: Shear force

F_p: Force at peak displacement

3.3.5.3 Results of regression analysis on envelope data Results of the regression analysis were classified according to the type of data used. The possible data sources were: 32 diaphragm tests (32 cases), virgin or stabilized envelope (2 cases), positive or negative envelope (2 cases), pre or post-peak region (2 cases). Since the number of regression models to be considered was 11, then the total number of regression analyses was 32x2x2x2x11= 2816. This number was too high to try to use a commercial software package such as STATISTICA (93) or SAS (96) to fit one model at the time. Even though that statistical packages included batch programming capabilities that may reduce the amount of runs, It was thought to be a better solution to write a computer program to do the job. A macro sheet program called BASE.XLM was developed and

tested against SAS and STATISTICA solutions. This macro sheet program runs under MS EXCEL (97) support, and is described according to the following steps:

- Transfer of data from other spreadsheets.
- Classify the data according to:
  - envelope type (virgin or stabilized).
  - data sign (positive or negative).
  - data region (pre-peak or post-peak region).
- Linearization of data (for those nonlinear models).
- Regression analysis (for each of the eleven different models).
- Evaluation of the standard error S_e and mean absolute error MAE.
- Print results.

A typical output for diaphragm Test 27 using BASE.XLM is presented in Table 4. After the 32 diaphragm test data were analyzed, a sorting of the results was made by the regression model for 31 of the 32 tests (Test 1 was monothonically loaded). To identify the best possible candidates for the regression model, mean values and 95% confidence intervals were evaluated for each set of 32 diaphragm tests. Selection of a model with the smallest average error is a logical choice, but the variability of the average error has to be taken into account. Therefore, another important parameter to consider is the confidence interval that provides information about the probability that the interval will contain the estimated parameter. Then for a given significance level, the narrowest the confidence interval the largest the reliability in the model. Since the variance of the population was unknown, the confidence interval was evaluated using the Student's t distribution as follows:

$$(1-\alpha)\%\ CI = \bar{y} \pm t_{\alpha/2,n-1}\left(\frac{s}{\sqrt{n}}\right) \qquad [3\text{-}6]$$

Table 4. Standard error and mean absolute error for test 27

		VIRGIN ENVELOPE				STABILIZED ENVELOPE			
model	Statistic	V+[a]	V+[b]	V-[a]	V-[b]	S+[a]	S+[b]	S-[a]	S-[b]
1	SEE	0.24	0.12	0.26	0.15	0.25	0.16	0.25	0.21
2	SEE	0.33	0.10	0.44	0.13	0.42	0.14	0.41	0.18
3	SEE	0.34	0.09	0.45	0.13	0.44	0.12	0.43	0.18
4	SEE	0.08	0.03	0.03	0.05	0.08	0.10	0.07	0.13
5	SEE	0.05	0.10	0.01	0.16	0.06	0.22	0.05	0.33
6	SEE	0.25	0.15	0.30	0.20	0.37	0.19	0.34	0.24
7	SEE	0.02	0.07	0.01	0.10	0.03	0.08	0.03	0.12
8	SEE	0.01	0.04	0.02	0.06	0.01	0.07	0.01	0.11
9	SEE	0.11	0.09	0.11	0.13	0.10	0.12	0.09	0.17
10	SEE	0.35	0.11	0.44	0.14	0.42	0.15	0.41	0.19
11	SEE	0.06	0.04	0.02	0.05	0.07	0.14	0.06	0.19
1	MAE	0.17	0.09	0.18	0.12	0.17	0.09	0.17	0.13
2	MAE	0.15	0.07	0.18	0.09	0.16	0.08	0.16	0.11
3	MAE	0.16	0.06	0.19	0.07	0.17	0.07	0.17	0.11
4	MAE	0.05	0.02	0.02	0.03	0.04	0.06	0.04	0.08
5	MAE	0.03	0.06	0.00	0.09	0.03	0.12	0.03	0.17
6	MAE	0.09	0.08	0.11	0.11	0.15	0.12	0.13	0.15
7	MAE	0.01	0.06	0.01	0.08	0.02	0.05	0.01	0.07
8	MAE	0.01	0.03	0.01	0.05	0.01	0.04	0.00	0.07
9	MAE	0.08	0.07	0.07	0.10	0.06	0.07	0.06	0.10
10	MAE	0.26	0.08	0.28	0.10	0.27	0.09	0.27	0.12
11	MAE	0.04	0.03	0.01	0.04	0.04	0.08	0.03	0.11

[a]Pre-peak region

[b]Post-peak region

where:

CI: confidence interval

$\bar{y}$: sample mean

$t_{\alpha/2,n-1}$: t statistic evaluated from the t distribution such that the probability of a random deviation numerically greater than $t_{\alpha/2,n-1}$ is α

s: sample standard deviation

n: number of observations

α: level of significance

An overall plot of the average MAE against envelope type and regression model for all tests is shown in Figure 15. In this figure the envelope type is identified by two letters and one number e.g. VP2. The first letter stands for virgin (V) or stabilized (S) envelope; the next letter stands for positive (P) or negative (N) envelope. Additionally, number one is associated with pre-peak envelope region and number two is associated with post-peak envelope region. An example of the mean values and 95% confidence intervals (CI) for virgin positive pre-peak envelope data per regression model is shown in Figure 16. A complete set of plots of confidence intervals and MAE values for all cases is shown in Appendix B (Figure B1-B8).

From the results and plots of MAE values and confidence intervals, the following patterns were identified:

- Positive and negative values for each envelope type had similar average MAE and confidence intervals; this may indicate that positive and negative diaphragm behavior is symmetrical. See Figures B9-B12 in Appendix B for a comparison between positive and negative envelope MAE average values.

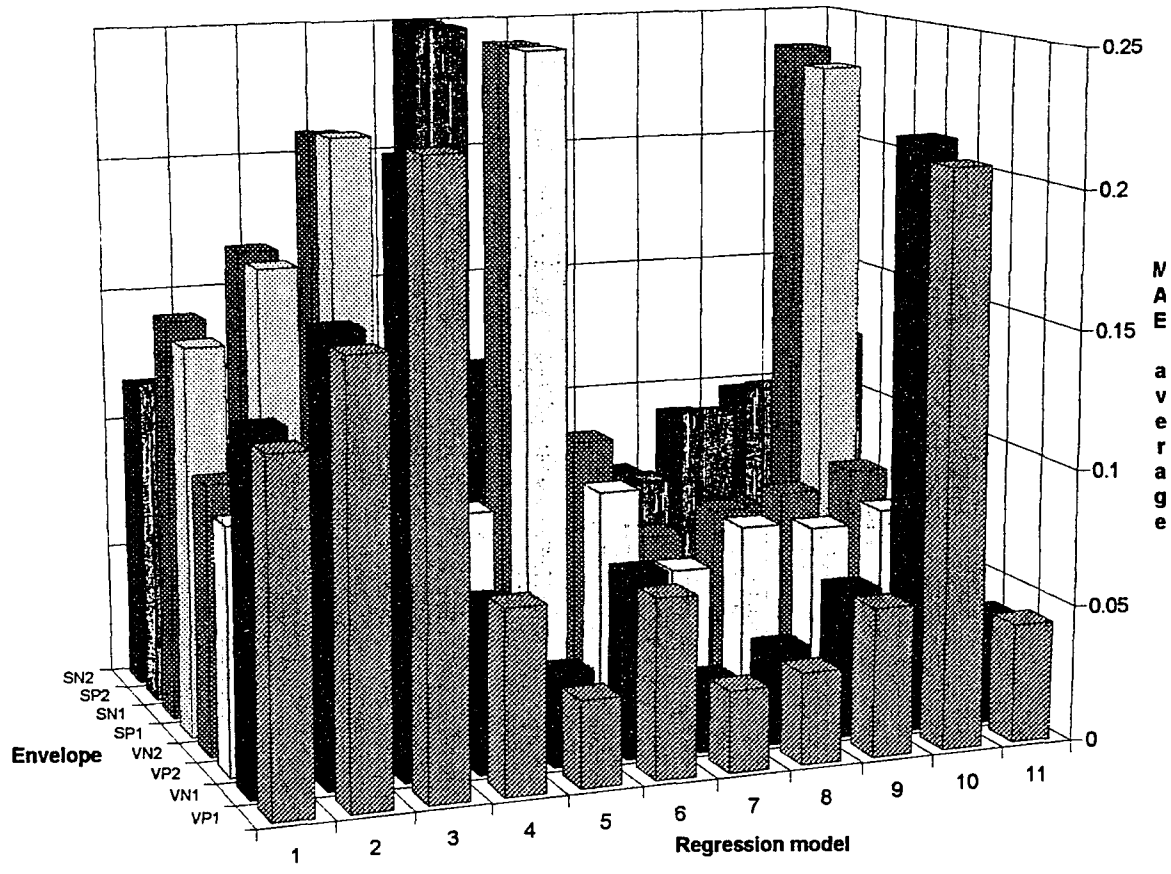

Figure 15. MAE average distribution per envelope type and regression model

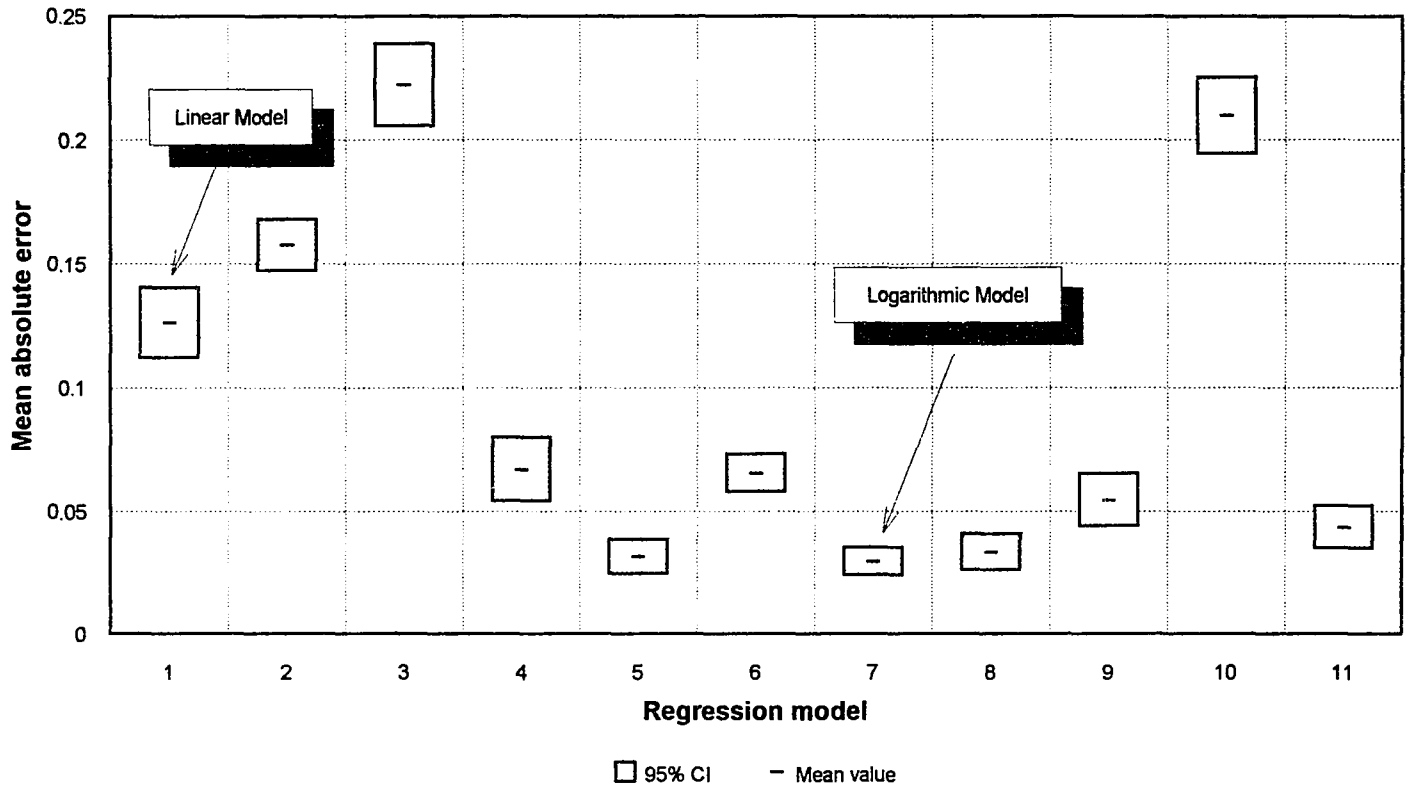

Figure 16. Mean values and 95% CI for virgin positive pre-peak region envelope data

- For all envelope types except stabilized positive post-peak region (Figure B7), the logarithmic-x regression model resulted in the lowest average MAE and smallest confidence interval. For the exception case, it had the second lowest average MAE (only 3% difference), but a smaller confidence interval, therefore the logarithmic-x model was a better predictor.

Based on the observed results of average MAE and CI, two hypotheses may be stated. The first hypothesis will state the possibility of a significant difference between positive and negative values of force envelope data. The second hypothesis will state the possibility of a significant difference between the logarithmic-x regression model and the other 10 regression models. The next two subsections will test these two hypotheses.

3.3.5.4 Test of Hypothesis I Test for significant difference between positive and negative envelope values may be made by considering each set of positive and negative envelope data as samples. Each sample was assumed to come from a population composed by diaphragms with the characteristics of the corresponding diaphragm tested. Testing for significant difference between two samples (positive and negative envelope values) was made using a Paired Samples Method, since each observation of positive envelope force is matched with a specific observation of negative envelope force for the same absolute displacement. A test was applied to each set of virgin and stabilized envelope data for each diaphragm specimen (except Diaphragm 1 that was monothonically loaded); therefore, the total number of sets was 2 (virgin and stabilized) x 31 (diaphragm tests) = 62. The following procedure was used in testing for significant difference between two paired samples:

- State the null (H_o) and alternative (H_a) hypotheses:

H_o: $\delta = \mu_1 - \mu_2 = 0$ (there is no significant difference between positive and corresponding negative envelope forces)

H_a $\delta = \mu_1 - \mu_2 \neq 0$

- Evaluate the sample difference, mean value and standard deviation as follows:

$$d_i = F_{i1} - F_{i2} \qquad [3\text{-}7]$$

$$\bar{x}_d = \frac{\sum_{i=1}^{n} d_i}{n} \qquad [3\text{-}8]$$

$$S_d = \sqrt{\frac{\sum_{i=1}^{n} (d_i - \bar{x}_d)^2}{n-1}} \qquad [3\text{-}9]$$

where:

F_{i1}: Positive envelope force

F_{i2}: Negative envelope force

d_i: difference of positive and negative force associated with the same absolute displacement

n: number of observations

$\bar{x}_d$: difference mean value

S_d: difference standard deviation

- Evaluate the test statistic t (t distribution since σ is unknown):

$$t = \frac{\bar{x}_d - 0}{\frac{S_d}{\sqrt{n}}} \qquad [3\text{-}10]$$

- For a defined significance level α and n-1 dof, determine the critical value of the statistic t_{cr} that defines the rejection region (two-tailed):

$$t_{cr} = t_{(\alpha/2,n-1)} \qquad [3\text{-}11]$$

- Rejection criterion is defined if $t>t_{cr}$ that is defined for a fixed value of α, or in a more general way a "variable" rejection criterion may be defined by using the observed significance level (p_{value}).

Graphical results of this analysis are shown in Figure 17, and numerical results are shown in Table B2 in Appendix B. Figure 17 shows observed confidence values for all the tests. Each test with a Pvalue greater or equal to a defined α value (e.g., 5%) means that there is no significant difference to reject the hypothesis H_0 which means that no significant difference exist between positive and negative envelope forces. Results showed that at the 5% level from a total of 62 tests (31 diaphragms x 2 envelopes), 13 tests showed significant difference, and at 1% level, only 2 tests showed significant difference.

From those tests with a significant difference at the 5% level, only one failed via the diagonal tension mode (Test 18 with twice the design gravity load), the other 12 failed under shear transfer mechanism and/or edge connection mode. These results agree with the observations made by Porter et al. (89) regarding the symmetrical failure crack pattern observed in diaphragms with diagonal tension failure. Additionally, shear transfer mechanism and edge connection failure modes are more of localized nature; therefore, a more unsymmetrical response is expected. In conclusion, the response pattern of diaphragms with the characteristics considered in this study (see Appendix A) under cyclic load is to have envelopes with symmetry respect to the origin, especially for those diaphragms with diagonal tension mode.

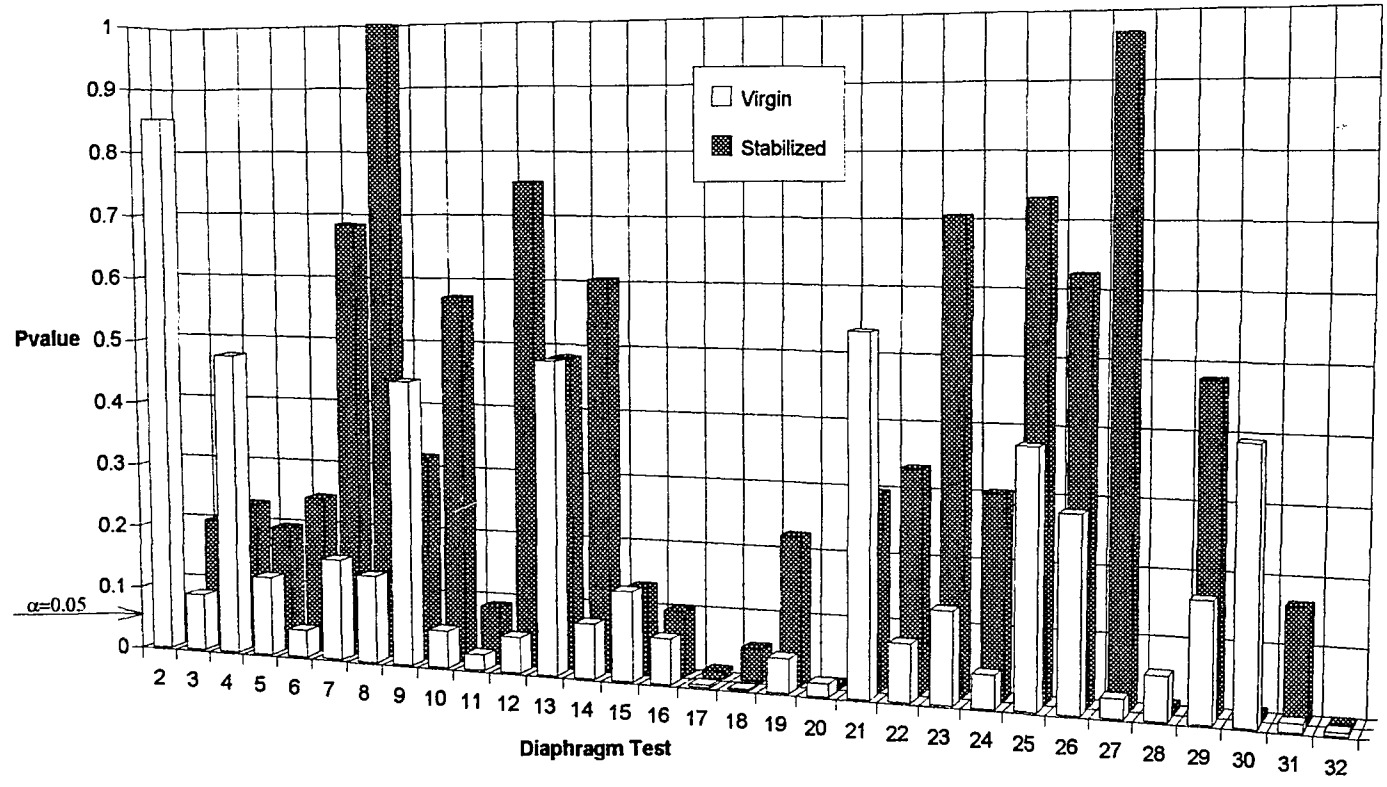

Figure 17. P_{value} **for positive and negative envelope force paired samples difference tests**

3.3.5.5 Test of Hypothesis II This second hypothesis will test if there is or there is not a significant difference among the logarithmic-x regression model MAE values and the MAE values from all the other regression models. From results presented in Figures 15-16, Table B1, and Figures B1-B8, the logarithmic-x regression model (Model 7) was found to have the lowest MAE for all tests, followed by the multiplicative regression model (Model 8). Testing for significant difference between these two models (Models 7 and 8) seems irrelevant because of the following reasons. First, both models are nonlinear from a mathematical point of view; therefore, both have the same degree of difficulty. Second, if there were no significant difference between both models; there is still an advantage in using the logarithmic-x regression model, since it is a linear model from a statistical point of view (see Section 3.2.1.4), meanwhile the multiplicative is not, and the criterion of least squares is valid only in the logY vs LogX domain.

Testing for significant difference between the logarithmic-x regression model and the linear regression model seems to be the most appropriate course to follow because among all models the linear is the most simple model to use. The criterion to be used is to compare the average MAE obtained for both models for each specific diaphragm. Use of the paired sample method again seems to be adequate because each MAE value was obtained from the same diaphragm test values under the two different models. For all diaphragm tests (Tests 2 to 32) a comparison was made for each envelope (virgin and stabilized), for each sign (positive, and negative), and for each region (pre-peak, and post-peak) for a total of 2x2x2=8 hypothesis tests.

The procedure to follow is similar to that used in the previous section, with the only difference is that now MAE values are used instead of force values as follows:

- State the null (H_o) and alternative (H_a) hypotheses:

H_o : $\delta = \mu_1 - \mu_2 = 0$ (there is no significant difference between MAE values of

linear and logarithmic-x regression models)

H_a : $\delta = \mu_1 - \mu_2 \neq 0$ (there is a significant difference between MAE values of both models)

- Evaluate the sample difference, mean value and standard deviation as follows:

$$d_i = MAE_{i1} - MAE_{i2} \quad [3\text{-}12]$$

$$\overline{x}_d = \frac{\sum_{i=1}^{n} d_i}{n} \quad [3\text{-}13]$$

$$S_d = \sqrt{\frac{\sum_{i=1}^{n} (d_i - \overline{x}_d)^2}{n-1}} \quad [3\text{-}14]$$

where:

MAE_{i1}: Mean Absolute Error value for Diaphragm *i* using linear model

MAE_{i2}: Mean Absolute Error value for Diaphragm *i* using logarithmic-x model

d_i: difference between MAE values for linear and logarithmic model

n: number of tests (31)

$\overline{x}_d$: difference mean value

S_d: difference standard deviation

- Evaluate the test statistic t according to Equation [3-10]
- Evaluate the critical value of the statistic t_{cr} according to Equation [3-11]
- Rejection criterion is defined for $t>t_{cr}$ for a certain fixed value of α. The rejection criterion may be also be defined by the observed significance level or p_{value}.

Results of this analysis showed a strong tendency to reject the null hypothesis H_o, since all the p_{values} were no significant, or in other words the statistical estimate t for all the cases was definitively in the rejection region as shown in Table 5. From these results, the conclusion is that there is a significant difference between the MAE values for all diaphragms when using the linear vs the logarithmic-x regression models; therefore, the logarithmic-x regression model (smallest average MAE values) is selected to predict the envelope forces for SDRC diaphragms.

3.3.5.6 Logarithmic-x regression model Results obtained in the previous subsection showed that the force envelope data may be described using the logarithmic-x regression model proposed in Section 3.2.1.4 (see Table 3), and obtained with the least squares method. A brief discussion of the assumptions used in the least squares method

Table 5. Difference of MAE values between linear and logarithmic-x regression models (paired samples method)

Envelope	VIRGIN				STABILIZED			
Section	Positive		Negative		Positive		Negative	
Region	Prepeak	Postpeak	Prepeak	Postpeak	Prepeak	Postpeak	Prepeak	Postpeak
$\bar{x}_d$	0.10	0.03	0.10	0.03	0.12	0.05	0.12	0.05
S_d	0.05	0.04	0.05	0.04	0.03	0.04	0.03	0.04
t	11.58	4.04	11.89	4.01	18.72	6.17	18.67	7.03
t_{cr}	2.05	2.04	2.05	2.04	2.05	2.06	2.05	2.05
p_{value}	--[a]	--[a]	--[a]	--[a]	--[a]	--[a]	--[a]	--[a]

[a]No significant values (P_{value}< 3E-04).

was presented in Section 3.2.1.3. Constant error variance was mentioned as one of the required assumptions. Section 3.3.4 also mentioned that the force envelope data has the standard deviation in some way proportional to the force mean value (Figure 14). To reduce the effect of heteroscedasticity or variance dependent of the mean value, different approaches may be used. The two most common procedures are the weighted least squares method and response transformation method.

The weighted least squares method introduces a small weight to observations whose large variances make them more unreliable, and larger weights are used for observations with smaller variances. Since the residual variances are not usually known, some kind of estimate has to be used. Use of weights based on poor estimates of variances may lead to useless regression coefficients (96).

The response transformation method is based on a similar criterion to that used by the weighted least squares method. The basic idea is multiply the response variable Y (force) by an appropriate transformation function (equivalent to the weight of the least squares method) to stabilize the variance. Appropriate variance stabilizing transformation function may be found elsewhere (92,94,91).

The force envelope data used in this work showed a variance dependent in the mean force values (see Figure 14), with data scattering increasing near to the peak load. One possible method of stabilize the variance is to normalize the data through the use of an especific scaling factor. Since the variance of data increase toward the peak load, one possibility may be to use as scaling factor the inverse of the peak load. The peak load and displacement at peak load of each diaphragm was used to normalize the diaphragm force displacement data. As result, each diaphragm data set was scaled from zero to unity, the variability data was reduced from a maximum to zero near the peak load. Additionally, the effect produced by the differences in peak loads from one diaphragm to

other was reduced, because due to the normalization of forces, each diaphragm had a normalized peak load of value unity.

The least squares method was applied using normalized force and displacement ratios. These dimensionless parameters were obtained by dividing each force and displacement value by the peak force and displacement at the peak respectively. Once the logarithmic-x model was found to be adequate to predict the envelope forces, the sample split method was again used to verify if there was stabilization of the variance by using the normalized parameters. The response and independent parameters used for the selected regression model were:

$$x = \ln\left(\frac{e}{e_p}\right) \qquad [3\text{-}15]$$

$$y = \frac{F}{F_p} \qquad [3\text{-}16]$$

Data was divided again into the pre-peak (x<0) and the post-peak regions (x>0). Figure 18 shows the results of the Split-Sample method for virgin envelope data. A comparison of Figure 18 with Figure 14 showed that, by using the force scaling factor, a partial stabilization of the variance was obtained. Additionally, a linearization effect produced by applying logarithms to the x variable was also obtained. Based in this results, a constant variance condition or homoscedasticity of the envelope data (normalized) was assumed.

The regression analysis used the least squares method. A typical output of a regression analysis is shown in Appendix B Table B3. As part of the output three sets of parameters were obtained: the regression statistics, the analysis of variance (Anova) and the parameter estimates. Since each of those statistical sets provides important

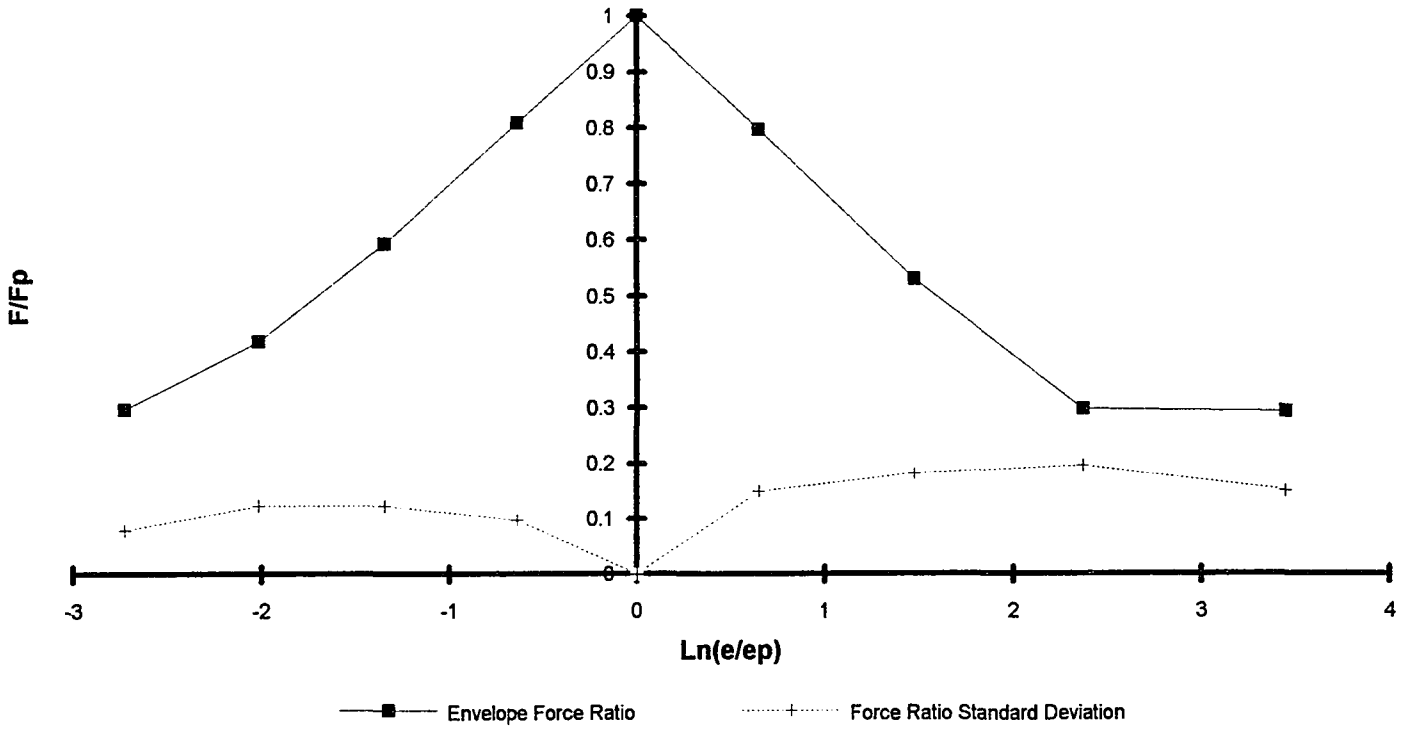

Figure 18. Mean and standard deviation values for the virgin envelope force data.

information about the relation between the input data and regression model, a brief description will be presented.

The regression statistics group, is formed basically by the correlation coefficient R, the coefficient of determination R^2, and the standard error of the estimate S_e. The correlation coefficient R is an index of the degree of linear association between two random variables (e.g., x, y). The magnitude of R indicates how accurate is the regression prediction of the criterion variable (y). A value of zero indicates no linear association between variables, meanwhile -1 (negative correlation) or +1 (positive correlation) indicates perfect association between variables. The sample correlation coefficient is given by:

$$R = \frac{\sum_{i=1}^{n}(x_i - \bar{x})(y_i - \bar{y})}{(n-1)S_x S_y} \qquad [3\text{-}17]$$

where:

$\bar{x}, \bar{y}$: x and y sample mean values, respectively.

S_x, S_y: x and y standard deviation values, respectively.

The coefficient of determination, or square of correlation coefficient R^2, is also an indicator of the accuracy of predictions, and measures the proportion of the total variance about the mean $\bar{y}$ explained by the regression line. Values of R^2 range among zero and unity, with unity standing for a full correlation. Usually, R^2 is expressed as follows:

$$R^2 = \frac{\text{SS due to regression}}{\text{Total SS, corrected for the mean } \bar{y}} \qquad [3\text{-}18a]$$

or

$$R^2 = \frac{\sum_{i=1}^{n}(\hat{y}_i - \bar{y})^2}{\sum_{i=1}^{n}(y_i - \bar{y})^2} \qquad [3\text{-}18b]$$

where:

$\bar{y}$: sample mean value

y: observed value

$\hat{y}$: predicted value

The standard error of the estimate is also an index of the accuracy of the prediction. In the absence of additional information on a given sample, the mean, $\bar{y}$, is the best estimate of the criterion variable, and the standard deviation, S_y, is an indication of accuracy. If y is related to a predictor variable (x), then the error of prediction is reduced from S_y to the standard error of estimate or S_e. In order to asses the reliability of the regression model, S_e should be compared with the bounds of zero and S_y, with values near to zero standing for good regression model. The standard error of the estimate is the standard deviation of the errors and may be evaluated using Equation [3-2].

The accuracy of a linear or linearized regression model may be evaluated by making inferences about the slope coefficient of the regression model. If the slope coefficient is no significantly different from zero then there is no relation between x and y and the best estimate for the data set is the mean value. The Student's t statistic or the analysis of variance (ANOVA) may be used to test for slope coefficients significantly different from zero. To use the Student's t statistic, an estimate of the slope coefficient is needed (it may be obtained from least squares method), and an estimate of the variance of the slope coefficient is also needed. The ANOVA uses the ratio of mean squares of the regression to a variance estimate, and compares it against an F statistic. The ratio used by the ANOVA is the square of the t estimate (92), therefore Student's t statistic and

ANOVA are equivalent procedures. Most of the professional statistical software such as SAS (96) or STATISTICA (93) use analysis of variance to asses the significance of the regression model. In general, the ANOVA test (see Table 6) is based on the follow procedure:

Model $y = \beta_0 + \beta_1 x + \varepsilon$ [3-19]

where:

β_0: intercept coefficient

β_1: slope coefficient

ε:: error term

Hypothesis:

H_0: $\beta_i = 0$, i=1,m; this hypothesis may be stated as "x_i does not contribute in the prediction of y"

H_a: $\beta_i \neq 0$; this hypothesis may be stated as "x_i contributes in the prediction of y using the linear model"

The null hypothesis is tested for significance using the ratio of the regression mean squares to the residual mean squares. This ratio F is the computed value of a random

Table 6. Formulation of an ANOVA table

Source of Variation	Sum of Squares	dof	Mean Squares	F	F_{cr}
Regression	$SS_{reg} = \sum(\hat{y}_i - \bar{y})^2$	1	$MS_{reg} = \frac{SS_{reg}}{1}$	$F = \frac{MS_{reg}}{MS_{res}} = \frac{MS_{reg}}{S_e^2}$	$F_{cr} = F_{[\alpha,1,n-2]}$
Residual	$SS_{res} = \sum(y_i - \hat{y}_i)^2$	n-2	$MS_{res} = \frac{SS_{res}}{n-2}$		
Total	$SS_{tot} = \sum(y_i - \bar{y})^2$	n-1			

variable having an F distribution. For a stated level of significance, α, the null hypothesis is accepted if F is less than the critical value, F_{cr}. The rejection region consists of all values of F greater than F_{cr}. The observed significance levels (p_{values}) may be an alternative in the testing procedure.

Finally, the third set of parameter estimates provides the coefficient values for the intercept and slope that are determined from expressions derived using the least squares criteria. The standard error of the intercept and slope coefficients are determined by applying directly the definition of mean and standard deviation to the least squares expressions of intercept and slope. The model parameter standard deviations may be used in testing for significant difference between each parameter and a pre-defined value, usually zero, but they are more frequently used to evaluate confidence intervals for the model parameters. The procedure used to test for significance and for the evaluation of confidence intervals is as follows:

Hypothesis:

H_0: β_1 (or β_0) = 0; this hypothesis may be stated as "there is no significant difference between the model parameter and zero"

H_a: β_1 (or β_0) $\neq$ 0; this hypothesis may be stated as "there is a significant difference between the model parameter and zero"

Statistical estimates:

for the slope term:

$$t = \frac{(\beta_1 - \beta_{10})}{S_{\beta_1}} \qquad [3\text{-}20]$$

$$S_{\beta_1} = \frac{S_{y/x}}{\sqrt{\sum (x_i - \bar{x})^2}} \qquad [3\text{-}21]$$

for the intercept term:

$$t = \frac{(\beta_0 - \beta_{00})}{S_{\beta_0}} \quad [3\text{-}22]$$

$$S_{\beta_0} = S_{y/x}\sqrt{\frac{\sum x_i^2}{n\sum (x_i - \bar{x})^2}} \quad [3\text{-}23]$$

where:

β_{10}, β_{00}: pre-defined values of population parameters

$S_{y/x}=S_e$: Standard error of estimate, see Equation [3-2]

Reject H_o if $| t | > t_{\alpha/2}$

Confidence intervals for intercept and slopes are given by:

Intercept CI $\beta_0 \pm t_{(\alpha/2,n-2)}S_{\beta_0}$ [3-24]

Slope CI $\beta_1 \pm t_{(\alpha/2,n-2)}S_{\beta_1}$ [3-25]

The procedures stated in this section were applied to the selected regression model (logarithmic-x model). Hypotheses test, and confidence interval results as well as other parameters are presented in tabular form in Appendix B (Table B4-B7). From these results the following conclusions may be stated: Correlation coefficients (R) as well as coefficients of determination (R^2) had mean values close to unity, suggesting a good correlation between variables as seen in Figure 19 and Table 7. Coefficient of determination showed a global mean value of 0.92 (1.00 value stands for perfect correlation) and a global mean standard error of 0.011. As expected, pre-peak values

Table 7. Descriptive statistics for R and R^2

Region	Pre-peak Virgin		Post-peak Virgin		Pre-peak Stab.		Post-peak Stab.	
Parameter	R	R^2	R	R^2	R	R^2	R	R^2
Mean	0.980	0.960	0.936	0.877	0.974	0.949	0.945	0.895
Std-error	0.003	0.007	0.006	0.011	0.005	0.010	0.009	0.017
Std-dev.	0.019	0.038	0.034	0.063	0.030	0.057	0.054	0.097
Minimum	0.923	0.851	0.871	0.758	0.888	0.788	0.780	0.610
Maximum	0.999	0.999	0.988	0.977	0.999	0.998	0.999	0.999

behave better than post-peak values, because larger diaphragm deterioration is associated with larger displacements. Such deterioration introduces more variability in the diaphragm response, therefore affecting the force-displacement curve (envelope).

The next result to discuss is given by the F values from Tables B4-B7 in Appendix B. The estimated F values were compared with critical F values defined for a certain α level as discussed eariier. A much easier way of observing this parameter is by evaluating the actual probability of finding an F value greater than the estimated F value (Sig F, or Pvalue of F test) and comparing with any desired α value. Result of significance F values (Sig F) displayed a global mean value of 0.002 (<<5%), therefore, the hypothesis H_0 : "the slope coefficient does not contribute in the prediction of the independent variable" is rejected and the alternate hypothesis is accepted. In other words, data seems to be well predicted by the proposed model. Figure 20 shows the significant F values for the envelope data using the Log-x regression model.

The logarithmic-x regression model is an intrinsically linear model from a statistical point of view (see Section 3.2.1.4), and is defined by the intercept and slope coefficients. This model uses as abscissas the logarithm of the normalized displacements respect to

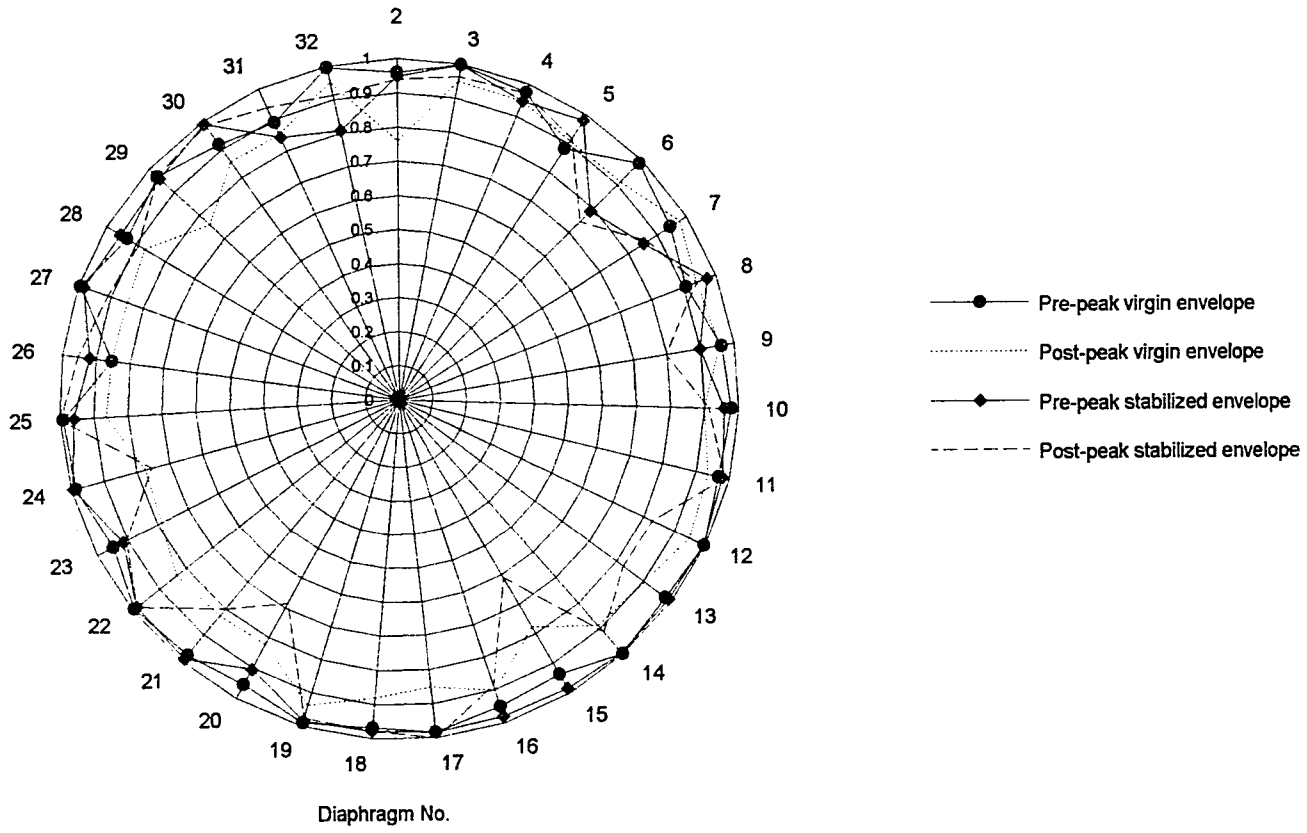

Figure 19. Coefficient of determination for log-x envelope regression model

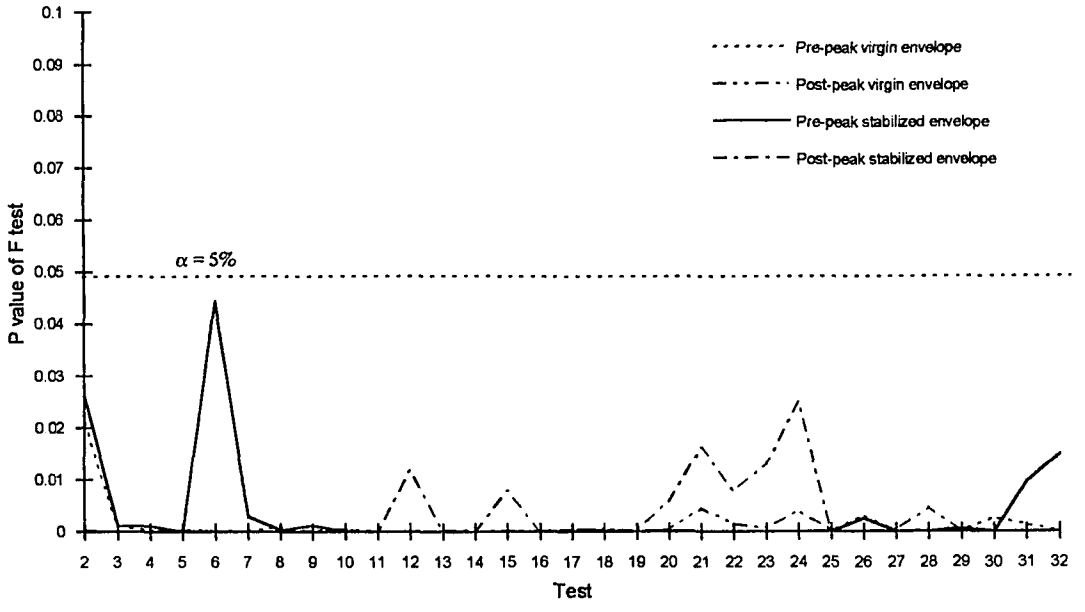

Figure 20. Significant F values (Pvalues for F test) for log-x regression envelope model

the peak displacement. Therefore at peak displacement the abscissa values is zero and the force normalized value is unity. As result, the regression model showed near to unity values of the intercept coefficient for all the diaphragms (see Tables B4 to B7).

Results of the slope coefficient are presented in two groups: First Pvalues associated with the slope are shown in Figure 21. Second, values of the mean and 95% confidence intervals are shown in Figures 22-25 (see Tables B4-B7). The hypothesis H_o associated with the slope coefficient analysis was stated as:"there is no significant difference between the slope coefficient and zero". P_{value} results shown in Tables B4-B7 and Figure 21, confirm that the slope coefficient was significantly different from zero (alternate hypothesis H_a accepted), consequently the proposed model seem to predict adequately the data (same conclusion than that previously obtained using the F values).

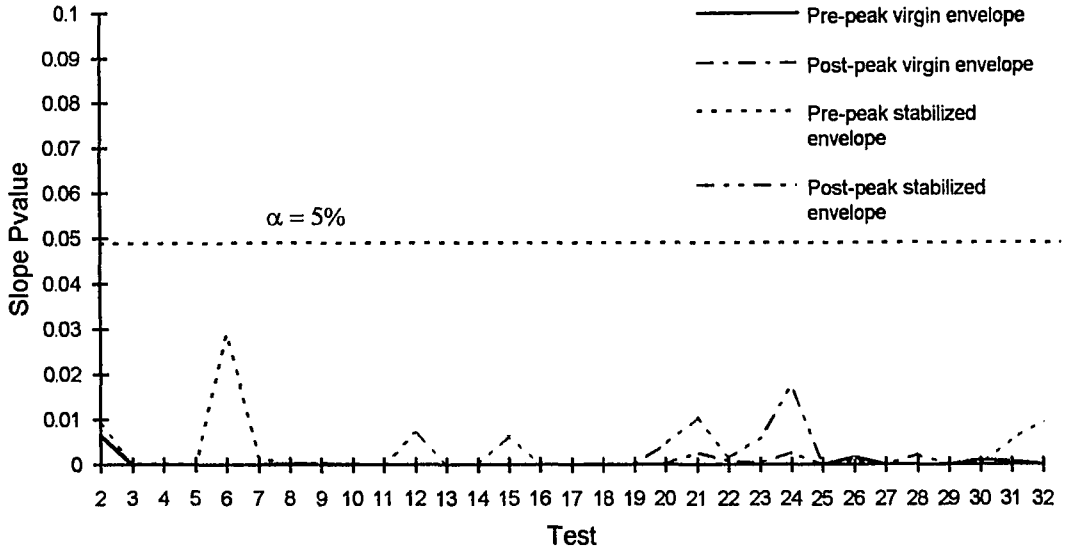

Figure 21. Observed significant slope P_{values}

Non-zero values for the slope coefficient, as well as 95% confidence intervals, were evaluated in the regression analysis. From Figures 22-25 and results from Tables B4-B7, a general tendency or pattern in the slope coefficient value can be established. Even that the confidence intervals were relatively small, the scatter of some groups of tests may be an indication that additional parameters are needed for a better explanation of the data. Before any additional work is described, a discussion on the source of variability in the data is presented.

Through the regression process, the population considered as source of data in each regression analysis has been assumed to be the collection of diaphragms with identical characteristics to the one analyzed. The main reason for considering such type of population in the analysis was due to the large range of parameters included in the experimental program. As example, consider the diaphragms with deck Type 1 (see

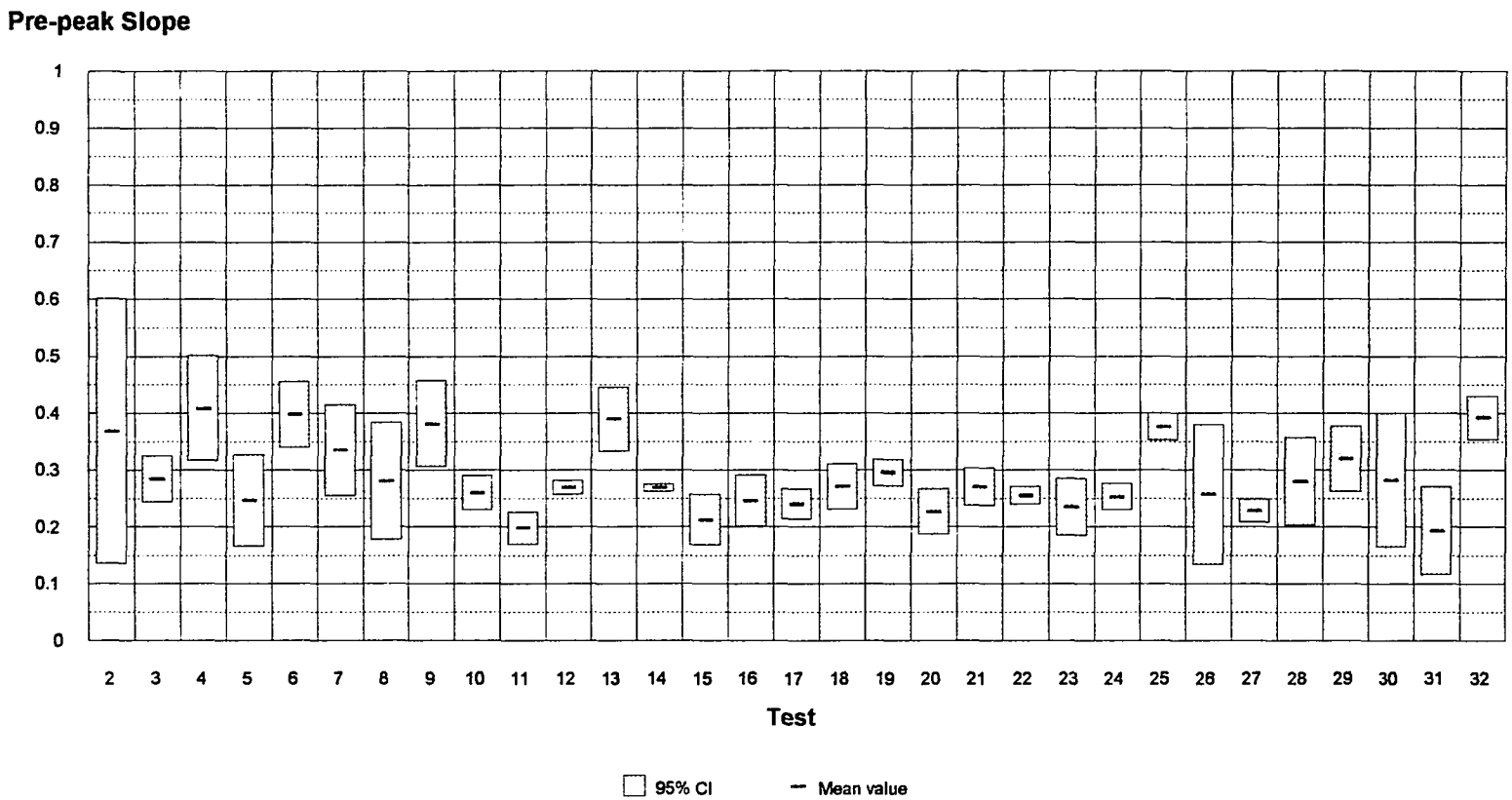

Figure 22. Pre-peak slope mean and 95% confidence interval values for virgin envelope data

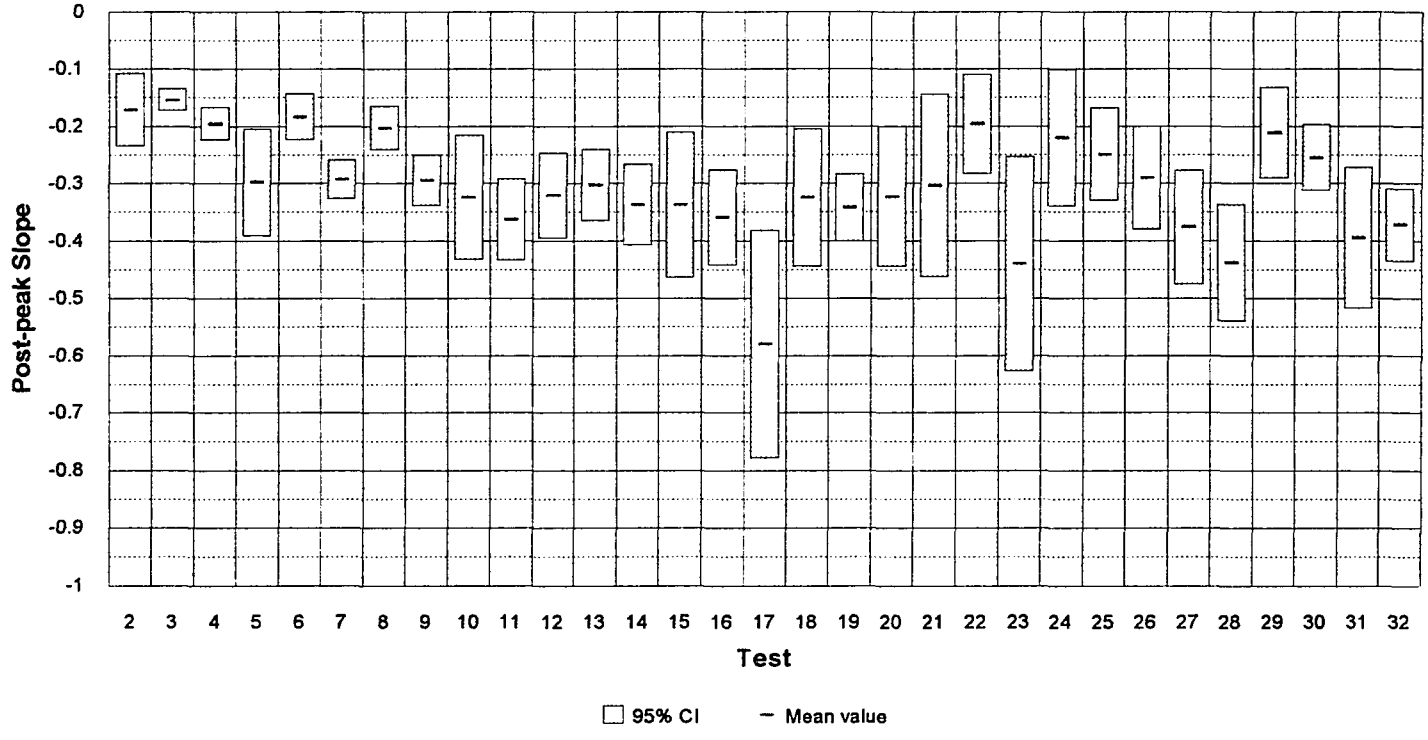

Figure 23. Post-peak slope mean and 95% confidence interval values for virgin envelope data

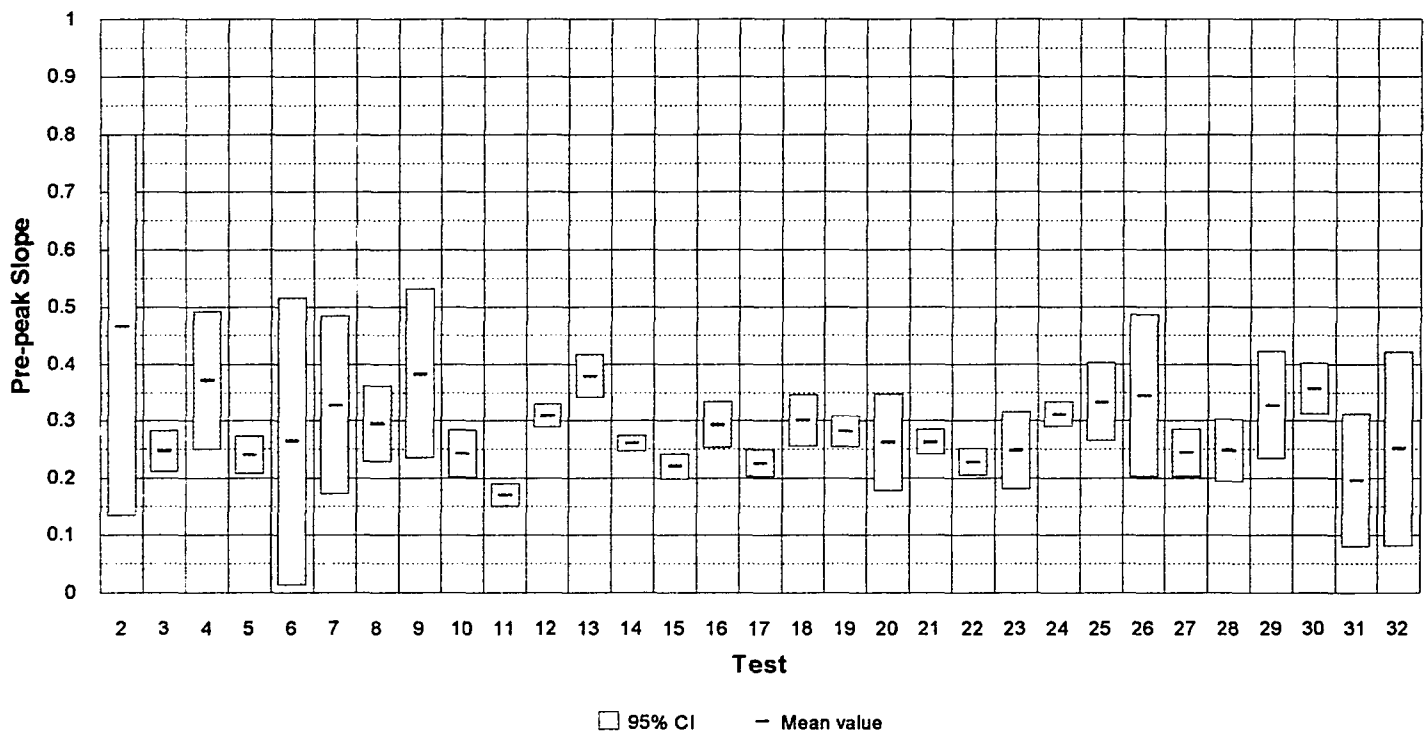

Figure 24. Pre-peak slope mean and 95% confidence intervals values for stabilized envelope data

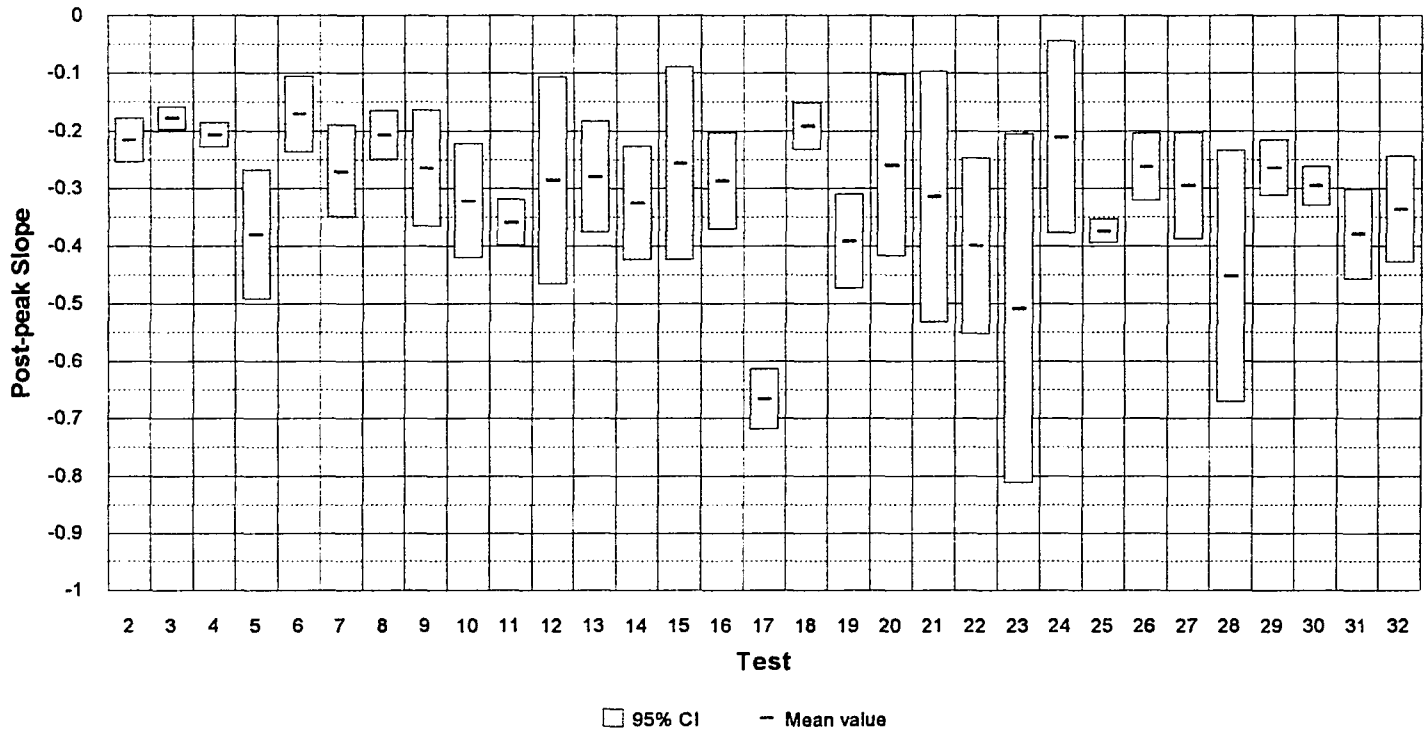

Figure 25. Post-peak slope mean and 95% confidence intervals values for stabilized envelope data

Appendix A, Table A1 and Figure A1). Deck Type 1 included diaphragm Tests 1,2,3,4, and 8. All of them had approximately the same concrete thickness, and the same steel deck thickness and yield strength. However, they are different in the concrete compressive strength or connection type. Tests 3 and 4 seem to be quite similar in compressive strength (4068/3849) and connection type, but Diaphragm 4 was tested with deck corrugations in East-West direction meanwhile Test 3 had North-South orientation. Similar mixed effects were included in the other deck type groups, leaving the experimental program with no one pair of tests with "identical" characteristics.

Results from the regression analysis showed some degree of scattering in the confidence intervals for the slope coefficients. Such scatter was assumed to be produced by effects not considered in the regression model. To improve the proposed model, additional terms were considered through the use of multiple regression analysis.

A source of additional terms to be included in the regression analysis, may be found by examination of the correlation matrix evaluated for the assumed important effects. The correlation matrix is a medium of presenting, in organized manner, the correlation between pairs of variables in a data set. This matrix is usually presented in triangular form because of its symmetry; also, the elements in the principal diagonal equal unity because the correlation between a variable and itself is unity. Each matrix coefficient is evaluated with Equation [3-17]. The correlation coefficient evaluated provides an index of the degree of linear association between pairs of variables.

To have an idea of a possible correlation between the slope coefficients and key experimental parameters, a matrix of correlation was evaluated. Only few parameters were considered in this preliminary analysis, including: initial experimental stiffness (K_i), deck thickness (Deck t), yield stress of steel deck (F_y), total concrete thickness (h), concrete thickness above the deck (top h), concrete compressive strength (f'_c), and

diaphragm side aspect ratio (L_1/L_2). Other factors were not included because there were too few samples (e.g., concrete light weight, deck corrugation orientation, supporting frame, etc.), or because they were variables with a qualitative nature (e.g., deck type, connection type).

Based in results shown in Table B8 in Appendix B, the following observations may be made:

- The four slope parameters showed the largest correlation associated with the concrete compressive strength (f'_c), with better correlation in the pre-peak envelope region.
- Concrete thickness above the deck seems to be the next largest correlation, especially for the post-peak envelope region.
- The independent-dependent variable correlations were low to moderate; the largest was 0.55 (S slope vs f'_c). Using the square of the correlation coefficient, the fraction of explained variation was 0.31. This low value suggest that more than one dependent variable may be necessary to estimate envelope force ratio accurately.

3.3.5.7 Multiple linear regression analysis

3.3.5.7.1 General Based on observations of the correlation matrix, a multiple regression analysis was considered as a viable option to increase the accuracy of the proposed regression model. The criterion applied for the analysis consisted of initially use as many variables or effects as possible, and later reduced them based on statistical criteria. Dimensionless parameters were used to reduce the number of different variables. A technique called stepwise regression was applied to identify which parameters had the

largest influence in the accuracy of the model. Qualitative effects such as deck type and connection type were considered by using dummy variables. A description of the variables included in the multiple regression analysis is presented in the next subsection.

3.3.5.7.2 Dependent variable The envelope force ratio Y, was considered as the dependent parameter Y. As stated previously in Equation [3-16], the force envelope ratio is given by:

$$Y = \frac{F}{F_p} \qquad [3\text{-}16]$$

Force ratio Y was identified according to the type of envelope (virgin or stabilized) and according to the position (pre-peak or post-peak region) as follows:

YV1: envelope pre-peak virgin force ratio

YV2: envelope post-peak virgin force ratio

YS1: envelope pre-peak stabilized force ratio

YS2: envelope post-peak stabilized force ratio

3.3.5.7.3 Independent variables A series of independent variables were identified and used in the multiple regression analysis. A brief description of each independent variable follows:

- Independent parameter, X. Based on previous regression analysis, the main independent parameter was found to be the values of the natural logarithm of the envelope displacement ratio (X) (see Equation [3-15]):

$$X = \ln(\frac{e}{e_p}) \qquad [3\text{-}15]$$

- Axial stiffness index, Q: This index included the effect of f'_c, the effect of the modular ratio, and the effect of the relative area between both materials through the use of equivalent thickness ratio.

$$Q = \frac{\frac{A_c E_c}{L}}{\frac{A_s E_s}{L}} = \frac{A_c}{A_s}\frac{E_c}{E_s} = \frac{t_{ec} E_c}{t_{es} E_s} \qquad [3\text{-}26]$$

$$E_c = w_c^{1.5} 33\sqrt{f'_c} \qquad [3\text{-}27]$$

where:

E_c: concrete modulus of elasticity, (psi)

E_s: steel modulus of elasticity (29E06 psi)

t_{ec}: effective concrete thickness, (in.)

t_{es}: effective steel thickness, (in.)

w_c: unit weight of concrete, (lb per cu ft)

- Side diaphragm aspect ratio, L1L2

$$L1L2 = \frac{L_1}{L_2} \qquad [3\text{-}28]$$

where:

L_1: Diaphragm length, (in.)

L_2: Diaphragm width, (in.)

- Deck shape type: This parameter was used to include the effect of the shape of the deck, not the deck type as described in Appendix A. Since deck Type 1, 3, and 4 had the same shape, they were assigned to the same shape type; the same happens between deck Type 6 and 11. Differences in thickness (one of the reasons to describe each shape as different deck type) were considered separately. To describe this effect, dummy variables were used as follows:

$$D1 = \begin{cases} 1 & \text{if deck type is 1,3, or 4} \\ 0 & \text{if none of the above} \end{cases}$$

$$D2 = \begin{cases} 1 & \text{if deck type is 2} \\ 0 & \text{if deck type is not 2} \end{cases}$$

$$D3 = \begin{cases} 1 & \text{if deck type is 5} \\ 0 & \text{if deck type is not 5} \end{cases}$$

$$D4 = \begin{cases} 1 & \text{if deck type is 6 or 11} \\ 0 & \text{if deck type is neither 6 or 11} \end{cases} \qquad [3\text{-}29]$$

$$D5 = \begin{cases} 1 & \text{if deck type is 7} \\ 0 & \text{if deck type is not 7} \end{cases}$$

$$D6 = \begin{cases} 1 & \text{if deck type is 8} \\ 0 & \text{if deck type is not 8} \end{cases}$$

$$D7 = \begin{cases} 1 & \text{if deck type is 9} \\ 0 & \text{if deck type is not 9} \end{cases}$$

$$D8 = \begin{cases} 1 & \text{if deck type is 10} \\ 0 & \text{if deck type is not 10} \end{cases}$$

The last expression associated with Deck 10, was used only when interaction terms were considered in the regression model. For regression analyses without interaction terms, condition for deck 10 was given when all previous deck shape parameters were zero.

- Gravity load effect, GL: Diaphragms 12-14 and 16-18 were tested including gravity load, using these dummy variables helped to test for significant difference between tests with and without gravity load.

$$GL = \begin{cases} 1 & \text{for Tests } 12,13,14,16,17,18 \\ 0 & \text{for any other tests} \end{cases} \qquad [3\text{-}30]$$

- Connection type, CT: Several types of connections were used (Appendix A, Table A1); but only connections with 60 welds per side were used repetitively. Therefore, for this analysis connection type were defined for those frequent cases.

$$CT = \begin{cases} 1 & \text{for diaphragms with 60 welds / side} \\ 0 & \text{for diaphragms without 60 welds / side} \end{cases} \qquad [3\text{-}31]$$

3.3.5.7.4 Stepwise regression analysis To identify the most important parameters to include in the final regression model, a technique called stepwise regression analysis was used. This method is a type of multiple regression analysis because it also calibrates a prediction equation. Additionally, the stepwise method uses statistical criteria to select which of the predictor variables (independent variables) may be included in the resulting regression model. The stepwise regression technique includes different

algorithms for selection of variables. There are basically two main algorithms to be used: backward and forward regression algorithms.

Forward regression algorithm starts using the predictor variable (independent variable) with the highest correlation associated with the criterion variable (dependent variable) and continues adding variables so that the explained variance is maximized at each step. A test of hypothesis is applied at each step to verify the inclusion of a variable in the model. Computation ends when all the statistically significant variables have been included. Backward regression algorithm begins with a model that included all the predictor variables. Variables with the least contribution to the explained variance are deleted first. Tests of hypothesis for significance of variables are applied at each step. More refined algorithms such as the forward stepwise regression with deletion, and the backward regression with addition, includes at each step in the analysis an additional check of the model to verify if all included variables are still statistically significant (91,92,94).

The multivariate linear model structure is given by:

$$y = b_0 + b_1 x_1 + b_2 x_2 + \ldots\ldots + b_q x_q \qquad [3\text{-}32]$$

where:

y dependent or criterion variable

x_i $(i = 1,2,\ldots,q)$ predictor variables

b_i $(i = 1,2,\ldots,q)$ regression coefficients

q number of predictor variables.

In applying the stepwise regression technique, two tests of hypothesis were used, the total F test, and the partial F test. The total F test was used to determine whether or not the independent variables were significantly related to the dependent variable,

therefore, it examined if the model was or was not a good predictor of the data. The null and alternative hypotheses were:

H_o: $\beta_1 = \beta_2 = ... = \beta_q = 0$

H_a: at least one regression coefficient is significantly different from zero.

where:

q number of predictor variables included in the equation

β_i (i=1,2...,q) population regression coefficients

The null hypothesis was tested using the following test statistics F:

$$F = \frac{\frac{R_q^2}{q}}{\frac{(1-R_q^2)}{(n-q-1)}} \qquad [3\text{-}33]$$

where:

R_q: multiple correlation coefficient for the equation containing q independent variables

n: number of observations

the null hypothesis was accepted if F was less or equal to the critical F value F_α, which was defined for the selected α level and the degrees of freedom (q, n-q-1).

The partial F test was used to test the significance of a specific predictor (independent) variable in the model. The null and alternative hypotheses were:

H_o: $\beta_k = 0$

H_a: $\beta_k \neq 0$

where β_k is the regression coefficient for the variable under consideration. The hypothesis was tested using the following test statistic:

$$F = \frac{\text{fraction increase in explained variation due to subject variable} / \upsilon_1}{\text{fraction of unexplained variation of the model equation} / \upsilon_2} \qquad [3\text{-}34]$$

where υ_1 and υ_2 are the degrees of freedom associated with the quantities in the numerator and denominator, respectively. Equation [3-34] may be evaluated as follows:

$$F = \frac{\left(R_i^2 - R_j^2\right)/1}{\left(1 - R_i^2\right)/(n-q-1)} \qquad [3\text{-}35]$$

where:

R_i , R_j are the correlation coefficients for models with i and j variables.

The null hypothesis was accepted when the test statistic F was less or equal to the critical F value, F_α.

The general procedure used by the forward method consisted of:

- Partial F Test. Compute the partial F values for all predictor variables that are not included in the model equation. The variable with the largest partial F values is selected to enter in the equation according to:

  a) for $F < F_\alpha$, the variable is not significant and the equation from the previous iteration is the final model.

  b) for $F > F_\alpha$, the variable is statistically significant, and it should be included in the equation (continue in Step 2).

- Total F test.

For this study, the forward stepwise regression with deletion was used. The statistical package STATISTICA (93) was used in this procedure. The model selected (see Equation [3-32]), had the following characteristics:

1. Variables were identified as numerical or quantitative variables, and dummy or qualitative variables. The use of dummy variables allowed to include qualitative effects (e.g., steel deck shape).

2. The model used was a half step between a first and second order model, since interaction effects are included. Second order models include all the first order terms (first order main effects), interaction terms, and second order main effects (quadratic terms). Examples of first and second order models are:

   First order model

   $$y(x) = \beta_0 + \beta_1 x_1 + \beta_2 x_2 \qquad [3\text{-}36]$$

   Second order model

   $$y(x) = \beta_0 + \beta_1 x_1 + \beta_2 x_2 + \beta_3 x_1 x_2 + \beta_4 x_1^2 + \beta_5 x_2^2 \qquad [3\text{-}37]$$

   The proposed model used all the first order terms and used some of the interaction terms corresponding to the second order model (e.g., $\beta_3 x_1 x_2$). The idea of using interaction terms came from the solution obtained for the first order regression model in Section 3.3.5.6. For the first order regression model was found intercept regression coefficients close to unity, and slope regression coefficient varying due to effects not included in the regression. The interaction terms affect directly the slope coefficient, meanwhile the first order main effects ($\beta_1 x_1$, $\beta_2 x_2$) affect the intercept coefficient.

The model used for the forward stepwise method used interaction terms related to the independent variable x, since the main reason for this analysis was the variability of the slope in the previous regression model and the slope was affected by this interaction effect. Initially, the proposed model was:

$$\begin{aligned} y = {} & b_0 + b_1 x + b_2 Q + b_3 L_1 L_2 + b_4 CT + b_5 GL + b_6 D_1 + b_7 D_2 + b_8 D_3 + b_9 D_4 + b_{10} D_5 \\ & + b_{11} D_6 + b_{12} D_7 + b_{13} Qx + b_{14} L_1 L_2 x + b_{15} CTx + b_{16} GLx + b_{17} D_1 x + b_{18} D_2 x + \\ & b_{19} D_3 x + b_{20} D_4 x + b_{21} D_5 x + b_{22} D_6 x + b_{23} D_7 x + \varepsilon \end{aligned} \qquad [3\text{-}38]$$

where:

b_i i=0,23 regression coefficients

for definition of each variable see Section 3.3.5.7.3

The regression analysis used four different groups of data specified by the envelope type (virgin or stabilized) and envelope region (pre- or post-peak region). Additionally, each group was formed with all the force-displacement ratios for the positive and negative envelopes for all tests (except Test 1). Therefore, the minimum number of force-displacement ratios used were approximately 240 pairs. As a first step in the analysis of results, the correlation coefficients between the dependent variable (force ratio) and all the other parameters were inspected. Table B9 in Appendix B, shows the correlation coefficients.

The interaction terms showed higher correlation coefficients (except for the x parameter), indicating that the variability of the data was explained better through these terms. This result was expected since the bivariate linear regression model previously obtained showed variability in the slope coefficient. The first analysis using stepwise regression also corroborated this result, since only interaction terms were selected as significantly different from zero to improve the explained variation.

After the first analysis using stepwise regression method, the model included the intercept coefficient and interaction terms associated with x (x=ln(e/ep)), but some of the regression coefficients were irrational. This effect was thought to be the result of the biased distribution of key experimental parameters, which may produce some problems in parameter estimation. For example, most of the stud connections were used in diaphragms with aspect ratio of 0.8 (L1/L2) and with deck Types 5, 9, 10, or 11. When many of the data points are not distributed but concentrated around a single x value any outlayer data point may introduce considerable amount of error in the parameter estimation. Also multicollinearity (two or more of the independent variables contribute redundant information) may be induced by this biased distribution. Therefore, the process

was continued but only those parameters with significant values (at 5% level) and with rational coefficients were considered, as suggested by some authors (91,94). Table B10 shows the parameters included in the second analysis.

General results from the stepwise regression are presented in Table 8, and more specific details are shown in Table B10 in Appendix B. From Table 8, the correlation coefficient for each envelope section ranged between 0.89 and 0.96 with a weighted average value (No. of cases being weight factors) of 0.93. Such range of values may be considered acceptable since a value of unity corresponds to perfect correlation. The coefficient of determination or proportion of explained variation ranged from 0.79 to 0.92 with a weighted average of 0.86. A better behavior was observed for the pre-peak regions in both virgin and stabilized envelopes. The same conclusion may be obtained from the resulting standard error of estimate S_e. Pvalues for the overall or total F test were too small (less than 2%); therefore, the null hypothesis stated as: "the regression model does not contribute to explain the normalized force", was rejected. Finally, intercept values ranged between 0.97 and 0.99, with close to unity values associated with the pre-peak envelopes. Main characteristics from these results are presented next:

- All the model parameters included in the second regression analysis had coefficients significantly different from zero (at 5% level) since all Pvalues showed values below 2%.
- The "x" parameter (natural logarithmic of the displacement ratio) was included in all four analyses as an interaction term in combination with all other parameters. This result was expected since interaction factors (associated with x) directly modify the slope of the x parameter.
- Axial stiffness index Q, was introduced in the post-peak region of both virgin and stabilized data envelopes. In both cases, the regression coefficient associated

Table 8. General results from the stepwise regression analysis

Region	Virgin Envelope		Stabilized Envelope	
parameter	Pre-peak	Post Peak	Pre-peak	Post-peak
# of Cases	260	354	236	265
R	0.95	0.92	0.96	0.89
R^2	0.90	0.84	0.92	0.79
S_e of Estimate	0.08	0.12	0.07	0.15
F	252.2	178.0	275.0	96.3
Pvalue	---[a]	---[a]	---[a]	---[a]
Intercept	0.99	0.99	0.99	0.97

[a]less than 0.02

with Q was positive, which means that as long as Q increases, the response (force) of the system increases.

- Gravity load was another effect included by the stepwise procedure. The effect of gravity appears for both regions (pre- and post-peak) and envelopes (virgin and stabilized). For the pre-peak region, their regression coefficient sign was negative (since x=ln(e/ep) was negative in this region) which means that gravity produced an increase in the force ratio diaphragm response. This phenomenon was thought to be the result of the increase in the friction between the steel deck and concrete, delaying the deterioration of the diaphragm. This effect was reduced with increased number of cycles (when moving from virgin to stabilized regions) since slip occurred in the interface. In the post-peak region, the effect of increased friction is minimum since, for this level of displacements, large slip

and deterioration had usually occurred and reduced force ratios response due to the nature of the out-of-plane gravity load was significant.

- Steel deck shapes were the other parameters introduced in the model by the regression process. The deck shape were the main source of explained variability, because their regression coefficient magnitudes were much larger than any other coefficient effects as shown in Table B10 in Appendix B. Results of regression coefficients between virgin and stabilized shape parameters for a given region (pre- or post-peak) were consistently similar, with only slight differences (Table B10).

3.3.5.8 Final envelope regression analysis Based on these observations, a final analysis to refine the regression model was made. The analysis included the following characteristics:

1) From the previous bilinear regression model and because of the nature of the input data ratios, a model with an intercept coefficient of value unity was needed. Since the multiple regression analysis allows the intercept to be defined as zero or different from zero only, a nonlinear regression analysis was used. This analysis was made using STATISTICA (93). The least squares criterion (minimization of the sum of the squares of deviations) was used as the objective function. As an initial estimate for the coefficients, those coefficients obtained from the multiple linear regression were used.
2) The intercept term was selected to be unity. Therefore, only interaction terms (associated with "x") were considered (and therefore the term D_8x was also included).
3) Gravity load effect was included.

4) Axial stiffness index Q was included for the post-peak regions.

5) An additional analysis was considered assuming an "average deck shape". Such analysis was made without differentiating between steel deck shapes, therefore results were assumed to be valid for any deck shape. Since the variation between shapes were considerable, results obtained for such average deck shape was less accurate. Nevertheless, the average deck shape approach may be used as a simple estimate when a deck shape not included especifically in the experimental program is used.

The new regression models were defined by:

For pre-peak regions

$$y = 1 + (a_1 GL + a_2 D_1 + a_3 D_2 + a_4 D_3 + a_5 D_4 + a_6 D_5 + a_7 D_6 + a_8 D_7 + a_9 D_8)x + \varepsilon \qquad [3\text{-}39]$$

For post-peak regions

$$y = 1 + (b_1 GL + b_2 Q + b_3 D_1 + b_4 D_2 + b_5 D_3 + b_6 D_4 + b_7 D_5 + b_8 D_6 + b_9 D_7 + b_{10} D_8)x + \varepsilon \qquad [3\text{-}40]$$

where:

$a_i \quad i = 1,2,..,9$: regression coefficients associated with the pre-peak region

$b_i \quad i = 1,2,..,10$: regression coefficients associated with the post-peak region

x: main effect, evaluated as the natural log of the normalized displacement ratio

GL: dummy variable describing the effect of gravity loads

Q: axial stiffness index

D_i: dummy variable describing the effect of deck shape

General results from the nonlinear regression analyses are presented in Table 9. More specific details from these results are presented in Table B11 in Appendix B.

Table 9. Correlation and determination coefficients from the nonlinear regression

Envelope	Virgin Envelope		Stabilized Envelope	
Parameter	Pre-peak	Post-peak	Pre-peak	Post-peak
S.S. Residuals	1.69	5.12	1.11	5.80
R	0.95	0.92	0.96	0.89
R^2	0.90	0.84	0.92	0.79

Results from the nonlinear regression were practically the same as those obtained from the multiple linear regression analyses (compare Tables 8 and 9), because for the multiple linear regression, the intercept coefficient was close to 1, meanwhile for the nonlinear regression it was assumed 1. After reordering terms in the proposed model of Equations [3-39] and [3-40], and using results presented in Table B11 from Appendix B, the proposed model in its final form was:

for Pre-peak envelope region

$$\frac{F(e)}{F_p} = \left[1 + \alpha \ln\left(\frac{e}{e_p}\right)\right]\xi \qquad [3\text{-}41]$$

for post-peak envelope region

$$\frac{F(e)}{F_p} = \left[1 + \beta \ln\left(\frac{e}{e_p}\right)\right]\xi \qquad [3\text{-}42]$$

where:

ξ: Strength degradation factor, applicable to virgin envelope only (see Section 3.3.5)

$$\alpha = \alpha_{GL} + \alpha_{DS} \qquad [3\text{-}43]$$

$$\beta = \beta_Q + \beta_{GL} + \beta_{DS} \qquad [3\text{-}44]$$

Table 10. Axial stiffness factor β_Q

Factor	Virgin Envelope	Stabilized Envelope
β_Q	$0.018Q^a$	$0.022Q^a$

[a]Q evaluated according to Equation [3-26]

Table 11. Gravity load factor α_{GL}, β_{GL}

Factor	Load Condition	Virgin Envelope	Stabilized Envelope
α_{GL}	Full gravity load[a]	-0.018	0.039
β_{GL}	Full gravity load[a]	-0.095	-0.046
α_{GL},β_{GL}	no gravity load	0.000	0.000

[a]Design gravity load

β_Q: axial stiffness factor (see Table 10).

α_{GL},β_{GL}: gravity load factors (see Table 11).

α_{DS},β_{DS}: deck shape factors (see Table 12).

Figure 26 shows a comparison between predicted and observed envelopes for Test # 4.

3.3.6 Envelope strength degradation

3.3.6.1 Degradation general information Structures under earthquake motion usually sustain many load reversals. Steel and concrete structures deform continuously with increased cycles of loading. Eventhough steel is ductile, steel members in frames may not be so ductile due to effects such as buckling or brittle failure of connections. Concrete structures generally show considerable degradation when subjected to load reversals.This effect is more marked when shear or bond failure takes place in the elements (3).

Table 12. Deck shape factors α_{DS}, β_{DS}

		α_{DS}		β_{DS}	
Shape Type	Deck Type	Virgin	Stabilized	Virgin	Stabilized
1	1	0.35	0.35	-0.38	-0.44
2	2	0.29	0.21	-0.39	-0.39
1	3	0.35	0.35	-0.38	-0.44
1	4	0.35	0.35	-0.38	-0.44
3	5	0.29	0.24	-0.40	-0.47
4	6	0.23	0.21	-0.52	-0.55
5	7	0.26	0.24	-0.43	-0.44
6	8	0.26	0.28	-0.42	-0.43
7	9	0.24	0.25	-0.59	-0.56
8	10	0.27	0.33	-0.44	-0.49
4	11	0.23	0.21	-0.52	-0.55
General Deck type		0.28	0.25	-0.42	-0.46

Usually the degradation effect is neglected in design practice, because is assumed to be small, or simply because the lack of knowledge to evaluate it. However, if degradation is inevitable, at least a gross estimation of such effect should be made.

Degradation effects are generally classified as strength degradation and stiffness degradation. Both effects may be associated with cyclic effects and/or monothonic effects. Cyclic strength degradation may be defined as the reduction in force capacity for an

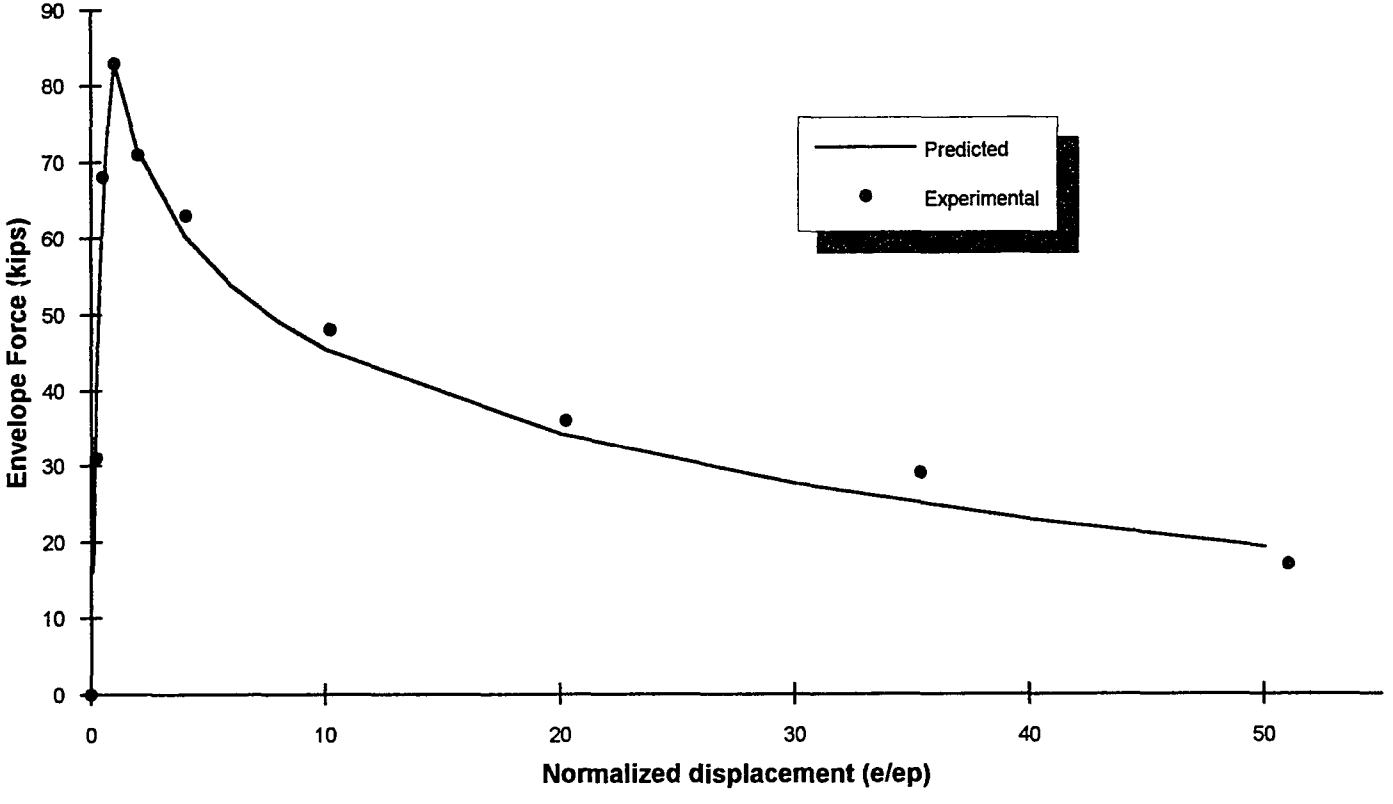

Figure 26. Diaphragm test 4 virgin envelope prediction

increased number of cycles at the same maximum displacement. Meanwhile basic strength degradation is the reduction in strength capacity (after peak load) for increased maximum displacement. Similar definitions may be stated for stiffness degradation (see discussion of stiffness degradation in Section 3.3.6.2.3). Figure 27 shows an example of cyclic strength degradation.

The state-of-the-art in hysteretic modelling of concrete structures suggests the evaluation of the cyclic strength degradation by either using a constant or a variable strength degradation factor. A very rough estimation of the strength degradation is obtained with the constant factor approach. This factor is applied to the actual force each time that a new cycle is made at the "same" maximum displacement (16,41). The second approach consists of using a variable strength degradation factor, usually a function of the number of cycles and other characteristic envelope parameters such as cyclic energy or maximum attained displacement (27,42,45,47). As part of this work, a discussion of the cyclic strength degradation effects on steel-deck-reinforced concrete diaphragms is made, and equations to evaluate such effects are presented in the next subsections.

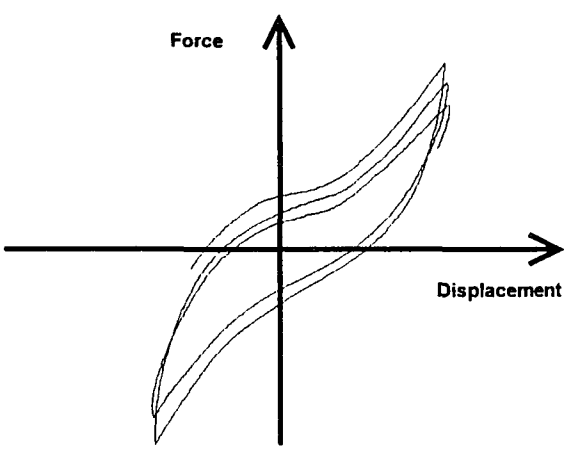

Figure 27. Cyclic strength degradation example

3.3.6.2 Input data As part of the experimental program on SDRC at ISU (see Appendix A), 32 diaphragms were tested. Reversed cyclic loading with displacement control was used for all test specimens, except for Test 1 that was monothonically loaded. A minimum of three complete cycles was applied at each level of displacement. The criterion used to increase displacement to the next level was that the load had to stabilize within a certain margin. Such margin was defined as being less than a 5% change in load from the previous cycle at the same displacement.

3.3.6.3 Basic patterns A database was created with the information required to evaluate the cyclic strength degradation as follows: for each diaphragm test, and for each displacement level, force vs cyclic number pairs of data were filed. To identify general trends in the data, a plot of average normalized force vs normalized displacement for each cycle number was made (see Figure 28). Force was normalized respect to the force associated with the maximum displacement for the virgin envelope (cycle n=1), and displacement was normalized respect to the displacement at the peak virgin load. Table B12 in Appendix B shows the average degradation factor and 95% confidence intervals for such factor. Results from Figure 28 and Table B12 showed the following trends:

- The strength degradation factor is a nonlinear function of the number of cycles, because the amount of reduction from first to second cycle was much greater than that from the second to third cycle.
- The degradation factor is also a function of the maximum reached displacement with a more pronounced slope for small displacements, and a stabilization zone or plateau for large displacements.
- For displacement ratios smaller than approximately one, the degradation factor was approximately constant for a given cycle number.

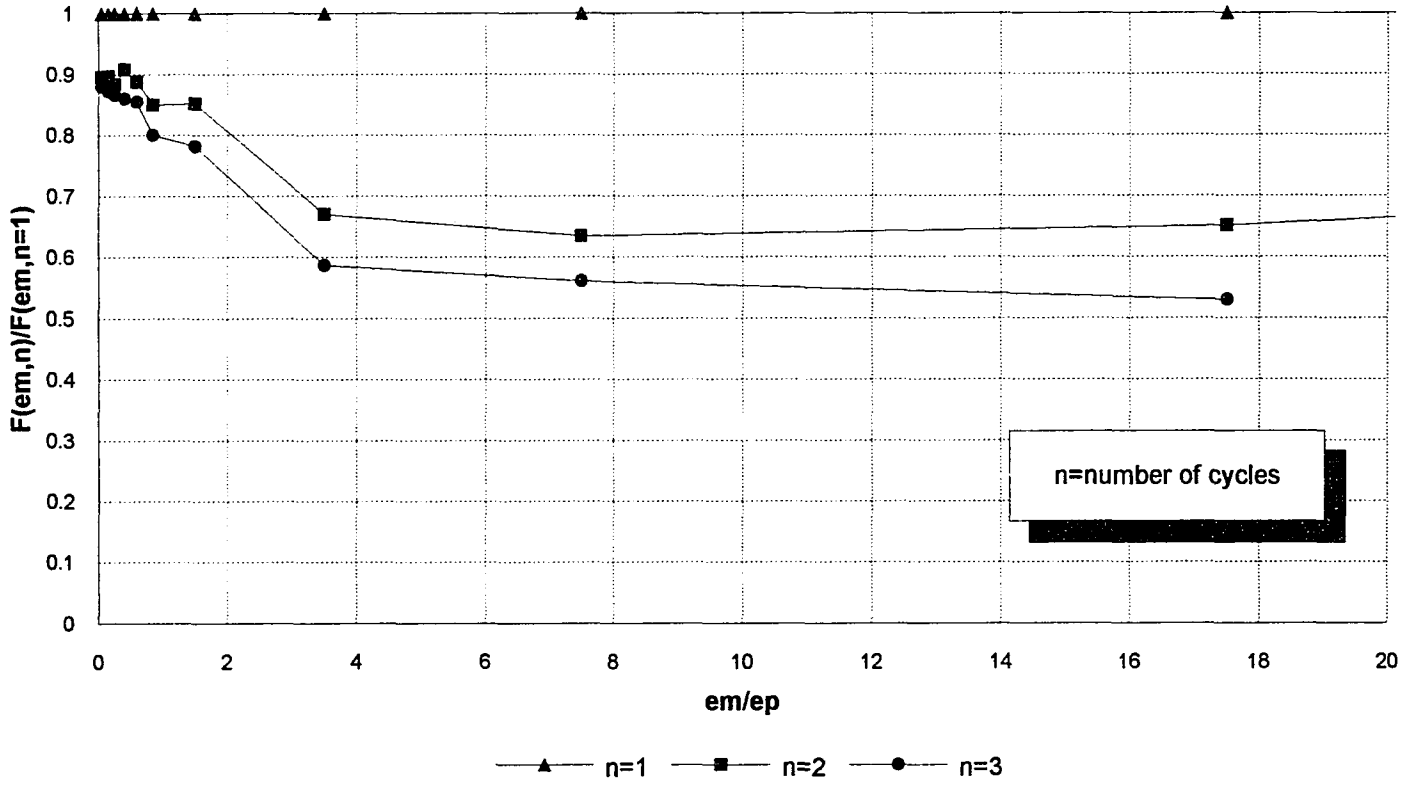

Figure 28. Normalized envelope force for a different number of cycles

3.3.6.4 Initial regression analysis

3.3.6.4.1 General The strength degradation factor was observed to be a function of the number of cycles, and the largest associated displacement. Other possible variables influencing this factor will be discussed in the next subsections. As a first step in predicting this effect, a regression analysis was made to investigate the type of model that better predicted the effect on the degradation due to the number of cycles and largest cyclic displacement. First, an analysis was made considering each of the two mentioned factors at the time (see Sections 3.3.6.4.2 and 3.3.6.4.3.). With the information obtained from this preeliminary analysis, a more generalized model was developed involving both effects (see Section 3.3.6.5).

3.3.6.4.2 Model considering number of cycles Under this model, the degradation factor was considered as a function only of the number of cycles. Any effect due to maximum reached displacement, type of steel deck, type of connection, etc., was neglected. Since the degradation factor was influenced by the largest attained displacement, the first objective was to investigate if the same type of regression model may predict the strength degradation as a function of the number of cycles at particular displacement levels. To study this condition, the data needed for the analysis was grouped for each diaphragm test according to three regions: Pre-peak region, peak point, and post-peak region. From each region an arbitrarily selected set of force versus cycle number pair of data was assumed to represent all pairs in the region (see Figure 29). The data selected for each region was taken from Diaphragms 2 to 32.

Each set of data was fitted to eleven different regression models (see Table 3). Therefore, for each diaphragm test (31 tests were considered), for each region (3 regions,

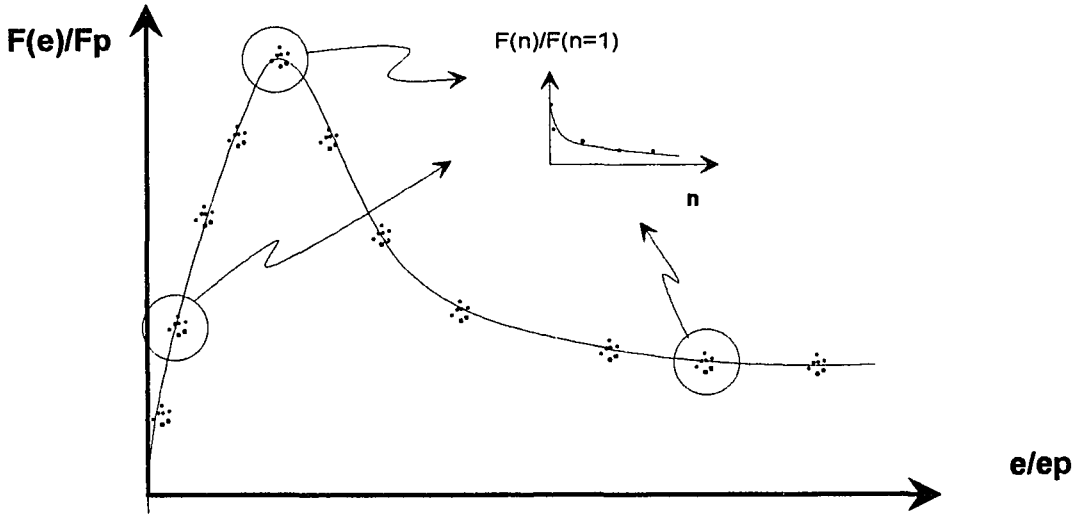

Figure 29. Degradation factor vs number of cycles at different regions

as previously described), eleven regression models were applied, giving a total of 31x3x11= 1023 fitted equations. Selection of the "best" regression model, as described earlier, was based on the mean absolute error (MAE) associated with each model. Graphical results of the analyses are shown in Figures B13-B15 in Appendix B. Numerical results are shown in Table 13, and discussed next.

According to results obtained from the regression analyses of strength degradation factor vs cycle number n, the following conclusions may be stated:

- Model 4 (reciprocal - x) had the lowest average MAE value for pre- and post-peak regions. For the peak region, Model 4 obtained the third lowest MAE value with a 6.5% difference respect to the smallest one. Model 7 (logarithmic - x), was ranked third, first, and third for the three mentioned regions, respectively.
- For pre-peak and peak regions, any of the tested regression models (Table 3) except model 6, may be used to predict the degradation effect. According to

Table 13. MAE mean values and 95% CI for regression models of degradation factor vs n

Region	Pre-peak			At peak			Post- peak		
Model	95% Confidence Interval		Mean	95% Confidence Interval		Mean	95% Confidence Interval		Mean
1	0.027	0.041	0.034	0.031	0.046	0.039	0.062	0.090	0.076
2	0.027	0.041	0.034	0.031	0.046	0.039	0.057	0.084	0.071
3	0.027	0.041	0.034	0.025	0.041	0.033	0.028	0.065	0.046
4	0.022	0.035	0.028	0.025	0.040	0.033	0.021	0.048	0.035
5	0.022	0.036	0.029	0.032	0.048	0.040	0.041	0.069	0.055
6	0.069	0.094	0.082	0.108	0.148	0.128	0.243	0.306	0.274
7	0.024	0.037	0.030	0.023	0.038	0.031	0.024	0.053	0.038
8	0.023	0.037	0.030	0.024	0.039	0.032	0.023	0.052	0.038
9	0.025	0.039	0.032	0.030	0.044	0.037	0.054	0.079	0.067
10	0.027	0.041	0.034	0.031	0.046	0.039	0.059	0.086	0.073
11	0.022	0.035	0.029	0.026	0.042	0.034	0.022	0.050	0.036

results (Figures B13-B15) there was no significant difference (5% level α) in MAE values between the models.

- For the post-peak region, any of 3, 4, 7, 8, and 11 regression models may be used, since there was no significant difference (5% level α) in MAE values between the regression models.

Pre-peak and peak regions had among their possible models the linear model. Although the linear model was included in the selection of possible models, the criteria used during testing to end a group of cycles at a prescribed displacement level clearly

suggested a non-linear pattern. Since not all the same models were selected for each region, a restriction was added to the analysis, that is, the degradation factor had to be described by the same type of regression model at any displacement level (any region). Some authors (27,45) had proposed a decaying exponential model to reproduce the strength degradation effect. However, according to results from Figure B15, for the post-peak region, there was a significant difference (at 5% level) in MAE values between the exponential model (regression Model 2) and any of Models 4, 7, 8 and 11. The selection was made for Model 7 or logarithmic-x model, because its intercept value was already defined (degradation factor has to be one at x=n=1 cycle), and, because from a statistical point of view, it is a linear model.

3.3.6.4.3 Model considering the maximum reached displacement

Under this approach, the variation pattern of the degradation factor with the maximum reached displacement was investigated. The data included in this analysis was considered to be all sets of data at a fixed number of cycles. The second and third cycles were selected because the data associated with the first cycle gave no useful information since the force ratio was unity for all the considered displacements. Since there was a tendency in the degradation factor to be approximately constant for small values of the normalized displacement, two regions were defined for analysis (pre- and post-peak regions). Therefore, for each diaphragm test (31 tests considered), and at each specified displacement level (e/ep), the corresponding force for the second and third cycle was selected. For each set of data (2 different n cycle levels), for each region (pre- and post-peak), for each diaphragm test (31 tests considered), 11 different regression models were fitted (see Table 3), for a total of 2x2x31x11=1364 regression models. The MAE (mean

absolute error) was the statistical estimate used to select the "best" regression model. Results are presented in Table 14, as well as in Figures B16-B19.

Results obtained showed that most of the proposed regression models may be used to predict the degradation effect vs e/ep because there was no significant difference among most of them ($\alpha = 0.05$). However, the linear model (Model 1) displayed the lowest average MAE value for all the analysis stages. Based on this result, the linear model was selected to introduce the parameter e/ep in the global model for the strength degradation factor.

3.3.6.5 Multiple linear regression analysis Previous subsections identified the possible model to use for the strength degradation factor vs cycle number and maximum reached displacement. According to Section 3.3.5.3.1, the strength degradation factor vs cycle number (for fixed values of e/ep) may be represented with a logarithmic-x model. Section 3.3.5.3.2 stated that for the variation of strength degradation factor vs maximum reached displacement (for fixed n values) a linear model may be used. The number of cycles and maximum displacements had been considered the significant factors in the strength degradation process according to some authors (27,45). However, others factors such as type of connections, gravity load, etc., may be of substantial influence. To identify other significant variables in the degradation process, a stepwise regression analysis (see Section 3.3.4.4) was made. Initially most of variables included in the experimental program were considered. The parameters consisting of light weight concrete, steel frame size members, and corrugation deck orientation were not included since there was only one test for each parameter. Only interaction terms associated with the number of cycles n were considered. Main (independent) terms associated only with maximum displacements were not included, because, by definition the cyclic strength

Table 14. Mean value and 95% CI for degradation factor vs e/ep regression models

	Pre-peak			Post-peak			Pre-peak			Post-peak		
	95% CI n=2			95% CI n=2			95% CI n=3			95% CI n=3		
Test	Lower	Upper	Mean	Lower	Upper	Mean	Lower	Upper	Mean	Lower	Upper	Mean
1	0.034	0.051	0.042	0.054	0.079	0.066	0.044	0.061	0.053	0.053	0.077	0.065
2	0.034	0.051	0.042	0.055	0.081	0.068	0.045	0.064	0.054	0.055	0.079	0.067
3	0.034	0.052	0.043	0.056	0.085	0.070	0.046	0.070	0.058	0.057	0.085	0.071
4	0.036	0.054	0.045	0.069	0.095	0.082	0.059	0.089	0.074	0.059	0.087	0.073
5	0.037	0.057	0.047	0.077	0.110	0.094	0.064	0.116	0.090	0.064	0.109	0.087
6	0.059	0.088	0.074	0.108	0.145	0.126	0.096	0.138	0.117	0.128	0.173	0.151
7	0.034	0.052	0.043	0.060	0.085	0.072	0.051	0.073	0.062	0.056	0.080	0.068
8	0.035	0.053	0.044	0.062	0.089	0.075	0.053	0.080	0.067	0.058	0.085	0.071
9	0.033	0.051	0.042	0.055	0.080	0.068	0.046	0.065	0.056	0.054	0.078	0.066
10	0.034	0.051	0.042	0.054	0.080	0.067	0.044	0.062	0.053	0.054	0.078	0.066
11	0.036	0.055	0.046	0.072	0.100	0.086	0.061	0.096	0.079	0.061	0.093	0.077

degradation effect was result of the cyclic displacement and not of the displacement alone. Accordingly, a maximum displacement variable had to show only as an interaction term. Additionally, not only quantitative variables but dummy variables were included to consider qualitative effects such as steel deck shape. A first intent for a model was proposed as follows:

$$\xi = b_0 + (b_1\bar{e} + b_2Q + b_3LL + b_4CT + b_5GL + b_6D_1 + b_7D_2 + b_8D_3 + b_9D_4 + b_{10}D_5 + b_{11}D_6 + b_{12}D_7 + b_{13}D_8)x \quad [3\text{-}45]$$

where:

$\xi = \frac{F(n)}{F(n=1)}$: strength degradation factor [3-46]

$x = \ln(n)$, n=cycle number [3-47]

$\bar{e} = \frac{e_m}{e_p}$ = ratio of maximum reached displacement to peak displacement

b_0: intercept coefficient

b_i, $i = 1,13$: regression coefficients

all other variables were defined in Section 3.3.4.4

The stepwise regression analysis was applied to two different sets of data, one for the pre-peak region, and other for the post-peak region. This range selection was made based on the preliminary data analyses from Section 3.3.5.2. A less steeped slope in the strength degradation factor plot for pre-peak regions was observed (Figure 28). The regression process was applied first including all the variables showed in Eqn. 3-45. Next, based on previous results from the stepwise method, a new selection of variables was made by removing all those variables with irrational regression coefficients.

Results showed that for both sets of data (pre- and post-peak regions), the strength degradation factor was mainly a function of the number of cycles (through its transformation, ln(n)), deck shape type (D's), and the maximum normalized displacement $\bar{e}$. The gravity load coefficient and the axial stiffness index displayed values significantly different from zero (at 5% level) for the post-peak region. Regression coefficients associated with deck shape parameters for post-peak region were at least three times larger than those associated with pre-peak region. Such a result agreed with the criteria of define degradation factors only for the post-peak region, as some authors suggest (16,41). The axial stiffness index was included and resulted with a positive regression coefficient meaning that for an increase in Q value (e.g., increase in concrete thickness or concrete compression strength f'_c) a reduction in the amount of degradation was obtained.

Gravity load resulted with a negative regression coefficient. therefore, the use of the design gravity load, increased the strength degradation. After this analysis, the proposed degradation factor model is

Pre-peak region:

$$\xi = b_0 + (b_1 D_1 + b_2 D_2 + b_3 D_3 + b_4 D_4 + b_5 D_5 + b_6 D_6 + b_7 D_7 + b_8 D_8 + b_9 \bar{e}) x \qquad [3\text{-}48]$$

Post-peak region

$$\xi = b_0 + (b_1 D_1 + b_2 D_2 + b_3 D_3 + b_4 D_4 + b_5 D_5 + b_6 D_6 + b_7 D_7 + b_8 D_8 + b_9 Q + b_{10} \bar{e} + b_{11} GL) x \qquad [3\text{-}49]$$

For both cases, the intercept regression coefficient was close to 1, 0.994 for pre-peak, and 0.968 for post-peak region. The expected value for the intercept coefficient was unity , because when the cycle number is one (n=1) then x which is the natural logarithm of n is zero and the amount of degradation is zero or ξ=1. Therefore, an additional analysis was made using a nonlinear regression analysis for a model given by Eqns. [3-48] and [3-49], but with an intercept value of 1. The regression coefficients obtained with the nonlinear regression analysis showed practically no difference with those previously obtained since the intercept values were close to unity.

To verify the improvement achieved by the regression model, a comparison between the standard error of estimate (S_e) and the standard deviation of the criterion variable (strength degradation factor ξ) was made, since the standard error is a realistic measure of the goodness of fit. For the pre-peak region, the standard error S_e was 0.065 and the standard deviation S_ξ was 0.101; therefore a reduction of 35% was obtained by using the regression model instead of the average ξ. For the post-peak region, the standard error S_e was 0.134 and the standard deviation S_ξ was 0.215; therefore, a

reduction of 38% was obtained. Results of regression analysis are shown in Tables B13-B14 in Appendix B.

The regression analysis showed that the strength degradation factor was function of the deck shape type as well as other parameters. Since the differences among some of the deck types were mainly in the embossment configuration, and because there are many different commercial deck types not considered in the experimental program, a strength degradation factor independent of the deck type could be helpful. Therefore, a new analysis was made and results were assumed to represent an "average deck type". After this last analysis, the strength degradation expression was proposed as follows:

1) Pre-peak regions:

$$\xi = 1 + (\delta_{DS} + \delta_e \frac{e_m}{e_p}) \ln(n) \qquad [3\text{-}50]$$

2) Post-peak regions:

$$\xi = 1 + (\delta_{DS} + \delta_e \frac{e_m}{e_p} + \delta_{GL} GL + \delta_Q Q) \ln(n) \qquad [3\text{-}51]$$

where:

$\xi = \frac{F(n)}{F(n=1)}$ = strength degradation factor [3-46]

n: cycle number

e_m: maximum reached displacement

e_p: displacement at peak load

Q: axial stiffness index (see Equation 3-26)

δ_{DS}: deck shape factor (Table 15)

δ_e: displacement factor (Table 15)

δ_{GL}: gravity load factor (Table 15)

δ_Q: axial stiffness factor (Table 15)

Figure 30 shows a comparison between predicted and observed envelope force ratio for different displacements vs number of cycles, for Diaphragm 12. As expected, the smaller the displacement level, the better the prediction is. The same observation applies for the number of cycles at a given displacement level.

3.3.7 Hysteresis curve

3.3.7.1 Basic curve description A hysteretic model predicts the force-displacement relation for a system using stiffness and strength information. The model is defined based on two main components: the envelope or skeleton curve, and the cyclic loop or hysteresis curve. As defined before, the hysteresis loop is the curve defined under load reversals.

The state-of-the-art in hysteretic models for concrete elements suggests the use of either, straight lines or polynomial equations for the description of the hysteresis curve (see Figures 4-6). Most of the hysteretic models used straight lines following a series of rules to describe the loops (3,8,9,10). The use of straight lines for loops has been used mostly to make the model being clear and uncomplicated, but the use of polynomial expressions (27,28,38,44) requires fewer rules and usually follows closer the actual cyclic behavior of the element.

Description of the loop by either approach requires the previous definition of some force-displacement points and slopes along the cyclic path. Then, the suggested equation is forced to satisfy the required boundaries. Typical points and slopes used in the description of cyclic loops are shown in Figure 31.

Table 15. Strength degradation equation coefficients

Deck Shape coefficients δ_{DS}		Region	
Deck shape type	Deck type[a]	Pre-peak	Post-peak
1	1	-0.05	-0.39
2	2	-0.12	-0.44
1	3	-0.05	-0.39
1	4	-0.05	-0.39
3	5	-0.11	-0.39
4	6	-0.14	-0.49
5	7	-0.15	-0.49
6	8	-0.13	-0.50
7	9	-0.11	-0.48
8	10	-0.16	-0.55
4	11	-0.14	-0.49
δ_{DS} for general steel deck		-0.12	-0.45
Axial stiffness index δ_Q		--[b]	0.02
Displacement factor δ_e		-0.07	-0.01
Gravity load factor δ_{GI}	full gravity load	--[b]	-0.06
δ_{GI}	no gravity load	--[b]	0.000

[a]According to description in Appendix A.
[b]Not apply

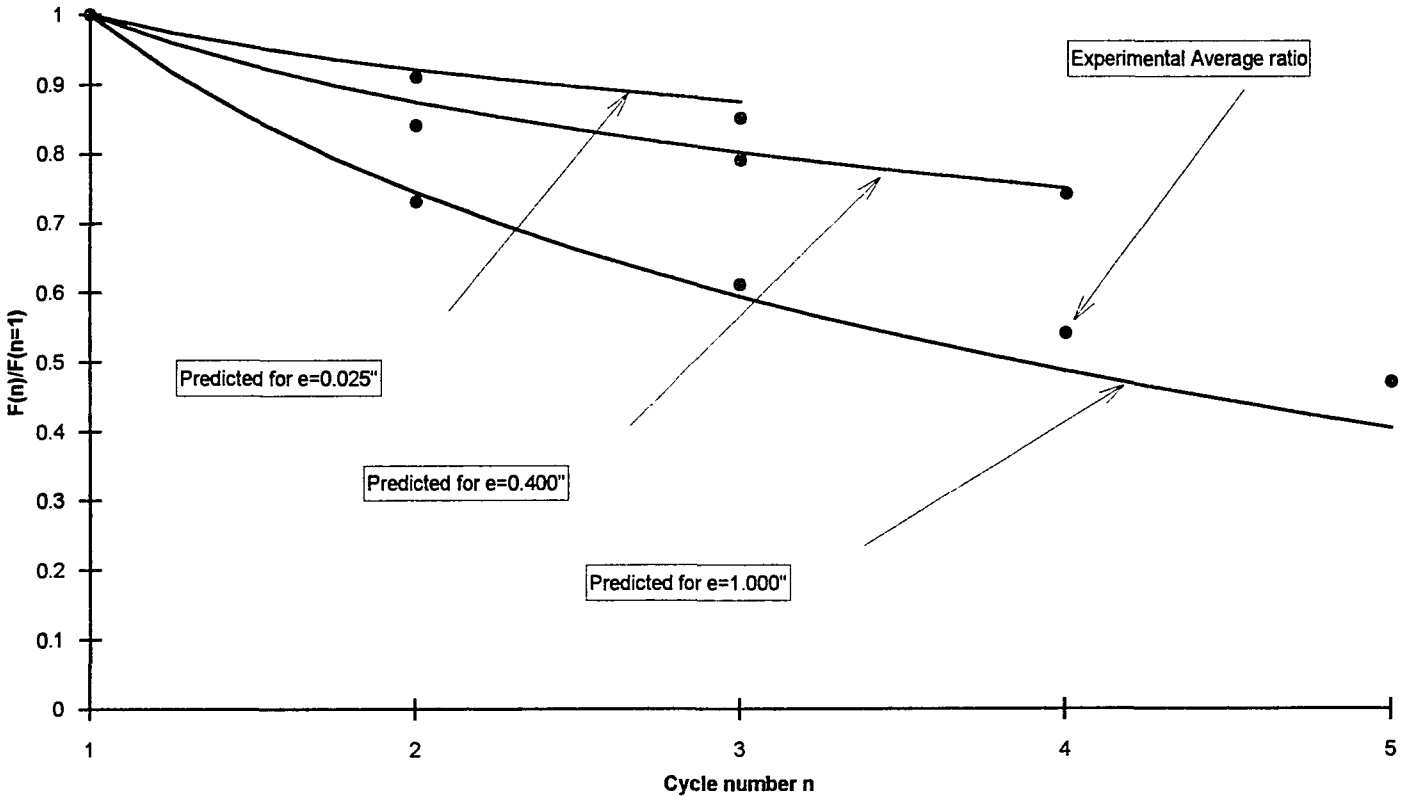

Figure 30. Comparison between predicted and observed strength degradation factors for test 12

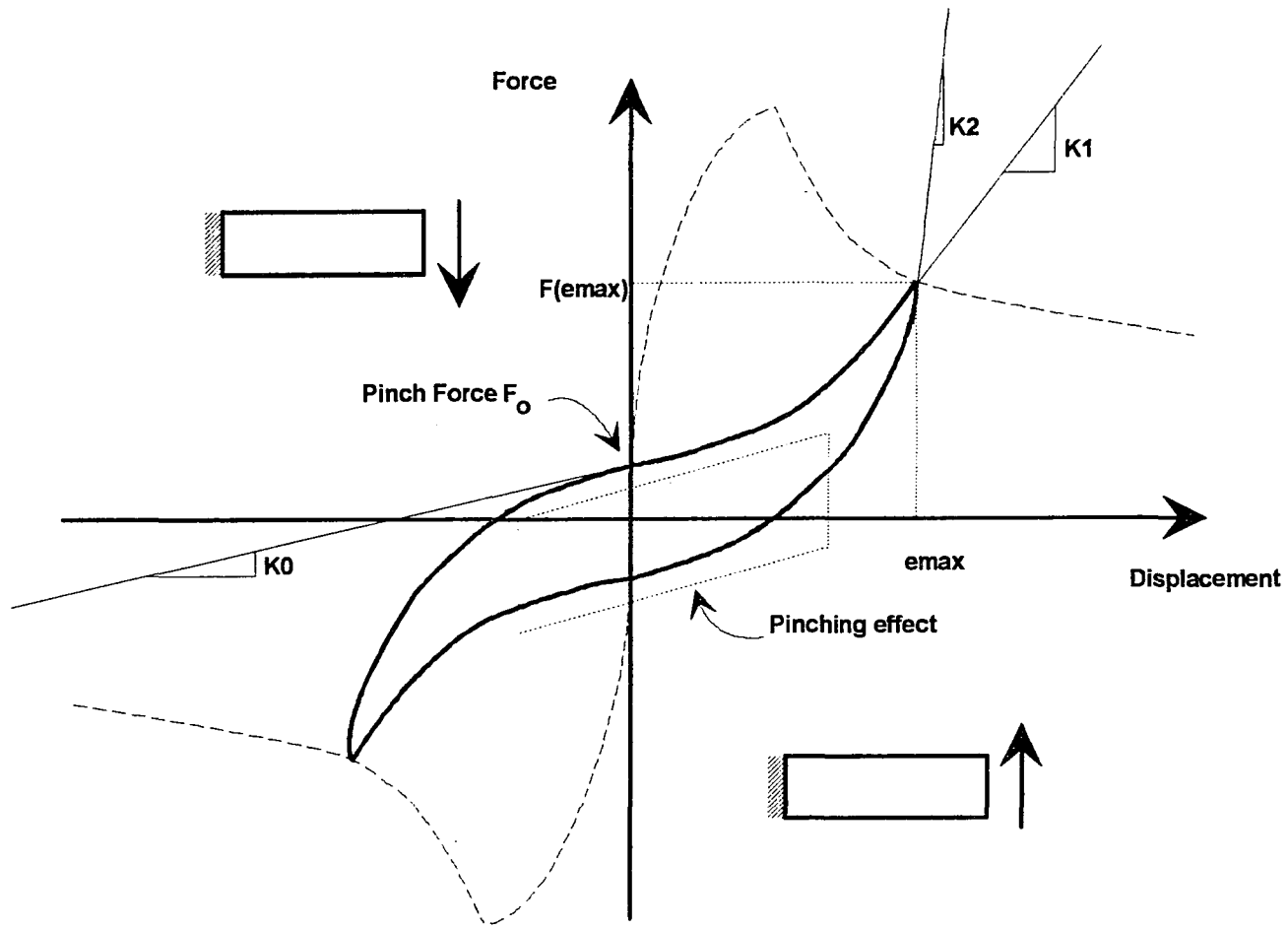

Figure 31. Typical hysteresis curve

The parameters used to define the hysteresis loop were : the pinch force F_0, maximum attached force and associated displacement for the cyclic, and the three characteristic slopes K_0, K_1, and K_2. Figure 31 showed a tendency in the cyclic loop for very low incremental stiffness near the origin followed by a stiffening, this is the so called pinching effect. The low stiffness may be produced by slip, yield of reinforcement, or opened cracks. Once the cracks closed and/or the slip was minimized by increased adherence or interlocking effect, the hysteresis loop showed a stiffening region. Pinch force accounted for why the load-displacement curve did not cross though the origin at zero displacement. Once these parameters were defined by constant values or expressions, the hysteresis loops may be defined by straight lines or by a nonlinear equations.

3.3.7.2 Pinch force prediction

3.3.7.2.1 General To predict the pinch force, a collection of data was made from test records. Plots of force vs displacement for each cycle recorded during test, were the only data source; therefore, the accuracy of these values was limited by the precision of the procedure used in the pinch force evaluation.

Pinch force predicted models had been reported in the literature for different types of hysteretic models (28,38,41,52). Kariotis et al. (41), expressed the pinch force as a constant fraction of the maximum force reached in the envelope, with this approach Kariotis reported a value of 0.15 for steel-deck diaphragms. Emori et al. (52) assessed indirectly the pinch force by fitting a third order polynomial to the hysteresis curve and evaluating such a polynomial expression at zero displacement. Porter and Yeomans

(28,38) found that a linear relation between pinch force and maximum displacement was a reliable predictor for hollow-core plank diaphragms.

3.3.7.2.2 Input data and basic patterns Pinch force values were obtained from cyclic plots of force vs displacement for each diaphragm test, except Test 1 which was monothonically loaded. Plots of pinch force vs displacement showed that the pinch force followed different paths before and after peak displacement; therefore, the data was grouped in two regions (pre- and post-peak). Additionally, virgin and stabilized pinch force data showed a difference in force magnitude, hence this effect was also considered in the sorting process. Figure 32 shows the pinch force displacement variation for Test 20. Research in pinch force prediction suggested two different models. First, a constant ratio of pinch force to the maximum associated envelope force was proposed for steel-deck diaphragms (41), and second, a linear relation between pinch force and maximum displacement was suggested for hollow-core plank diaphragms (28,38). The use of the first approach was discarded after plotting F_o vs F(e) for some of the diaphragm tests and notice a very weak linear relation between both parameters (see Figure 33).

3.3.7.2.3 Regression analysis The procedure used to define an empirical model for pinch force prediction, was similar to that used to identify a model for the envelope curve. That is, a group of eleven different models (see Table 3) were proposed. The mean absolute error (MAE) was used as goodness of fit measure.

The pairs of data (x, y) used in the regression analysis were the normalized pinch force and its respective maximum normalized displacement. The pinch force was normalized with respect to the peak force; meanwhile, the maximum associated displacement was normalized respect to the peak displacement. The regression analysis

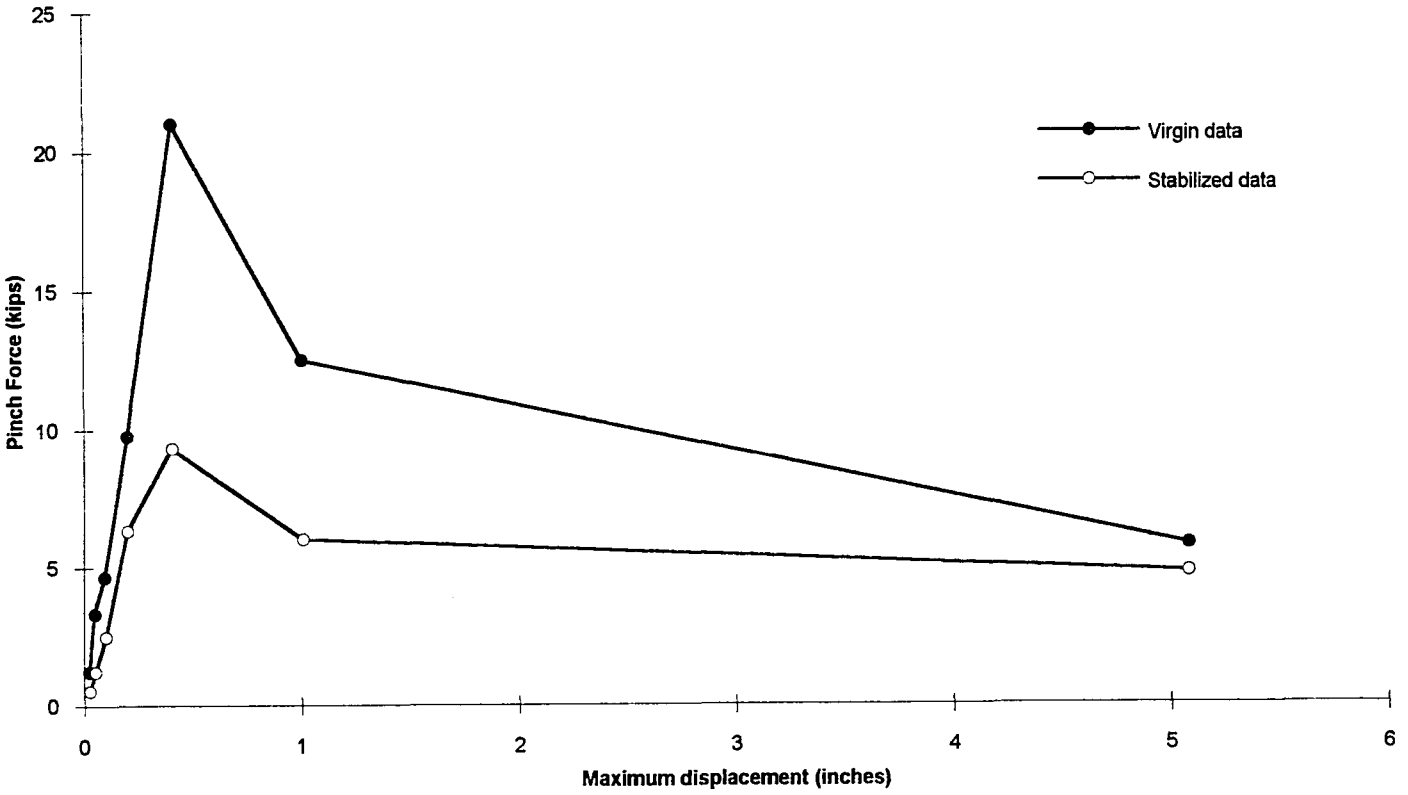

Figure 32. Pinch force vs maximum displacement for test 20

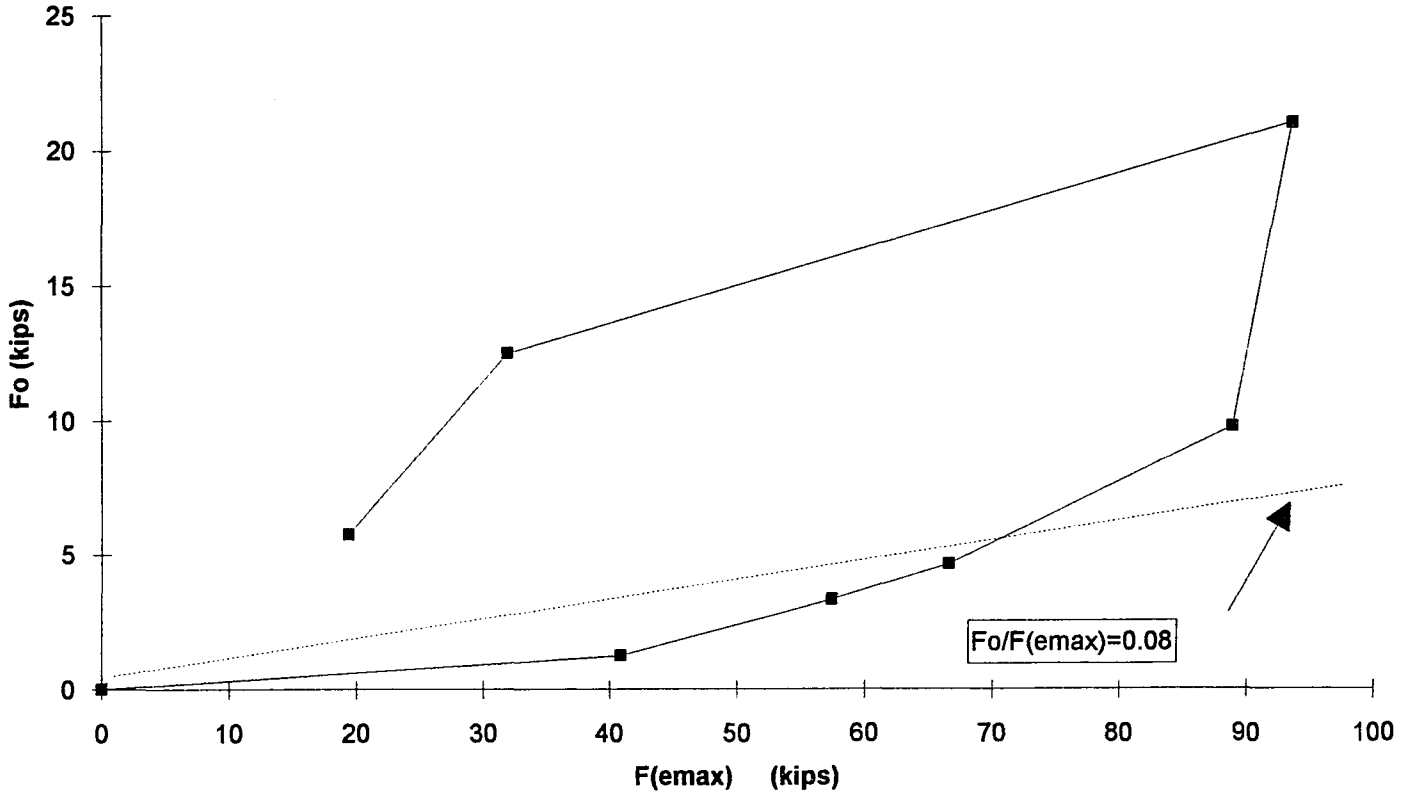

Figure 33. Fo vs F(emax) for test 20

was applied to all diaphragm tests (except Test 1), for both sources of data (virgin and stabilized), for both displacement ranges (pre- and post-peak region), and for all 11 models from Table 3, resulting in a total of 31x2x2x11=1364 fitted expressions.

Results of the regression analyses are shown in Table B15 and graphical representations of the results are shown in Figures B20-23 in Appendix B. Conclusions from these analyses were:

- The pinch force for pre-peak virgin region and pre-peak stabilized region may be predicted by either linear (regression Model 1) or multiplicative (regression Model 8) models, because both had approximately the same mean value and almost the same confidence interval. Additionally, there was no significant difference (at 5% level) in the error evaluation for these two models Figures B20 and B22).
- The pinch force for both virgin and stabilized post-peak regions may be predicted by almost any of the proposed models (except Model 5) since all the confidence intervals were overlapped.

Based on the conclusions previously stated, the linear model may be the best model for pre-peak regions and at least as good as any other proposed model for post-peak regions. Therefore, the linear model was proposed to predict the pinch force of steel-deck-reinforced concrete diaphragms. Once the pinch force regression model was selected, an inspection of the corresponding regression coefficients and its confidence intervals was made to identify if other parameters were necessary to improve the explained variation of data. First of all, statistical tests were made to verify if the intercept coefficient for the pre-peak region was significantly different from zero. Results showed that there was no significant difference (at 5% level) between such intercept and zero (as expected), therefore the analysis continued using no intercept at pre-peak regions. Regression coefficients (slope for pre-peak region, slope and intercept for post-peak region) and their

confidence intervals are shown in Tables B16 and B17. From these results, the following conclusions may be stated:

- Slope coefficients for pre-peak regions in both virgin and stabilized data showed less variability since their confidence intervals were the smallest.
- For some cases, slope and intercept coefficients for post-peak regions showed confidence intervals including the zero value. The inclusion of zero in the confidence interval may be due mainly to the small number of data points available for this region. Note that the t statistic (see Eqns. 3-24 and 3-25) at α =5% for n=3 is 12.71 for n=4 is 4.30 and for n=5 is 3.18; therefore, the smaller the samples, the wider the confidence intervals obtained. The general trend for slope and intercept coefficients may be identified by observing the average values at the end of Tables B16-B17, where significantly different from zero values are suggested.
- A comparison among different test regression coefficients and the confidence intervals showed considerable scatter. This scatter may be due to the exclusion of other parameters (e.g., gravity load, deck shape, etc.) in the regression analysis; and/or to the lack of precision method of collecting pinch force data; and/or pure random error.

In order to identify if additional parameters may help in the prediction of the pinch force, a multiple regression analysis was used as explained in the next subsection.

3.3.7.2.4 Multiple linear regression analysis Based on conclusions in the previous section, a multiple linear regression analysis was made to investigate if the explained variation may be increased by adding more parameters to the proposed model. This analysis, was applied to four data sets: pre-peak virgin, pre-peak stabilized, post-peak

virgin, and post-peak stabilized. Additional parameters considered were :shape of deck (D's), axial stiffness index (Q), gravity load effect (GL), connection type (CT), and aspect ratio (L1L2). For the pre-peak region, only interaction terms (those affecting the slope) were included in the proposed model, because the previous linear regression analyses showed values not significantly different from zero for the intercept coefficient. For the post-peak region, since both regression coefficients were needed, a more general model was proposed. The proposed multiple linear regression models for both regions were:

1) Pre-peak regions

$$\frac{F_0}{F_p} = (a_1 GL + a_2 CT + a_3 L_1 L_2 + a_4 Q + a_5 D_1 + a_6 D_2 + a_7 D_3 + a_8 D_4 + a_9 D_5 + a_{10} D_6 + a_{11} D_7 + a_{12} D_8)\frac{e_{\max}}{e_p} + \varepsilon \quad [3\text{-}52]$$

2) Post-peak regions

$$\frac{F_0}{F_p} = b_0 + b_1 GL + b_2 CT + b_3 L_1 L_2 + b_4 D_1 + b_5 D_2 + b_6 D_3 + b_7 D_4 + b_8 D_5 + b_9 D_6 + b_{10} D_7 + \begin{pmatrix} b_{11} GL + b_{12} CT + b_{13} I_1 L_2 + b_{14} D_1 + b_{15} D_2 \\ + b_{16} D_3 + b_{17} D_4 + b_{18} D_5 + b_{19} D_6 + b_{20} D_7 + b_{21} D_8 \end{pmatrix} \frac{e_{\max}}{e_p} + \varepsilon \quad [3\text{-}53]$$

Results of analyses showed that for both regions the deck shape parameters were significant in explaining variation. Additionally, the axial stiffness index Q was also significant for post-peak regions by increasing the slope of the straight line model (and increasing pinch force) for an increasing value of Q. A measure of the goodness of fit may be made by comparing the standard deviation of force ratio Fo/Fp vs standard error of regression analysis. For pre-peak virgin region, the standard deviation was 0.034 and the

standard error of estimate was 0.021. Therefore, a reduction of approximately 38% in the unexplained variation was obtained through the regression model. For the pre-peak stabilized region, the standard deviation was 0.025 and the standard error of estimate was 0.017 for a total reduction of 32%. The post-peak virgin region showed a standard deviation of 0.074 and a standard error of estimate of 0.047 for a 36% reduction. Post-peak stabilized region had a standard deviation of 0.060 and a standard error of 0.040 for a reduction of 33%. Reduction values were equal or greater to 32%, therefore there were a significant improvement in using the regression model against the use of the pinch force mean values.

Based on results obtained from this section, the pinch force model is proposed as follows:

Pre-peak region:

$$\frac{F_0}{F_p} = \lambda_D \frac{e_{\max}}{e_p} \qquad [3\text{-}54]$$

Post-peak region:

$$\frac{F_0}{F_p} = \lambda_{D0} + \lambda_Q \frac{e_{\max}}{e_p} \qquad [3\text{-}55]$$

where:

Fo: Pinch force

Fp: Peak force

e_{max}: maximum envelope displacement for the actual cycle

e_p: displacement at peak load

λ_D, λ_{D0}: shape deck factor (Table 16)

λ_Q: axial stiffness factor (Table 16)

Additional results to those presented in Table 16 are shown in Table B18 in Appendix B. A comparison between predicted and observed pinch forces is shown in Figure 34. Predicted values seemed to adequately predict the experimental values. Note the clear definition of regions (pre- and post-peak regions) as well as the difference between virgin and stabilized pinch force to peak load ratios.

3.3.7.3 Characteristic slopes prediction

3.3.7.3.1 General Similarly to pinch force source data, the characteristic slope values were determined (visually) from plots of force vs displacement for each cycle; therefore, the accuracy of such values is limited due to the process used.

Most of the reinforced concrete degrading type hysteretic models used a similar formula to evaluate the degrading stiffness in one or more segments of a cyclic force-displacement path (1,6,9,16,28,40,53). Such an expression had been proposed as:

$$\frac{K(e_{max})}{\overline{K}} = f(\frac{\hat{e}}{e_{max}}) \qquad [3\text{-}56]$$

Typically, the function of the normalized displacement has been used as a multiplicative model or square root model with no intercept (see Table 3). The nominal stiffness ($\overline{K}$) and nominal displacement ($\hat{e}$) had been proposed differently from one model to other. Takeda (9) suggested for the nominal stiffness, the slope of a line joining the yield point in one direction to the cracking point in the other direction (trilinear skeleton curve). Kariotis et al. (16,41) suggested the initial stiffness for the nominal stiffness value. Nominal displacement has been proposed as the yield displacement (9), or the ratio of peak load to initial stiffness (41, 28). In any case, all of the expressions are similar in form since used the same model structure.

Table 16. Pinch force shape deck factor λ_D

Steel deck		Virgin Data		Stabilized Data	
Shape	Type	λ_D Pre-peak	λ_{D0} Post-peak	λ_D Pre-peak	λ_{D0} Post-peak
1	1	0.12	0.22	0.06	0.14
2	2	0.18	0.27	0.14	0.20
1	3	0.12	0.22	0.06	0.14
1	4	0.12	0.22	0.06	0.14
3	5	0.16	0.25	0.10	0.17
4	6	0.15	0.15	0.09	0.09
5	7	0.17	0.25	0.15	0.18
6	8	0.20	0.29	0.12	0.20
7	9	0.18	0.15	0.07	0.09
8	10	0.09	0.16	0.09	0.08
4	11	0.15	0.15	0.09	0.09
General deck		0.16	0.21	0.09	0.14
Axial stiffness factor λ_Q		--[b]	$\frac{Q}{550} - 0.023$[a]	--[b]	$\frac{Q}{730} - 0.016$[a]

[a]axial stiffness factor Q evaluated according to Eqn.3-26
[b]not apply

The parameters used for the characteristic slope analysis were based on previous work made by the author in a hysteretic model for hollow-core plank diaphragms (28), where the following normalized parameters showed good correlation:

$$x = \frac{\bar{e}_p}{e_{\max}} = \frac{F_p}{K_i e_{\max}} \qquad [3\text{-}57]$$

$$y = \frac{K_j}{K_i} \qquad [3\text{-}58]$$

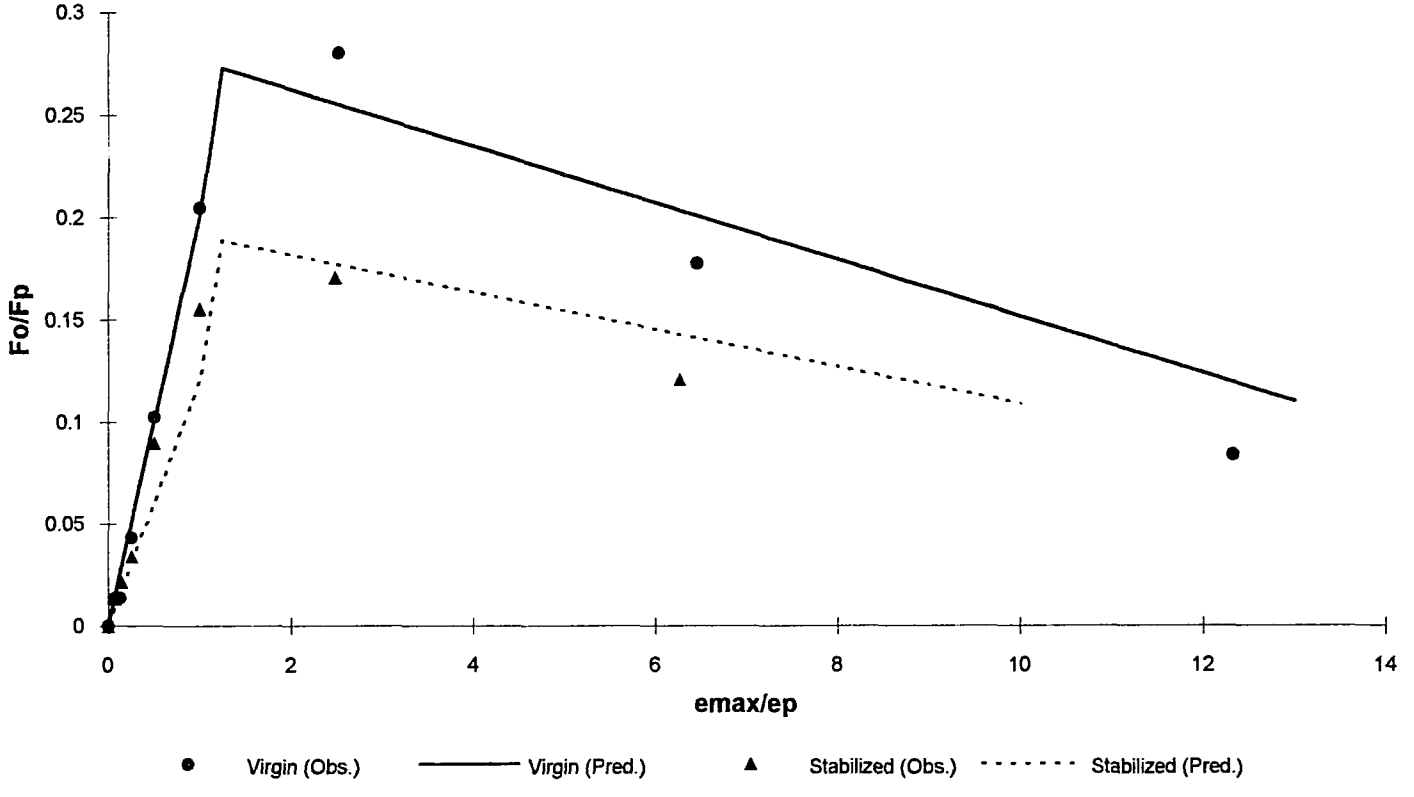

Figure 34. Predicted vs observed pinch force for test 19

where:

Fp: peak load

K_i: initial (envelope) stiffness

e_{max}: maximum associated displacement

$K_j, j = 0,1,2$: characteristic slopes (see Figure 31)

$\bar{e}_p$: elastic peak displacement

For the analysis related to characteristic slopes, two different force terms were initially considered, the peak force (Fp) and the envelope force associated with e_{max} (F(emax)). Results showed no significant difference between both cases. Since an expression with a constant term is easier to use, the peak force was considered for this investigation.

3.3.7.3.2 Input data and basic patterns Characteristic slope values were visually obtained from cyclic plots of force vs displacement for each diaphragm test except Test 1 that was monothonically loaded. Since there were no cyclic plots available for Tests 1-9, a graphical approach was used in these cases, that is a continuous curve was plotted through the available experimental force-displacement data points. Since there had to be continuity between points through the curve, the pinch force and characteristic slope K0 evaluation were assumed to be not considerably affected by this approach. But, the other two slopes K1 and K2 were assumed to be affected because they were evaluated at the end of the cycle loop. A reduced influence was considered for K1 and K2 slope values for Tests 1-9 in the final estimation of regression coefficients. Plots of characteristic slope vs associated maximum displacement showed a continuous degrading curve with a steeper initial region and a final low value plateau at large displacements. Small differences were observed for virgin and stabilized values

especially after peak displacements. Figure 35 shows an example of characteristic slope vs displacement for Test 15. This plot shows the typical pattern followed by the characteristic slopes for all the diaphragm tests.

3.3.7.3.3 Regression Analysis In order to identify an empirical model for characteristic slope prediction, a similar procedure to that used previously for pinch force and envelope force was used. A group of eleven different models (Table 3) was proposed as possible predictive models. Regression analysis was applied on the normalized data (Eqns. 3-57 and 3-58), and measures of error in prediction were evaluated. The mean absolute error (MAE) was used as goodness of fit measure. The model selected was function of the MAE values and its confidence intervals. The regression analysis was applied for all diaphragms (except Test 1), for both sources of data (virgin and stabilized), for all 11 models from Table 3, resulting in a total of 31x2x11=682 fitted expressions for each of the three different characteristic slopes (see Figure 31). Results of the regression analyses for the three characteristic slopes are shown in Tables B19-B20 and graphical representations of results (MAE values and confidence intervals) are shown in Figures B24-B29 in Appendix B. Based on these results the following conclusions were stated:

- The magnitude of error was considerably smaller for K0 and K1 characteristic slopes. Some reduction in the average error was also observed from virgin to stabilized.
- Virgin slopes were best predicted (smallest error) using Model 9 (square root model). A comparison between model 9 and the linear model showed significant (5%) differences between them since confidence intervals were not overlapped. For K2 slope, Model 7 (logarithmic-x model) showed a smaller

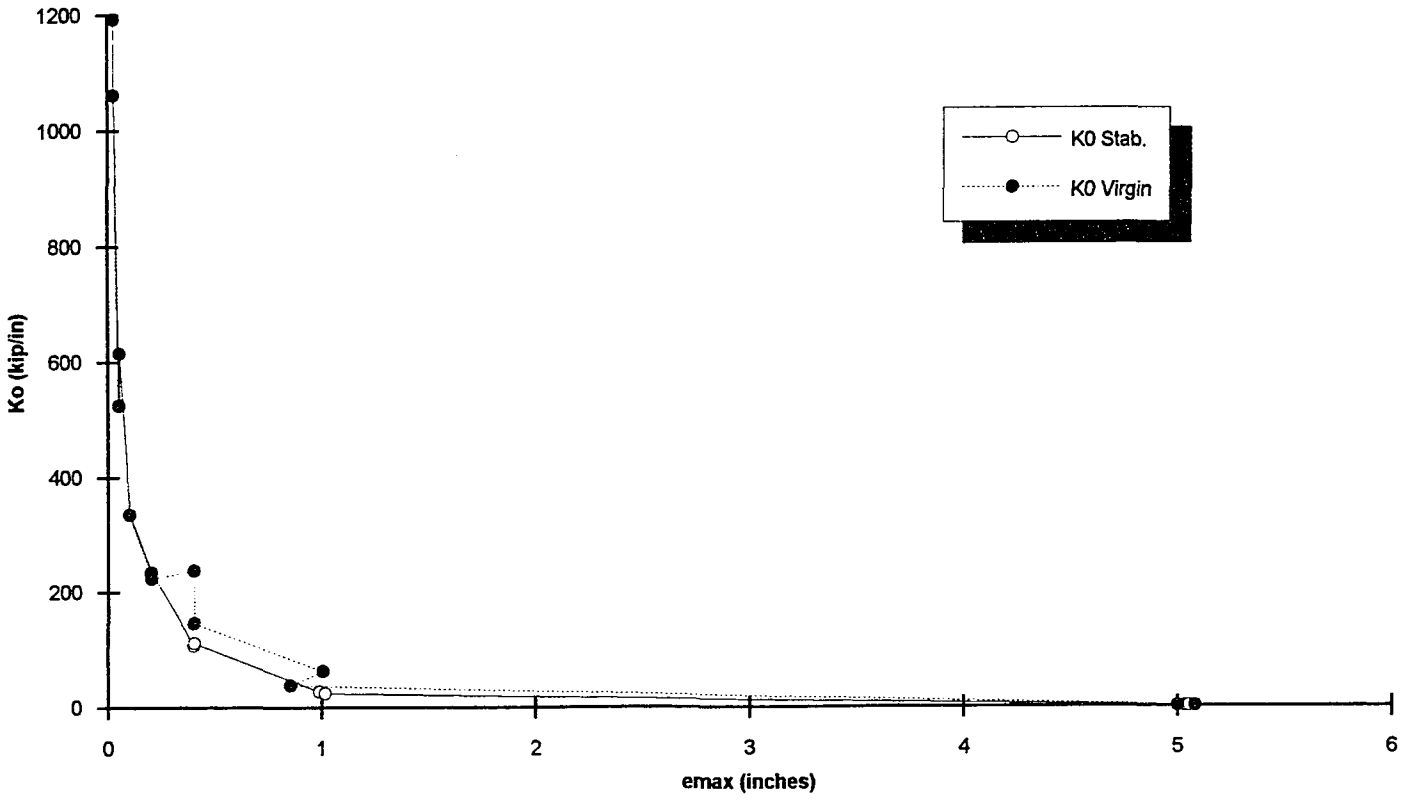

Figure 35. Ko characteristic slope for test 15

average error than Model 9, but there was no significant difference between them (at 5% confidence level).

- Stabilized slopes may be predicted using Model 9. For K0, Model 9 and Model 1 (linear model) showed no significant difference, but Model 9 had a smaller confidence interval. For K1, there were significant differences between linear and square root model (Model 9). Finally for K2, logarithmic model (Model 7) had the smallest average error, but showed no significant difference with thesquare root model.

Conclusions from last results showed a tendency in the data to be better described with the square root model. This conclusion agreed with the type of expression previously used to model stiffness degradation for other hysteretic models.

Once the square root model had been proposed to describe stiffness degradation for steel-deck-reinforced concrete diaphragms, the next step was to analyze the results of linear regression model related to regression coefficient values and confidence intervals. Such an analysis was applied to each diaphragm data set separately with the following model:

$$\frac{K_j}{K_i} = a + b\sqrt{\frac{F_p}{K_i e_{\max}}} \qquad [3\text{-}59]$$

where:

a,b: regression coefficients

other variables were defined in Section 3.3.7.3.1

Regression analysis for the model proposed in Eqn. 3-59 was made considering two cases: with and without an intercept coefficient. Results showed for some tests an intercept coefficient significantly different from zero, which physically means that some

characteristic slopes for large displacements had a negative value. Such result was assumed to be consequence of the inaccuracy in the procedure used for slope evaluation. Therefore, a non-intercept option was selected. Since the resulted slope coefficients seem to be similar for virgin and stabilized sets, a paired sample analysis was applied on the slope regression coefficients. Results for K0 showed no significant difference between mean values from both sets (Pvalue = 0.997 for a two tailed test). Similar results were obtained for K2 with a Pvalue of 0.26. Test for difference between virgin and stabilized results for K1 showed a significantly difference between both data sets, which had a physical explanation. Slope K1 value for n=1 really was the slope of the envelope curve and not really the slope of part of a cycle. The first loop was created when after reaching a specific displacement a complete set of unloading and reloading steps occurred; therefore, the value called K1 for n=1 cycle (the virgin K1 value) should not be defined as virgin K1 value. Values of K1 after the "first" cycle are much closer to those from the stabilized cycle, and the cyclic loop showed basically strength degradation but not significant stiffness degradation. Results from regression analyses are shown in Tables B21-B23. Some scatter was observed in the slope regression coefficient which may be an indication of missing parameter effects in the proposed model. Therefore, a multiple regression analysis was applied to investigate the effects of other parameters. Such analysis is explained in the next subsection.

3.3.7.3.4 Multiple linear regression analysis Results from the previous section showed some scatter in the slope regression coefficient for the proposed model, which may be an indication of missing parameter effects such as gravity load, deck shape, aspect ratio, connection type, or axial stiffness index. To investigate if additional variation may be explained through the inclusion of some or all the listed parameters, a multiple

linear regression analysis was made. The analysis was applied on a model that included no intercept coefficient since zero values of the characteristic slopes were expected for large displacements. Analysis was applied for virgin and stabilized data, for each characteristic slope. The data from Tests 2-9 were not included in the evaluation of regression coefficients associated with K1 and K2, because of the lack of precision on the method used to evaluate such data (see discussion in Section 3.3.7.3.2). The proposed model was:

$$\frac{K_j}{K_i} = (b_1 GL + b_2 Q + b_3 CT + b_4 L_1 L_2 + b_5 D_1 + b_6 D_2 + b_7 D_3 + b_8 D_4 + b_9 D_5 + b_{10} D_6 + b_{11} D_7 + b_{12} D_8) \sqrt{\frac{F_p}{K_i e_{\max}}} \qquad [3\text{-}60]$$

where:

$K_j, j = 0,1,2$: characteristic slopes

b_r, r=1,2,..12: regression coefficients

all other parameters had been defined in previous sections.

Results of the multiple linear regression analyses showed that the major contributor to the slope term was the deck shape (D's terms). Additionally for K0 and K1 a slightly contribution from the gravity load effect was found (approximately 10% of total slope coefficient). The final model for each characteristic slope was:

$$\frac{K_j}{K_i} = (\rho_{GL} + \rho_{DS}) \sqrt{\frac{F_p}{K_i e_{\max}}} \qquad [3\text{-}61]$$

where:

$K_j, j = 0,1,2$: Characteristic slopes

K_i: initial stiffness

F_p: virgin or stabilized peak force

e_{max}: maximum displacement

ρ_{GL}: gravity load factor (Table 17)

ρ_{DS}: deck shape factor (Table 17)

Results in Table 17 show also a general deck shape factor evaluated with an analysis using all the data without diferentiating between steel deck shapes. Due to the variation between shapes, results obtained for such general deck were less accurate. Nevertheless, the general deck shape may be used as a simple estimate for those decks not included in the experimental program. Standard errors of parameters are shown in Table B24 in Appendix B. A plot of predicted-observed characteristic slope is shown in Figure 36. A comparison of the confidence intervals for the three characteristic slopes in Table B24 showed that there was no significant difference between virgin and stabilized coefficients for characteristic slopes K0 and K2. Therefore, the effect of cyclic stiffness degradation may be considered negligible for these two characteristic slopes. For K1, there was a significant difference between virgin and stabilized values. This may suggest a cyclic stiffness degradation effect, but based on the discussion of Section 3.3.7.3.3 related to the procedure used to evaluate the virgin value of K1, a negligible stiffness degradation was also assumed. Additionally, those coefficient values associated with the stabilized region were suggested also as virgin values.

3.3.7.4 Cyclic loop equation State-of-the-art in hysteretic models for reinforced concrete elements suggestes the use of either straight lines or polynomial curves to define the force-displacement cyclic path. Using either of both approaches requires the previous definition of some boundaries such as pinch force, characteristic slopes, etc. Then the line or curve is forced to adjust to those boundaries. The use of straight lines to model the

Table 17. Deck shape and gravity load factors for characteristic slope equation

Deck Shape	Deck Type	K_0		K_1		K_2	
		ρ_{DS} Virgin	ρ_{DS} Stabilized	ρ_{DS} Virgin	ρ_{DS} Stabilized	ρ_{DS} Virgin	ρ_{DS} Stabilized
1	1	0.63	0.62	0.52	0.58	1.06	1.12
2	2	0.64	0.62	0.65	0.67	1.28	1.38
1	3	0.63	0.62	0.52	0.58	1.06	1.12
1	4	0.63	0.62	0.52	0.58	1.06	1.12
3	5	0.50	0.53	0.49	0.61	1.34	1.37
4	6	0.54	0.49	0.48	0.66	1.55	1.56
5	7	0.45	0.52	0.44	0.58	1.35	1.48
6	8	0.42	0.40	0.41	0.54	1.44	0.93
7	9	0.47	0.45	0.44	0.62	1.63	1.54
8	10	0.44	0.46	0.50	0.63	1.58	1.35
4	11	0.54	0.49	0.48	0.66	1.55	1.56
General Deck		0.54	0.55	0.51	0.61	1.40	1.34
Gravity load factor ρ_{GL}		-0.09	-0.09	-0.05	-0.06	--[a]	--[a]

[a]not apply

cyclic behavior of diaphragms results in a model uncomplicated in definition, but more empirical rules are needed to define a cycle. Using a curve to define the cycles increases model complexity but improves the force-displacement prediction.

Use of the straight line approach for cyclic prediction of SDRC diaphragms follows the empirical rules described in most of the degrading type models such as Takeda model (9) or Sina model (10). Necessary modifications to those models are:

- Substitute the bilinear or trilinear skeleton curve by the nonlinear expression defined in previous Section 3.3.5
- Include the effect of strength degradation.
- Substitute the degrading stiffness expressions of those models with the characteristic slopes defined in Section 3.3.6.2
- Include the pinch force parameter as an additional condition in defining cyclic path.

Figure 37 displays the nonlinear path observed by the force-displacement behavior of Test 21. Observation of all cyclic loops available for diaphragm tests from which Figure 37 is a typical example, reinforce the use of the the nonlinear cyclic approach. Nonlinear expressions are an alternative to describe the cyclic force-displacement behavior, particularly polynomial expressions had been more frequently used. Soroushian et al. (27) suggested the use of a 4th order polynomial equation to describe the half-cyclic behavior of masonry shear walls. Nakata et al. (44) proposed the use of a third order polynomial to describe each quarter-cycle for reinforced concrete column force-displacement behavior. Porter and Yeomans (28,38) proposed the use of a 5th order polynomial for a half cycle force-displacement of hollow-core plank diaphragms.

To investigate the degree of polynomial expression that may be used for SDRC cycles, and to evaluate the goodness of fit of polynomial expressions, a regression

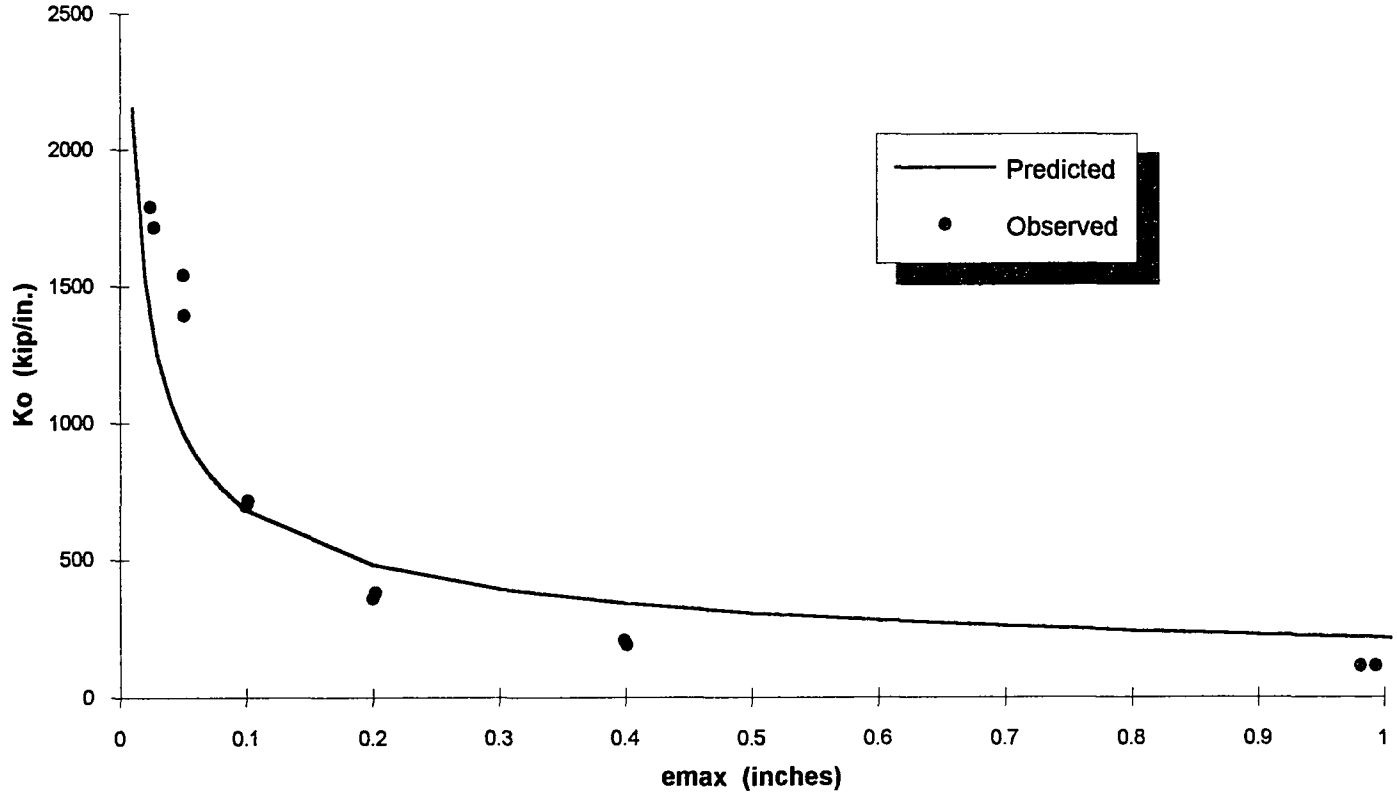

Figure 36. Predicted vs observed stabilized Ko for test 12

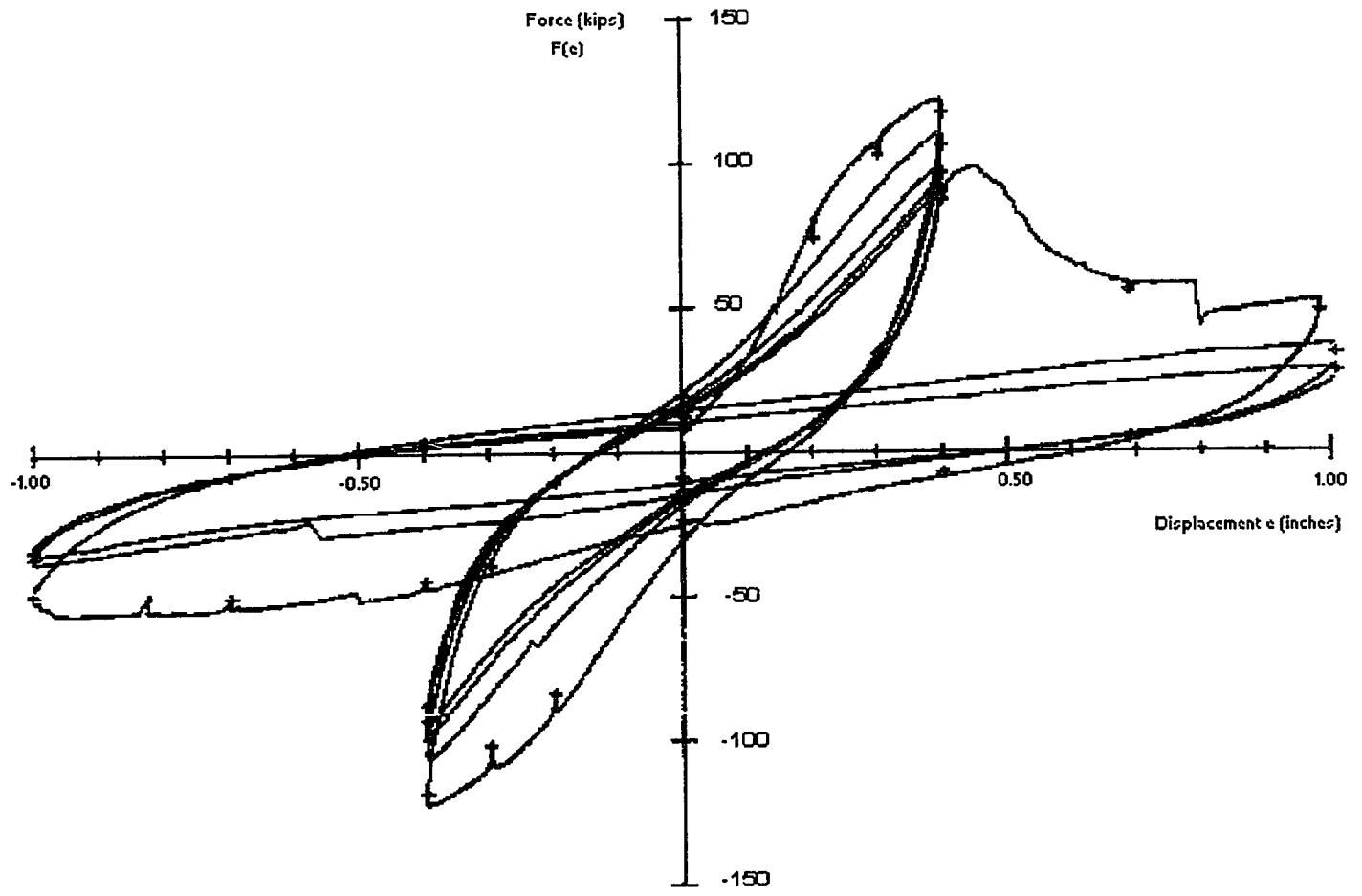

Figure 37. Cyclic force-displacement path at 0.4 and 1.00 in. displacement for test 21

analysis was made. A series of cycles from different diaphragm tests were selected. Cycles associated with different displacements were included. For each cycle, the force-displacement values were normalized with respect to the maximum force in the cycle and maximum displacement in the cycle, so a comparison between cycles at the same displacement level but from different tests may be made. Stepwise regression analysis was applied in the experimental cyclic data using as a limiting model, a 5th order polynomial model. The stepwise regression method selects only the polynomial terms that improved the explained variation. The polynomial equation may be defined for a complete half cycle or for a quarter cycle; therefore two different sets of data were used. First, data with complete half cycles (from maximum positive displacement to maximum negative displacement) was used, and later, a second data set with quarter cycles (from maximum positive or negative displacement to zero displacement) was utilized. Results from this analyses are shown in Table B25 in Appendix B. The following conclusions may be stated:

- Explained variation using polynomial models were considerably large with an average above 0.95 for the investigated cycles. Small reduction in explained variation was found for large displacement cycles.
- Quarter cycles were well defined by second order polynomials. Half cycles may be defined by third order polynomials

Results obtained from the statistical analysis were confirmed by observing the following characteristics from the cyclic plots:

- Plots of cyclic loading showed an inflection point only when moving from a set of cycles at a fixed displacement to the next larger displacement (cycle n=1). For all other loading cycles (n>1) at the same displacement level, the cyclic plot showed no reversals in curvature.

- Paths of cyclic unloading showed no reversal in curvature for any cycle.

A third or higher order polynomial is needed to model reversals in curvature, therefore, to describe quarter cycles, a second order polynomial is suggested since there is no reversal in curvature (unless n=1). If a complete half cycle is described with a polynomial expression, a third or higher order is needed because the pinching effect introduces a reversal in curvature (see Figure 38).

Based on results of regression analysis and observations from all available cyclic plots for diaphragm tests, second and third order polynomial equations for different cycle paths were proposed. Expressions were forced to fit defined boundaries. A full cycle was divided in four sections as shown in Figure 39. Each section was defined by the following boundaries: the pinch force point, the maximum cyclic force point and its characteristic slope. Boundary conditions were applied to the general 3rd order polynomial Eqn. [3-62] as follows:

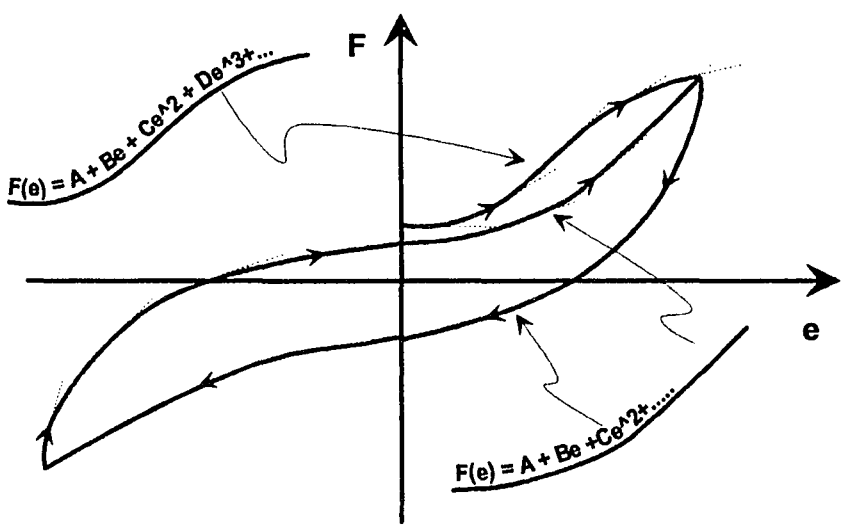

Figure 38. Curvature variation of a cyclic force-displacement path

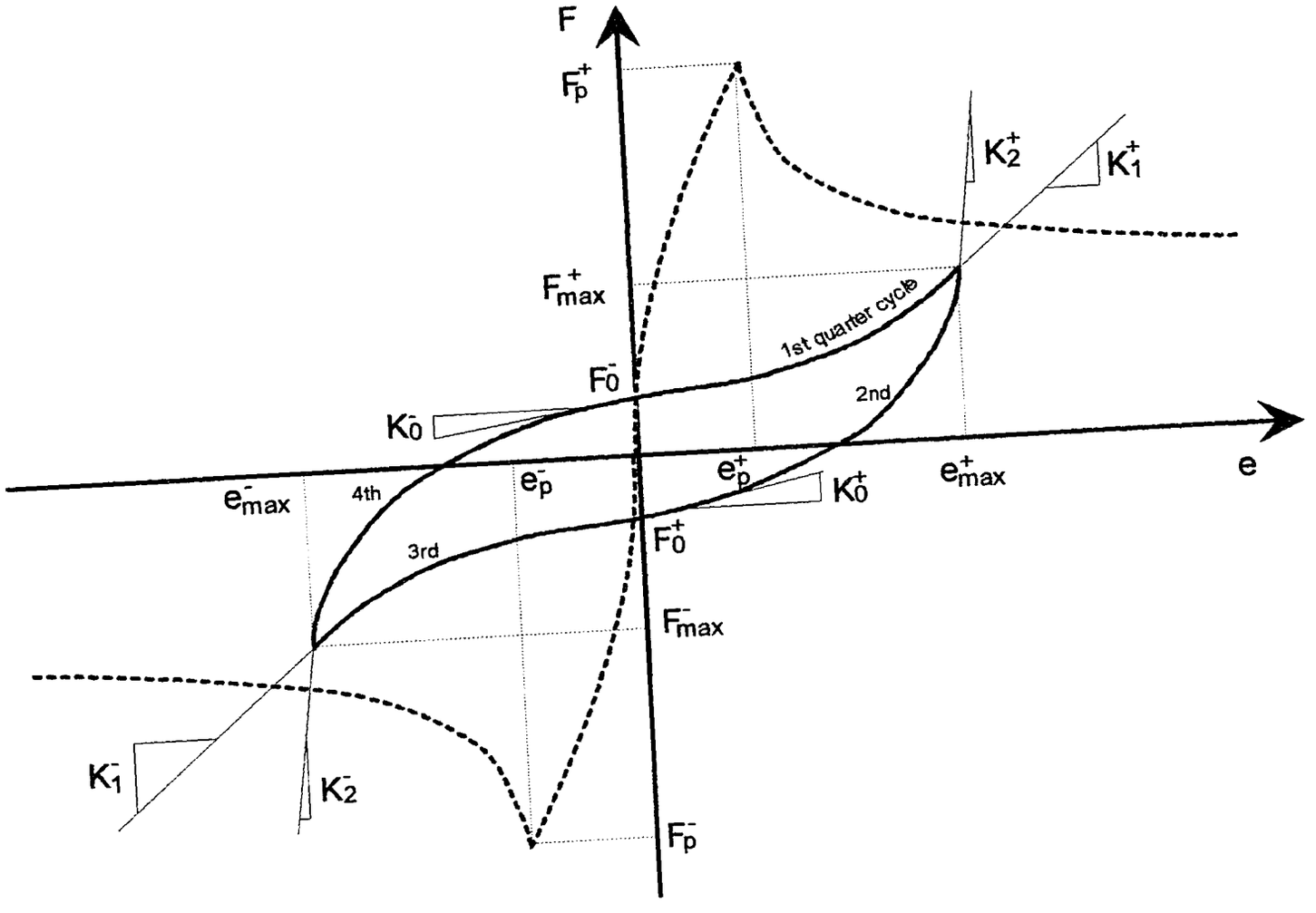

Figure 39. Definition of parameters for cyclic polynomial equation

$$F(e) = A + Be + Ce^2 + De^3 \qquad [3\text{-}62]$$

- 1st quarter cycle

Conditions:

$$at\ e = 0,\quad F(e) = F_0^-$$

$$at\ e = 0,\quad F'(e) = K_0^-$$

$$at\ e = e_{max}^+,\quad F(e) = F_{max}^+ \qquad [3\text{-}63]$$

$$at\ e = e_{max}^+,\quad \frac{dF}{de} = K_1^+$$

substituting [3-63] into [3-62] and evaluating the constants:

$$A = F_0^-$$

$$B = K_0^-$$

$$C = \frac{\left[3\left(F_{max}^+ - F_0^-\right) - \left(2K_0^- + K_1^+\right)e_{max}^+\right]}{e_{max}^{+\,2}} \qquad [3\text{-}64]$$

$$D = \frac{\left[-2\left(F_{max}^+ - F_0^-\right) + \left(K_0^- + K_1^+\right)e_{max}^+\right]}{e_{max}^{+\,3}}$$

following a similar procedure, the four constants for each of the other segments are:

- 2nd quarter cycle

$$A = F_0^+$$

$$B = K_0^+$$

$$C = \frac{\left[3\left(F_{max}^+ - F_0^+\right) - \left(2K_0^+ + K_1^+\right)e_{max}^+\right]}{e_{max}^{+\,2}} \qquad [3\text{-}65]$$

$$D = \frac{\left[-2\left(F_{max}^+ - F_0^+\right) + \left(K_0^+ + K_1^+\right)e_{max}^+\right]}{e_{max}^{+\,3}}$$

- 3rd quarter cycle

$$A = F_0^+$$

$$B = K_0^+$$

$$C = \frac{\left[3\left(F_{\max}^- - F_0^+\right) - \left(2K_0^+ + K_1^-\right)e_{\max}^-\right]}{e_{\max}^{-2}} \qquad [3\text{-}66]$$

$$D = \frac{\left[-2\left(F_{\max}^- - F_0^+\right) + \left(K_0^+ + K_1^-\right)e_{\max}^-\right]}{e_{\max}^{-3}}$$

- 4th quarter cycle

$$A = F_0^-$$

$$B = K_0^-$$

$$C = \frac{\left[3\left(F_{\max}^- - F_0^-\right) - \left(2K_0^- + K_1^-\right)e_{\max}^-\right]}{e_{\max}^{-2}} \qquad [3\text{-}67]$$

$$D = \frac{\left[-2\left(F_{\max}^- - F_0^-\right) + \left(K_0^- + K_1^-\right)e_{\max}^-\right]}{e_{\max}^{-3}}$$

All parameters have a sign associated with them according to the direction of axes as shown in Figure 39. $F_{\max}^{\pm}$ is the force at the virgin envelope when the number of cycles is n=1 (ξ=1 in Eqns. [3-41] and [3-42]), and is the degraded envelope force when n>1. Pinch forces and characteristic slopes are also function of their respective (±) maximum displacement $e_{\max}^{\pm}$. The proposed model has the capability to deal with asymmetrical behavior, such as that produced when parallel supporting beams have different cross-section, or for continuous panels when distance between parallel supporting beams are not symmetrically positioned.

3.3.7.5 Hysteresis rules The following hysteresis rules were based on observations of cycle plots. Due to the procedure used in the load-displacement program,

only full or complete cycles were applied, no partial cycles or small amplitude cycles were considered. Therefore, rules associated with small amplitude cycles were based on definitions proposed for reinforced concrete models, specifically Takeda's model (9) and Ozcebe et al. model (45). Additionally, typical errors made in the hysteresis rule definitions as explained by Ridell and Newmark (4) were considered in defining the rules for the proposed model. Rules for large and small amplitude cycles are shown in Figure 40. Definition of those hysteresis rules follows.

The most significant characteristics of the model were: The envelope curve was defined by the peak force and peak displacement and included the effect of deck shape, gravity load, and axial stiffness ratio. Strength degradation was considered as function of number of cycles and other parameters (see Section 3.3.6.5). Cyclic curve or hysteresis curve was defined through a series of characteristic slopes and pinch force, which were found to be function of the amount of deformation and other parameters (see Sections 3.3.7.2 and 3.3.7.3). A series of rules to describe the hysteresis curve follows.

The following definitions apply:

- Loading: Increasing the force in one direction
- Unloading: decreasing the force in one direction
- Load reversal: Change of force sign in the same step
- Reloading: Increasing the force in one direction after being unloading it in the same direction

® **RULE 1**

Loading: follows the envelope according to:

$e \le e_p$ $$\frac{F(e)}{F_p} = \left[1 + \alpha \ln\left(\frac{e}{e_p}\right)\right]\xi \qquad [3\text{-}68]$$

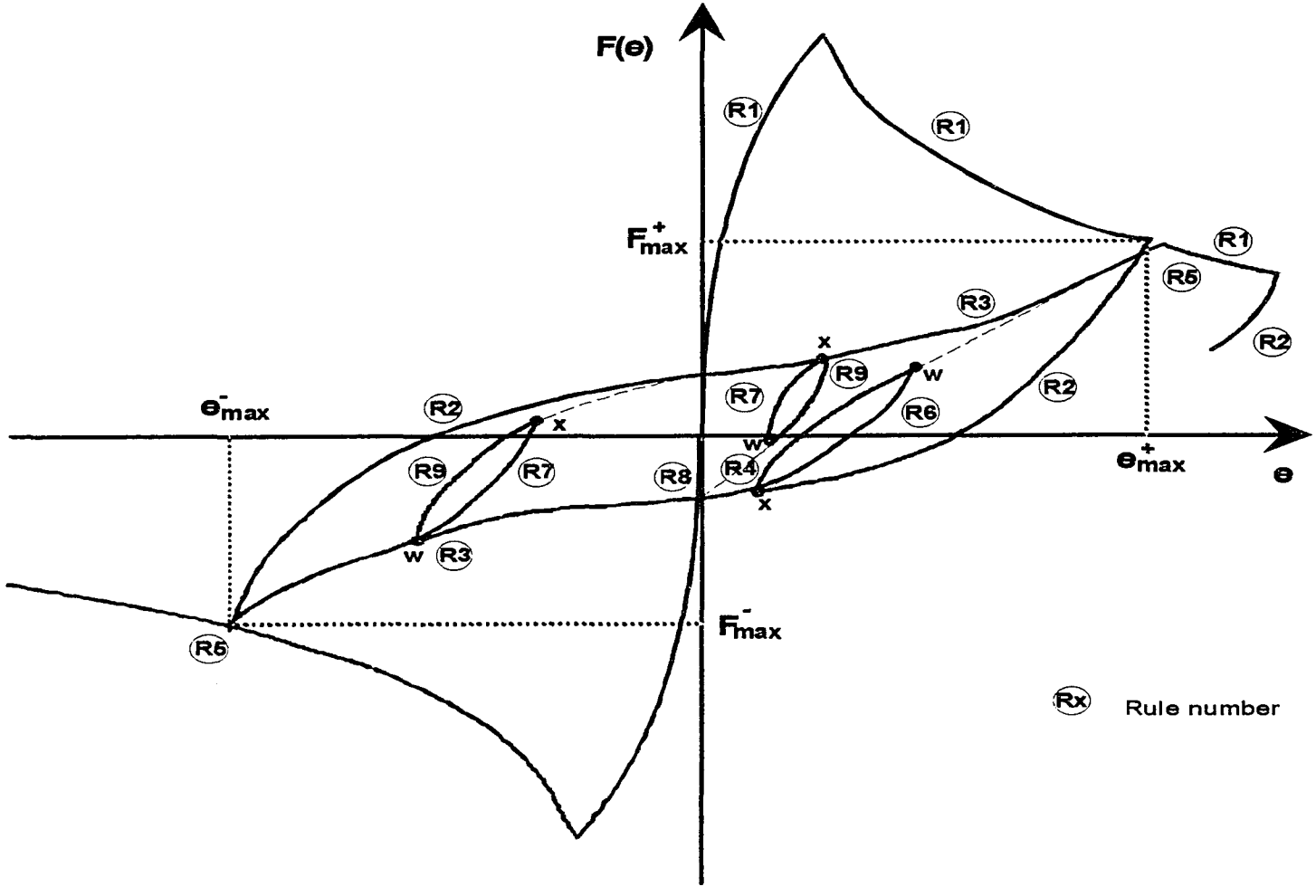

Figure 40. Hysteresis rules definition

$$e > e_p \qquad \frac{F(e)}{F_p} = \left[1 + \beta \ln\left(\frac{e}{e_p}\right)\right]\xi \qquad [3\text{-}69]$$

for small displacements, the envelope is defined by a straight line as follows:

$$\text{if } e \le 2e_p e^{-1/\alpha} \text{ then } F(e) = \frac{\xi[\alpha \ln 2]F_p e}{2e_p e^{-1/\alpha}} \qquad [3\text{-}70]$$

if $|e| \ge |e_{max}|$ then: GO TO RULE 1

if $|e| \le |e_{max}|$ then:: GO TO RULE 2

® **RULE 2**

Unloading (and load reversal if needed) follows a path toward the pinch force point described by a polynomial expression as follows:

if $|e| \le |e_p|$ then:

use constant set defined by Eqns. [3-65] or [3-67] according with the sign of the actual displacement.

if $|e| \ge |e_p|$ then:

use a second order polynomial expression. The set of constants for the case of positive displacement are:

$$F(e) = A + Be + Ce^2$$

$$A = F_0^+$$

$$B = \frac{\left[-K^+ e_{max}^+ + 2\left(F_{max}^+ - F_0^+\right)\right]}{e_{max}^+} \qquad [3\text{-}71]$$

$$C = \frac{\left[K_2^+ e_{max}^+ - \left(F_{max}^+ - F_0^+\right)\right]}{e_{max}^{+\,2}}$$

additionally, if a minimum or maximum is introduced, then use a straight line joining

the point of intersection of the cuadratic expression with x axis and the pinch point.

if $|e| \leq |e_{previous}|$ then: GO TO RULE 2

if $|e| \geq |e_{previous}|$ then: GO TO RULE 4

and

if $e \geq 0$ and $e_{previous} \leq 0$, or $e \leq 0$ and $e_{previous} \geq 0$ then GO TO RULE 8 (If first excursion in such direction) otherwise GO TO RULE 3

® **RULE 3**

This rule describes the reloading process. The path is defined by a third order polynomial expression with constants defined by [3-64] or [3-66] according with the sign of the actual displacement. All the times the force values has to be in the range defined by the pinch force and the maximum force. Additionally, to eliminate any inflection point in the path, a limiting value of the pinching characteristic slope is defined as follows:

$$K_0 \leq \frac{F_{\max} - F_0}{e_{\max}} \qquad [3\text{-}72]$$

if $|e| \geq |e_{\max}|$ then GO TO RULE 5

if $|e| \leq |e_{previous}|$ then GO TO RULE 9

if $|e| \geq |e_{previous}|$ then GO TO RULE 3

® **RULE 4**

This rule describes the reloading after partial unloading (partial cycle). A second order polynomial expression is used with the following coefficients (the signs associated to coefficients are introduced according with the sign of the actual displacement):

$$A = \frac{\left[F_x e_{\max}^2 + F_{\max}\left(e_x^2 - 2e_x e_{\max}\right) + K_1 e_x\left(e_{\max}^2 - e_x e_{\max}\right)\right]}{\left(e_x - e_{\max}\right)^2}$$

$$B = \frac{\left[-2e_{\max}\left(F_x - F_{\max}\right) + K_1\left(e_x^2 - e_{\max}^2\right)\right]}{\left(e_x - e_{\max}\right)^2} \qquad [3\text{-}73]$$

$$C = \frac{\left[F_x - F_{\max} - K_1\left(e_x - e_{\max}\right)\right]}{\left(e_x - e_{\max}\right)^2}$$

if $e \le 0$ and $e_{previous} \ge 0$ then GO TO RULE 3

if $e \ge 0$ and $e_{previous} \le 0$ then GO TO RULE 3

if $|e| \ge |e_{\max}|$ then GO TO RULE 1

if $|e| \le |e_{previous}|$ then GO TO RULE 6

if $|e| \ge |e_{previous}|$ then GO TO RULE 4

® **RULE 5**

Loading after reaching the maximum attached displacement in that direction follows a straight line until the envelope force-displacement path is reached:

$e > 0$ (starts from the upper end of 1st quarter cycle)

$$F(e) = F_{\max}^{+} + K_{1virgin}^{+}\left(e - e_{\max}^{+}\right) \qquad [3\text{-}74]$$

loading with $|F(e)| < |F(e)_{envelope}|$: GO TO RULE 5

loading with $|F(e)| \geq |F(e)_{envelope}|$: GO TO RULE 1

unloading ($|e| \leq |e_{previous}|$): set maximum associated force and displacement, GO TO RULE 2

$e < 0$ (starts from the lower end of the 3rd quarter cycle)

$$F(e) = F^{-}_{\max} + K^{-}_{1virgin}(e - e^{-}_{\max}) \qquad [3\text{-}75]$$

loading with $|F(e)| < |F(e)_{envelope}|$: GO TO RULE 5

loading with $|F(e)| \geq |F(e)_{envelope}|$: GO TO RULE 1

unloading($|e| \leq |e_{previous}|$): set maximum associated force and displacement, GO TO RULE 2

® **RULE 6 and 7**

Unloading after reloading in the same direction follows a second order polynomial from the point where unloading started (w point) toward the last point (point x) in the respective quarter cycle segment. The only difference between rules six and seven is that rule six is directed toward the first or third quarter cycle segment. Rule seven is directed toward the second or fourth quarter cycle segment. The coefficients describing the polynomial expression are presented in a general form, sign associated to the different parameters are selected according with the sign of the current displacement.

$$F(e) = a + be + ce^2$$

where:

$$A = \frac{\left[F_x e_w (e_e - 2e_x) + F_w e_x^2 + K_x e_x e_w (e_x - e_w)\right]}{(e_x - e_w)^2}$$

$$B = \frac{\left[2e_x (F_x - F_w) - K_x (e_x^2 - e_w^2)\right]}{(e_x - e_w)^2} \qquad [3\text{-}76]$$

$$C = \frac{\left[F_w - F_x + K_x (e_x - e_w)\right]}{(e_x - e_w)^2}$$

For Rule 6:

if $|e| \geq |e_{previous}|$ then GO TO RULE 4

if $|e| \leq |e_x|$ then GO TO RULE 2

if $|e_x| \leq |e| \leq |e_w|$ then GO TO RULE 6

For Rule 7:

if $|e| \leq |e_{previous}|$ then GO TO RULE 9

if $|e| \geq |e_x|$ then GO TO RULE 3

if $|e_w| \leq |e| \leq |e_x|$ then GO TO RULE 7

® **RULE 8**

This rule describes the first displacement incursion in the opposite direction. A straight line is used to join the pinch force point (zero displacement point) and the envelope curve.

$$F(e) = A + Be$$

when coming from second quarter cycle:

$$A = F_0^+$$

$$B = K_0^+ \qquad [3\text{-}77A]$$

when coming from fourth quarter cycle:

$$A = F_0^-$$

$$B = K_0^- \qquad \text{[3-77B]}$$

if $|e| \le |e_{previous}|$ then GO TO RULE 4

if $|e| \ge |e_{previous}|$ then GO TO RULE 8

® **RULE 9**

This rule describe the path for unloading after loading under the first or third quarter cycle segment. A second order polynomial expression is used to describe the cycle path which joins the last point on the quarter cycle segment (point x) and the pinch force point. The coefficients describing such a path are as follows(signs of different parameters are selected according with the sign of the current displacement):

$$F(e) = A + Be + Ce^2$$

$$A = F_0$$

$$B = K_0 \qquad \text{[3-78]}$$

$$C = \frac{\left[(F_x - F_0) - K_0 e_x\right]}{e_x^2}$$

if $e \le 0$ and $e_{previous} \ge 0$ or $e \ge 0$ and $e_{previous} \le 0$ then GO TO RULE 3

if $|e| \ge |e_{previous}|$ then GO TO RULE 6

otherwise GO TO RULE 9

3.4 Analytical Method

3.4.1 Introduction

The definition of the diaphragm envelope curve using the statistical method presented in Section 3.3 was based on the previous knowledge of the diaphragm peak load and displacement at peak load. The force-displacement characteristics may be evaluated approximately by scaling the experimental values using scale factors based on length ratios as proposed by Ewing et al. (117), or by an analytical approach based on equilibrium and compatibilty considerations (33,71,89).

The definition of the envelope force-displacement relationship of SDRC diaphragms by analytical means consists in the prediction of the force and respective displacement using stress-strain material relationships, compatibility conditions, as well as equilibrium equations. Such definition of the envelope curve is usually determined by assuming a monothonic loading procedure. Next section presents a review of the approaches used in describing the force-displacement envelope curve for diaphragms.

3.4.2 Review of previous work

The modelling of structural elements may be approached through micro- or macro-modelling as was mentioned in Section 2.3. Usually the macro modelling approach is used for the analysis of a complete structure, but the properties definition of its elements are based on a micro-modelling. Micro modelling includes techniques such as finite element analysis and fiber model analysis. For the evaluation of the force-displacement envelope curve of diaphragms, two of the most used approaches reported in the literature are: the finite element approach (71,89), and the beam approach or fiber model analysis (42,71).

A prediction of the SDRC envelope curve using finite element analysis was presented by Porter and Easterling (89). The basic philosophy used to modelate the diaphragm was similar to that previously developed by Porter and Greimann (78). A two-dimensional analysis was used, since in-plane loading effects as well as excentricity of the applied load were assumed to have minimal influence. Diaphragms were modelled using beam elements, plate elements, and spring elements. Beam elements were used to model the supporting steel frame. Four node isoparametric plane stress finite elements were used to model the concrete as well as the steel deck . The steel deck was modelled as an orthotropic material because the presence of the corrugated profile. Spring elements were used to model the edge fasteners as well as the interface between concrete and steel deck. Nonlinearity effects were considered in modelling fasteners and deck-to-concrete interface. Perimeter supporting steel beams, concrete and steel deck were assumed to behave linearly elastic. The concrete was assumed to behave linearly elastic because the model was intended to reproduce the edge connection failure and shear transfer failure which developed little or none cracking state.

Nakashima et al. (71) used a 2D plane stress nonlinear finite element model to simulate the in-plane behavior of reinforced concrete diaphragms. A four node isoparametric quadrilateral element was used. Material nonlinearities of concrete and steel were considered. The reinforcing steel was considered as an orthrotropic material with bi-linear stress strain relationship. Effect of bond slip was neglected. A comparison of the predicted behavior versus results of three floor panels tested showed good accuracy of the model to predict satisfactorily the diaphragm behavior.

Porter and Greimann (78) at Iowa State University developed analytical expressions to evaluate the initial stiffness and strength of steel deck reinforced concrete diaphragms. The initial stiffness equation was developed by modelling the diaphragm as

a deep beam with the steel supporting frame forming the flanges and the steel deck and concrete forming the web. Ultimate strength equations were determined by considering three failure modes, which were diagonal tension mode, edge connector mode and shear transfer mechanism mode. Both sets of equations were in part based on the edge zone concept proposed by the authors. The edge zone concept recognized that for those diaphragms without positive shear transfer devices, such as studs, the shear force must be transferred through the deck concrete interface.

Nakashima et al. (71) used a deep beam analogy to evaluate the initial in-plane stiffness as well as the inelastic in-plane stiffness of reinforced concrete diaphragms. The total deflection was considered to be built by the flexural and shear contributions. For the initial in-plane analysis, the effective moment of inertia value was found to be very close to the nominal moment of inertia of the diaphragm regardless of the moment-to-shear ratio or the relative beam size. The effective shear area was found to be affected for such variables, but an effective shear area evaluated in the cross sectional area of the panel without edge beams represent well the shear area. For the inelastic in-plane behavior an attempt to use the deep beam analogy was made. The stiffness degradation was considered by evaluating an equivalent flexural stiffness and equivalent shear stiffness. Using experimental and analytical results the flexural and shear deflections were plotted. From this plot was found that the proportion in relative deflection remained approximately the same regardless of the load level for all the examined panels. Based on this finding, the authors stated that the flexural and shear stiffness degrade proportionally independently of the loading and support conditions, or the load level.

Reinhorn et al. (42) used a generalized fiber model analysis to evaluate the moment-curvature and the force-displacement envelope curve of reinforced concrete diaphragms. Via this approach, the diaphragm cross section was sub-divided into a

number of parts depending on the variation of reinforcement or the appearance of longitudinal beams. Each part was then additionally subdivided into fibers for a monothonic loading analysis. Equilibrium and strain compatibility conditions were applied through an iterative process until the equilibrium was satisfied and then the moment and curvature were evaluated. Results of this analytical beam approach was favorable compared with available experimental reinforced concrete diaphragm tests (71).

The use of strain compatibility analysis in a similar procedure to that used for beams and columns in the evaluation of moment-curvature curve or ultimate moment capacity of reinforced concrete shear walls has been widely used (75, 101, 109). Cardenas et al. (109) derived an equation for the moment capacity of reinforced concrete walls with uniformly distributed vertical steel. Such equation was obtained by assuming a linear strain distribution and evaluating the compressive concrete forces using the rectangular block approximation.

The analytical model based on finite element approach used by Porter and Easterling (89) showed its accuracy by duplicating the pre-peak experimental load versus deflection curve satisfactorily, but the model was oriented to predict force-displacement relationships for those failure modes without limiting crack development, therefore the diagonal tension mode of failure was not included. To include the diagonal tension mode of failure in the finite element formulation presented by Porter and Easterling, nonlinearity of concrete and steel elements in addition to that due to edge connectors and interface elements has to be considered. An alternate and more simple procedure to include the nonlinear effects of steel and concrete in the response of SDRC diaphragms is the fiber model analysis or strain compatibility analysis. Such approach modified to include the effect of interfacial slip as well as the effect of edge connectors is presented in the next sections.

3.4.3 Fiber model approach

3.4.3.1 Basic considerations The analytical definition of the pre-peak envelope curve may be used for the evaluation of the peak load and associated displacement needed for the statistical definition of the envelope, or may be used instead of the statistical envelope in the analysis. Additionally, the analytical approach may also be used to generate the moment-curvature curves for interior and end diaphragm sections required for the structural analysis.

The procedure used in the fiber model approach to evaluate the force-displacement envelope curve of a SDRC diaphragm consisted in the division of the diaphragm element in a serie of flexural-shear spring sub-elements (see Figure 41). An specific moment-curvature relationship was assigned to each subelement. A monothonic loading procedure was used and for each increment of load, the flexural moment acting on each subelement was evaluated. Using the moment-curvature relationship the associated curvature for each subelement was determined. By integrating the curvatures of each subelement the flexural component of deflection was then evaluated. Such flexural component of deflection had implicitly the effects of the flexibility of edge connections and the flexibility due to concrete-steel deck interface. The shear component of deflection was obtained by keeping the relative proportion between flexural and shear deflection, that is by assuming that the flexural and shear stiffnesses degrade proportionally independently of the load level as suggested for reinforced concrete diaphragms by Nakashima et al. (71).

The evaluation of the moment-curvature relationship for an specific diaphragm cross section was made following the same fiber model analysis used for RC diaphragms by Reinhorn et al. (42). This procedure was also similar to the strain compatibility analysis

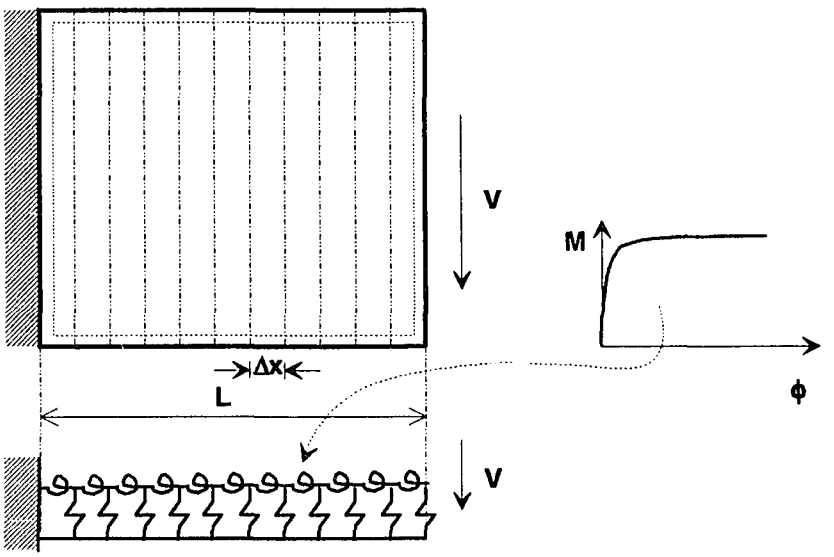

Figure 41. Discretization of a diaphragm in sub-elements

used in reinforced concrete shear walls (75,101,109). That is, a strain compatibility analysis was applied to the diaphragm cross section which was sub-divided into a serie of subelements or fibers formed by segments of steel deck, concrete, interface, edge connectors, and edge framing beams. The interface and concrete elements were assumed to act as springs in series. Similarly, the edge connection and edge framing beam were assumed to be in series. Nonlinear properties were considered not only for the edge connection and interface element but also for the concrete, steel deck and framing edge beam.

3.4.3.2 Assumptions In order to evaluate the moment-curvature relationship of SDRC diaphragms, the following assumptions were made:

- Initially plane sections remain plane after bending. For beams with large depth to span ratios (deep beams) a significant departure from a linear strain profile

may occur. Smith et al. (110) showed that the type of loading and support conditions play an important role in the distribution of the strain profile through the beam depth. Beams with load transmitted by shear and with reactions applied to the sides showed close to linear stress profile through the depth.

- The shear component of deflection is evaluated assuming that the flexural and shear stiffnesses degrade proportionally independently of the load level as suggested for reinforced concrete diaphragms by Nakashima et al. (71).
- Slip between concrete and steel deck is included in the strain compatibility analysis. Slip effects are included through a ficticious interface element modelled as a spring with nonlinear characteristics as proposed by Prins (76) and later modified by Easterling (29).
- Concrete in compression follows a parabolic stress-strain distribution. Concrete tension stress-strain distribution is assumed linear and ignored after cracking.
- The steel deck stress-strain characteristics is idealized as a trilinear material including elastic, plastic and strain-hardening effect.
- Studs and arc spot welds are modelled as springs with nonlinear characteristics using the available information summarized by Porter and Easterling (89).

3.4.3.3 Material model

3.4.3.3.1 Concrete and steel Concrete was assumed to follow a parabolic stress-strain distribution under compression stress and a linear distribution under tension stress as shown in Figure 42a. Stress-strain relationship for steel beams and steel-deck were modelled with a trilinear distribution that includes elastic, plastic and strain-hardening stages as shown in Figure 42b. Analytical expressions for the mentioned

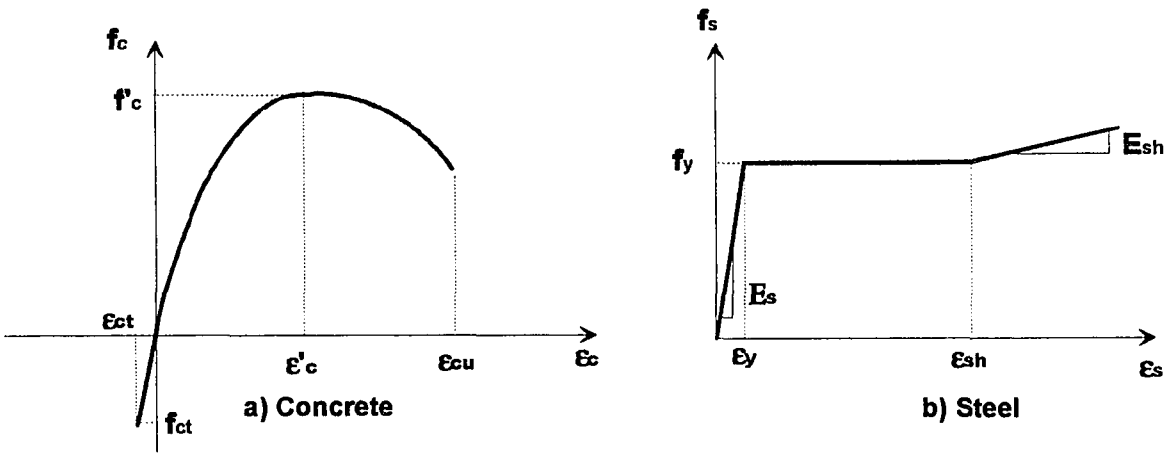

Figure 42. Stress-strain relationships. a) Concrete, b) Steel

stress-strain relationships are presented as Equations [4-49] and [4-50] in Section 4.4.3.2.

The steel deck had a corrugated profile, but for analysis purposes was assumed unifomly distributed with a constant thickness given by:

$$t_{se} = t_s \frac{d}{s} \qquad [3\text{-}79]$$

where:

t_{se}: equivalent steel deck thickness

t_s: steel sheet thickness

d: corrugation spacing

s: total length of deck (perimeter) per corrugation

Concrete was also considered with an equivalent thickness. The thickness used was the average thickness including the trapezoidal shape of the filled deck.

3.4.3.3.2 Edge fasteners Two types of edge fasteners were used in the study: headed shear studs and arc spot welds. For analysis purposes both types of fasteners were used similarly. Only the analytical model describing each type was different. All fasteners on each side were considered to be uniformly distributed on the side and acting in parallel. Therefore, the initial stiffness and peak load of an individual fastener was multiplied by the ratio of total number of fasteners on the side to the length of the side, and finally multiplied by the segment width Δx (or Δy) of the interior or end segment analyzed. Additionally, the strength of individual fasteners were modified to consider the perpendicular vector of forces result of shear and bending. Thus the assumption was made that those fasteners located at sides parallel to the direction of loading were subjected to perpendicular forces; a vertical component due to shear and a horizontal component due to bending. Meanwhile the edge fasteners located at the edges perpendicular to the loading direction were assumed to be subjected only to horizontal component of forces due to bending. Fasteners subjected to perpendicular components of forces were assumed to have a maximum force acting at 45°, therefore the strength of individual fasteners was multiplied by 0.7071. Similar approach was used by Porter and Easterling (89) to define the strength capacity of SDRC diaphragms based on fastener failure.

Headed shear studs were modeled using an empirical stud load-displacement curve proposed by Ollgaard et al. (105). The empirical expression was given by

$$Q = Q_{sol}\left(1 - e^{-18\Delta}\right)^{2/5} \qquad [3\text{-}80]$$

where:

Q: load on stud connector

Q_{sol}: strength of a stud connector embedded in a solid slab

Δ: displacement

The strength of a stud connector embedded in a solid slab was evaluated using also an empirical expression proposed by the same authors (105):

$$Q_{sol} = 0.00666 A_{st} f_c'^{0.3} E_c^{0.44} \quad [3\text{-}81]$$

where:

A_{st}: cross-sectional area of a stud (in^2)

f_c': concrete compressive strength (psi)

E_c: concrete modulus of elasticity (psi)

The strength of a stud connector embedded in a solid slab Q_{sol} may need to be reduced due to different effects such as edge distance, deck orientation, stud length, number of studs per rib, effects of rib height and width. Equations used to modify Q_{sol} due to the mentioned effects are presented in References (111,112).

The general information regarding the load-displacement behavior of arc spot welds was to some extent limited. A summary of most of the available information on arc spot welds was presented by Easterling (29). Based on such information Easterling constructed analytical weld curves formed by a series of linear segments.

In order to facilitate the evaluation of force-displacement characteristics for arc spot welds, a regression model was suggested in this work. A regression analysis was applied to the force-displacement data points proposed by Easterling. A second order polynomial equation produced the best fit, but such equation predicted a maximum before the peak load, therefore other nonlinear models were investigated. The double reciprocal model as presented in Table 3 produced excellent results, since the determination coefficient for all the data sets were over 0.99. Such model was compared against other empirical model (exponential type) presented in Reference (112) for the load-displacement curve of fillet

welds. The exponential model from Reference (112) obtained also excellent results but the variability of the regression coefficients from one data set to other was considerably large. Therefore, the double reciprocal model was used as a base to predict force-displacement behavior of arc spot weld data from Reference (29). The proposed model was

$$F_w = \frac{\Delta}{a + b\Delta} \leq F_{wp} \qquad [3\text{-}82]$$

where:

F_w: weld force

F_{wp}: peak weld force

Δ: displacement

a,b: constants

Constants a and b were defined by satisfying the following boundary conditions:

$$\text{at } \Delta = 0, \ \frac{dF_w}{d\Delta} = K_w, \ \text{therefore } a = \frac{1}{K_w} \qquad [3\text{-}83]$$

$$\text{at } \Delta = \Delta_p, \ F_w = F_{wp}, \ \text{therefore } b = \frac{1}{F_{wp}} - \frac{1}{K_w \Delta_p} \qquad [3\text{-}84]$$

where:

Δ_p: weld displacement at the peak

K_w: elastic weld stiffness

The AISI (113) was used to evaluate the peak weld force F_w of arc spot welds according to the smaller of:

$$F_{wp} = 0.625 d_e^2 F_{xx} \qquad [3\text{-}85]$$

or one of the following

$$\text{if } \frac{d_a}{t} \leq 0.815\sqrt{\frac{E}{F_u}} \ \text{ then } \ F_{wp} = 2.20 t d_a F_u \qquad [3\text{-}86]$$

$$\text{if } 0.815\sqrt{\frac{E}{F_u}} < \frac{d_a}{t} < 1.397\sqrt{\frac{E}{F_u}} \text{ then } F_{wp} = 0.280\left(1+\frac{5.59t\sqrt{E}}{d_a\sqrt{F_u}}\right)td_aF_u \quad [3\text{-}87]$$

$$\text{if } \frac{d_a}{t} > 1.397\sqrt{\frac{E}{F_u}} \text{ then } F_{wp} = 1.40td_aF_u \quad [3\text{-}88]$$

where

d: weld diamter (in.)

d_a: average diameter of arc spot weld at mid-thickness (d-t for single sheet, d-2t for double sheet) (in.)

d_e: effective diameter of fused area $= 0.7d - 1.5t \leq 0.55d$ (in.)

t: thicness of sheet (in.)

F_u: ultimate strength of sheet (ksi)

F_{xx}: AWS weld designation strength (ksi)

E: 29500 (ksi)

Few references only were found in the literature regarding elastic stiffness of arc spot welds. Davies and Bryan (114) suggest a nominal flexibility value of 0.01 mm/KN which results in a nominal stiffness value of 571 Kip/in. Lutrell (115) proposed the follwing expression to evaluate the flexibility of 5/8" diameter arc spot welds:

$$S_f = \frac{1.15x10^{-3}}{\sqrt{t}} \quad [3\text{-}89]$$

therefore the stiffness expression is given by

$$K_w = 870\sqrt{t} \quad [3\text{-}90]$$

where

S_f: arc spot weld flexibility (in./kip)

t: sheet thickness (in.)

Equation [3-89] was used to evaluate the weld stiffness but a lower bound of 571 Kip/in as suggested by Davies and Bryan (114) was imposed to the expression. Based on the weld data plots from Reference (29), weld displacement at the peak load was arbitrarily defined to be given by $2F_{wp}/K_w$. After the peak weld force was reached, a series of straight lines, similarly to those from Easterling (29) model, were used to define the weld force-displacement. Figure 43 shows a typical force-displacement curve for arc spot weld.

3.4.3.3.3 Deck-to-concrete interface Deck-to-concrete interface was described by Prins (76) using a load displacement relationship shown in Figure 44. Such relationship was arbitrarily defined, but influenced by the behavior of elemental test results (see Appendix A for a summary of elemental test used). Easterling (29) modified slightly the relationship proposed by Prins by including a third segment on the curve as shown in

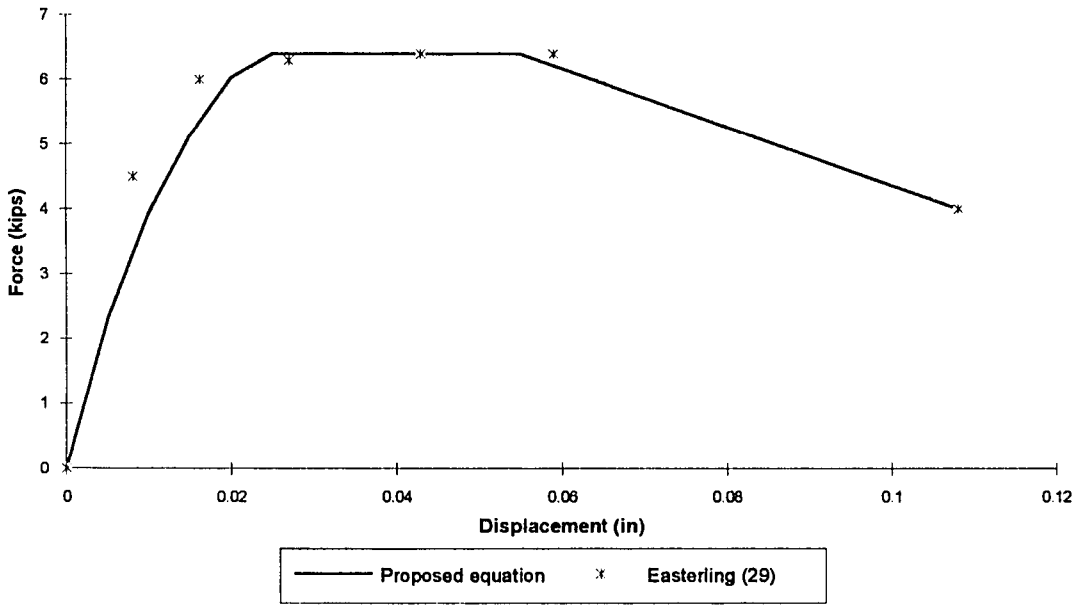

Figure 43. Typical arc spot weld force-displacement curve

Figure 44. It was emphasized by Easterling (29) that "the relationships used to modelate the concrete-deck interface were very approximate. The elemental tests were not designed to yield load vs. displacement information of the type that was required for the finite element analysis."

The approximate force displacement relationship modified by Easterling (29) as shown in Figure 44 was used in this work.

3.4.3.4 Methodology

3.4.3.4.1 Moment-curvature relationship The moment curvature relationship was evaluated at all sections associated with a change in reinforcement, distribution of edge fasteners, or any change that can modify such relationship. For the SDRC diaphragms there were two sections to analyze: a typical interior section, and an end section. Interior section was considered to be formed by the steel deck, concrete, deck-to-concrete interface elements, edge fasteners and edge supporting steel beam. The end section had additionally the back edge fasteners.

To obtain the moment curvature relationship the SDRC diaphragm was segmented. First, the diaphragm was sectioned in the longitudinal direction (orthogonal to loading direction) by a series of segments of length Δx identified as end or interior segment. Second, for a particular segment, a new discretization was made through the segment depth and fibers or subelements of size Δy were identified. Figure 45 shows both types of discretization. Once the sections were discretized a strain compatibility step-by-step analysis similar to that described in Section 4.4.3.2 was used to evaluate the moment-curvature relationship. The process started by aplying a linear strain distribution on the

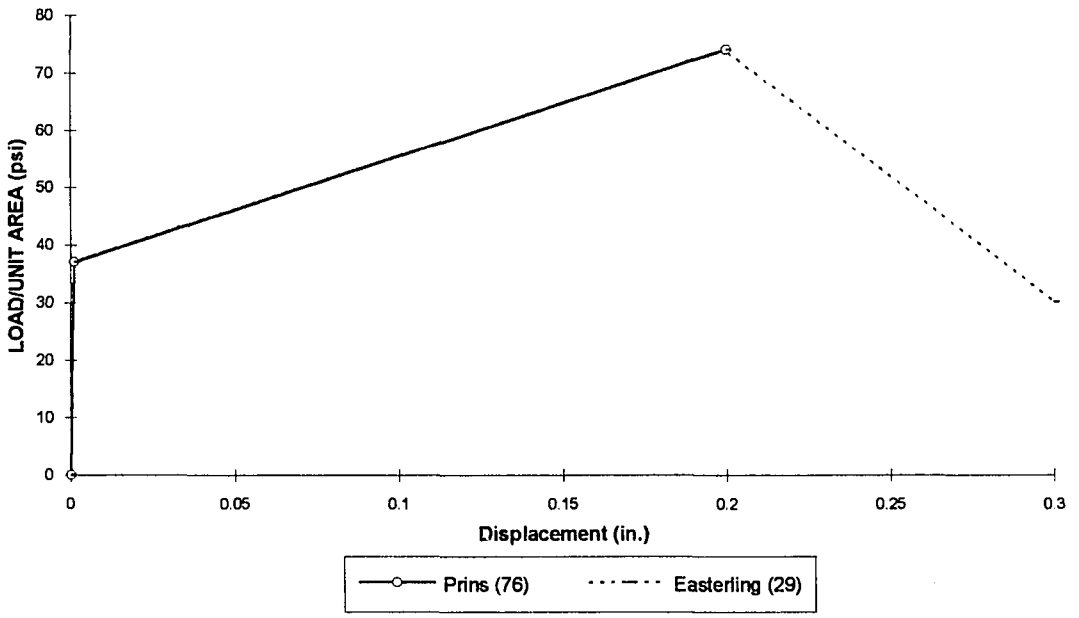

Figure 44. Deck-to-concrete interface (modified from reference 29)

steel deck. Such distribution was defined by the maximum strain at top and bottom. Based on the proposed strain distribution, the strain at each fiber or subelement was evaluated, and the corresponding segment displacement and force (see Figure 46). Next a verification of the longitudinal equilibrium of forces was made; if equilibrium had not be accomplished, a new value for the bottom strain was defined and a new cycle started again. Once the longitudinal equilibrium had been accomplished, the strains at top and bottom were used to define the curvature, and the fiber forces were used to evaluate the bending moment.

For each assumed strain, an iterative procedure was applied on each subelement of the section to find the strain distribution. There was a difference in the process when applied to an interior or end sections. For an interior section, the linear strain distribution

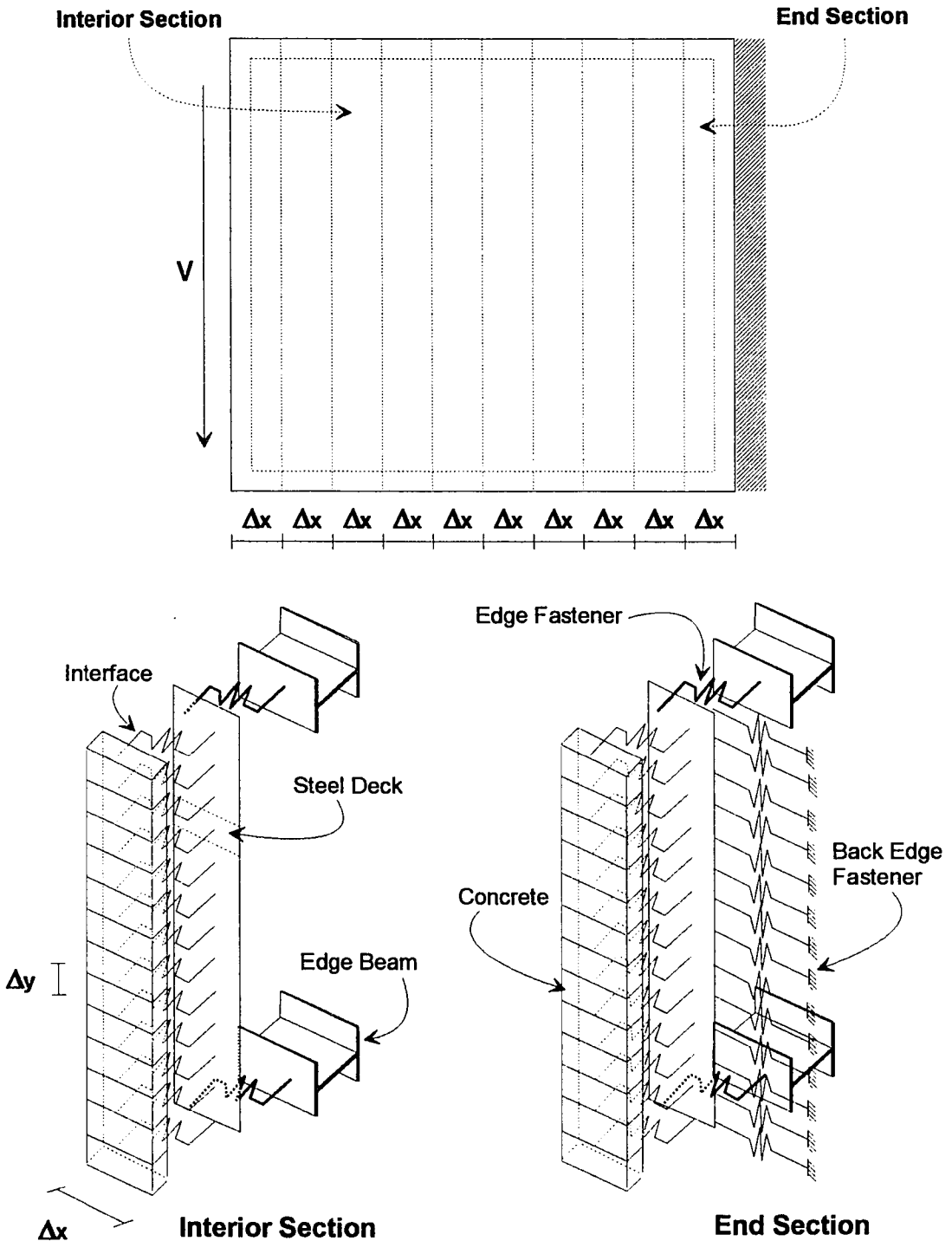

Figure 45. Diaphragm interior and end section

was assumed to be applied on the steel deck, therefore strains, stresses and forces on the deck were evaluated. Next the interface and concrete elements were considered to act as spring in series subjected to a total strain given by the corresponding deck element strain. The Newton-Raphson method was applied to find the distribution of deformation and the force acting on the subelements. Similarly, the edge connector and edge steel beam were assumed to act as springs in series, therefore, an iterative process was applied to find the distribution of deformation as well as the force acting on them.

For an end section, the assumed strain distribution was applied on the steel deck and back edge fasteners which were assumed to be acting as spring in series. An iterative process was applied to distribute the strains and to evaluate the force acting on them. Once the strain on each subelement of the deck was defined, the process continued similarly to that described for an interior section.

3.4.3.4.2 Force-displacement relationship Force-displacement envelope curves for pre-peak region of SDRC diaphragms were obtained by adding the flexural and shear components of deflection. The flexural component of deflection which also included the edge connector flexibility as well as the interface flexibility effect was evaluated through the use of the moment-curvature relationship. Next the shear component of deflection was obtained by assuming proportional degradation of flexural and shear stiffnesses independently of the loading level, as suggested by Nakashima for reinforced concrete diaphragms (71).

The procedure used to evaluate the flexural component of deflection started with the evaluation of the moment-curvature relationship for all the different diaphragm sections (interior and end sections) according to the methodology presented in Section 3.4.3.4.1. Next, assuming a monothonic loading procedure, the diaphragm was subjected to a serie

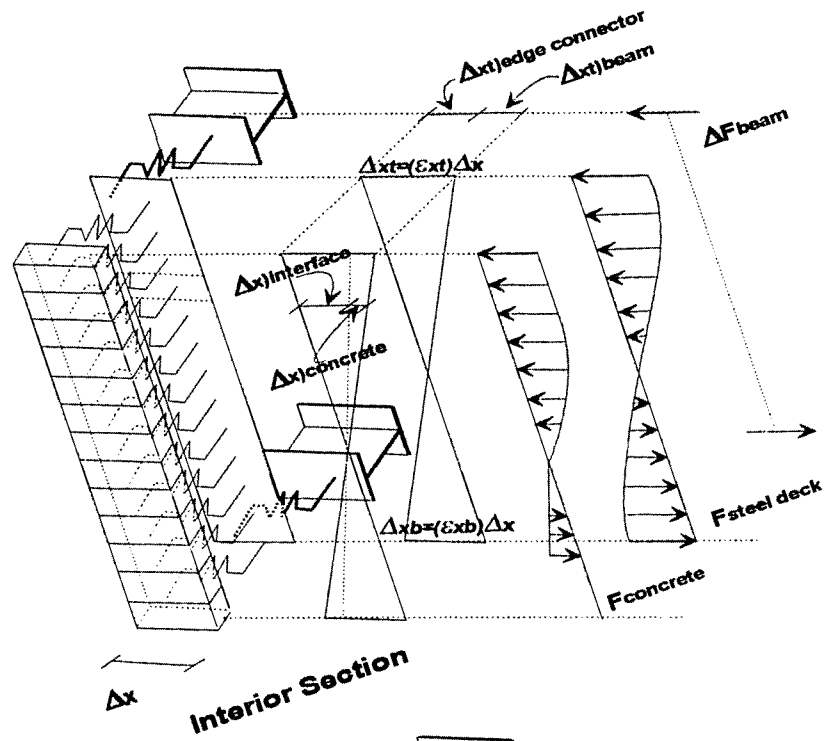

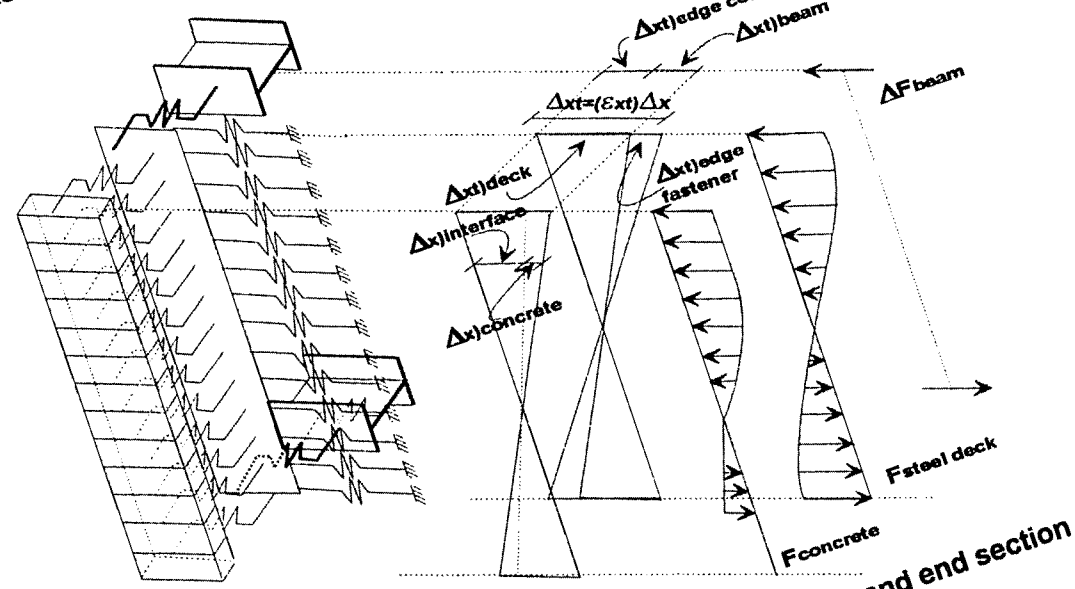

Figure 46. Typical force-deformation acting on an interior and end section

of loads, one at the time. For each load, the bending moment at each segment location was evaluated. Using the respective moment-curvature relationship, the associated curvature was obtained. According to Figure 47, the flexural moment acting on a segment at any distance x from the end was given by:

$$M_x = V(L - x) - \sum_{j=1}^{i-1} \Delta F_j h \qquad [3\text{-}91]$$

where:

M_x: Flexural moment

V: Shear force

L: Diaphragm span

x: distance from the diaphragm end to any segment

h: diaphragm depth

ΔF_j: increment of axial force on supporting beam at any diaphragm segment

Once the curvature was evaluated at each segment location, the flexural component of deflection was evaluated by integration as follows:

$$\delta_f = \sum_{i=1}^{n} \phi_i (L - x_i) \Delta x_i \qquad [3\text{-}92]$$

where:

δ_f: flexural component of deflection

ϕ_i: curvature at segment i

Δx_i: segment length

x_i: ith segment position

The shear component of deflection was evaluated assuming proportional degradation of flexural and shear stiffnesses independently of the loading level.

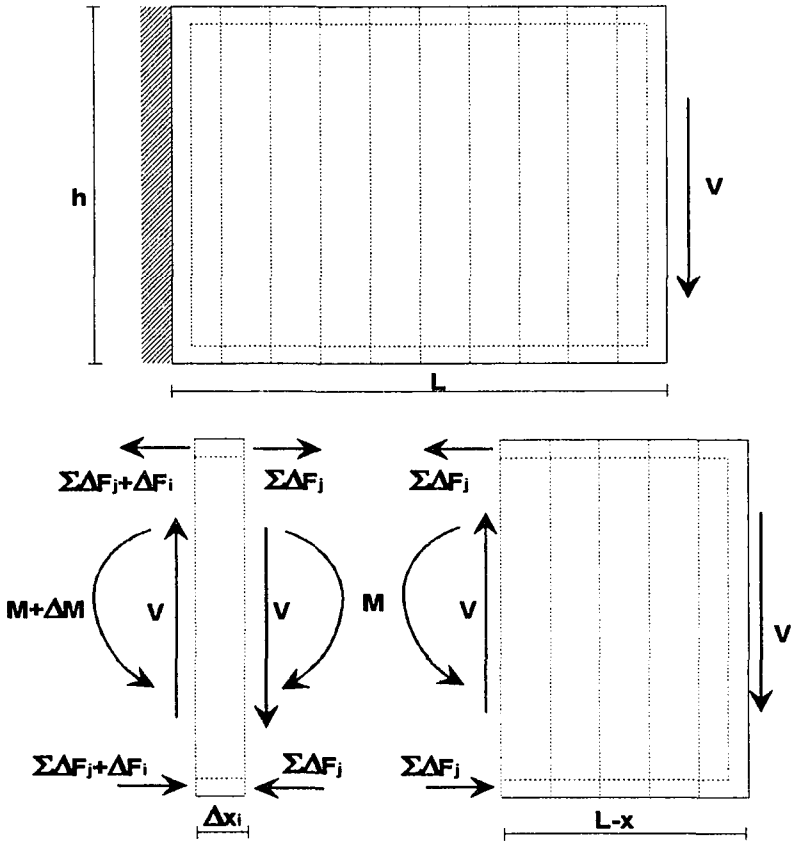

Figure 47. Acting moment on a diaphragm segment

Nakashima et al. (71) found that for RC diaphragms, the proportion of shear deflection to total deflection remained approximately constant regardless the load level. Based on this criteria, the ratio of components of deflection was evaluated as follows:

$$\frac{\delta_v}{\delta_{total}} = \frac{\delta_v}{\delta_v + \delta_f} = \kappa = \text{ constant} \qquad [3\text{-}93]$$

The components of deflection under elastic stage were evaluated as follows:

$$\delta_v = \frac{VL}{A_e G} = \frac{VL}{\frac{A_e E}{2(1+\mu)}} = \frac{2VL(1+\mu)}{A_e E} \qquad [3\text{-}94]$$

$$\delta_f = \frac{VL^3}{3EI} \qquad [3\text{-}95]$$

Substituting Equations [3-94] and [3-95] into [3-93]

$$\delta_v = \frac{\kappa\delta_f}{1-\kappa} = \kappa_v\delta_f \quad \text{where} \quad \kappa = \frac{1}{1+\dfrac{A_eL^2}{6I(1+\mu)}} \qquad [3\text{-}96]$$

Nakashima suggested that the effective shear area evaluated with the cross sectional area of the panel without edge beams represented well the shear area. Therefore assuming that only the web was effective:

$$\kappa = \frac{1}{1+\dfrac{(t_c+nt_{se})hL^2}{6(t_c+nt_{se})\dfrac{h^3}{12}(1+\mu)}} \qquad [3\text{-}97]$$

By simplifying Equation [3-97], the ratio κ_v between components of deflections was

$$\delta_v = \kappa_v\delta_f \quad \text{where} \quad \kappa_v = \frac{h^2(1+\mu)}{2L^2} \qquad [3\text{-}98]$$

where

δ_v: shear component of deflection

δ_f: flexure component of deflection

κ_v: ratio of shear to flexural component of deflection

μ: poisson ratio

h: diaphragm depth

L: diaphragm span

3.4.3.5 Application and verification of the model

3.4.3.5.1 General The main objective of the proposed model was to predict the force-displacement behavior of SDRC diaphragms for the pre-peak region of

the envelope curve. Also the determination of the moment-curvature relationships needed for the analysis of structures with continuous diaphragms was an important objective. In order to give credence to the model and consequently the results, particular experimental tests were modeled and predicted and experimental results were compared. Specific details of the modeling as well as the results obtained are presented next.

3.4.3.5.2 Diaphragm 20 This test was selected because a diaphragm with a shear transfer mechanism failure was considered an important target, and also because the same diaphragm was modeled by Easterling (29) using a nonlinear 2D finite element analysis and a comparison of both predictive approaches may be of interest.

Diaphragm test 20 was a 15 by 15 feet side especimen constructed with a deck type 9 (see Figure A3 in Appendix A) with a 2.5 in. deep, 20 gage (0.037 in.) steel deck and with a 3.05 in. concrete cover above the top flange of the steel deck. 40 arc spot welds with 0.75 in. diameter were used per side.

As first step in the analysis, the diaphragm was divided in the longitudinal direction forming segments and in the transverse direction forming fibers. A total of 20 segments were considered in the longitudinal direction and 100 fibers in the transverse direction. All the calculations were made on a spreadsheet using Microsoft Excel as supporting software (97). Once the diaphragm was divided, the moment-curvature curves for a typical interior section as well as for an end section were evaluated. As expected, the moment curvature curve for an interior section showed more strength and energy capacity than the end section curve, because the end section curve was limited by the back edge fastener strength. Figure 48 shows a comparison of both curves.

For analysis purposes, when the distributed flexibility approach is used (see Section 4.5.2.2) the interior section moment-curvature relationship should be used for an

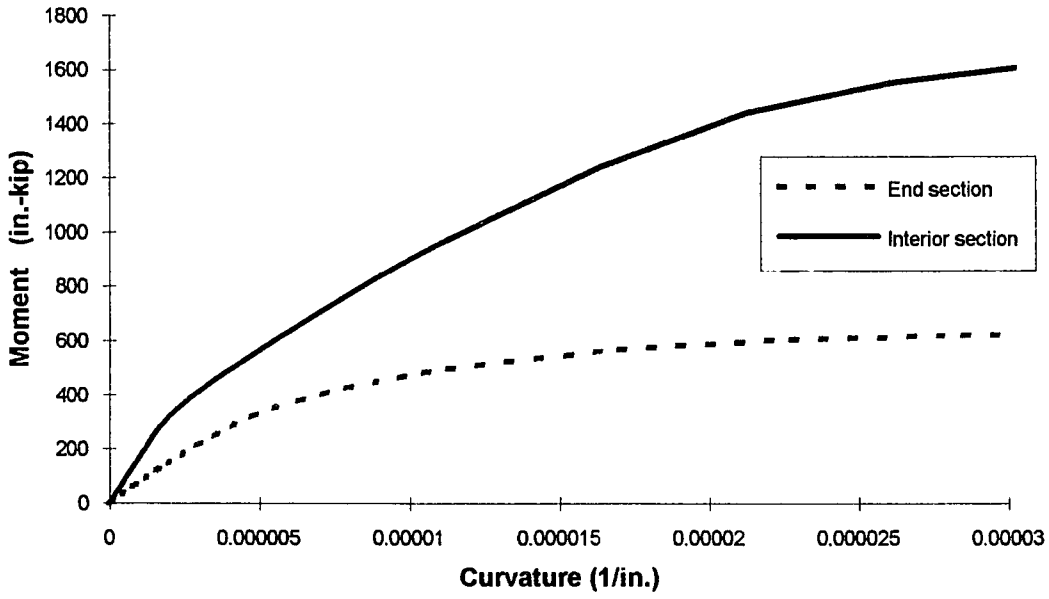

Figure 48. Diaphragm 20 moment-curvature curves for end and interior section

interior diaphragm node because the associated continuity provided by one diaphragm member on the neighbor. Meanwhile the end section moment-curvature relationship should be used in the exterior diaphragm node since on that end there were no diaphragm continuity and only the resistance offered by the end connection keep the end of rotate freely.

Once the moment-curvature relationship for both sections were defined, the force displacement relation was obtained as shown in Figure 49. Since the same diaphragm was modeled by Easterling (29) using nonlinear 2D finite element analysis, a comparison of both predictive methods against the experimental results was made. Solutions presented by Easterling are shown as FEA-20-A and FEA-20-B which stands for finite element analysis (FEA) model 20-A and model 20-B. The difference between model 20-A and 20-B was that different load-displacement relationships were assigned to the weld and

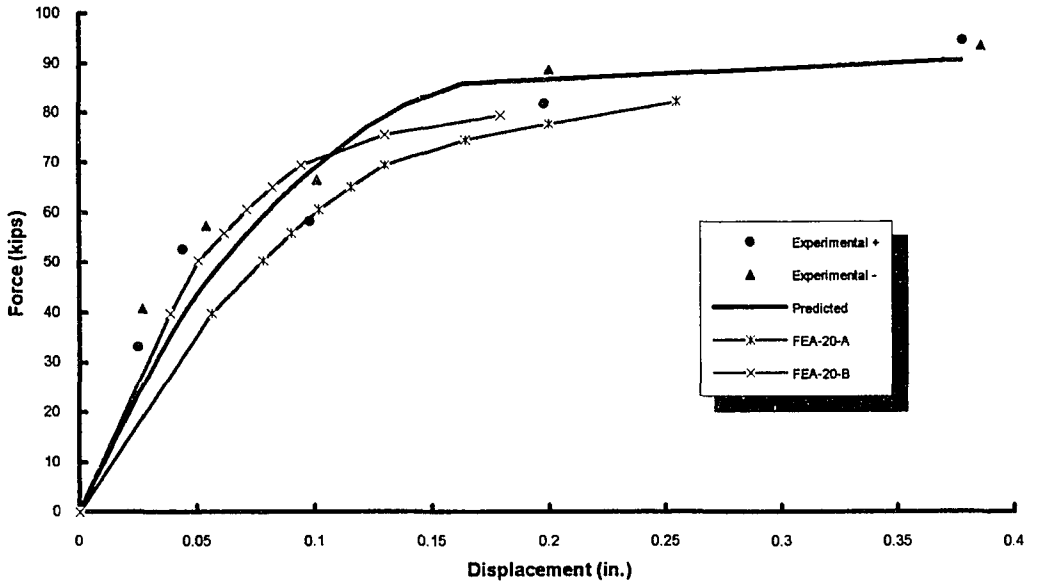

Figure 49. Comparison of predicted pre-peak envelope for diaphragm 20

to the interface. As observed in Figure 49 both approaches (finite element and fiber model) predict satisfactorily the diaphragm behavior.

3.4.3.5.3 Diaphragm 32 This test was selected because had a different distribution of welds on each side and had a number of fasteners that permited a connection failure to occur. Additionally the supporting frame for this diaphragm was made with a much lighter beam section, and a smaller span to depth diaphragm ratio was used. The diaphragm test 32 was a 15 by 12 feet side especimen constructed with a deck type 11 (see Figure A2 in Appendix A) with 3 in. deep, 20 gage steel deck and with 2.66 in. concrete cover above the top flange of the steel deck. 30 arc spot welds with 0.75 in. diameter were used on sides parallel to loading direction, and 23 arc spot welds with 0.75 in. diameter on sides orthogonal to loading direction.

Results of the analysis are presented graphically in Figure 50. The predicted peak load was 69 kips which was 15 percent higher than the experimental value. Easterling (29) using the strength predictive equations based on the edge zone concept predicted a peak load of 74 kips which was 23 percent higher than the experimental peak load value. Comparing the deck section with previous deck types, diaphragm 32 used 24 in. wide deck section which required that an additional deck strip were added. That condition forced to put a seam near to the edge with five seam welds. According to Easterling (29), end slip measurements during the experimental testing showed that the seam near to the edge failed limiting the strength. Therefore in order to avoid a premature failure due to seam weld failure, the location of the seams near to an edge should be avoided or the number of seam welds should be incremented.

3.4.3.5.4 Diaphragm 2 This test was selected because was constructed with headed stud connectors allowing a diagonal tension failure. Diaphragm 2 was a 15 by 15 feet side specimen constructed with a deck type 1 (see Figure A1 in Appendix A) with a 3 in. deep, 20 gage steel deck and with a 2.5 in. concrete cover above the top flange of the steel deck. 30 headed shear studs with 0.75 in. diameter were used per side. The fiber analysis or strain compatibility analysis when applied to diaphragms fastened with headed shear studs was made assuming that the fasteners transmitted the force directly from the loading beam to the concrete. Therefore the effect of the interface which actually was lessened by the restraining force from the studs was neglected. As result, the concrete and steel deck were assumed to be subjected to the same strain level.

The moment-curvature relationship was obtained using the procedure stated previously in Section 3.4.3.4.1. A modification on the obtained curve was needed for those diaphragms under diagonal tension mode of failure, because a displacement-

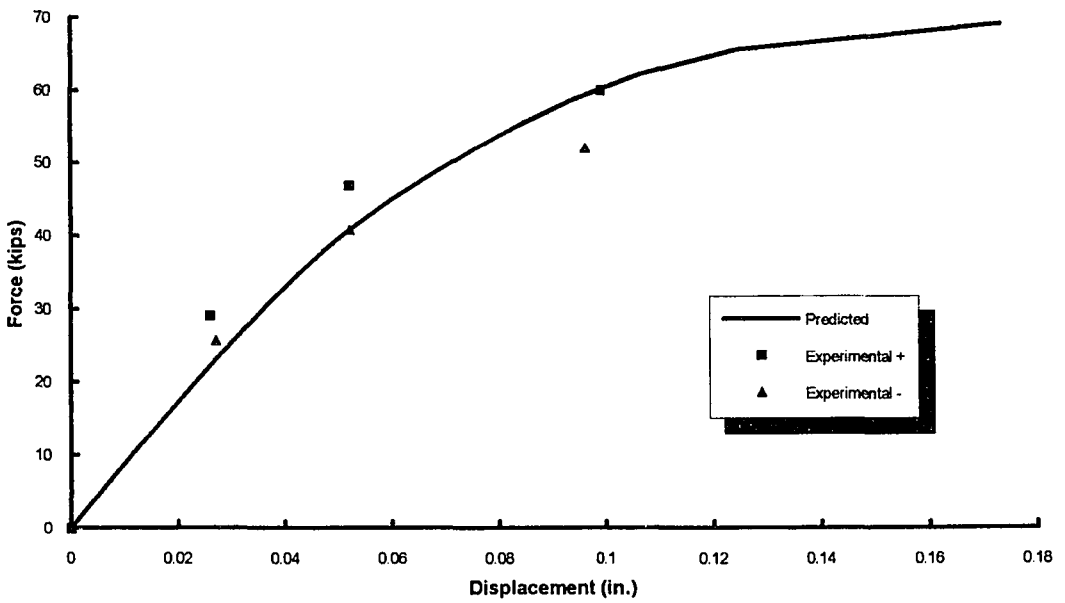

Figure 50. Experimental and predicted pre-peak envelope for diaphragm 32

controlled loading was used in the strain compatibility analysis. Therefore the shape of the curve showed a drop in strength after the more distant concrete fibers started to crack. Such path is not likely to occur under actual loading conditions.

Two approaches were considered to deal with the mentioned effect. First, as an upper bound approach, the smallest values of curvature were associated with a given moment. This approach led to a moment-curvature path I as shown in Figure 51, and to a force-displacement relationship called "Predicted I" shown in Figure 52. The second approach was based on a RC diaphragm study (42). Reinhorn et al. (42) observed the same drop in strength behavior on reinforced concrete diaphragms, and based on the observed experimental data specifically by comparing monothonic and cyclic curves a linear modelling of the first sections of the curve was suggested. The Deviation from the initial elastic portion of the curve was observed to take place at approximately 1/3 of the

cracking strength. The second linear segment intersected the curve at the smaller of the following two estimates: 1) at a point along the curve which yields a slope equal to 5 percent of the initial elastic slope, and 2) at 6 times the cracking curvature. Based on those estimates, the modified moment curvature curve for Diaphragm 2 was obtained as shown in Figure 51 (path II). The force-displacement relationship using this second approach is shown as "Predicted II" case in Figure 52.

For the definition of the force-displacement envelope curve, a similar procedure to that stated in Section 3.4.3.4.2 was followed, but an upper bound or limiting force value was added according to the following discussion. The ACI Code (63) recognises two types of shear failures on RC shearwalls, the web-shear cracking and the flexure-shear cracking. Web-shear cracking occurs when the diagonal tension stress in the vecinity of

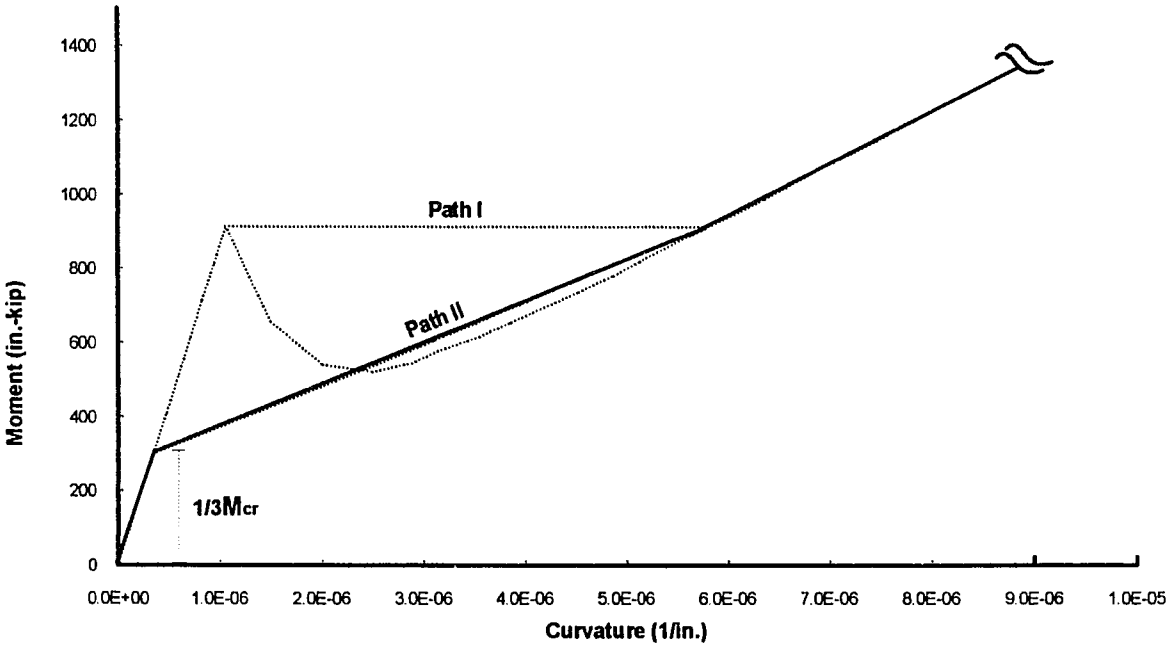

Figure 51. Moment-curvature curve for diaphragm 2

the neutral axis becomes equal to the principal tensile stress in the concrete of approximately $4\sqrt{f_c'}$. This type of failure is produced by a biaxial state of stress. Flexure-shear cracking occurs when the diagonal tension stress at the end of the flexural tension cracks exceeds the flexural tensile stress in the concrete of $6\sqrt{f_c'}$. This type of failure is more of the uniaxial nature. Since the moment-curvature relationship was evaluated based on a uniaxial state of stress and from that curve the shear force-displacement curve was derived, then using the fiber model approach, the predicted shear failure is a flexure-shear type of failure. Because both types of failure have to be considered, a limiting value of the shear force based on the web-shear type of failure is also applied. The expression to evaluate the web-shear diagonal tension force of failure was proposed by Porter and Easterling (89) based on the ACI (63) shear wall equation. The expression was:

$$V = 3.2 t_e h \sqrt{f_c'} \qquad [3\text{-}99]$$

$$t_e = t_c + n t_{se} \qquad [3\text{-}100]$$

where

h: diaphragm depth (in.)

f_c': 28 day concrete compressive strength (psi)

t_e: effective diaphragm thickness (in.)

Based on Eqaution [3-99], Diaphragm 2 has a limiting shear force value of 179 kips. A comparison of predicted and experimental envelope curve for Diaphragm 2 showed a satisfactory prediction of the diaphragm behavior for this type of failure (see Figure 52). Additionally, the first approach used to consider the moment-curvature drop, showed a better prediction of the experimental values for the small displacement range (Predicted I case).

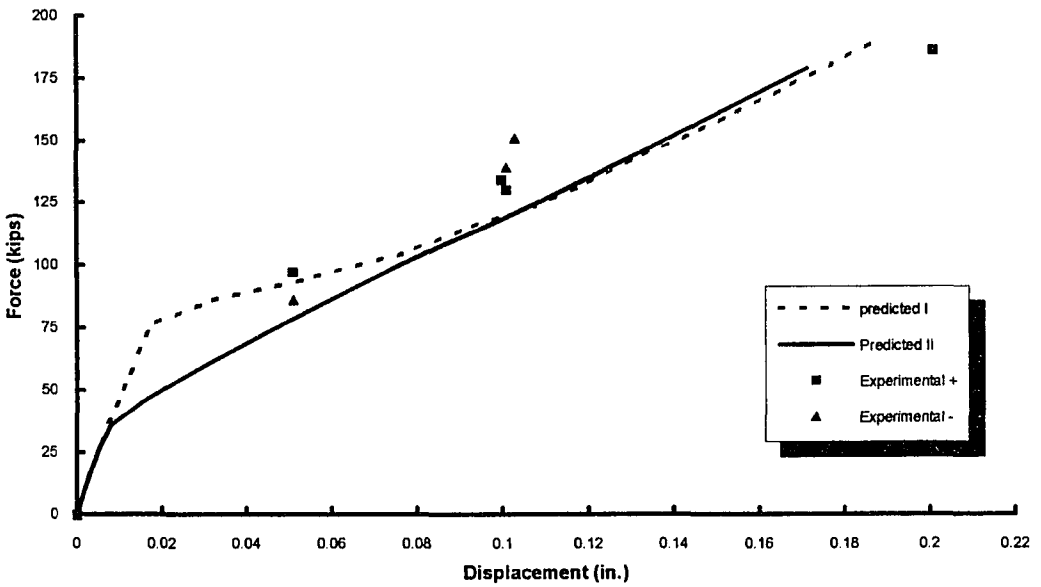

Figure 52. Experimental and predicted pre-peak envelope for diaphragm 2

3.4.3.5.5 Diaphragm 29 Diaphragm 29 was selected because was built with a smaller number of headed shear studs than Diaphragm 2 and it still had a diagonal tension failure. This diaphragm was a 15 by 12 feet side specimen constructed with a deck type 11 (see Figure A2 in Appendix A) with 3 in. deep, 20 gage steel deck and with 2.55 in. concrete cover above the top flange of the steel deck. 16 studs with 0.75 in. diameter were used in edges parallel to loading direction, and 11 studs were used in edges transverse to loading direction.

This diaphragm showed basically the same pattern as the previous Diaphragm test 2. That is, a similar strength drop in the moment-curvature curve was obtained. The same two approaches to consider the effect of the moment-curvature drop were used. The predicted peak load based on the diagonal tension web-shear failure was 143 kips. Predicted Force-displacement envelope curve were satisfactory when compared with the

experimental data as shown in Figure 53. Again, the first approach used to consider the effect of moment-curvature drop showed a better prediction of the experimental values especially for small displacement range.

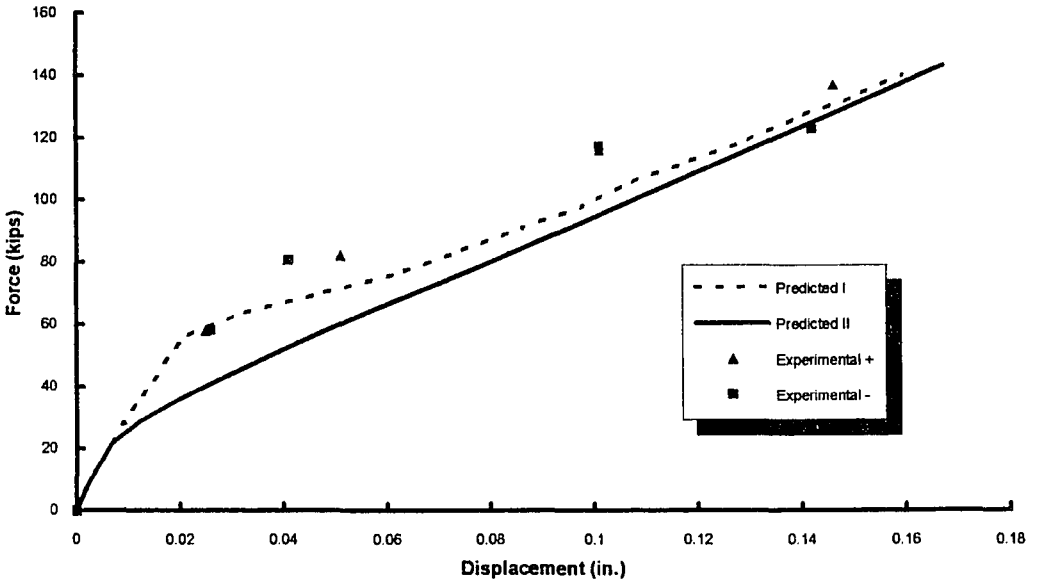

Figure 53. Experimental and predicted pre-peak envelope for diaphragm 29

4. STRUCTURAL MODELLING USING DIAPHRAGMS

4.1 Introduction

In the analysis of structures, the floor system is often assumed to be perfectly rigid in its own plane. This assumption, although acceptable for many structures such as regular frame buildings, is not realistic for certain building configurations. The influence of diaphragm flexibility is more evident in frame-wall structures built with shear walls and flexible frames, and buildings with long and narrow floor plans (33,37,39,42,70,72).

The assumption of diaphragm rigidity or flexibility has to be made considering not only the diaphragm properties (material, dimensions, etc.), but also including the interaction with surrounding members. The same diaphragm may change from rigid to flexible behavior just by changing the arrangement of walls and frames. Therefore, diaphragm flexibility or rigidity has to be considered as a relative term function of the diaphragm properties and its interaction with the structure.

Diaphragm rigidity may be considered as an unchanging or variable term according to the level of forces applied on it. Such is the case of steel-deck reinforced concrete diaphragms that under small force level have a close to linear elastic response But, the same diaphragm when subjected to strong in-plane forces shows a completely inelastic behavior with a stiffness parameter varying with the strain level. Shear in-plane forces generated by earthquakes are distributed to the vertical resisting system through the diaphragm. Reinforced concrete structures usually develop inelastic deformations when subjected to strong ground motions. Therefore, the seismic response analysis of concrete structures requires realistic analytical models that can predict the continually varying stiffness of the structure under cyclic loading.

The objective of this chapter is to state the limitations and procedures required to perform the structural analysis of concrete structures subjected to ground motions considering the varying stiffness of their components as well as including the effect of steel-deck reinforced concrete diaphragms.

4.2 Modelling of Structural System

4.2.1 Introduction

The modelling of reinforced concrete structures for dynamic analysis purposes had been improved over the years. Originally, nonlinear structural analysis used shear beam representation of multi-story buildings supplemented with some kind of shear-force-drift relation (57). Elastoplastic model was first used, followed by bilinear and trilinear representations of the force-displacement relation that allowed for cracking and yielding effects. Besides the envelope curve properties, models of restoring force characteristics were proposed.

One of the first macro-models used, was the shear beam model. Shear beam modelling was associated with a story behavior of weak column-strong beam type, but in many instances the opposite may have occurred. Therefore, to include the possibility of a different behavior, a member-by-member approach has been used. The actual state-of-the-art in reinforced concrete modelling is almost completely focused in this later approach.

A different scheme for the member-by-member approach has been suggested. Early examples of such schemes are the two-component model of Clough (58), the multi-component model of Aoyama and Sugano (59), and the one-component approach of Gilberson (60). A next development in this path, was the inclusion of the distributed

flexibility concept for reinforced concrete members (15, 32, 50, 51, 53, 66). The actual tendency in concrete member modelling follows the distributed flexibility approach.

For a more detailed and complete description of member models, refer to Sections 2.3 and 2.4 of this report and to References (6, 50, 51, and 90).

4.2.2 Structural modelling

The structural modelling presented in this section has been oriented mainly to reinforced concrete elements and steel-deck-reinforced concrete elements, but steel members may be included as long as envelopes and restoring force-displacement characteristics are supplied. Current developed software for inelastic analysis of reinforced concrete structures such as IDARC2 (42) includes most of the modeling features presented in this section.

The structure to be analyzed is idealized as a series of plane steel and/or reinforced concrete frames and shear-walls joined by steel-deck-reinforced concrete diaphragms. Frames may be considered as shear frame substructures as long as weak column-strong beam behavior describes them. The structure is analyzed considering the member-by-member modelling approach. Different type of elements may be considered, each one with its own hysteretic model. A brief description of each element type follows (see Figure 54):

- Diaphragm element. This element is discretized from the slab through the definition of its boundaries described by the surrounding frames and walls. A diaphragm element is modeled considering shear and flexure characteristics; other effects are also included through modification of the envelope force-displacement curve (see Section 4.4.1). Two nodes with two degrees of freedom per node describes the element. In-plane rotation and lateral translation are the two degrees of freedom considered.

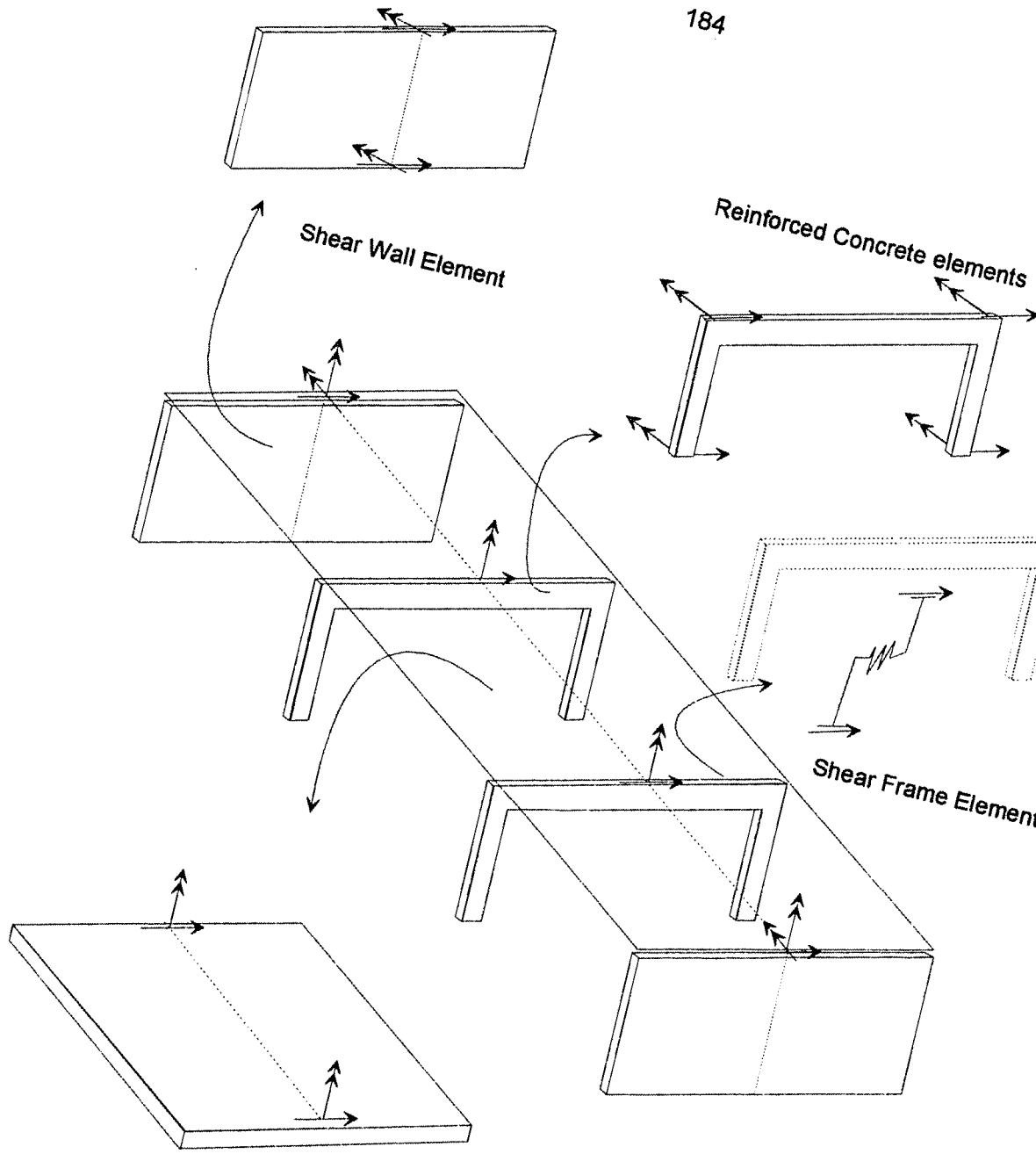

Figure 54. Member discretization for a frame-wall structure

Flexural effects are included through the distributed flexibility concept. That is, a linear variation of curvature is assumed; such variation is defined by the end member moments. Shear effects for steel-deck-reinforced concrete diaphragms are included throughout a hysteretic model developed in Chapter 3 of this report.

- Reinforced concrete beam element. This element may be used for beam and columns (when axial load is small). Flexural and shear effects are included by coupling both effects through an equivalent spring. Two degrees of freedom per node are considered, that is, rotation and lateral translation.
- Steel frame substructure. Steel frame may be considered as an equivalent truss or spring element, with a stiffness defined by the condensed lateral resisting force. This type of model is more accurate for weak column-strong beam frame systems. Only one degree of freedom is needed under this approach.
- Steel beam element. Two degrees of freedom per node are needed for steel beams and columns. One component model such as that proposed by Gilberson (60) and shown in Figure 7 may be used in conjunction with a hysteretic model for the end moment-curvature relation. Typical hysteretic models used in this case include the bilinear model and the Jennings model (7).
- Shear wall element. This element is modelled similarly to the diaphragm element, but with different shear contribution. Two degrees of freedom (dof) per node are considered (three dof when axial loads are significant), with an equivalent stiffness matrix result of the flexural and shear contributions. The flexural contribution is considered through the use of the flexibility distributed concept. The shear contribution may be obtained from different hysteretic models. For reinforced-concrete shear walls, the shear hysteretic model proposed by Ozcebe and Saatcioglu (45) may be used. For masonry walls, the model proposed by Soroushian et al. (27) or the

EKEH model (nonlinear spring type number 11) proposed by Kariotis et al. (41) are suggested.

- Torsional frame element. This imaginary element is included to consider the restraining torsional effect of frames or shear walls on the in-plane rotation of the diaphragm element. Torsional rigidity of the frame may be evaluated with the flexural stiffness of the vertical shear wall or frame members subjected to lateral deflection (in perpendicular direction to the frame plane).

4.3 Basic Assumptions

As part of the overall dynamic modelling of structures with diaphragm flexibility; a compromise is needed among accuracy, simplicity, and reality resulting in a simple but realistic representation of the real structure. The simplifications considered for the analysis are:

- Each member of the structure is a massless line element considered acting along its centroidal axis.
- Deformations are considered to be small, therefore the undeformed configuration of the structures is used through the analysis.
- Masses are lumped at locations where the horizontal degrees of freedom are defined.
- Axial deformation of columns, beams, diaphragms and shear walls is neglected.
- Elements connected to the foundation are assumed to be rigidly fixed.
- Stiffness properties of each member in the structure are assumed to remain unchanged over each increment of time.
- Gravity effects, if any, will be only included in the shear envelope of diaphragms.

- Ground motion occurs in the horizontal and parallel direction to the diaphragm supporting frames and walls.
- Only external lateral forces are considered in the analysis; any vertical force or moment at the structure nodes is considered to be zero.

The nonlinear dynamic analysis is applied by linearizing the problem over a short time. A step-by-step numerical integration method is used for such procedure. That is, the solution continues in a step-by-step form using a series of linear systems with changing stiffness characteristics. As result of this process, basic assumptions used in elastic analysis are considered to be valid.

4.4 Force-Deformation Relationship

4.4.1 Basic considerations

Inelastic dynamic analysis requires a proper selection of hysteretic models and member models. A hysteretic model is used to describe a force-displacement relationship at a specific location in the element, meanwhile the member model uses the localized effect (hysteresis effect) to describe the overall member response.

A hysteretic model is defined by the envelope curve and by a series of hysteretic rules describing the cyclic loop. The force-deformation relationship defining the envelope curve, is described either by a series of straight lines joined at critical points or by continuous curves. Such envelope curve is considered to be the same as the force-displacement relationship under monothonic loading.

The force-deformation relationship is usually evaluated for flexural behavior (moment-curvature/rotation), shear behavior (force-displacement), or a combination of both effects. Other effects such as bond-slippage of beam reinforcement, shear transfer

flexibility of steel deck-concrete interface, connection flexibility, etc., are included as equivalent flexural or shear effects by incorporating the specific effects in the envelope curve. When shear and flexure are evaluated separately, a coupling effect is considered by including both effects in the flexibility matrix (see Section 4.5.2.5).

Flexural effects are evaluated through a moment-curvature (or rotation) relationship. This relation may be obtained by either a series of discrete moment-curvature points (cracking, yield, and ultimate stage) joined by straight lines, or more accurately by the step-by-step method based on moment-curvature relationships applied on segments of the cross section (filament,fiber or layer approach). Shear effects are either assumed constant (10,52) or defined by a force-displacement relationship (45). Different points along the force-displacement envelope curve are usually defined by empirical equations (32, 54), or by analytical means (99,100).

The following sections describe the procedure used to define the force-displacement relationship for the different elements of the structure.

4.4.2 Reinforced concrete beam elements

4.4.2.1 Introduction Force-displacement relationship for a reinforced concrete beam is given by an equivalent flexural envelope that includes other effects such as elastic shear, bond-slippage, etc. Many hysteretic models have been proposed for this type of element, probably that proposed by Takeda et al. (9), or by Saiidi and Sozen (53) are among the most used.

The moment-curvature relationship is needed to evaluate the flexural properties of the elements. For simply or double-reinforced concrete beam and columns, explicit expressions for moment and curvature may be determined. For other more complex

sections, such as those with various steel layers, probably the layer or fiber approach is more adequate option (see Section 4.4.3). In the next subsections, explicit expressions for moment and curvature are given at three specific stages, at cracking, at yield, and at ultimate stage.

4.4.2.2 Cracking stage Flexural cracking is assumed to occur when the stress in the extreme tension fiber reaches the tensile strength of the concrete. The cracking moment is then evaluated using beam theory (see Figure 55). The equations required to evaluate the moment and curvature at cracking stage are as follows:

$$M_{cr} = C_c\left(\frac{2\kappa_r d}{3}\right) + C_s'(\kappa_r d - d') + T_s(d - \kappa_r d) + T_c\frac{2}{3}(h - \kappa_r d) \qquad [4\text{-}1]$$

$$\phi_{cr} = \frac{\varepsilon_c}{\kappa_r d} \qquad [4\text{-}2]$$

$$\rho = \frac{A_s}{bd} \qquad [4\text{-}3]$$

$$\rho' = \frac{A_s'}{bd} \qquad [4\text{-}4]$$

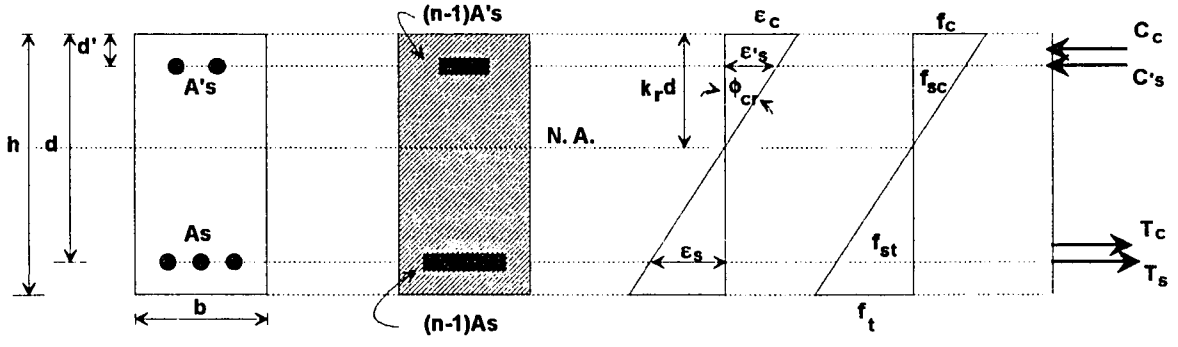

Figure 55. Reinforced concrete beam section at cracking stage

$$\kappa_r = \frac{(n-1)\left[\rho+\rho'\left(\frac{d'}{d}\right)\right]+\frac{1}{2}\left(\frac{h}{d}\right)^2}{(n-1)(\rho+\rho')+\left(\frac{h}{d}\right)} \quad [4\text{-}5]$$

$$f_t = f_r = 7.5\sqrt{f'_c} \quad [4\text{-}6]$$

$$T_c = \frac{f_t b(h-\kappa_r d)}{2} \quad [4\text{-}7]$$

$$\varepsilon_c = \frac{\kappa_r f_t}{\left(\frac{h}{d}-\kappa_r\right)E_c} \quad [4\text{-}8]$$

$$f_c = \varepsilon_c E_c \quad [4\text{-}9]$$

$$C_c = \frac{f_c b \kappa_r d}{2} \quad [4\text{-}10]$$

$$\varepsilon_s = \left(\frac{d-\kappa_r d}{\kappa_r d}\right)\varepsilon_c \quad [4\text{-}11]$$

$$f_s = \varepsilon_s E_s \le f_y \quad [4\text{-}12]$$

$$f_{st} = \left(\frac{d-\kappa_r d}{\kappa_r d}\right)f_c \quad [4\text{-}13]$$

$$T_s = A_s(f_s - f_{st}) \quad [4\text{-}14]$$

$$\varepsilon'_s = \left(\frac{\kappa_r d-d'}{\kappa_r d}\right)\varepsilon_c \quad [4\text{-}15]$$

$$f'_s = \varepsilon'_s E_s \le f_y \quad [4\text{-}16]$$

$$f_{sc} = \left(\frac{\kappa_r d-d'}{\kappa_r d}\right)f_c \quad [4\text{-}17]$$

$$C'_s = A'_s\left(f'_s - f_{sc}\right) \quad [4\text{-}18]$$

where:

M_{cr}: cracking moment

ϕ_{cr}: curvature at cracking

h: element depth

d: effective depth of tension steel

d': distance from extreme compression fiber to centroid of compression steel

Ec: modulus of elasticity of concrete

E_s: modulus of elasticity of steel

n: modular ratio of elasticity

A_s: area of tension steel

A'_s: area of compression steel

4.4.2.3 Yield stage Concrete in compression under this stage is assumed to remain elastic up to yielding of the tension reinforcement (see Figure 56). The equations required to evaluate the moment and curvature at yield stage are as follows:

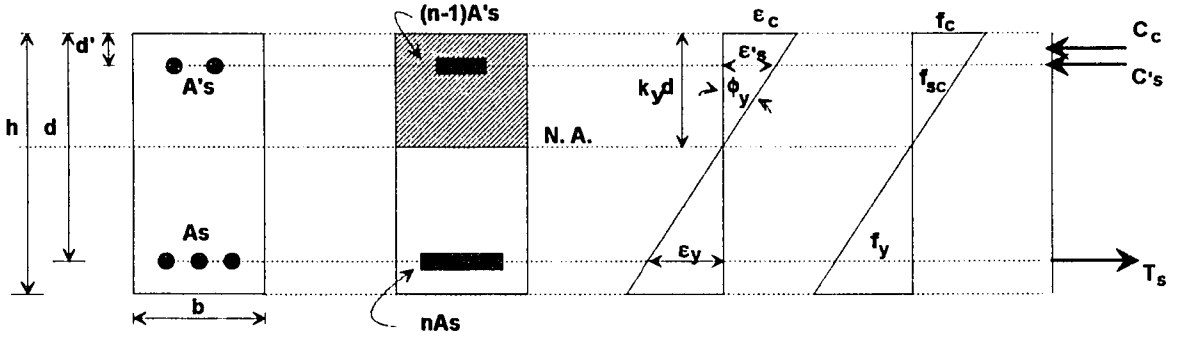

Figure 56. Reinforced concrete beam section at yield stage

$$\alpha = \frac{\rho'}{\rho} \qquad [4\text{-}19]$$

assume $\gamma = 1$, and solve for κ_y

$$\kappa_y = \rho\left\{\sqrt{\left[(n-\gamma)\alpha + n\right]^2 + \frac{2}{\rho}\left[(n-\gamma)\alpha\frac{d'}{d} + n\right]} - \left[(n-\gamma)\alpha + n\right]\right\} \qquad [4\text{-}20]$$

if, $d' > \kappa_y d$, then set $\gamma=0$ and evaluate κ_y again

$$M_y = C_c\left(\frac{2\kappa_y d}{3}\right) + C_s'\left(\kappa_y d - d'\right) + T_s\left(d - \kappa_y d\right) \qquad [4\text{-}21]$$

$$\varphi_y = \frac{\varepsilon_y}{d - \kappa_y d} \qquad [4\text{-}22]$$

$$\varepsilon_c = \frac{\kappa_y d}{d - \kappa_y d}\varepsilon_y \qquad [4\text{-}23]$$

$$\varepsilon_s' = \frac{\kappa_y d - d'}{\kappa_y d}\varepsilon_c \qquad [4\text{-}24]$$

$$f_c = \varepsilon_c E_c \le f_c' \qquad [4\text{-}25]$$

$$f_{sc} = \frac{\kappa_y d - d'}{\kappa_y d} f_c \qquad [4\text{-}26]$$

$$f_s' = \varepsilon_s' E_s \le f_y \qquad [4\text{-}27]$$

$$C_s' = A_s'\left(f_s' - f_{sc}\right) \qquad [4\text{-}28]$$

$$C_c = T_s - C_s' \qquad [4\text{-}29]$$

where:

M_y: moment at yield of tension reinforcement

φ_y: curvature at yield

4.4.2.4 Ultimate stage For ultimate strength, a rectangular concrete compressive stress distribution is used (see Figure 57). Equations are expressed as a function of the ultimate concrete strain ε_{cu}, , which according to ACI code (63) shall be assumed equal to 0.003. The equations required to evaluate the moment and curvature at ultimate stage are as follows:

Assume γ_2 =1 and solve for the compressive steel stress f's

$$f_s' = \frac{\left(\rho f_y + E_s \varepsilon_{cu} \rho' + 0.85 f_c' \gamma_2 \rho'\right) - \sqrt{\left(\rho f_y + E_s \varepsilon_{cu} \rho' + 0.85 f_c' \gamma_2 \rho'\right)^2 + 4\rho' E_s \varepsilon_{cu}\left(0.85\beta_1 f_c' \frac{d'}{d} - \rho f_y - 0.85 f_c' \rho' \gamma_2\right)}}{2\rho'} \quad [4\text{-}30]$$

$$\left|f_s'\right| \le f_y \quad [4\text{-}31]$$

$$c = \frac{E_s \varepsilon_{cu} d'}{E_s \varepsilon_{cu} - f_s'} \quad [4\text{-}32]$$

if d' > β_1c then set γ_2=0 and evaluate f'$_s$ again

$$\beta_1 = 0.85 \quad f_c' \le 4000 \text{ psi}$$
$$\beta_1 = 0.85 - \frac{0.05}{1000}\left(f_c' - 4000\right) \ge 0.65 \quad f_c' > 4000 \text{ psi} \quad [4\text{-}33]$$

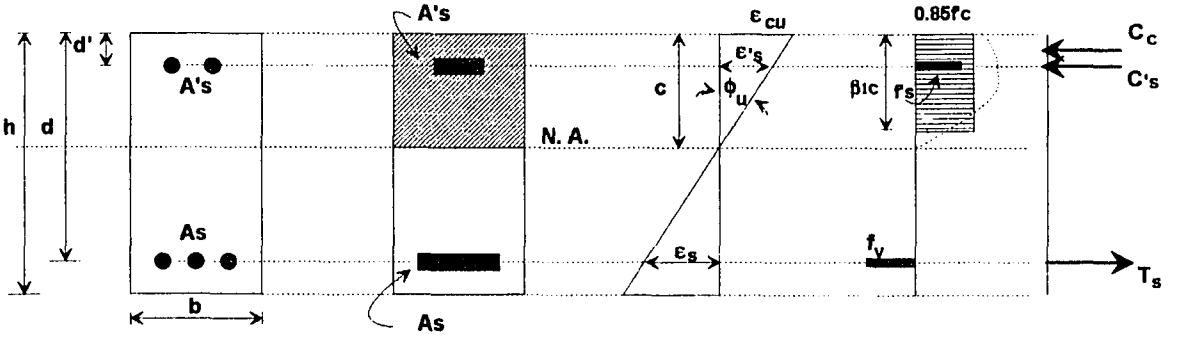

Figure 57. Reinforced concrete beam section at ultimate stage

$$M_{nu} = 0.85f_c'\beta_1 cb\left(d - \frac{\beta_1 c}{2}\right) + A_s'\left(f_s' - 0.85f_c'\gamma_2\right)(d - d') \quad [4\text{-}34]$$

$$\varphi_u = \frac{0.85\beta_1 f_c'\varepsilon_{cu}}{\left[\rho f_y - \rho'\left(f_s' - 0.85f_c'\gamma_2\right)\right]d} \quad [4\text{-}35]$$

4.4.2.5 Other inelastic components of deformation Some references (10,52,54,98) suggest the inclusion, in the total curvature value, of the equivalent curvature terms due to bond-slippage, and inelastic shear deformation. This approach is supported by the fact that such effects increase rotation in the element.

Curvature due to bond-slippage had been defined by Park et al. (54) based on available pullout data (98). According to Park, the slippage of tension bars at yield is expressed as follows:

$$\frac{S}{D} = 0.0003 f_y^{1.5} \tau_m^{-0.75} \quad [4\text{-}36]$$

where:

S: slippage of tension bars

D: bar diameter

f_y: yield strength of reinforcement

τ_m: maximum bond strength of concrete, a mean value of 1.2 ksi is suggested.

An equivalent curvature due to bond-slippage is evaluated assuming linear curvature distribution along the element. From Figure 58, the following geometric relations may be stated:

$$S = (d - d')\theta \quad [4\text{-}37]$$

$$\delta = L\theta \quad [4\text{-}38a]$$

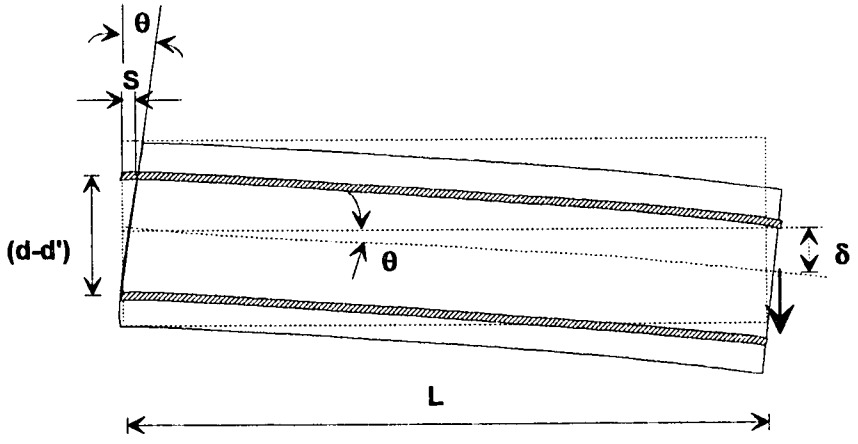

Figure 58. Bond-slippage component of deformation (modified from reference 54)

$$\delta = \frac{LS}{(d-d')} \qquad [4\text{-}38b]$$

For a cantilever beam subjected to a linear moment, the deflection is given by:

$$\delta = \frac{VL}{EI}\frac{L}{2}\frac{2L}{3} = \frac{VL}{EI}\frac{L^2}{3} = \frac{M_{end}}{EI}\frac{L^2}{3} \qquad [4\text{-}39]$$

substituting the curvature at the fixed end:

$$\frac{d^2y}{dx^2} = \varphi = \frac{M}{EI}$$
$$\varphi = \frac{3\delta}{L^2} \qquad [4\text{-}40]$$

Finally substituting Eqn. [4-38] into Eqn. [4-40], the equivalent curvature due to bond-slippage at yield is given by:

$$\varphi_{sb} = \frac{3S}{L(d-d')} \qquad [4\text{-}41]$$

Note, that here L is the shear span length.

The equivalent curvature due to the inelastic shear deformation is produced by the rotation of the member section at each crack (98). Details of the model may be found in Reference (98). Equations predicting this behavior are presented.

$$\varphi_{shear} = 3\left[\frac{1}{L} + \frac{1-\left(\frac{L_s'}{L}\right)^2}{2(d-d')}\right]\Theta_s \qquad [4\text{-}42]$$

$$L_s' = \frac{M_{cr}}{\left[\left(M_y L - bd\sqrt{f_c'}\right) + (d-d')\right]} \qquad [4\text{-}43]$$

ρ_w= stirrup ratio in percentage (>0.2%)

$$u = \frac{\tau_b}{\sqrt{f_c'}} \qquad [4\text{-}44]$$

τ_b= average bond stress

$$\Theta_s = \frac{0.002}{\frac{L}{d} - 0.5} \quad u < 5, \quad \frac{L}{d} > 4$$

$$\Theta_s = \frac{0.002}{\frac{L}{d} - 0.5}\left[1 + 0.27(u-5)\right] \quad u > 5, \quad 2.5 < \frac{L}{d} < 4 \qquad [4\text{-}45]$$

$$\Theta_s = \frac{0.002}{\frac{L}{d} - 0.5}\left[1 + 0.185\frac{(u-5)}{\sqrt{\rho_w} - 0.4}\right] \quad u > 5, \quad \frac{L}{d} < 2.5$$

Θ_s inelastic shear rotation

4.4.2.6 Elastic shear component of deformation The elastic shear component of deformation is included in the analysis by coupling it with the flexural deformation in the element flexibility matrix as explained in Section 4.5.2.5.

4.4.3 Shear wall and diaphragm elements

4.4.3.1 Introduction Force-displacement relationship for reinforced concrete shear walls, and steel-deck-reinforced concrete diaphragms are given by flexural and shear effects coupled as spring in series. For steel-deck-reinforced concrete diaphragms a shear force versus total displacement relationship is evaluated for a cantilever guided system as presented in Sections 3.3 and 3.4. Such relation includes the effect of bending, concrete shear, shear transfer flexibility, as well as connection flexibility. The equivalent shear displacement (that include all effects except bending) may be evaluated by subtracting the flexural component of deflection as proposed in Section 4.5.2.6.

Shear walls may follow a similar procedure to that described for steel-deck diaphragms when the same type of force-displacement relationship is provided. When a direct shear force-shear displacement relationship is given, a coupling of flexure and shear may be applied. Such is the case of reinforced concrete shear walls as presented in Reference (54), where an empirical relation between shear force and shear displacement is provided.

To describe the flexural behavior of diaphragms and shear walls, an origin-oriented hysteretic model has been recommended according to References (43,71). For a one-story building, shear walls act as cantilever systems and may be directly modeled as spring elements.

The next section presents a suitable method to evaluate the moment-curvature relationship of shear walls, and diaphragms. Such method is an extension of the strain compatibility analysis used for reinforced concrete beam and is called fiber or layer method. Coupling of shear and flexure effects are presented in Section 4.5.2.5.

4.4.3.2 Moment-curvature relationship A step-by-step method may be used to evaluate the moment-curvature relationship for any section under bending. This approach has been widely used in reinforced concrete beam strain compatibility analysis and has been also applied for shear walls (54,101) and diaphragms (33).

To apply the method, the cross section is divided into a number of elements. Each element is assumed to be subjected to a uniform strain and stress. To define the response, two equilibrium equations and one strain compatibility relationship are used. The procedure consists in assume a maximum compressive strain value ε_{cm} and by trial-and-error find the corresponding neutral axis depth "c" that satisfy the longitudinal force equilibrium equation. Once the neutral axis depth has been found, the bending moment and curvature can be obtained.

The flexural characteristics of the element are evaluated based on proposed stress-strain relationships for concrete and steel. The stress-strain variation of concrete (Figure 42) is frequently expressed by a parabolic equation (99-102). The stress-strain relationship for the steel is idealized by three segments for linear, plastic, and "strain-hardening" stages (Figure 42).

The equations describing the stress-strain relationship for concrete are:

$$f_c = f_c^{'}\left[2\frac{\varepsilon_c}{\varepsilon_c^{'}} - \left(\frac{\varepsilon_c}{\varepsilon_c^{'}}\right)\right] \qquad [4\text{-}49]$$

where:

f_c: stress in concrete

ε_c: strain in concrete

$f_c^{'}$: compressive strength of concrete

$\varepsilon_c^{'}$: strain at peak stress f'c (=2f'c/Ec, or 0.002 is suggested)

ε_{cu}: concrete ultimate compression strain. A 0.003 value is suggested (63).

The equations describing the stress-strain relationship for steel are:

$$f_s = E_s \varepsilon_s, \qquad \varepsilon_s \le \varepsilon_y$$

$$f_s = f_y, \qquad \varepsilon_y \le \varepsilon_s \le \varepsilon_{sh} \qquad [4\text{-}50]$$

$$f_s = f_y + E_{sh}(\varepsilon_s - \varepsilon_{sh}) \le f_u, \quad \varepsilon_s > \varepsilon_{sh}$$

where:

f_s: stress of steel

ε_s: strain of steel

f_y: yield stress of steel

ε_y: strain at yield

f_u: ultimate stress of steel

ε_{sh}: strain at initiation of hardening (with $12\varepsilon_y$ as typical value)

E_s: modulus of elasticity of steel

E_{sh}: modulus defining stiffness at strain hardening range

(approximately 3% of Es)

The procedure step-by-step to evaluate the moment-curvature relationship follows (see Figure 59):

- STEP 1

  select a value for maximum concrete compressive strain ε_{cm}

- STEP 2

  select a value for the neutral axis depth c

- STEP 3

  evaluate the strain and stress on each concrete and steel layer

  at any location x the strain ε_x is given by:

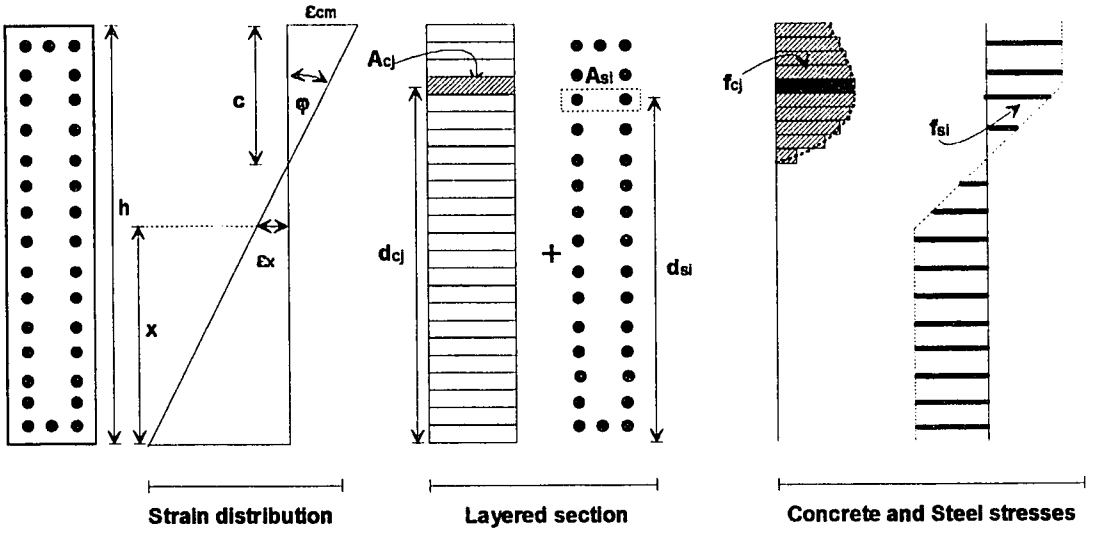

Figure 59. Element discretization for moment-curvature evaluation

$$\varepsilon_x = \left(1 - \frac{h - d_x}{c}\right)\varepsilon_{cm} \qquad [4\text{-}51]$$

where:

h: section depth

d_x: position where ε_x is evaluated

for the jth concrete layer the compressive stress is given by Eqn. [4-49]. Concrete tension is neglected. The concrete force F_{cj} in such layer is given by:

$$F_{cj} = A_{cj} f_{cj}, \quad j = 1, ncl \qquad [4\text{-}52]$$

where:

ncl: number of concrete layers

for the ith steel layer the stress is given by Eqn. [4-50]. The steel force is given by:

$$F_{si} = A_{si} f_{si}, \quad i = 1, nsl \qquad [4\text{-}53]$$

where:

nsl: number of steel layers

- STEP 4

  evaluate the resultant force R

$$R = \sum_{i=1}^{nsl} F_{si} + \sum_{j=1}^{ncl} F_{cj} \qquad [4\text{-}54]$$

- STEP 5

  if $|R| \leq$ tolerance, goto STEP 6

  if $|R| >$ tolerance, goto STEP 2

- STEP 6

  evaluate moment M and curvature φ

$$M = \sum_{i=1}^{nsl} F_{si} d_{si} + \sum_{j=1}^{ncl} F_{cj} d_{cj} \qquad [4\text{-}55]$$

$$\varphi = \frac{\varepsilon_{cm}}{c} \qquad [4\text{-}56]$$

where:

d_{si}: location of the ith steel layer with respect to the bottom

d_{cj}: location of the jth concrete layer with respect to the bottom

4.4.4 Steel beam elements

4.4.4.1 Introduction The force-displacement relationship for a steel beam is given by a flexural envelope defined through the moment-curvature relationship. Typical hysteretic models used in steel element are the bilinear model (3) and the Jennings model (7). The Jennings model has been limited in use because the relations describing the

envelope and cycles are presented as implicit equations. For beam sections with small shape factor (plastic to yield moment ratio), the moment-curvature relationship may be idealized by two straight lines. The first line goes from the origin to the point defined by the plastic curvature and moment. The second line starts at the end of the first line and continues horizontally. Sections with large shape factor may be idealized by two lines as described before, but considerable error may be associated for predictions close to the intersection of both lines.

4.4.4.2 Moment-curvature relationship To define different moment-curvature points, a stress-strain relationship for steel similar to that used in Section 4.4.3.2 is used. The assumptions used for the analysis are:

- Beams have compact sections, that is section capable of developing a fully plastic stress distribution and therefore allowing enough inelastic rotation capacity.
- Effects due to residual stress, stress concentration, strain hardening, axial and shear force are not considered.

The moment-curvature equations for an I or W sections as presented in Reference (103) are:

$$M = \varphi EI, \quad \frac{\varphi}{\varphi_y} \le 1 \qquad [4\text{-}57]$$

$$\frac{M}{M_y} = \frac{\varphi}{\varphi_y}\left(1 - \frac{b_f d^2}{6S}\right) + \frac{b_f d^2}{4S}\left[1 - \frac{1}{3}\left(\frac{\varphi_y}{\varphi}\right)^2\right], \quad 1 < \frac{\varphi}{\varphi_y} < \frac{\frac{d}{2}}{\frac{d}{2} - t_f} \qquad [4\text{-}58]$$

$$\frac{M}{M_y} = \frac{Z}{S} - \frac{t_w d^2}{12S}\left(\frac{\varphi_y}{\varphi}\right)^2, \quad \frac{\frac{d}{2}}{\frac{d}{2} - k} < \frac{\varphi}{\varphi_y} < \infty \qquad [4\text{-}59]$$

$$M_y = S\sigma_y \quad [4\text{-}60]$$

$$\varphi_y = \frac{2\varepsilon_y}{d} \quad [4\text{-}61]$$

where:

M: bending moment

φ: curvature

M_y: yielding moment

φ_y: curvature at yield

S: section modulus

Z: plastic modulus

d: total beam depth

b_f: flange width

t_f: flange thickness

t_w: web thickness

k: distance from outer face of flange to web toe of fillet

4.5 Element Stiffness Matrix

4.5.1 Basic considerations

The dynamic analysis of frame-wall structures including diaphragm effects may be made using the stiffness matrix method. This method requires the evaluation of the element stiffness matrices, the assemblage of these matrices into a global stiffness matrix, the formation of a vector of forces, and the solution of the equations of motion system. Since the changes in displacement are the unknown parameters, the equations of motion

are presented in an incremental form. In the following subsections, the incremental element stiffness matrix of different type of members is presented.

4.5.2 Reinforced concrete elements

4.5.2.1 Introduction The distributed flexibility approach is incorporated in the evaluation of the stiffness matrix of reinforced concrete elements. This approach is based on the fact that for reinforced concrete members, the inelasticity is not restricted to the end of the element, but it is spread through the member length. Different models for the distribution of flexibility have been proposed (15,32,50,51,53,66). Up to date, the proposed models do not describe exactly the behavior of the element, since some kind of rough assumptions has to be made regarding the distribution of flexibility, e.g., the location of the inflection point and/or the way in which the flexibility changes. A linear distribution of flexibility as proposed by Park et al. (32,54) is considered for this work, because allows variation of the contraflexure point.

The material included in the next subsections is general in the sense that applies to beam, diaphragm and shear wall elements. The difference in the stiffness matrix for each element comes from the instantaneous flexural and shear rigidity values.

4.5.2.2 Distribution of flexibility approach The stiffness matrix developed via the distributed flexibility approach, corresponds to the stiffness matrix of a prismatic/non-prismatic member. For small rotations at the end of the member, the flexibility factor 1/EI corresponds to that of elastic members, and the element behaves as a prismatic member. For large end rotations, the element may show sections with elastic and inelastic behavior, therefore a different flexibility factor 1/EI should be provided to each section. A linear

distribution of the flexibility factor is assumed, based on the flexibility values at the end member. The flexibility factors at the end member are continually monitored through the analysis and updated using a hysteretic model.

According to the sign of end-member moments, an element may bent in reverse curvature or in single curvature (Figure 60). For elements deformed in reverse curvature, the cross section at the contraflexure point is assumed to have an elastic value for the flexibility factor. Flexibility factor values at the member ends are evaluated considering the previous history of deformation by using a hysteretic model. The flexibility terms as function of the position along the member are given by:

- For single curvature

$$\frac{1}{EI} = \frac{1}{EI_i} + \left(\frac{1}{EI_j} - \frac{1}{EI_i}\right)\frac{x}{L} \qquad [4\text{-}62]$$

- For reverse curvature

$$\frac{1}{EI} = \frac{1}{EI_i} - \left(\frac{1}{EI_i} - \frac{1}{EI_e}\right)\frac{x}{\alpha L}, \quad x \le \alpha L$$
$$\frac{1}{EI} = \frac{1}{EI_e} + \left(\frac{1}{EI_j} - \frac{1}{EI_e}\right)\frac{x-\alpha L}{L(1-\alpha)}, \quad x > \alpha L \qquad [4\text{-}63]$$

$$\alpha = \frac{M_i}{M_i + M_j} \qquad [4\text{-}64]$$

where:

$\frac{1}{EI}$: flexibility factor

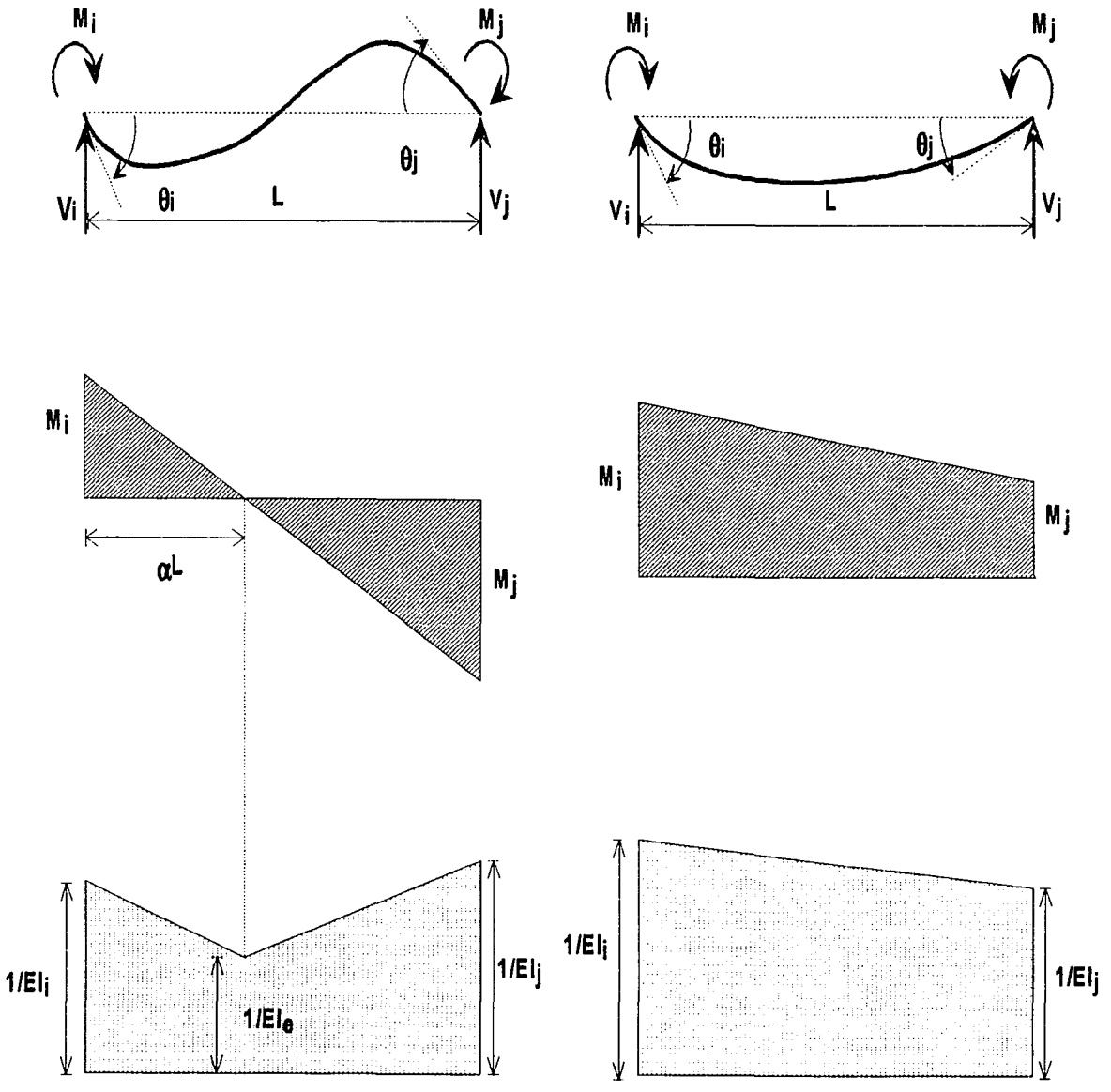

Figure 60. Distribution of flexibility (modified from reference 42)

$\frac{1}{EI_i}$: flexibility factor at end member i

$\frac{1}{EI_j}$: flexibility factor at end member j

$\frac{1}{EI_e}$: flexibility factor at the contraflexure point

4.5.2.3 Flexibility matrix for a released element To evaluate the stiffness matrix of an element considering both flexural and shear effects a relation between end-actions and end-displacements has to be found (see Figure 61a). Such relation is obtained by evaluating the flexibility matrix of a released element (see Figure 61b), and then by matrix operations, the stiffness matrix of the element may be obtained.

To begin the formulation, the flexibility matrix of the released member (Figure 61b) is obtained. Such element is arbitrarily fixed at the i end and free at the j end. Thus, the displacements at the j end are relative displacements of the j end with respect to the i end. The flexibility matrix for displacements and actions shown in Figures 61b-c is:

$$\begin{Bmatrix} \theta_1 \\ \delta_2 \end{Bmatrix} = \begin{bmatrix} f_{11} & f_{12} \\ f_{21} & f_{22} \end{bmatrix} \begin{Bmatrix} M_1 \\ V_2 \end{Bmatrix}$$

or

$$\overline{\theta}_j = \overline{F}_j \cdot \overline{M}_j \qquad [4\text{-}65]$$

where:

$\overline{\theta}_j$: end member displacement vector

$\overline{F}_j$: flexibility matrix

$\overline{M}_j$: end member action vector

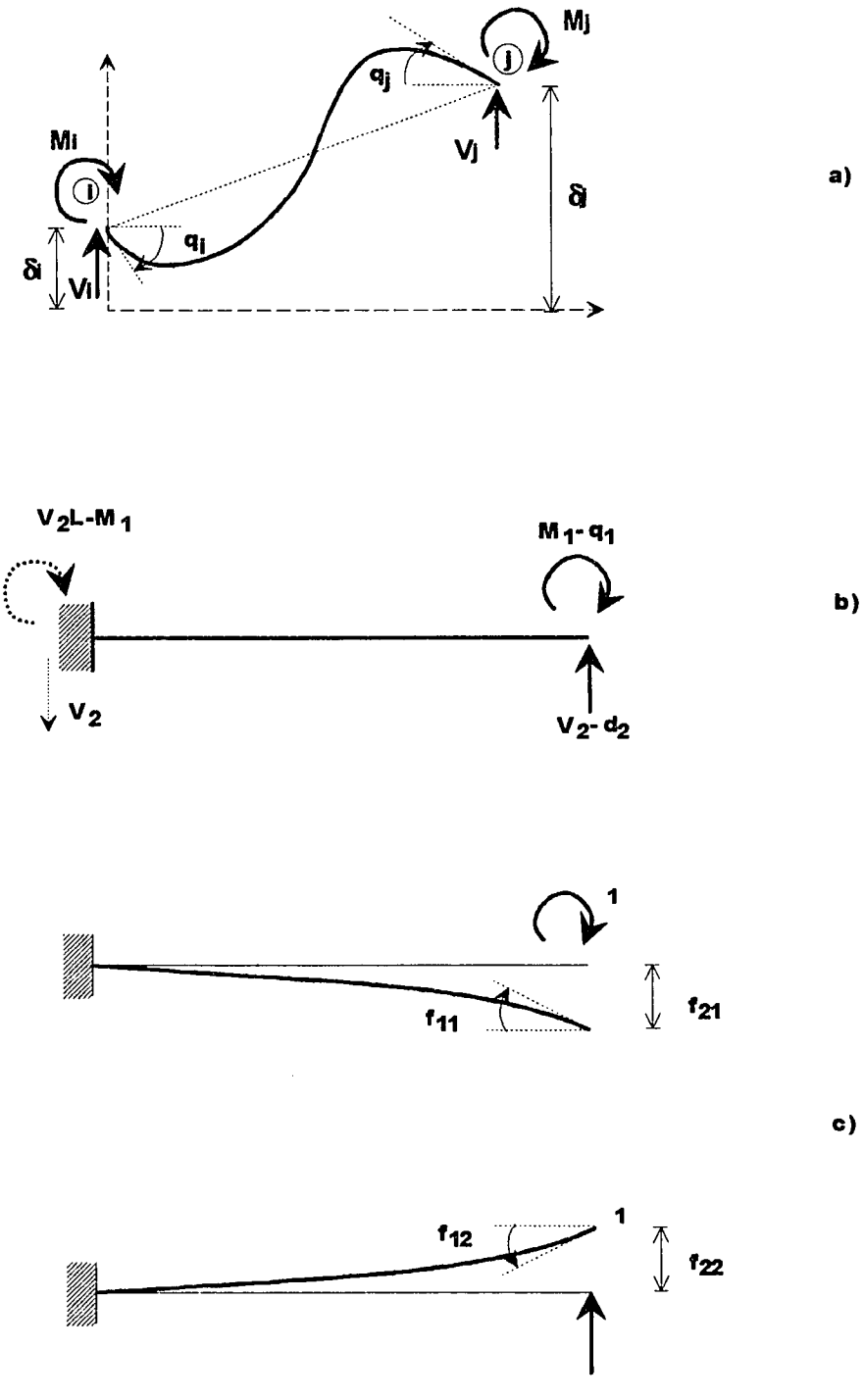

Figure 61. **Reinforced concrete member. a) End-member actions and displacements. b) Released element. c) Definition of flexibility terms**

4.5.2.4 Stiffness matrix The stiffness matrix of the released member may be obtained by inverting the flexibility matrix:

$$\overline{K}_j = \frac{1}{f_{11}f_{22} - f_{12}f_{21}} \begin{bmatrix} f_{22} & -f_{12} \\ -f_{21} & f_{11} \end{bmatrix} \qquad [4\text{-}66]$$

where the stiffness matrix of the released element relates end member actions and displacements:

$$\begin{Bmatrix} M_1 \\ V_2 \end{Bmatrix} = \left[\overline{K}_j\right] \begin{Bmatrix} \theta_1 \\ \delta_2 \end{Bmatrix}$$

or

$$\overline{M}_j = \overline{K}_j \cdot \overline{\theta}_j \qquad [4\text{-}67]$$

Based on equilibrium considerations, the relation between the end member actions for the general element (Figure 61a) and the released member (Figure 61b) is:

$$\begin{Bmatrix} M_i \\ V_i \\ M_j \\ V_j \end{Bmatrix} = \begin{bmatrix} -1 & L \\ 0 & -1 \\ 1 & 0 \\ 0 & 1 \end{bmatrix} \begin{Bmatrix} M_1 \\ V_2 \end{Bmatrix}$$

or

$$\overline{M} = \overline{T} \cdot \overline{M}_j \qquad [4\text{-}68]$$

where:

$\overline{M}$: end member actions for the general element

$\overline{T}$: transformation matrix

The end member displacements at end j for the released structure may be related to the end member displacements of the general elements. Based on the condition that

end displacements for the released element are relative displacements of the j end with respect to the i end, the following relation is found (see Figure 62):

$$\theta_1 = \theta_j - \theta_i$$
$$\delta_2 = L\sin\theta_i + (\delta_j - \delta_i)\cos\theta_i \approx L\theta_i + (\delta_j - \delta_i) \qquad [4\text{-}69]$$

or in matrix form:

$$\begin{Bmatrix}\theta_1\\ \delta_2\end{Bmatrix} = \begin{bmatrix}-1 & 0 & 1 & 0\\ L & -1 & 0 & 1\end{bmatrix}\begin{Bmatrix}\theta_i\\ \delta_i\\ \theta_j\\ \delta_j\end{Bmatrix}$$

$$\overline{\theta}_j = \overline{T}^T \cdot \overline{\theta} \qquad [4\text{-}70]$$

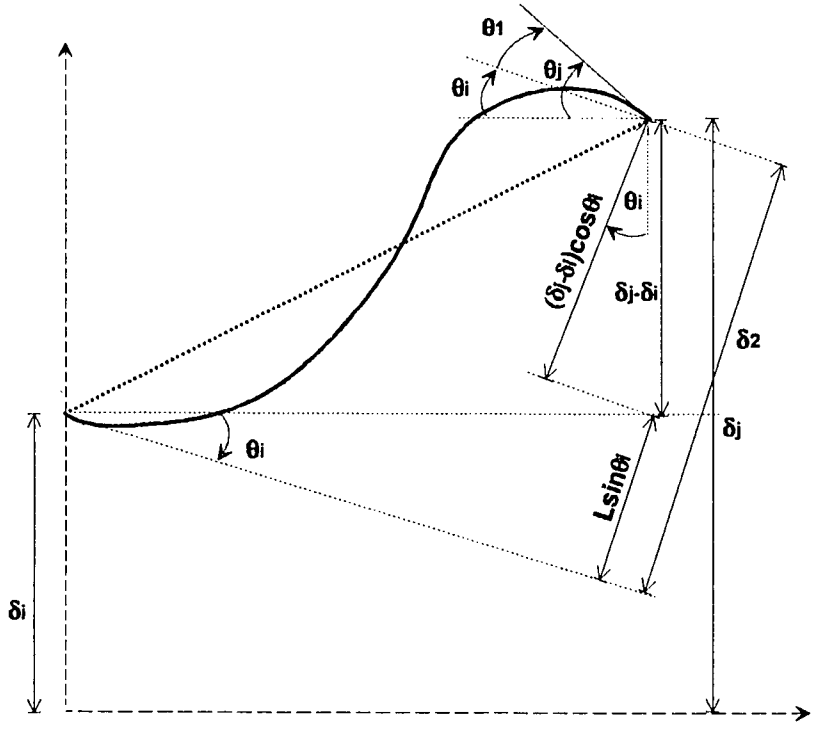

Figure 62. Relation of end member displacements between the released member and the general element

where:

$\overline{T}^T$: transpose of the transformation matrix

Substituting Eqn. [4-67] into Eqn. [4-68]:

$$\overline{M} = \overline{T} \cdot \overline{K}_j \cdot \overline{\theta}_j \qquad [4\text{-}71]$$

Substituting Eqn. [4-70] into Eqn. [4-71], the member stiffness matrix is obtained:

$$\overline{M} = \overline{T} \cdot \overline{K}_j \cdot \overline{T}^T \cdot \overline{\theta} \qquad [4\text{-}72]$$

or expressing the end member actions and displacements in incremental form:

$$\Delta\overline{M} = \overline{K} \cdot \Delta\overline{\theta}, \qquad \overline{K} = \overline{T} \cdot \overline{K}_j \cdot \overline{T}^T \qquad [4\text{-}73]$$

The element stiffness matrix for a general element (prismatic or nonprismatic), considering two degrees of freedom per node (rotation and translation perpendicular to the member axis) is:

$$\overline{K} = \frac{1}{D}\begin{bmatrix} f_{22} + 2f_{21}L + f_{11}L^2 & -(f_{21} + f_{11}L) & (f_{22} + f_{21}L) & (f_{21} + f_{11}L) \\ -(f_{21} + f_{11}L) & f_{11} & f_{21} & -f_{11} \\ -(f_{22} + f_{21}L) & f_{21} & f_{22} & -f_{21} \\ (f_{21} + f_{11}L) & -f_{11} & -f_{21} & f_{11} \end{bmatrix} \qquad [4\text{-}74]$$

where:

$D = f_{11}f_{22} - f^2{}_{21}$

Since the cross flexibility terms f_{12} and f_{21} are equal, only f_{21} has been included in the development of the stiffness matrix. The evaluation of the flexibility factors is presented in the next subsection.

4.5.2.5 Evaluation of flexibility factors This section presents the evaluation of the flexibility factors defined in Section 4.5.2.3. The evaluation includes effects due to the distributed flexibility as well as the shear deformation.

To evaluate the displacements in the released element (Figure 61c) due to unit loads (flexibility terms), the unit-load method is used. This method assumes small displacements, and linear elastic material. Even that the material considered is non linear and inelastic, the nonlinear dynamic analysis is applied by linearizing the problem over a short time, therefore during such small period of time it is assumed that the material behaves linear and elastic. Flexural and shearing effects are considered in the determination of the flexibility terms as follows:

$$1 \times \Delta = \int_0^L \frac{mM}{EI} dx + \int_0^L \frac{v\,V}{A^{*}G} dx \qquad [4\text{-}75]$$

where:

EI: flexural rigidity

A*G: shear rigidity

- Evaluation of f_{11}

$$\begin{aligned} m(x) &= -1 \\ M(x) &= -1 \\ v(x) &= 0 \\ V(x) &= 0 \end{aligned} \qquad [4\text{-}76]$$

$$f_{11} = \int_0^L \frac{1}{EI} dx \qquad [4\text{-}77]$$

- Evaluation of f_{21}

$$m(x) = L - x$$
$$M(x) = -1$$
$$v(x) = -1$$
$$V(x) = 0 \qquad [4\text{-}78]$$

$$f_{21} = -\int_0^L \frac{L - x}{EI} dx \qquad [4\text{-}79]$$

- Evaluation of f_{12}

$$m(x) = -1$$
$$M(x) = L - x$$
$$v(x) = 0$$
$$V(x) = -1 \qquad [4\text{-}80]$$

$$f_{12} = -\int_0^L \frac{L - x}{EI} dx \qquad [4\text{-}81]$$

- Evaluation of f_{22}

$$m(x) = L - x$$
$$M(x) = L - x$$
$$v(x) = -1$$
$$V(x) = -1 \qquad [4\text{-}82]$$

$$f_{22} = \int_0^L \frac{(L - x)^2}{EI} dx + \int_0^L \frac{1}{A^* G} dx \qquad [4\text{-}83]$$

Section 4.5.2.2 showed expressions for the flexibility factor 1/EI as function of the position x, as well as function of the type of curvature (single or reverse). Substituting Eqns.[4-62] to Eqn. [4-64] into the expressions for the flexibility factors results:

- For single curvature

$$f_{11} = \frac{L}{2}\left(\frac{1}{EI_i} + \frac{1}{EI_j}\right)$$
$$f_{12} = f_{21} = -\frac{L^2}{6}\left(\frac{2}{EI_i} + \frac{1}{EI_j}\right) \qquad [4\text{-}84]$$
$$f_{22} = \frac{L^3}{12}\left(\frac{3}{EI_i} + \frac{1}{EI_j}\right) + \frac{L}{A^*G}$$

- For double curvature

$$f_{11} = \frac{L}{2EI_i}\alpha + \frac{L}{2EI_e} + \frac{L}{2EI_j}(1-\alpha)$$
$$f_{12} = f_{21} = \frac{L^2}{6EI_i}\alpha(\alpha-3) + \frac{L^2}{6EI_e}(\alpha-2) - \frac{L^2}{6EI_j}(\alpha-1)^2 \qquad [4\text{-}85]$$
$$f_{22} = \frac{L^3}{12EI_i}\left(\alpha^3 - 4\alpha^2 + 6\alpha\right) + \frac{L^3}{12EI_e}\left(\alpha^2 - 3\alpha + 3\right) - \frac{L^3}{12EI_j}(\alpha-1)^3 + \frac{L}{A^*G}$$

where α is defined by Eqn. [4-64].

4.5.2.6 Evaluation of element stiffness matrix The element stiffness matrix obtained in the previous sections applies for all the reinforced concrete elements, including beam, shear walls and steel-deck diaphragms. Main differences are in the hysteretic models used for each element. The hysteretic models are responsible for the instantaneous stiffness parameters (flexural EI, and shear A*G values) of the member.

In order to use a flexural hysteretic model (moment-curvature) to obtain the stiffness value EI for the next increment of time, an estimate of the actual curvature was needed. To evaluate the curvature, an iterative procedure was used to increase the accuracy of it. Such procedure started with elastic values for the flexural stiffnessis EI and degradation was allowed using the current curvature value in the origin oriented flexural hysteretic model. The expressions used for the curvature evaluation were obtained by dividing the first and third row of the member stiffness matrix (Eqn. [4-74]) by the respective EI value. The expressions used were:

$$\phi_i = \frac{\left[\left(f_{22} + 2f_{21}L + f_{11}L^2\right)\theta_i - \left(f_{21} + f_{11}L\right)\delta_i - \left(f_{22} + f_{21}L\right)\theta_j + \left(f_{21} + f_{11}L\right)\delta_j\right]}{DEI_i} \qquad [4\text{-}86]$$

$$\phi_j = \frac{\left[-\left(f_{22} + f_{21}L\right)\theta_i + f_{21}\delta_i + f_{22}\theta_j - f_{21}\delta_j\right]}{DEI_j} \qquad [4\text{-}87]$$

Once the curvature at each end is known, the corresponding bending moment may be evaluated from the hysteretic model. With values of curvature and moment obtained in the previous time, the incremental moment and curvature values may be evaluated. Next, the new flexibility factors are evaluated as follows:

$$\frac{1}{EI_i} = \frac{\Delta\phi_i}{\Delta M_i}, \quad \Delta\phi_i = \phi_{i,t+\Delta t} - \phi_{i,t}, \quad \Delta M_i = M_{i,t+\Delta t} - M_{i,t}$$
$$\frac{1}{EI_j} = \frac{\Delta\phi_j}{\Delta M_j}, \quad \Delta\phi_j = \phi_{j,t+\Delta t} - \phi_{j,t}, \quad \Delta M_j = M_{j,t+\Delta t} - M_{j,t} \qquad [4\text{-}88]$$

Beam elements may use a flexural hysteretic model such as Sina model (10) or Takeda model (9). As presented in Section 4.4.2.5, other inelastic components of deformation may also be included in the envelope moment-curvature.

For shear walls and diaphragms, an origin-oriented flexural hysteretic model, may be used as proposed by Nakashima et al. (71) and Kabeyazawa et al. (43). Shear effects are also included in the element stiffness through the shear rigidity term A*G. Different approaches have been presented for the inclusion of shear effects in the elastic and inelastic phases of behavior.

Reinforced concrete beams may consider the shear effects by dividing elastic and inelastic effects. Inelastic effects are included in the flexural envelope directly as proposed by Park et al. (98) (see Section 4.4.2.5.) The elastic shear effects are directly included by evaluating the elastic shear rigidity A*G. Other approaches go from neglecting shear effects; assume a constant elastic shear rigidity value (55); and finally assume shear rigidity degrading in proportion to the flexural stiffness (43). The last assumption has been also verified experimentally by Nakashima et al. (71) for reinforced concrete diaphragms.

Effect of shear in diaphragms and shear walls may work similarly to that of beams; the only difference is the hysteretic models used. Typically, the hysteretic models for shear walls and diaphragms are evaluated for a cantilever guided configuration, therefore this discussion applies for hysteretic models of force versus displacement (at the tip) of the cantilever system. To obtain the instantaneous shear rigidity value to be used in the next analysis step; the abscise value of the hysteretic model has to be known for input. Such abscise value may be the total displacement (including shear and bending as well as other effects), or shear displacement (all effects except bending). For models with abscise value defined by the total displacement, such as the steel-deck reinforced concrete diaphragms described in this work; the following procedure applies:

- Step 1: Assume that the flexural stiffness for the next increment of time has been evaluated according to the procedure described at the beginning of this section.
- Step 2: To evaluate the shear effect, the total lateral displacement as cantilever system has to be evaluated. By observing Figure 62, the lateral displacement δ_2 is used as the total displacement of a cantilever system and as input value for the hysteretic model. With Eqn. [4-69] the lateral displacement as cantilever is evaluated and the corresponding shear force is obtained from the hysteretic model.
- Step 3: In the evaluation of shear displacement, the lateral displacement δ_2 includes also bending effects, therefore the net shear displacement may be evaluated approximately by either of the following approaches:

  Approach A.

  the net shear deflection may be obtained by deducting bending deflection from δ_2

  as follows:

  $$\delta_{shear} \cong \delta_2 - \left(V_j f_{22}^* - M_j f_{21}\right) \qquad [4\text{-}89]$$

  where:

  f_{22}^* is the flexibility factor from Eqn. [4-84] or Eqn. [4-85] without the shear component.

  Approach B.

  the net shear deflection may be evaluated by assuming a constant ratio between the shear deflection and the total deflection as found experimentally for R/C diaphragms by Nakashima et al. (71).

- Step 4: Once the shear force and shear displacement have been evaluated, by recalling the same terms from the previous step, an incremental expression to evaluate the shear rigidity is used:

$$A^{*}G = \frac{\Delta V \cdot L}{\Delta \delta_{shear}}, \quad \Delta V = V_t - V_{t-\Delta t}, \quad \Delta \delta_{shear} = \delta_{shear,t} - \delta_{shear,t-\Delta t} \qquad [4\text{-}90]$$

In order to relate the hysteretic model with the member model, some assumptions associated with the deflected shape of the element have to be made. Common assumptions are:

- The inflection point is located at midlength (10,52,66)
- The element behave elastically with inelastic end springs (60).
- The flexibility factor 1/EI varies linearly (54), or parabolically (50,51).

For the especific case of shear walls and diaphragms, similar assumptions have to be considered in order to relate the hysteretic model with the member model. Typically, the hysteretic models for shear walls and diaphragms are presented as force vs displacement at the tip of a cantilever guided system. Then, a relation between the cantilever member and the continuous element is used (see Figure 62 and Eqn. [4-69]). In using such relation, the moment at the j end influence the lateral displacement; such effect is not present in the force-displacement relation of shear walls and diaphragms acting as cantilever systems and subjected only to lateral in-plane force. Due to the usually large bending stiffness of shear walls and diaphragms, the influence of this effect was assumed negligible.

4.5.3 Steel members

4.5.3.1 Introduction Steel members are oftenly analyzed under the assumption of concentrated plasticity behavior (plastic hinge model). This assumption holds as long as compact steel sections being used. See Section 4.4.4.2 for other assumptions involved. Modeling of steel structures follows basically two approaches: the shear beam approach, and the member-by-member approach. The shear beam approach consists in the concentration of the lateral resistance of all columns in a specific story as a single spring shear type element. Such approach is restricted to weak column-strong beam structural systems. The member-by-member approach is more general in the sense that may be applied to any type of structural system. Under this approach the member is modeled typically as an elastic element with inelastic rotational springs at the ends. This model assumes that plastic hinges are created only at the member ends which is typically a column type behavior. Steel beams may develop plastic hinges toward the midlength due to gravity load in combination with lateral load.

4.5.3.2 Member-by-member approach Under this approach the element is assumed to be form by an elastic central member and inelastic rotational springs. The following presentation assumes that inelastic rotational springs have elastoplastic behavior. The steel beam member is assumed to have two degrees of freedom at each end (rotation and lateral translation). According to the level of end deformation, a typical member may behave as: elastic member, fixed-hinge member, and hinge-hinge member. The incremental stiffness matrix has to consider all these possible stages.

Figure 63 shows end actions and displacement for a typical element. The incremental stiffness matrix based on these conditions was developed by Gilberson (60) and is presented here:

$$\begin{Bmatrix} \Delta M_i \\ \Delta V_i \\ \Delta M_j \\ \Delta V_j \end{Bmatrix} = \begin{bmatrix} S_a & -\frac{S_a+S_b}{L} & S_b & \frac{S_a+S_b}{L} \\ -\frac{S_a+S_b}{L} & \frac{S_a+2S_b+S_c}{L^2} & -\frac{S_b+S_c}{L} & -\frac{S_a+2S_b+S_c}{L^2} \\ S_b & -\frac{S_b+S_c}{L} & S_c & \frac{S_b+S_c}{L} \\ \frac{S_a+S_b}{L} & -\frac{S_a+2S_b+S_c}{L^2} & \frac{S_b+S_c}{L} & \frac{S_a+2S_b+S_c}{L^2} \end{bmatrix} \begin{Bmatrix} \Delta\theta_i \\ \Delta\delta_i \\ \Delta\theta_j \\ \Delta\delta_j \end{Bmatrix} \quad [4\text{-}91]$$

Expressions of the stiffness coefficients Sa, Sb, and Sc are function of the degree of end deformation in the member. Additionally, expressions for the rotation of the plastic hinge are needed to observe any change in the direction of hinge rotation. Such expressions may be evaluated using virtual work and are presented here for each stage of member end-deformation:

- Elastic stage

$$S_a = \frac{4EI}{L}, \quad S_b = \frac{2EI}{L}, \quad S_c = \frac{4EI}{L} \quad [4\text{-}92]$$
$$\Delta\alpha_i = 0, \quad \Delta\alpha_j = 0$$

- Plastic hinge at end i, elastic at end j

$$S_a = 0, \quad S_b = 0, \quad S_c = \frac{3EI}{L} \quad [4\text{-}93]$$
$$\Delta\alpha_i = \Delta\theta_i + \frac{\Delta\theta_j}{2} - \frac{3}{2L}\left(\Delta\delta_i - \Delta\delta_j\right), \quad \Delta\alpha_j = 0$$

- Elastic at end i, plastic hinge at end j

$$S_a = \frac{3EI}{L}, \quad S_b = 0, \quad S_c = 0$$
$$\Delta\alpha_i = 0, \quad \Delta\alpha_j = \Delta\theta_j + \frac{\Delta\theta_i}{2} - \frac{3}{2L}\left(\Delta\delta_i - \Delta\delta_j\right) \qquad [4\text{-}94]$$

- Plastic hinges at ends i and j

$$S_a = 0, \quad S_b = 0, \quad S_c = 0$$
$$\Delta\alpha_i = \Delta\theta_i - \frac{\Delta\delta_i - \Delta\delta_j}{L}, \quad \Delta\alpha_j = \Delta\theta_j - \frac{\Delta\delta_i - \Delta\delta_j}{L} \qquad [4\text{-}95]$$

where:

S_a, S_b, S_c: stiffness coeficients

$\theta_i, \delta_i, \theta_j, \delta_j$: member end displacement

α_i, α_j: plastic hinge rotation at end i and j respectively

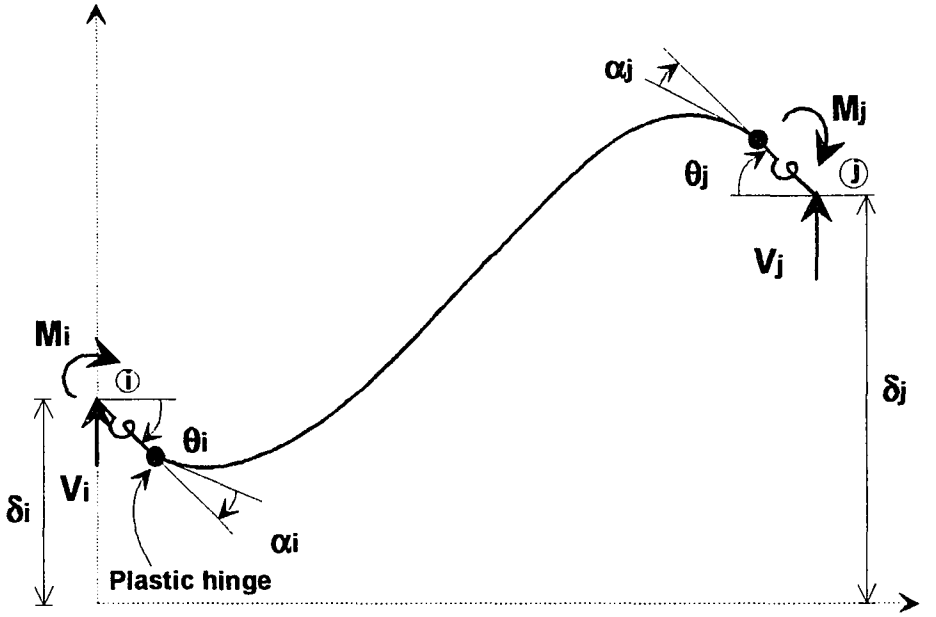

Figure 63. End forces and displacements for a typical steel member

For the solution process the following steps applies:

- Step 1: At the end of the time step the incremental displacements as well as the total displacements have been evaluated. Evaluate the end-member action using the respective incremental displacements and the element stiffness matrix from previous step.
- Step 2: Verify the plasticity condition, that is, the bending moment has to be less or equal to the plastic moment. If at any end, the moment is greater or equal to the plastic moment, then a plastic hinge has been form.
- Step 3: If from a previous time the member has plastic hinges, the hinge rotation has to be consistent with the sign of moment. That is the plastic hinge is free to rotate in one direction only, and in the opposite direction, the section returns to behave elastically.

4.5.3.3 Shear beam approach This model is appropriate for weak column-strong beam structural systems with lateral plastic mechanism of collapse. Under this approach, a series of columns at the same story level are substituted by one spring member with an equivalent lateral resistance. The spring member is assumed to behave with an elastoplastic force displacement relationship. This is true as long as all the substituted members reach their yield strength at the same lateral displacement, otherwise, the relationship is formed by a series of straight lines creating a more curved response.

Assuming an elastoplastic behavior for the substitute element, the stiffness matrix is given by:

$$\begin{Bmatrix} \Delta V_B \\ \Delta V_T \end{Bmatrix} = \begin{bmatrix} k & -k \\ -k & k \end{bmatrix} \begin{Bmatrix} \Delta \delta_B \\ \Delta \delta_T \end{Bmatrix} \qquad [4\text{-}96]$$

where:

ΔV_B: incremental force at the bottom of the story columns

ΔV_T: incremental force at the top of the story columns

$\Delta \delta_B$: incremental lateral displacement at the bottom of the story columns

$\Delta \delta_T$: incremental lateral displacement at the top of the story columns

k: stiffness of the equivalent spring element

The determination of the stiffness of the equivalent spring element is based on the following assumptions:

- Steel members have compact sections; that is sections with capacity to develop inelastic rotation capacity in the range of 7 to 9 times the elastic rotation capacity (104).
- All the elements substituted in the story, reach the yield strength at the same lateral translation.
- Other assumptions as stated in Section 4.4.4.2

From Figure 64, the stiffness of the equivalent spring member is obtained as follows:

The elastic stiffness of the equivalent spring element is given by:

$$K_e = \sum_{i=1}^{ncol} K_i = \sum_{i=1}^{ncol} \frac{V_{y,i}}{\Delta_{y,i}} = \sum_{i=1}^{ncol} \frac{12EI_i}{h^3} \qquad [4\text{-}97]$$

The inelastic stiffness of the equivalent spring element is given by:

$$K_p = \sum_{i=1}^{ncol} \frac{V_{p,i} - V_{y,i}}{\Delta_{p,i} - \Delta_{y,i}} = \sum_{i=1}^{ncol} \frac{2(M_{p,i} - M_{y,i})}{h(\Delta_{p,i} - \Delta_{y,i})} = \sum_{i=1}^{ncol} \frac{12EI_i}{h^3} \frac{(f_i - 1)}{(\mu_i - 1)} \qquad [4\text{-}98]$$

where:

V_y, V_p: shear at yield and plastic stage respectively

M_y, M_p: moments at yield and plastic stage respectively

Δ_y, Δ_p: deflections at yield and plastic stage respectively

$f = \frac{Z}{S} = \frac{M_p}{M_y}$ shape factor (approximately 1.12 in average for W shapes)

$$\mu = \frac{\Delta_u}{\Delta_y} = \frac{\theta_u h}{\theta_y h} = \frac{\theta_u}{\theta_y} = \frac{(R+1)\theta_y}{\theta_y} = R+1 \qquad [4\text{-}99]$$

R: inelastic rotation capacity ranging from 7 to 9 according to AISC (104]

Based on the average value of shape factor for W shapes and using an R value of 9, the inelastic slope of the equivalent spring element is approximately 1.3% of the elastic stiffness.

4.5.4 Frame and shear wall torsional stiffness

4.5.4.1 Assumptions Structural modeling considering the torsional stiffness of frames due to the rotational degree of freedom in the diaphragm has been suggested by Reinhorn et al. (42). The torsional stiffness of frames is generally negligible when compared with the flexural stiffness of diaphragms; but this not necessary the case when torsional stiffness of shear walls is considered.

In evaluating the torsional stiffness of frames and shear walls, the following assumptions are considerd:

- The rotational degree of freedom of the diaphragm is assumed to take place at the center of the shear wall or frame
- The torsional members behave linearly elastic
- Connection flexibility, between diaphragm ans supporting system, when used is assumed to behave elastically
- the torsional element (frame or shear wall) when subjected to rotation displaces linearly as shown in Figure 65.

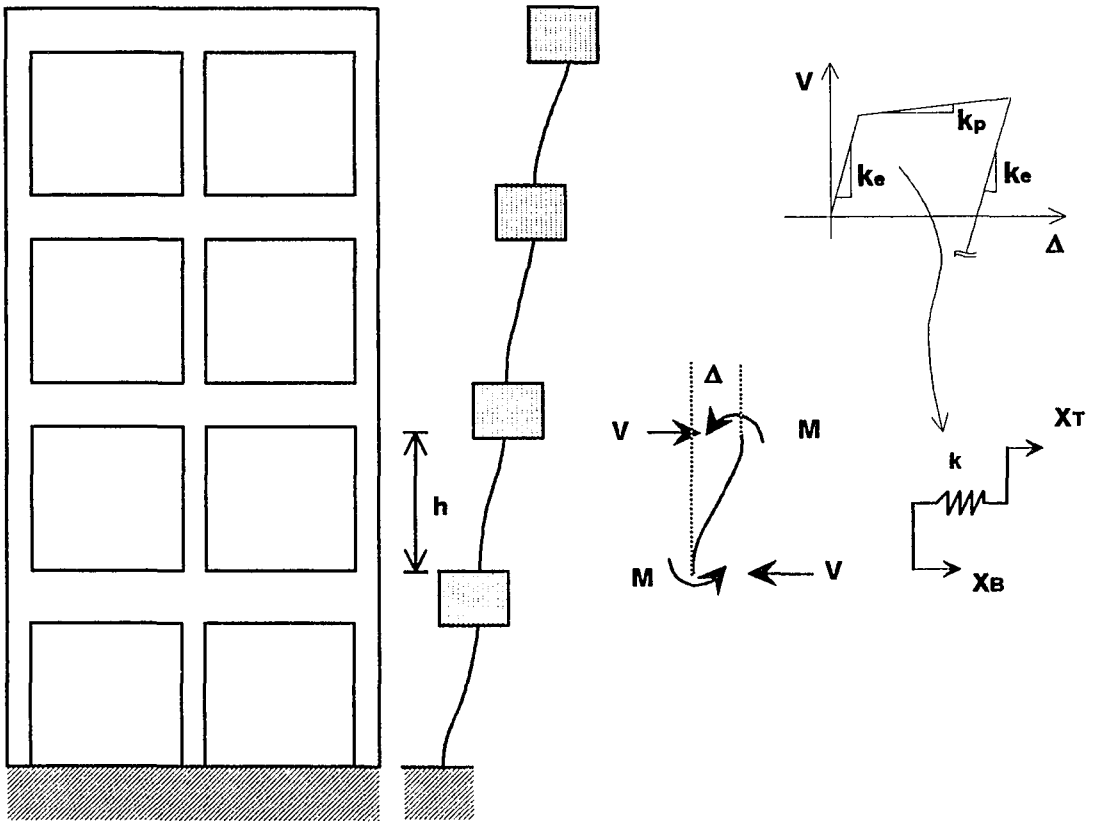

Figure 64. Typical shear frame structure

4.5.4.2 Frame torsional stiffness Based on the assumptions previously stated, the torsional frame element stiffness in incremental form is given by:

$$\begin{Bmatrix} \Delta M_T \\ \Delta M_B \end{Bmatrix} = \begin{bmatrix} k_t & -k_t \\ -k_t & k_t \end{bmatrix} \begin{Bmatrix} \Delta\theta_T \\ \Delta\theta_B \end{Bmatrix} \qquad [4\text{-}100]$$

The torsional moment is obtained by adding the aportations of each vertical element, then:

$$M_t = \sum_{i=1}^{ncol} V_i x_i \qquad [4\text{-}101]$$

Each vertical element is subjected to a horizontal force V_i given by the stiffness of the element times the corresponding lateral horizontal displacement (see Figure 65), therefore the torsional moment is given by:

$$M_t = \sum_{i=1}^{ncol} k_{ci}(\theta x_i)x_i = \left(\sum_{i=1}^{ncol} k_{ci}x_i^2\right)\theta \qquad [4\text{-}102]$$

Finally by setting the rotation equal to unity, the torsional stiffness coefficient is:

$$k_t = \sum_{i=1}^{ncol} k_{ci}x_i^2 \qquad [4\text{-}103]$$

where:

k_{ci}: flexural stiffness of the ith vertical element

x_i: distance from the center of the diaphragm to the ith vertical member

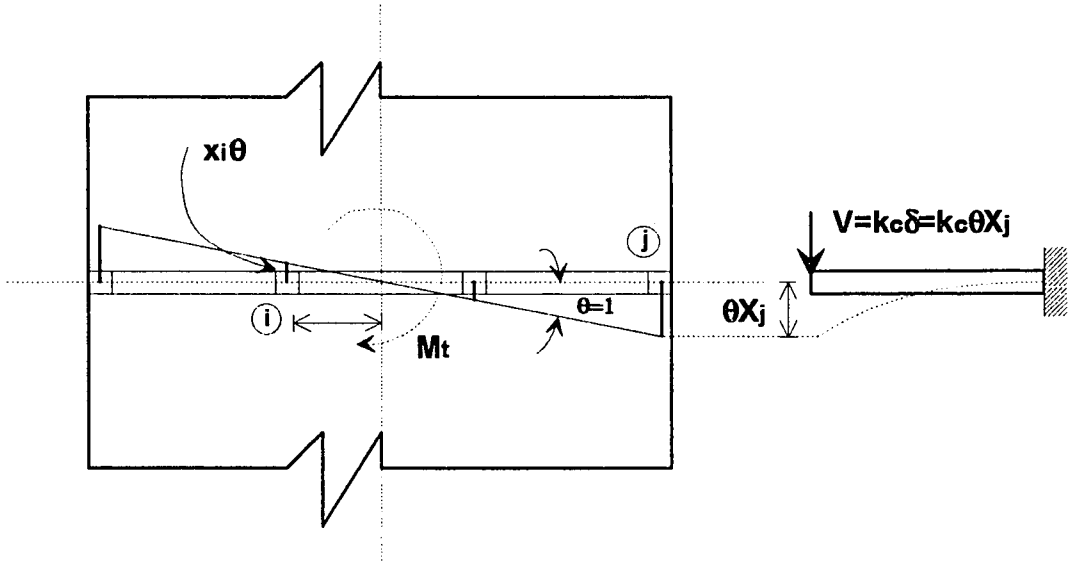

Figure 65. torsional frame element (modified from reference 42)

4.5.4.3 Shear wall torsional stiffness The torsional stiffness coefficient provided by a shear wall parallel to the lateral loading direction is evaluated considering the flexibility of connection between wall and diaphragm. The rotational degree of freedom of the diaphragm is assumed to be applied at the center of the diaphragm forcing the shear wall to move along a line as shown in Figure 66.

At any distance x from the center of the diaphragm, a differential force dF is acting on the diaphragm. Such differential force is result of the opposition to distort by the connection and shear wall. The sum of the differential moments produced by dF have to equilibrate the torsional moment, that is:

$$M_t = \int dM = 2\int_0^{\frac{L}{2}} x dF \qquad [4\text{-}104]$$

The lateral displacement at any position is given by the rotation θ times x. This displacement is also equal to the component of displacement generated at the connection and the shear wall (as shown in Figure 66), that is:

$$\Delta(x) = \theta x = \delta_{conn} + \delta_{sw} \qquad [4\text{-}105]$$

A relation between the components of displacement and the applied force is given by the stiffness coeficient (per unit length) of each segment. From such relation, the components of displacement may be obtained as follows:

$$\begin{aligned} dF &= (\bar{k}_{sw} dx)\delta_{sw} \Rightarrow \quad \delta_{sw} = \frac{dF}{\bar{k}_{sw} dx} \\ dF &= (\bar{k}_{conn} dx)\delta_{conn} \Rightarrow \quad \delta_{conn} = \frac{dF}{\bar{k}_{conn} dx} \end{aligned} \qquad [4\text{-}106]$$

Substituting Eqn. [4-106] into Eqn. [4-105] and solving for dF:

$$dF = \frac{xdx}{\left(\frac{1}{\bar{k}_{sw}} + \frac{1}{\bar{k}_{conn}}\right)}\theta \qquad [4\text{-}107]$$

Substituting Eqn. [4-107] into Eqn. [4-104] and setting θ equal 1:

$$k_t = 2\int_0^{\frac{L}{2}} \frac{x^2 dx}{\left(\frac{1}{\bar{k}_{sw}} + \frac{1}{\bar{k}_{conn}}\right)} = \frac{L^3}{12}\frac{\bar{k}_{sw}\bar{k}_{conn}}{\bar{k}_{sw} + \bar{k}_{conn}} \qquad [4\text{-}108]$$

where:

$\bar{k}_{sw}$: out-of-plane flexural stiffness of shear wall per unit length

$\bar{k}_{conn}$: connection stiffness per unit length

L: shear wall length

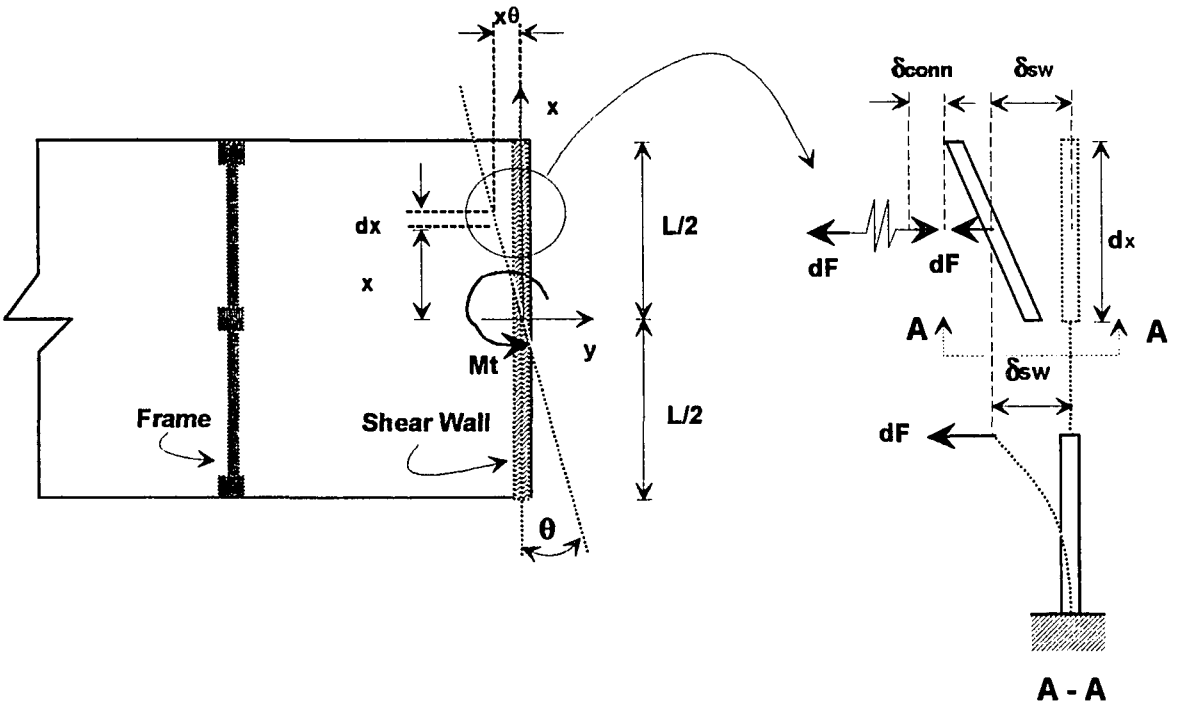

Figure 66. Diaphragm-shear wall interaction schematic

Force-displacement relationships for different types of connections are available in the literature. For bond slippage of embedded steel, a relation between stress in the steel bar and the amount of slippage is available in Reference (98). An empirical relationship between load and deflection for studs is available in Reference (105).

4.6 Global Stiffness Matrix

4.6.1 Assembled stiffness matrix

The global stiffness matrix of the structural system was obtained by accumulating the contributions of all element stiffness matrices. Local degrees of freedom (dof) were related to global degrees of freedom, then, element stiffness matrices were accumulated into the global stiffness matrix at appropiate locations.

Each node in the structure had defined a rotational degree of freedom. Since axial deformation was neglected, all joints connected by series of members at the same level, displaced equally in horizontal direction and introduced only one degree of freedom.

The structural system was discretized by elements. Additionally, the mass of the system was also discretized or lumped to translational degrees of freedom, these resulted in a number of massless degrees of freedom. Degrees of freedom were classified as primary and secondary. Primary dof were all those associated with a translational degree of freedom, therefore a lumped mass was associated with them. Secondary dof were all those related to rotational degree of freedom. Since no rotational inertia was considered for the masses, then, secondary degrees of freedom were masless dof.

Only external lateral loads were considered in the analysis, therefore, external vertical forces and moments at joints of the structure were assumed to be zero.

4.6.2 Static condensation

Static condensation was applied on the secondary degrees of freedom (sdof). The condensation was applied to the stiffness matrix. Additionally, rows and columns associated with the secondary degrees of freedom were deleted because those were masless dof. The global stiffness matrix with coefficients associated only to free joint displacements was partitioned as follows:

$$[K]\cdot\{y\}=\{F\} \qquad [4\text{-}109]$$

or

$$\left[\begin{array}{c|c}[K_{ss}] & [K_{sp}]\\ \hline [K_{ps}] & [K_{pp}]\end{array}\right]\cdot\left\{\begin{array}{c}\{y_s\}\\ \hline \{y_p\}\end{array}\right\}=\left\{\begin{array}{c}\{0\}\\ \hline \{F_p\}\end{array}\right\} \qquad [4\text{-}110]$$

where:

s: associated with secondary dof

p: associated with primary dof

After applying matrix operations, a reduced stiffness matrix $\overline{K}$ was obtained:

$$[\overline{K}]\cdot\{y_p\}=\{F_p\} \qquad [4\text{-}111]$$

where:

$$[\overline{K}]=[K_{pp}]-[K_{ps}][K_{ss}]^{-1}[K_{sp}] \qquad [4\text{-}112]$$

Practical aplication of the static condensation method did not require the evaluation of the inverse matrix K_{ss}. By using the Gauss-Jordan elimination procedure up to the elimination of the secondary dof y_s (Eqn. [4-112b]) the reduced stiffness matrix was obtained.

4.7 Mass Matrix

The mass matrix of the structural system was obtained assuming that the entire mass was concentrated in the points at which the translational dof were defined (primary dof). Structural elements were considered masless line elements. The lumped-mass matrix was a diagonal matrix with zero diagonal elements for the rotational dof, since static condensation was used, all diagonal elements were nonzero:

$$[M] = \begin{bmatrix} m_1 & & & 0 \\ & m_2 & & \\ & & . & \\ & & & . \\ 0 & & & m_p \end{bmatrix} \qquad [4\text{-}113]$$

where:

$[M]$: diagonal mass matrix of order pxp

m_i: lumped mass at the primary ith dof

p: number of primary dof

4.8 Damping Matrix

The damping forces are usually assumed to be proportional to the velocity of the points were dof are defined, for this condition, damping is identified as viscous type of damping. For this work, the damping matrix was considered at the structural level, and expressed as a linear combination of the mass and global stiffness matrices.

$$[C] = a_0[M] + a_1[K] \qquad [4\text{-}114]$$

where:

$[C]$: viscous damping matrix

a_0, a_1: proportionality constants

The proportionality constants were related to the damping ratio and frequency by:

$$\xi_n = \frac{a_0}{2\omega_n} + \frac{a_1\omega_n}{2} \qquad [4\text{-}115]$$

The two damping factors a_0, and a_1 were evaluated through the solution of a pair of simultaneous equations. By defining a pair of damping ratios ξ_n for two specific frequencies and substituting into Eqn. [4-115], the simultaneous equations were:

$$\begin{aligned} \xi_1 &= \frac{a_0}{2\omega_1} + \frac{a_1\omega_1}{2} \\ \xi_2 &= \frac{a_0}{2\omega_2} + \frac{a_1\omega_2}{2} \end{aligned} \qquad [4\text{-}116]$$

where:

ξ_1, ξ_2: damping factors for the two first modes

Even though exist more simple approaches to evaluate the damping matrix, the linear combination of the mass and stiffness matrix was selected because include the effect of lower and higher frequencies. It can be seen from Eqn. [4-116] that when the damping matrix is proportional to the mass matrix only (a_1=0) the damping ratio is small for higher frequencies of vibration (inversely proportional to the frequency). If a stiffness proportional damping matrix is considered (a_0=0), the damping ratio is large for higher frequencies. Then, the contribution of the higher modes to the response is less significant. According to Clough and Penzien (64), neither of these two proportional damping approaches are suitable for multi degrees of freedom system with a wide range of

frequencies because the relative amplitude of either the higher or lower modes will be distorted by inadequate damping ratios.

4.9 Differential Equation of Motion

By considering the dynamic equilibrium of all the forces on the structure, a system of equations of motion can be formulated. A step-by-step integration procedure was used for the analysis of the nonlinear response equations. To apply the step-by-step procedure, an incremental formulation of the equations of motion was used as follows:

At time t

$$\{F_i\}_t + \{F_d\}_t + \{F_s\}_t = \{F_p\}_t \qquad [4\text{-}117]$$

At time $t + \Delta t$

$$\{F_i\}_{t+\Delta t} + \{F_d\}_{t+\Delta t} + \{F_s\}_{t+\Delta t} = \{F_p\}_{t+\Delta t} \qquad [4\text{-}118]$$

Evaluating the differences between vector equilibrium equations, the incremental equilibrium equation was obtained:

$$\Delta F_i + \Delta F_d + \Delta F_s = \Delta F_p \qquad [4\text{-}119]$$

where:

$$\begin{aligned} \Delta F_i &= \{F_i\}_{t+\Delta t} - \{F_i\}_t = [M]\{\Delta \ddot{y}\} \\ \Delta F_d &= \{F_d\}_{t+\Delta t} - \{F_d\}_t = [C]\{\Delta \dot{y}\} \\ \Delta F_s &= \{F_s\}_{t+\Delta t} - \{F_s\}_t = [K]\{\Delta y\} \\ \Delta F_p &= \{F_p\}_{t+\Delta t} - \{F_p\}_t = -[M]\{\Delta \ddot{y}_g\} \end{aligned} \qquad [4\text{-}120]$$

where:

[M]: mass matrix

[C]: damping matrix

[K]: stiffness matrix

$\{\Delta\ddot{y}\}$: incremental acceleration vector

$\{\Delta\dot{y}\}$: incremental velocity vector

$\{\Delta y\}$: incremental displacement vector

$\{\Delta\ddot{y}_g\}$: incremental ground acceleration vector

The elements of the incremental stiffness matrix were defined at the beginning of the time increment and assumed constant during the increment of time, therefore the incremental expressions in the left side of Eqn. [4-119] were only an approximation. The system of equations of motion of a structural system change to nonlinear in nature when some of its components are nonlinear themselves. For reinforced concrete systems subjected to strong motions the demand of ductilty on the system usually force the component members to go into the nonlinear range, resulting in a nonlinear set of equations of motion.

4.10 Numerical Solution of Equations of Motion

4.10.1 General considerations

Numerical step-by-step integration is a general procedure for the solution of linear and nonlinear set of equations of motion. In this method, the response is divided into a sequence of small, usually equal time steps, and during each time increment the response is evaluated for a linear system having the stiffness properties existing at the starting of the time increment. At the end of each time increment the stiffness properties are updated according to the previous history of member deformation. Since the stiffness coefficients are assumed constant during each time increment, the nonlinear analysis may be seen as a sequence of analysis of successively changing linear systems.

Several implicit and explicit methods are available for performing the step-by-step integration of the equations of motion. Newmark's β method (106) has been widely used for linear and nonlinear analysis because its versatility and efficiency. For linear systems, specific values of its parameter β make this method unconditionally stable, that is, the solution does not grow out-of-bound for any time step. For nonlinear problems, the Newmark's β method tend to be unstable (108).

For the numerical solution of the equations of motion, the cost of an analysis (i.e., the number of operations used) is directly proportional to the size of the time step that has to be used for accuracy and stability (107). Bathe, et al. (107) investigated stability limits, period elongation and amplitude decay in the dynamic response of linear systems. Bathe discussed the selection of time step, starting with the rule of one tenth of the smallest period. Clough et al. (64) suggest a time step smaller than the smallest period divided by 1.8 In selecting the smallest period to consider, attention may be given to:

- Largest frequencies and mode shapes in lumped systems are only crude approximations to the exact values (107).
- Recording of earthquake excitation with period smaller of approximately 0.05 sec. are not accurately made (52).

4.10.2 Algorithm of solution

The Newmark's β method (106) was considered in the solution of the nonlinear system of equations. This method introduces two coefficients (β, γ) in the incremental displacement and acceleration equations. The parameter γ may introduce numerical or artificial damping within the time step. For γ values smaller than 1/2, artificial negative damping is included, values above 1/2 introduces positive damping, and γ equal 1/2 introduces no damping. The parameter β controls the variation of acceleration within the

time step. A value of zero results in the constant acceleration approach (64,65,107), value of 1/4 introduces the average acceleration approach, and a β value of 1/6 results in a linear acceleration approach.

Using the algorithm equations for Newmark's β method with γ equal to 1/2, and β equal to 1/4, the incremental velocity and displacement equations are:

$$\Delta\dot{y}_i = \left[(1-\gamma)\ddot{y}_i + \gamma\ddot{y}_{i+1}\right]\Delta t_i = \ddot{y}_i\Delta t_i + \tfrac{1}{2}\Delta\ddot{y}_i\Delta t_i \qquad [4\text{-}121]$$

$$\Delta y_i = \dot{y}_i\Delta t_i + \left[\left(\tfrac{1}{2}-\beta\right)\ddot{y}_i + \beta\ddot{y}_{i+1}\right]\Delta t_i^2 = \dot{y}_i\Delta t_i + \left(\tfrac{1}{2}\ddot{y}_i + \beta\Delta\ddot{y}_i\right)\Delta t_i^2 \qquad [4\text{-}122]$$

Solving Eqn. [4-122] for $\Delta\ddot{y}_i$ and substituting into Eqn. [4-121] results:

$$\Delta\dot{y}_i = \frac{1}{2\beta\Delta t_i}\Delta y_i - \frac{1}{2\beta}\dot{y}_i - \left(\frac{1}{4\beta}-1\right)\ddot{y}_i\Delta t_i \qquad [4\text{-}123]$$

Now, substituting Eqn. [4-123] into the incremental differential equation of motion (Eqn. [4-119] and Eqn. [4-120]) results in:

$$\begin{aligned}
&\hat{K}_i\Delta y_i = \Delta\hat{F}_i \\
&\hat{K}_i = \frac{[M]}{\beta\Delta t_i^2} + \frac{[C]}{2\beta\Delta t_i} + [K] \qquad [4\text{-}124] \\
&\Delta\hat{F}_i = \Delta F_i\left(\frac{\dot{y}_i}{\beta\Delta t_i} + \frac{\ddot{y}_i}{2\beta}\right)[M] + \left[\frac{\dot{y}_i}{2\beta} + \left(\frac{1}{4\beta}-1\right)\ddot{y}_i\Delta t_i\right][C]
\end{aligned}$$

After solving Eqn. [4-124] for Δy_i, updated values for displacement, velocity, and acceleration may be obtained:

$$y_{i+1} = y_i + \Delta y_i \qquad [4\text{-}125]$$

$$\Delta\dot{y}_i = \frac{1}{2\beta\Delta t_i}\Delta y_i - \frac{1}{2\beta}\dot{y}_i - \left(\frac{1}{4\beta} - 1\right)\ddot{y}_i\Delta t_i \qquad [4\text{-}126]$$

$$\dot{y}_{i+1} = \dot{y}_i + \Delta\dot{y}_i$$

$$\Delta\ddot{y}_i = \frac{1}{\beta\Delta t_i^2}\Delta y_i - \frac{1}{\beta\Delta t_i}\dot{y}_i - \frac{1}{2\beta}\ddot{y}_i \qquad [4\text{-}127]$$

$$\ddot{y}_{i+1} = \ddot{y}_i + \Delta\ddot{y}_i$$

The evaluation of the updated acceleration using Eqn. [4-127], is usually substituted by solving for the acceleration directly from Eqn. [4-118].

4.11 Computer Program

4.11.1 Introduction

A computer program called INEDAV8 (INElastic Dynamic Analysis Version 8) was developed for the nonlinear dynamic analysis of lumped parameter structures. The code is based in a series of 25 FORTRAN subroutines, and was prepared for a 386 IBM personal computer or compatible system. As input, the code accepts either of time-histories of earthquakes or nodal forces. A library of elements is used to model the behavior of different structural systems. Particularly, the code included the following element models:

- Linear elastic translational spring.
- Linear elastic rotational spring.
- Linear elastic beam element.
- Elasto-plastic shear-beam element.
- Inelastic concrete beam element.
- Inelastic flexural-shear spring model.

The program was developed for the two dimensional analysis of 3D structural systems. Under such scheme all the frames parallel to the direction of loading are

connected by transverse elements such as beams and diaphragms, allowing flexural-torsional coupling. The main steps used during the program are presented in the flowchart of Figure 67.

4.11.2 Numerical validation

Since, there were no experimental dynamic test results available for a wall-frame-SDRC diaphragm structure, the computer program was validated through comparison of analytical results of typical frame structures behaving inelastically. Specifically, numerical solutions obtained from Biggs (120), Clough and Penzien (64), and Paz (121) were used to test the capabilities of the program in handling elasto-plastic behavior of one-, two- and three-story frames. A comparison of displacement versus time response for the different examples showed basically no difference. A typical three-story steel frame subjected to load-time nodal forces was solved by Biggs (120). The structure was assumed to have an elasto-plastic behavior. A comparison of the response obtained with INEDAV8 as well as the solution from Reference (120) is shown in Figure 68, where a good agreement is observed.

In order to test the capacity of the program to handle the distributed plasticity model for reinforced concrete members, a five-story reinforced concrete shearwall (20' by 60' by 7.625") subjected to El Centro N-S 1940 was analyzed and displacement response was compared with the solution presented for the same problem by Kariotis, et al. (123). Both approaches considered variation of the flexural stiffness EI, at a given time Kariotis approach assumes constant EI value for the element, meanwhile the distributed plasticity model used a distributed flexibility approach that accounts for the spread of the plastic zone. As shown in Figure 69, the general response pattern was similar.

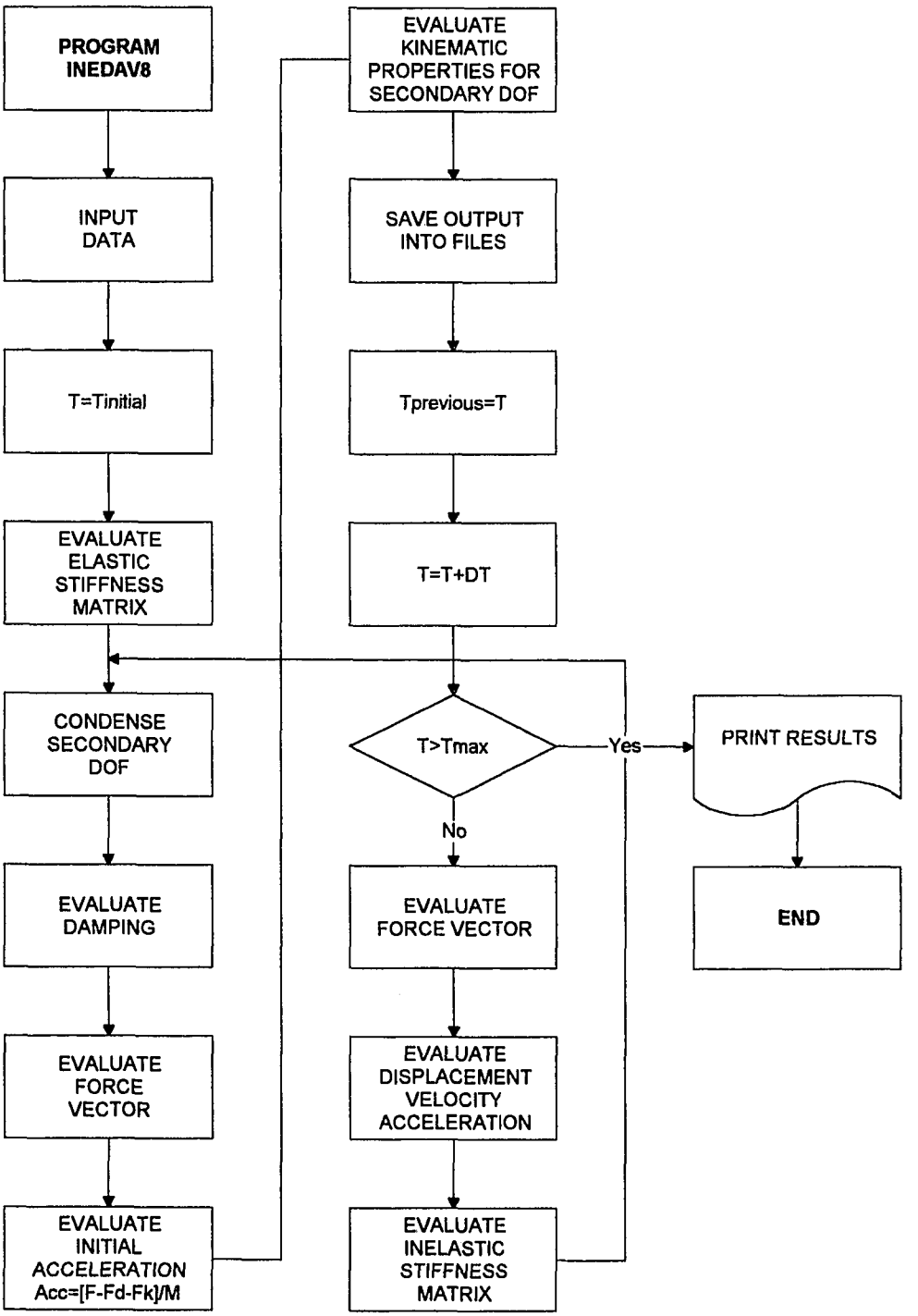

FIGURE 67. Computer program flowchart

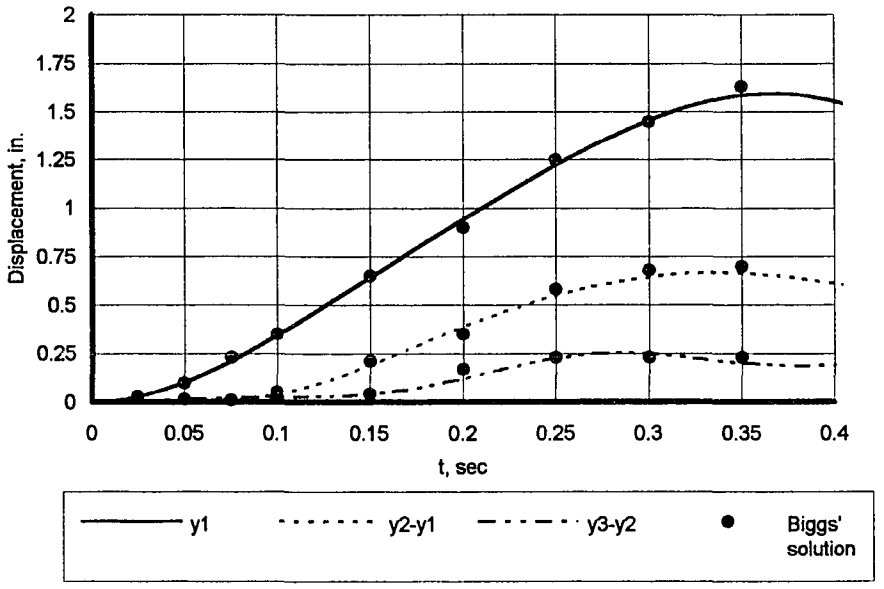

Figure 68. Elasto-plastic response of a three story steel frame under load-time nodal forces

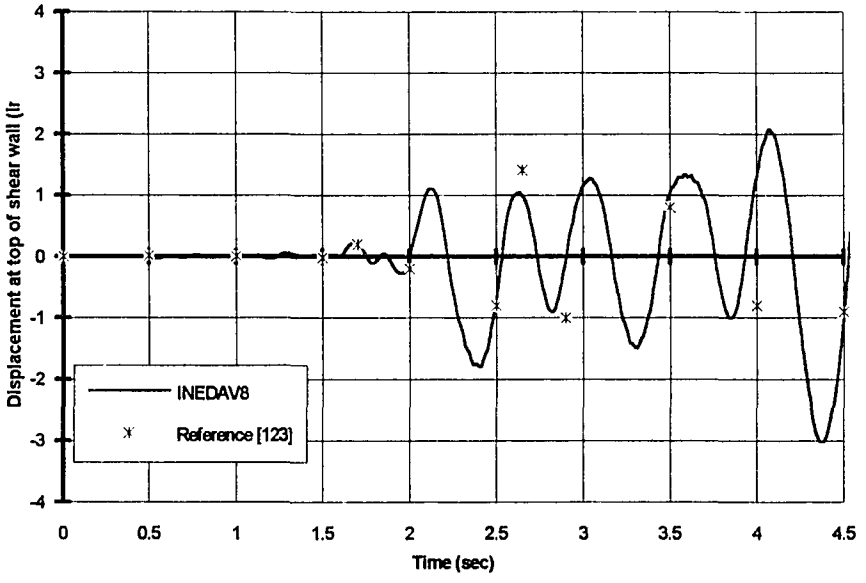

Figure 69. Comparison of response for a R/C shear wall subjected to EL CENTRO N-S 1940

4.12 Model and Analysis of a Wall-Frame-Diaphragm Structure

4.12.1 Model of a selected structure

As a final part of this study, a nonlinear and linear dynamic analysis of a one-story building subjected to ground motion was made. In order to do the analysis, a computer program (INEDAV8) was developed. For analysis purposes, a typical one-story building was selected (Figure 70). The building consisted of a steel-deck reinforced concrete diaphragm supported on a pair of reinforced concrete shearwalls at the ends and moment resisting steel frames at interior supports. The structure was designed according to the Uniform Building Code specifications (122) for gravity as well as wind and seismic loads. For seismic analysis purposes, the structure was assumed to be located in a seismic zone Region 4 that corresponds to a horizontal peak acceleration of 0.4g with 90 percent probability of not being exceeded in 50 years (124).

For the diaphragm system, a steel-deck reinforced concrete diaphragm was selected. A 3 in. steel-deck with a 2.5 in. concrete on top for a total slab depth of 5.5 in. was used. The diaphragm was connected to the supporting system by 3/4 in. ∅ 4 in. long headed studs at every 6 in. o. c.. The proposed diaphragm corresponded to that numbered as Diaphragm 2 in the experimental test program at ISU, which showed a diagonal tension failure. The coefficients required to define the shear force hysteretic model of such diaphragm were obtained from the respective Tables in Chapter 3. For the flexural capacity of the diaphragm the moment-curvature curve shown in Figure 51 was used as envelope of an origin oriented hysteretic model.

The reinforced concrete shearwall used was assumed to be 8 in. thick with a 4 ksi compressive strength. The minimum amount of reinforcement according to the ACI code (63) was used, that is #4 @ 6 in. Based in these characteristics, the moment-curvature

curve was obtained (see Figure 71), and used as the envelope curve in the origin oriented hysteretic model. The shear wall was modeled with the same hysteretic model used for diaphragms, but since the wall was designed for flexural failure type, the post-peak envelope curve of the shear hysteretic model was assumed to remain constant.

The moment resisting steel frame was assumed to behave as a shear frame, therefore an inelastic shear spring was used for the hysteretic model. Considering both frame columns, the total elastic stiffness was 47.6 kip/in, for the plastic region, a plastic slope of 1.3% of the elastic stiffness was used.

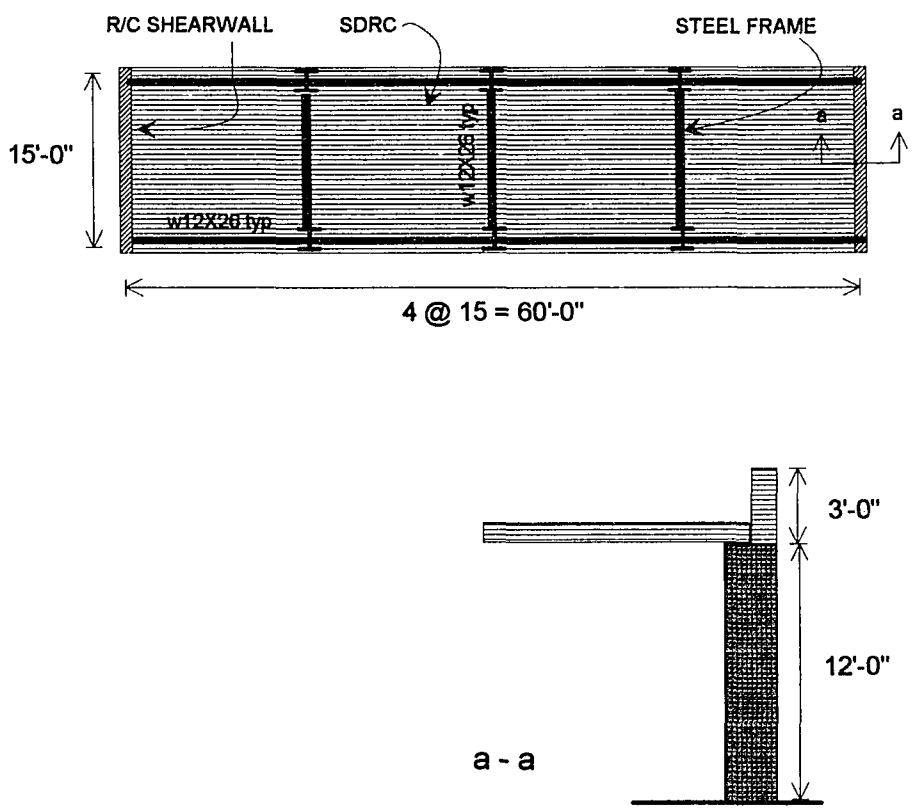

Figure 70. Typical one story building

For the analysis, the symmetry of the structure about the middle frame was considered, therefore, only half structure was analyzed. Since the structure was divided in half, the mass associated with the centerline DOF was also divided, and the middle steel frame was then modeled with half the stiffness and strength of the regular frame.

Torsional spring elements were included to consider the torsional restraint produced by the steel frames and shear walls against diaphragm rotation. For the steel frames the elastic torsional stiffness was evaluated using Equation [4-106] given a total of 8166 kip-in. For the shear walls, the elastic torsional stiffness was evaluated using Equation [4-111]. Since the moment curvature envelope of the diaphragm included the flexibility of the fastener connection, the torsional stiffness value was evaluated assuming an infinite value of the connection stiffness. The shear wall elastic torsional stiffness value was found to be 128515 kip-in.

The structural system was represented by a lumped parameter model as shown in Figure 72. The floor system was divided into several segments defined by the frame axis and a concentrated mass was located at each segment interface. Each lumped mass included the tributary mass of the respective diaphragm segment as well as the tributary side wall mass.

4.12.2 Analysis of the selected structure

The dynamic analysis considered was formulated including the following effects:

1. A structure with 15 by 60 feet plan dimension was considered.
2. The dynamic analysis was applied using elastic and inelastic behavior of the structural elements.
3. 2% of stiffness proportional damping was considered.

4. The first ten seconds of the acceleration time history of the EL CENTRO N-S 1940 earthquake was used. Since the structure was assumed to be located in a seismic Region 4 (UBC-91), the ground acceleration of EL CENTRO was scaled by a factor of 1.25 to give the 0.4g required peak acceleration. Figure 73 shows the scaled EL CENTRO accelerogram.

For the dynamic analysis of the structure using the step by step integration method, a time step has to be selected. Clough, et al. (64) suggest a time step smaller than the smallest period divided by 1.8. An eigenvalue problem was solved for the condensed stiffness matrix and lumped mass matrix of Case I structure.

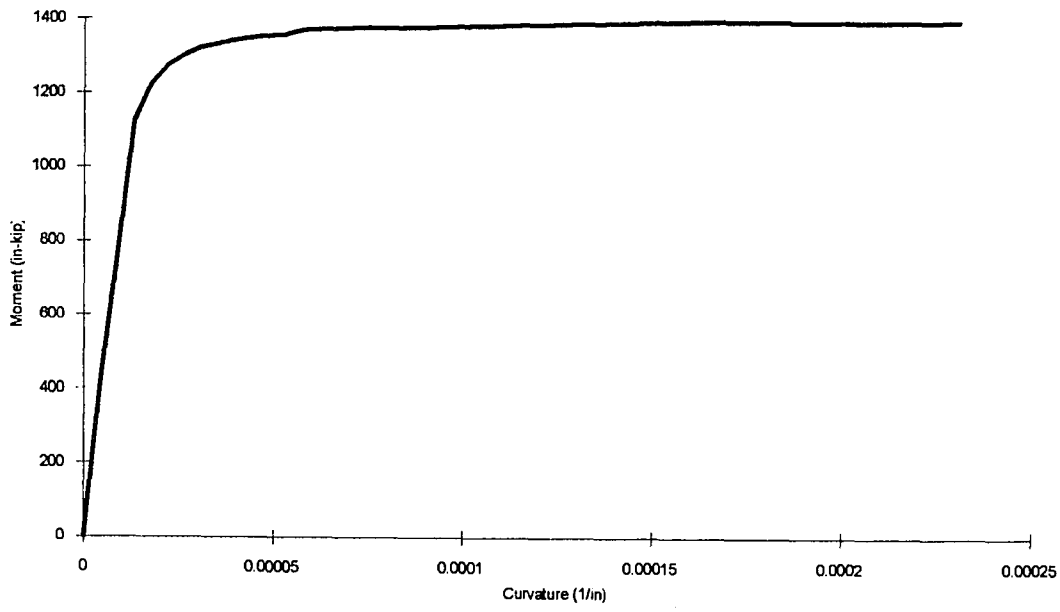

Figure 71. Moment-curvature curve for the proposed R/C shear wall

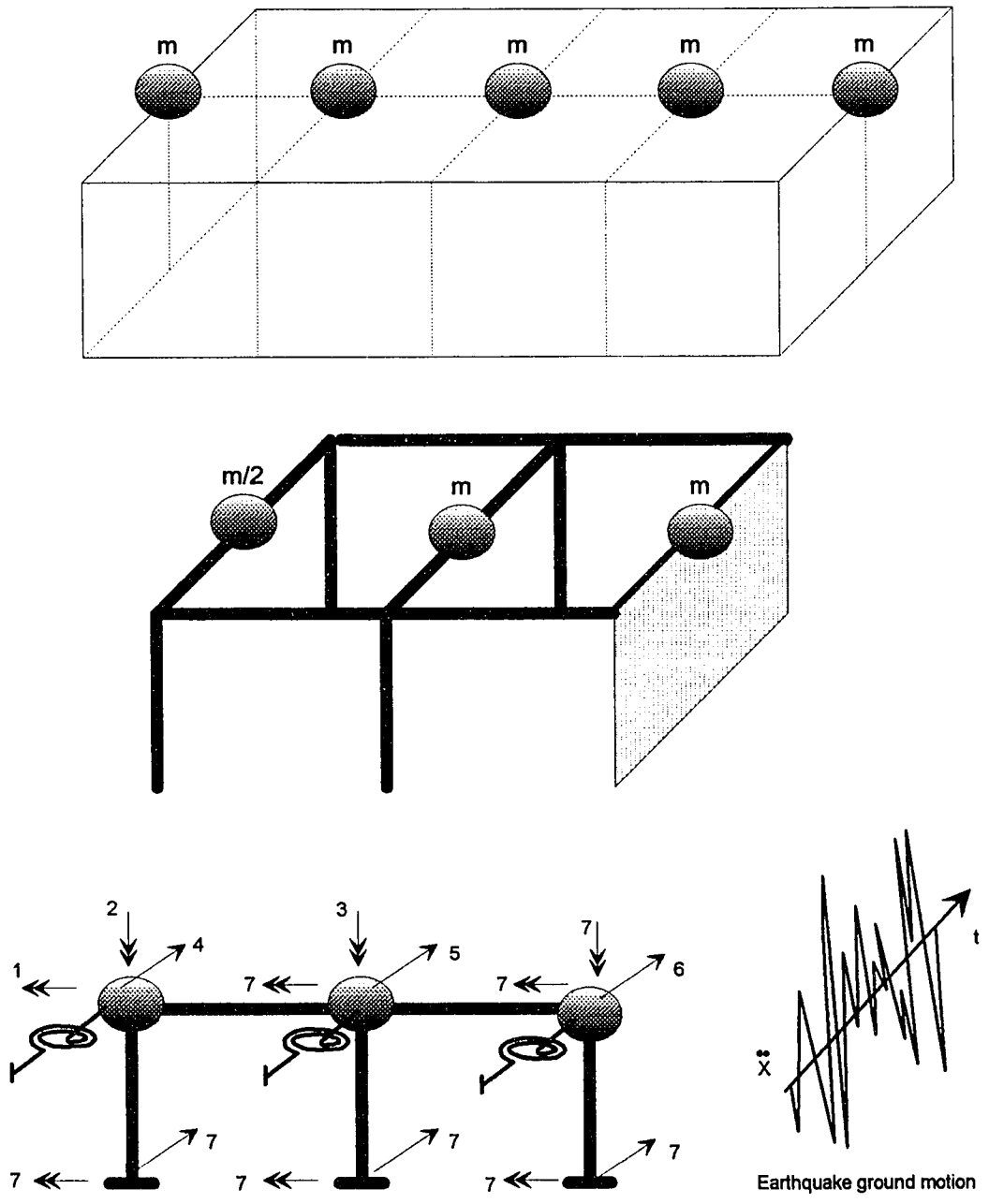

Figure 72. Lumped mass model

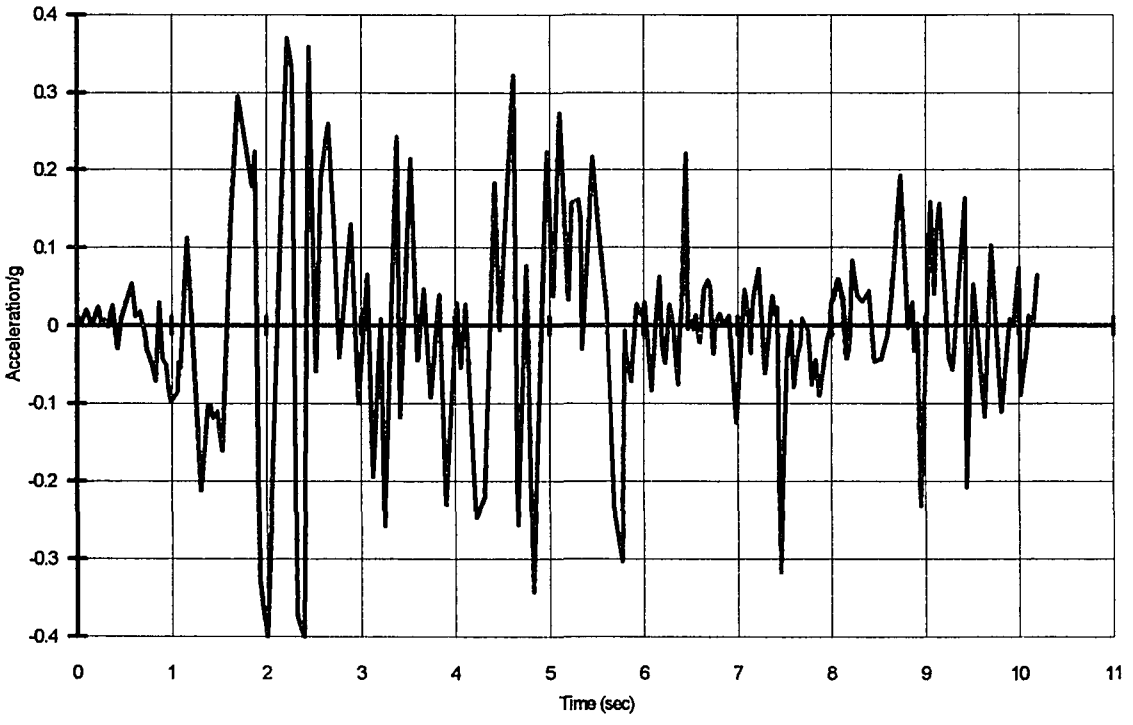

Figure 73. El Centro N-S 1940 ground motion

The smallest period was 0.0166 sec therefore the time step should be less than 0.009 sec. The selected time step for all the analysis was 0.005 sec. This small value was selected after a couple of trial and error solutions, the criterion was to generate the hysteretic model rules without discontinuties which may occur if the time step is large.

A total of 2000 time steps were used for each of the two analyses. Comparison of displacements at diaphragm midlength, and at top of wall was made. Investigation of the time for yielding of each hysteretic model was also made. The next section discussed the results of such analysis.

4.12.3 Results of the dynamic analysis

Two dynamic analyses were made assuming linear elastic and inelastic behavior. Figure 74 shows a comparison between the elastic and inelastic diaphragm midlength displacement. From this figure is observed that for the two first seconds of the earthquake motion the structure behaves elastically. At approximately 2.5 seconds, the shearwall reached the yield force of 116 kips, next half cycle also reached the yield capacity in the opposite direction. The magnitude of the yield force was evaluated as the flexural capacity of the shear wall divided by the wall height. Note that the shear capacity of the shear wall according to the ACI code (63) was 402 kips, forcing the wall to have a ductile behavior since the flexural failure is controlling. Figure 75 shows the shear force vs total lateral displacement for the shear wall. Note that a flat constant post-peak envelope is obtained and not a decaying envelope because the capacity was limited by flexure.

The steel deck reinforced concrete diaphragm behavior was different to that of the shear walls. The shear capacity of the diaphragm was 189 kips for a diagonal tension failure. Therefore, the diaphragm was expected to show a degrading strength after the peak load was reached. At approximately 5 seconds, the first interior diaphragm segment reached their maximum capacity in one direction and immediately after that reached its maximum capacity in the opposite direction and started to degrade. Before the first diaphragm segment reached its shear capacity, the interior steel frames reached the yield strength at approximately 4.5 sec and started to behave elastic-plastic. This effect forced the system to redistribute the shear force through the diaphragm and triggered the diaphragm degradation. Figure 76 shows the force-displacement behavior for the first interior diaphragm.

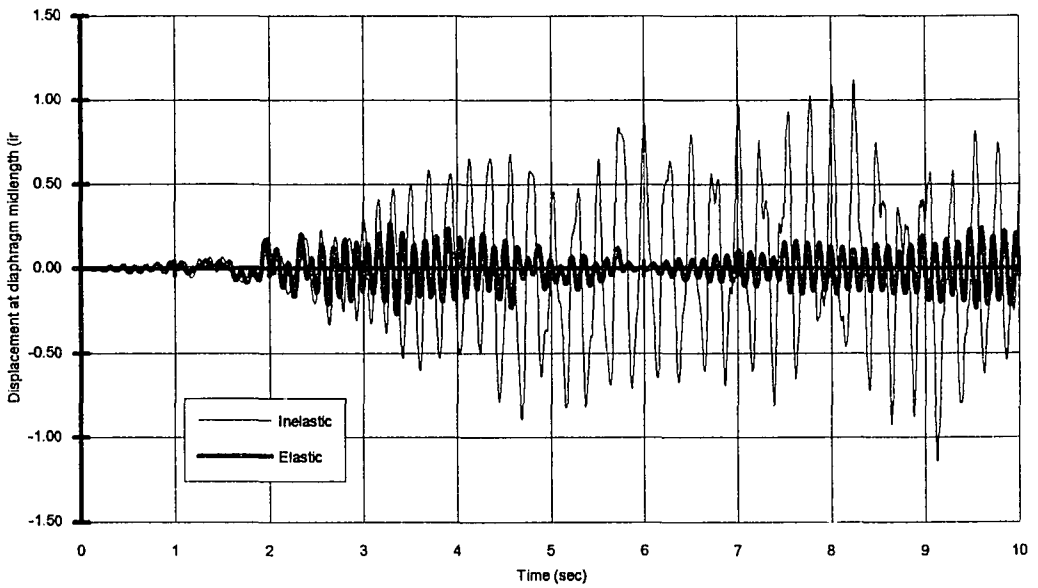

Figure 74. Comparison of elastic and inelastic displacements at diaphragm midlength

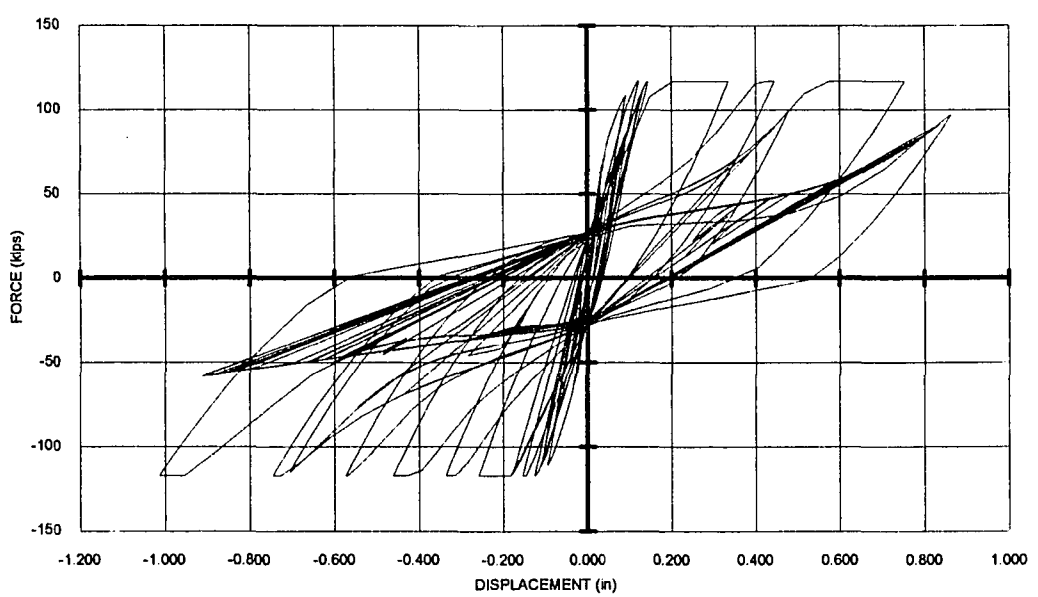

Figure 75. Force-displacement behavior of the R/C shear wall

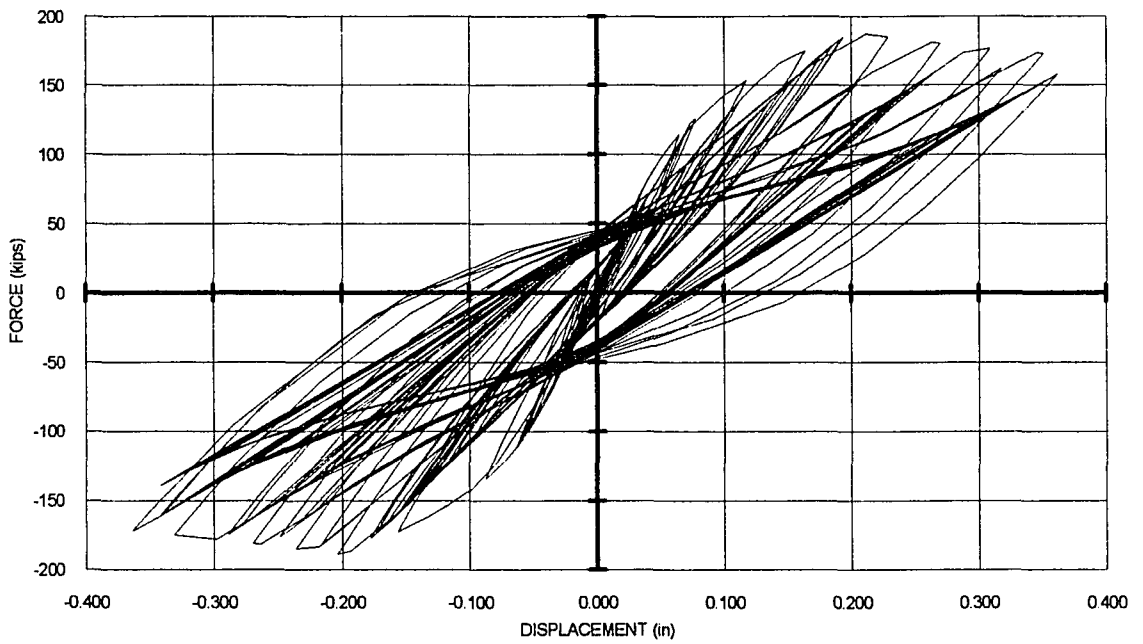

Figure 76. Force-displacement behavior of first interior diaphragm segment

The steel frame members reached the yield strength at approximately 4.5 sec of the initiated ground motion. After the shear wall reached yield capacity, larger displacements were allowed at the top of the wall, therefore, larger displacements started to occur at top of steel frames initiating the yielding process. Figure 77 shows the force displacement behavior of the first interior steel frame.

Finally, once the first interior diaphragm reached its maximum strength, a more flexible system was generated because the loss in stiffness, such effect causes a redistribution of force forcing the interior diaphragm to yield. The force-displacement curve for the second diaphragm segment is similar to that shown in Figure 76 and is not reproduced.

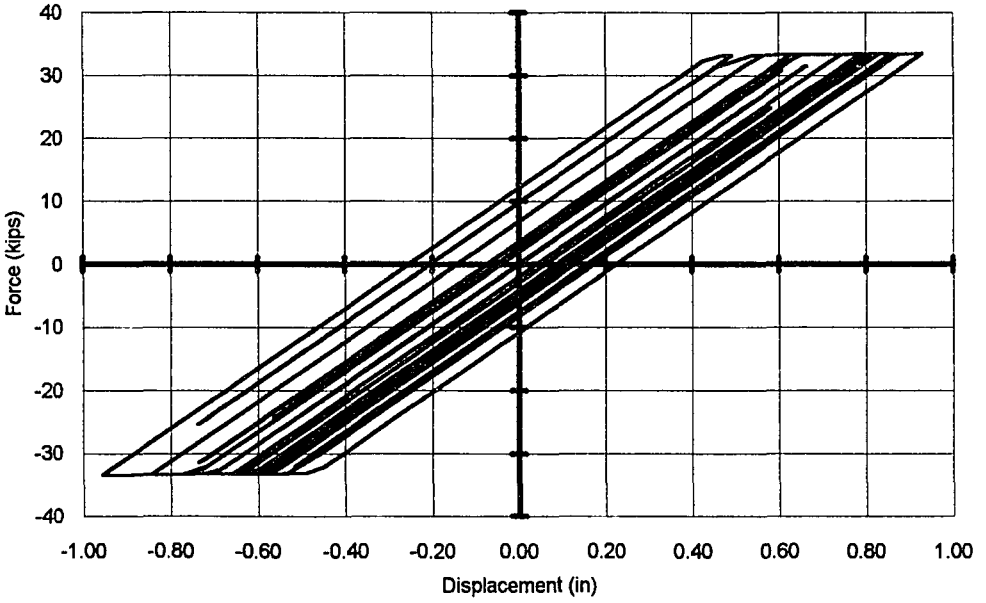

Figure 77. Force-displacement behavior of the first interior steel frame

5. SUMMARY, CONCLUSIONS AND RECOMMENDATIONS

5.1 Summary

This investigation on seismic modeling of structures with steel-deck-reinforced concrete diaphragms was part of the overall research program conducted at Iowa State University dealing with the investigation of floor diaphragms constructed with steel-deck-reinforced concrete. The overall research program was divided into three phases: Phases I and II had as objective the investigation of behavioral and strength characteristics of SDRC floor diaphragms. Phase III had as objective the dynamic modeling of SDRC floor diaphragms.

Before this analytical phase (Phase III) of the research, nine specimens were tested in Phase I and the results were reported by Porter and Greimann (78). Additionally to the full-size tests, 97 elemental tests conducted at ISU were reported by Dodd (18) and Prins (76). Twenty-three full size diaphragms were tested as part of Phase II and the results were reported by Porter and Easterling (89).

Phase I of the research developed predictive equations for initial stiffness and strength of SDRC diaphragms. These equations were based on an edge zone concept with edge force distributions based on a linear elastic finite element analysis. Force distributions at ultimate load levels were assumed. Phase II of the research program verified the previously assumed edge force distribution at ultimate based on a nonlinear finite element analysis. Additionally, design recommendations based on the experimental and analytical results were also developed.

Phase III of the overall research program had as main objective the analytical investigation of the nonlinear inelastic behavior of steel-deck-reinforced concrete diaphragms under seismic loads. As part of this study, previous diaphragm research was

reviewed. Both SDRC diaphragms and RC diaphragm research were considered. An extensive review was made in hysteretic models for reinforced concrete elements, as well as in member macro-modelling of concrete and steel elements. Finally a review of the state-of-the-art on dynamic modelling of diaphragms and the structural interaction was also made.

Specific objectives of Phase III were the development of a hysteretic model with nonlinear, inelastic, degrading and pinching capabilities to predict the in-plane shear response of SDRC diaphragms under earthquake loads, and the definition of the steps needed for the modeling of structures incorporating the diaphragm action.

The development of the diaphragm hysteretic model included the definition of all the model components needed to describe the force-displacement characteristics of the SDRC diaphragm. Envelope curve equation, pinch force expression, loop stiffness equations, cyclic loop equation, strength degradation, and hysteresis rules were the model components developed to describe the diaphragm hysteretic behavior. Two approaches were presented to describe the envelope curve equation: statistical, and analytical approach. Experimental results were extensively used for the development of the hysteretic model with the statistical approach. Particularly, these included force-displacement results for the cyclic displacement, pinch force values or force at zero cyclic displacement, and slopes of cyclic loops at different locations in the displacement history of all the diaphragm tests.

An analytical approach based on strain compatibility and equilibrium conditions were developed and used in the prediction of the force-displacement envelope curve. A major component of the analytical approach consisted in the definition of the flexural characteristic of diaphragms including the edge connection flexibility and deck-concrete interface flexibility. The method used in the analytical definition of the envelope curve

was presented as an easy and simple alternative to the more complicated nonlinear finite element analysis proposed by Porter and Easterling (89).

A review of the state-of-art on modeling of structures subjected to earthquakes loads was made, and modifications were made to include the diaphragm flexibility, as well as the interaction frame-diaphragm and shearwall-diaphragm.

A computer program for the nonlinear dynamic analysis of structures with steel-deck reinforced concrete diaphragms was developed. The program (INEDAV8) included the following elements models: linear elastic translational spring, linear elastic rotational spring, linear elastic beam element, elasto-plastic shear-beam element, inelastic concrete beam element, and inelastic flexural-shear spring model.

Finally, a procedure was presented for the dynamic analysis of structures with diaphragms.

5.2 Conclusions

The following conclusions were based on the results of the investigation summarized above:

1. Tests for normality were applied on the experimental forces of the envelope curve for all the specimens. Two different tests, the Kolmogorov-Smirnov and the Chi-Square, showed that at 5% significance level the Hypothesis of normality can not be rejected.
2. Positive and negative force-displacement envelope data was tested for significant difference or symmetry to the origin. Data was grouped into two sections: virgin and stabilized envelope data, resulting in a total of 62 sets. Results showed that at 5% level from a total of 62 sets, 13 sets (21%) showed significant difference, and at 1% level, only two sets (3%) showed significant difference From those tests with a significant difference at the 5% level, only

one failed via the diagonal tension mode. In conclusion, the response pattern of diaphragms with characteristics considered in this study under cyclic load is symmetrical respect to the origin.

3. A series of eleven models (Table 3) was selected as possible candidates to fit the force-displacement envelope curve of SDRC diaphragms. The normalized data was grouped into six sections for each specimen: virgin and stabilized envelope, positive and negative envelope, pre- and post-peak envelope segment, resulting in a total of 248 data sets. Results showed (Figures 16 and B1-B8) that from all eleven suggested models the logarithmic-x regression model resulted with the lowest mean absolute error (MAE) and the smallest confidence interval (at 5% level). Therefore, the logarithmic-x model was selected to predict the force-displacement envelope curves for SDRC diaphragms.
4. Statistical analyses were applied on each of the experimental envelope data using the selected logarithmic-x model. Specifically, analyses of variance to test for significance in the regression coefficients, as well as other statistical indices were evaluated for each specimen (Tables 7 and B4-B7). Coefficients of determination showed a global mean value of 0.92 (unity stands for perfect correlation), and a global mean standard error of 0.011. F tests were used to verify the strength of the proposed model. Significance F values displayed a global mean value of 0.2% (<5%), that strongly support the proposed model.
5. Multiple regression analyses were used with the proposed log model to involve other parameters in the prediction. From a list of parameters identified (Section 3.3.5.7.3) the axial stiffness Q, the gravity load index, and the steel deck shape parameter exhibited influence in the envelope prediction, because

they showed regression coefficients that improved the explanation of variability (at 5% level). Results of the multiple regression analysis showed a global mean value for the correlation coefficient ranging among 0.89 to 0.96, with a better prediction for the pre-peak envelope curves (Table 9).

6. A parameter to estimate the reduction in strength capacity for an increased number of cycles at the same displacement level was developed. This cyclic strength degradation factor was initially analyzed separately against two parameters: the number of cycles for a given displacement level, and maximum reached displacement for a given number of cycles. From the analysis for the first parameter using the eleven proposed models from Table 3, and based on the obtained MAE values, the logarithmic-x regression model was selected. For the analysis using the second parameter, the linear model displayed the lowest average MAE value for all the tests. Applying multiple regression analysis, both described parameters as well as other possible variables were attempted to be combined. Results showed that for both sets of data (pre- and post-peak regions) the strength degradation factor was mainly a function of the number of cycles (through its transformation, ln(n)), deck shape type, and the maximum normalized displacement. Additionally for the post-peak region, the axial stiffness index and the gravity load index were also significantly different from zero (at 5% level). As a measure of improvement respect to use only the mean average value for the degradation factor, a comparison between standard error of the estimate and standard deviation of the degradation factors was made. A 35% and 38% in reduction were obtained for pre-peak and post-peak regions, respectively.

7. To describe the cyclic behavior of SDRC diaphragms, an expression for the pinch force or force at zero cyclic displacement was developed. First, normalized pinch force experimental values and normalized displacements were fitted against eleven suggested models from Table 3. Data was grouped into four sections: virgin and stabilized values, and pre- and post-peak region, resulting in a total of 124 sets of data. The linear model showed to be as good option as other nonlinear models, since there was no significant difference (at 5% level) between their MAE values. A multiple regression analysis was applied to investigate the possible improvement of the explained variation by including more parameters. Results showed that for the pre-peak region the shape deck parameter and normalized displacement ratio were significant. For the post-peak region the normalized displacement ratio, the shape deck parameter, and the axial stiffness index Q was also significant (5%). As a measure of goodness of fit a comparison between standard deviations and standard errors were made. Reduction on the standard deviation ranged from 32% to 36%.
8. Expressions to evaluate the slope at three specific locations of a force-displacement cyclic loops were developed. The characteristic slopes were evaluated at zero cyclic displacement (k0), at maximum cyclic displacement for a loading stage (k1), and maximum cyclic displacement for an unloading stage (k2). Initially, the experimental data was fitted using a pool of eleven suggested models (Table 3). From these analyses, the square root had in most of the cases the smallest MAE, therefore was selected as basic model. Next, multiple regression analysis was also applied to investigate if variation may be explained through the inclusion of additional parameters. Results

showed that deck shape parameter was the major contributor to the definition of the regression coefficients, and in lesser degree (10% or less of the total coefficient value) was the gravity load index. Additionally, a comparison of the confidence intervals for the three characteristic slopes (Table B24) showed that there was no significant difference (5% level) between virgin and stabilized coefficients. Therefore, the effect of cyclic stiffness degradation may be considered negligible.

9. Cyclic loop equations were developed assuming polynomial type of expression according to References (27,28,38,44). To investigate the degree of the polynomial expression to be used a stepwise regression analysis was applied, using 5th order polynomial as an upper bound. Force-displacement values were normalized with respect to the maximum cycle force and displacement, and grouped into quarter cycle and half cycle sets. Results showed a large explained variation (coefficient of determination) for the polynomial expressions used, with an average above 0.95 (unity stands for perfect fit). Additionally, for all the cases tested, quarter and half cycles may be predicted by second and third order polynomial expressions, respectively.
10. A series of six rules were stated to describe the hysteretic behavior of steel-deck-reinforced concrete diaphragms.
11. An analytical procedure (fiber model approach) to predict the pre-peak envelope force-displacement curve of SDRC diaphragm was presented. The procedure was based on uniaxial strain compatibility analysis and considered effects such as material non linearity of the components, edge connection flexibility, and deck-concrete flexibility was suggested as an alternative to the more complex nonlinear finite element approach presented in Reference (89).

Comparison of the predicted response against experimental results as well as to nonlinear finite analysis predictions, showed that the suggested procedure even though its simple and approximate approach did a good job in the force-displacement prediction of the experimental specimens.

12. The presented fiber model approach enabled the evaluation of the moment-curvature curves for the diaphragm sections especially those located at the end of the diaphragm. These curves show the effect of edge connection as well as deck-concrete interface flexibility, needed for the dynamic analysis of the overall structure.
13. Only one expression to evaluate the flexibility of 5/8 in. diameter arc-spot welds could be found during this study. However, force-displacement curves were not generally available for various arc-spot weld diameters made in various strength steels, except for analytical curves proposed in Reference (29).
14. The used fiber model approach assumes a uniform edge connector force-displacement distribution. Therefore, modelling of diaphragms with few connectors resulting in a non-uniform distribution (e.g., Diaphragm 8) should be avoided and more sophisticated analysis, such as finite element methods, should be utilized.
15. The distributed flexibility approach, from Reference (42), was used to form the stiffness matrix of the diaphragm elements. Flexural and shearing effects were accounted for, in the evaluation of the flexibility coefficients, by adding the components of deflection accordingly. In addition, a step by step procedure was described to update the diaphragm stiffness matrix during the analysis.

16. A procedure for the evaluation of torsional stiffness of the diaphragm supporting system was developed. This procedure also included the connection flexibility needed to represent a more realistic behavior of the interactive systems.
17. A computer program was developed (INEDAV8) for the nonlinear dynamic analysis of diaphragm-wall-frame structures subjected to earthquakes. Such code was verified against analytical solutions available in the literature.
18. A numerical example of inelastic dynamic analysis of a SDRC diaphragm structure was made with the objective of establish a step by step procedure for the modeling and analysis of frame-wall structures with SDRC diaphragms. Result seem to be reasonable.

5.3 Recommendations for Continued Study

1. Perform additional full-scale diaphragm tests with similar characteristics to increase the number of elements in the samples with specified attributes (e.g., light weight concrete, aspect ratio, deck orientation, etc.). This will lead to identify any possible statistically significance of such parameters, and improve the statistical predictive model.
2. Experimentally investigate the force-displacement relationships for deck-to deck and deck-to-structure welds made with different diameters and deck steel strength.
3. Perform additional full-scale diaphragm tests under an improved displacement history. Such displacement history should include degradation cycles as in

the sequential phase displacement program proposed by Porter (116), but with additional displacement paths such as half cycles. This improvement could lead to new rules for loading and unloading of the hysteretic model.

4. Incorporate into the analytical prediction of the moment-curvature relationship the effect on the concrete due to tension stiffening and shear force level. Constitutive relationships for concrete such as those proposed by Vecchio and Collins in their modified compression field theory (100) may be used.
5. Experimentally and analytically investigate the effects of the size and location of openings in the force-displacement characteristics of SDRC diaphragms.
6. Experimentally investigate the effect on the diaphragm due to intermediate supports members such as steel joists, and compare results with those predicted analytically using the fiber model approach.
7. Analytically investigate on SDRC diaphragms the three-dimensional loading effects such as out-of-plane loading and eccentricity of applied in-plane load.
8. Using the computer program developed, made a sensitivity analysis of the parameters required to describe the hysteretic model.
9. Experimentally investigate the behavior of steel-deck reinforced concrete diaphragms under quasi-dynamic testing such as shaking table tests. Such testing program will help to experimentally verify the computer code developed, as well as provide insight in the strain rate phenomenon not included in previous experimental programs.
10. Prepare a set of recommendations for the dynamic analysis of structures using steel-deck-reinforced concrete diaphragms.

REFERENCES

1. Porter, M. L., F. S. Yeomans, and A. W. Johnson. "Assembly of Existing diaphragm data." U.S.-Japan Coordinated Program for Masonry Building Research, Final Report Task 5.2. Department of Civil and Construction Engineering, Iowa State University, Ames, Iowa, 1990.

2. Wakabayashi, M. "Studies on Damping and Energy Absorption of Structures." Symp. on Resistance and Ultimate Deformability of Structures acted on by Well-Defined Repeated Loads. International Association of Bridge and Structural Engineering, Lisbon, 1973.

3. Wakabayashi, M. Design of Earthquake-Resistant Buildings. New York: McGraw-Hill Book Company, 1986.

4. Riddell, R., and N. M. Newmark. "Force-Deformation Models for Nonlinear Analyses." ASCE Journal of the Structural Division 105, ST12 (Dec. 1979): 2773-2778.

5. Otani, S. "Hysteresis Models of Reinforced Concrete for Earthquake Response Analysis." Proc. of the Eight World Conference on Earthquake Engineering. Englewood Cliffs, New Jersey: Prentice Hall, 1984.

6. Sozen, M. A. "Hysteresis in Structural Elements." Applied Mechanics in Earthquake Engineering, ASME, AMD, 8 (Nov. 1974): 63-98.

7. Jennings, P. C. "Periodic Response of a General Yielding Structures." Proc., ASCE Journal of the Engineering Mechanic Division 90, EM2 (April 1964): 131-166.

8. Clough, R. W., and S. B. Johnston. "Effect of Stiffness Degradation on Earthquake Ductility Requirements." Proc. at Second Japan Earthquake Engineering Symposium. Tokyo, 1966.

9. Takeda, T., M. A. Sozen, and N. N. Nielsen. "Reinforced Concrete Response to Simulated Earthquakes." Proc. ASCE, Journal of the Structural Division 96, ST12 (Dec. 1970): 2557-2573.

10. Saiidi, M., and M. A. Sozen. Simple and Complex Models for Nonlinear Seismic Response of Reinforced Concrete Structures. University of Illinois, Urbana-Champaign, Structural Research Series #4. Champaign: University of Illinois Press, 1979.

11. Tanabashi, R., and K. Kaneta. "On the Relation between the Restoring Force Characteristics of Structures and the Pattern of Earthquake Ground Motions." Proc. First Japan Earthquake Engineering Symposium, Tokyo, 1962.

12. Iwan, W. D. "The Steady State Response of the Double Bilinear Hysteretic Model." Trans. ASME Journal of Applied Mechanics 32 (1965): 921-925.

13. Ramberg, W., and W. R. Osgood. "Description of Stress-Strain Curves by Three Parameters." National Advisory Committee on Aeronautics Technical Note 902, 1943.

14. Meyer, R. J. "Effect of Plank Depth Parameter on Seismic Resistance of Precast Hollow-Core Plank Diaphragms." M.S. Thesis, Iowa State University, Ames, Iowa, 1988.

15. Otani, S. "SAKE-A Computer Program for Inelastic Response of R/C Frames to Earthquake." Civil Engineering Studies, Structural Research Series No. 413, University of Illinois, Urbana, November 1975.

16. Ewing, R. D., J. C. Kariotis, and A. El-Mustapha. "LPM/I. A Computer Program for the Nonlinear, Dynamic Analysis of Lumped Parameter Models." National Science Foundation, Tech. Rept. 2.3-1, August, 1987.

17. Neilsen, M. K. "Effect of gravity load on composite floor diaphragm behavior." M.S. Thesis, Iowa State University, Ames, Iowa, 1984.

18. Dodd, S. M. "Effect of edge fasteners on the seismic resistance of composite floor diaphragms." M.S. Thesis, Iowa State University, Ames, Iowa, 1986.

19. Tremel, P. M. "Boundary Conditions and Orientation Behavioral Characteristics for Hollo-Core Planks." M.S. Thesis, Iowa State University, Ames, Iowa, 1988.

20. Rosenblueth, E., S. E. Ruiz, and C. C. Thiel, Jr., "The Mexico Earthquake of September 19, 1985" Earthquake Spectra. Vol 5, Number 1, February 1989.

21. Porter, M. L. "Highlights of New ASCE Standard on Composite Slabs." Proceedings of the 8th International Specialty Conference on Cold-Formed Steel Structures. University of Missouri-Rolla, Rolla, Mo. (1986): 433-452.

22. Porter, M. L. "Two-Way Analysis of Steel Deck Floor Slabs." Proceedings of the 9th International Specialty Conference on Cold-Formed Steel Structures, University of Missouri-Rolla, Rolla, Mo., (1988): 331-342.

23. Porter, M. L., and L. F. Greimann. "Composite Steel Deck Diaphragm Slabs- Design Slabs." Proceedings of the 6th International Specialty Conference on Cold-Formed Steel Structures. University of Missouri-Rolla, Rolla, Mo. (1982): 467-484.

24. Porter, M. L., and L. F. Greimann. "Shear-Bond Strength of Studded Steel Deck Slabs." Proceedings of the 7th International Specialty Conference on Cold-Formed Steel Structures. University of Missouri-Rolla, Rolla, Mo. (1984): 285-306.

25. American Society of Civil Engineers Composite Steel Deck Slabs Standards Committee of the Technical Council on Codes and Standards. Specifications for the Design and Construction of Composite Slabs. ANSI-ASCE Standard. (ASCE3) New York: ASCE, 1985.

26. American Society of Civil Engineers Composite Steel Deck Slabs Standards Committee of the Technical Council on Codes and Standards. Specifications for the Design and Construction of Composite Slabs. ANSI-ASCE Standard. (ASCE3 and ASCE9) New York: ASCE, To be Published in 1993.

27. Soroushian, P., K. Obaseki, and K. Choi. "Nonlinear Modeling and Seismic Analysis of Masonry Shear Walls." ASCE Journal of Structural Engineering Division, 114, No. 5 (May 1988): 1106-1119.

28. Yeomans, F. S. "A Hysteretic Model for Precast Prestressed Hollow Core Plank Diaphragms." M.S. Thesis, Iowa State University, Ames, Iowa, 1990.

29. Easterling, W. S. "Analysis and design of steel-deck-reinforced concrete diaphragms." Dissertation, Iowa State University, Ames, Iowa, 1987.

30. Ewing, R. D., T. J. Healey, and M. S. Agbabian. "Seismic Analysis of Wood Diaphragms in Masonry Buildings." Proc. of a Workshop on DESIGN OF HORIZONTAL WOOD DIAPHRAGMS. Applied Technology Council (ATC), Berkeley, California, Dec. 1980.

31. Celebi, M., E. Safak, and A. G. Brady. "Seismic Response of a Large-Span Roof Diaphragm." Earthquake Spectra, Vol. 5, No. 2, (1989): 337-350.

32. Kunnath, S. K., A. M. Reinhorn, and Y. J. Park. "Analytical Modeling of Inelastic Seismic Response of R/C Structures." ASCE Journal of Structural Engineering. Vol. 116, No. 4, (April 1990): 996-1017.

33. Kunnath, S. K., N. P. Panahshahi, and A. M. Reinhorn. " Seismic Response of RC Buildings with Inelastic Floor Diaphragms." ASCE Journal of Structural Engineering. Vol. 117, No. 4, (April 1991): 1218-1237.

34. Kunnath, S. K. "IDARC: A Computer Program for Seismic Damage Evaluation of Structures." NCEER Bulletin. (April 1991): 8-13.

35. Tena-Colunga, A. "Seismic Evaluation of Unreinforced Masonry Structures with Flexible Diaphragms." Earthquake Spectra. Vol. 8, No. 2, (1992): 305-318.

36. Saffarini, H. S., and M. M. Quadaimat. "In-Plane Floor Deformations in RC Structures." ASCE Journal of Structural Engineering. Vol. 118, No. 11, (Nov. 1992): 3089-3102.

37. Panahshahi, N., A. M. Reinhorn, S. K. Kunnath, L. L. Huang, and K. Yu. "Seismic Response of a 1:6 Reinforced Concrete Scale-Model Structure with Flexible Floor Diaphragms." ACI Structural Journal. Vol. 88, No. 3, (May-June 1991): 315-324.

38. Porter, M. L., and F. S. Yeomans. "A Hysteretic Model for Hollow-Core Plank Diaphragms." Proc. of the Sixth Annual Meeting of the U.S.-Japan Joint Technical Coordinating Committee on Masonry Research. Seattle, Washington, 1990.

39. Nakashima, M., T. Huang, and L. Lu. "Expeimental Study of Beam-Supported Slabs Under Plane Loading." ACI Structural Journal. Vol. 79, No. 8, (Jan.-Feb. 1982): 59-65.

40. Anderson, J. C., and W. H. Townsend. "Models for RC Frames with Degrading Stiffness." ASCE Jorunal of Structural Engineering . Vol. 103, No. ST12, (Dec. 1977): 2361-2376.

41. Kariotis, J. C., A. M. D. Rahman, O. M. Waqfi, and R. D. Ewing. "LPM/I Version 1.03, A Computer Program for the Nonlinear, Dynamic Analysis of Lumped Parameter Models." U.S.-Japan Coordinated Program for Masonry Building Research." National Science Foundation, Report No. 2.3-4, Ewing/Kariotis/Englekirk &, February, 1992.

42. Reinhorn, A. M., S. K. Kunnath, and N. Panahshahi. "Modeling of R/C Building Structures with Flexible Floor Diaphragms (IDARC2)." National Center for Earthquake Engineering Research (NCEER), Technical Report NCEER-88-0035, Sept., 1988.

43. Kabeyasawa, T., H. Shiohara, S. Otani, and H. Aoyama. "Analysis of the Full-Scale Seven-Story Reinforced Concrete Test Structure." Journal of the Faculty of Engineering, The University of Tokyo. Vol. XXXVII, No. 2, (1983): 431-477.

44. Nakata, S., T. Sproul, and J. "Mathematical Modelling of Hysteresis Loops for Reinforced Concrete Columns." Earthquake Engineering Report Center (EERC), Report No. UCB/EERC-78/11, Berkeley, Cal., 1978.

45. Ozcebe, G., and M. Saatcioglu. "Hysteretic Shear Model for Reinforced Concrete Members." ASCE Journal of Structural Engineering. Vol. 115, No. 1, (January 1989): 132-148.

46. Bowker, A. H., and G. J. Lieberman. Engineering Statistics. 2nd Edition. Englewood Cliffs, N.J.: Prentice-Hall Inc., 1986.

47. Saatcioglu, M., A. T. Derecho, and W. G. Corley. "Modelling Hysteretic Behaviour of Coupled Walls for Dynamic Analysis." Earthquake Engineering and Structural Dynamics. Vol. 11, (1983): 711-726.

48. Griffin, M. J. "Comparative Analysis of Two Numerical Methods for Computing Dynamic Response of Nonlinear Systems." M.S. Thesis, University of California, Irvine, 1988.

49. Villaverde, R., and R. C. Lamb. "Scheme to Improve Numerical Analysis of Hysteretic Dynamic Systems." ASCE Journal of Structural Engineering. Vol. 115, No. 1, (January 1989): 228-233.

50. Takizawa, H., "Notes on Some Basic Problems in Inelastic Analysis of Planar R/C Structures (Part I)." Transactions of Architectural Institute of Japan. No. 240, (February 1976): 51-62.

51. Takizawa, H., "Notes on Some Basic Problems in Inelastic Analysis of Planar R/C Structures (Part II)." Transaction of Architectural Institute of Japan. No. 241, (March 1976): 65-77.

52. Emori, K. and W. C. Schnobrich. "Analysis of Reinforced Concrete Frame-Wall Structures for Strong Motion Earthquakes." Report No. UILU-ENG 78-2025, University of Illinois at Urbana-Champaign, Urbana, Illinois, Dec., 1978.

53. Saiidi, M., and M. A. Sozen. "Simple and Complex Models for Nonlinear Seismic Response of Reinforced Concrete Structures." Report No. UILU-ENG-79-2013, University of Illinois at Urbana-Champaign, Urbana, Illinois, Aug., 1979.

54. Park, Y. J., A. M. Reinhorn, and S. K. Kunnath. "IDARC: Inelastic Damage Analysis of Reinforced Concrete Frame-Shear-Wall Structures." Technical Report NCEER-87-0008, National Center for Earthquake Engineering Research (NCEER), State University of New York at Buffalo, July, 1987.

55. Aktan, A. E., and V. Bertero. "Seismic Response of R/C Frame-Wall Structures." ASCE Journal of Structural Engineering. Vol. 110, No. 8, (August 1984): 1803-1821.

56. Collins, M. P. "The response of Reinforced Concrete Elements Subjected to Shear." Proc. of a Workshop on Concrete Shear in Earthquake. Edited by T. Hsu, and S. Mau, University of Houston Texas, January, 1991.

57. Penzien, J. "Elasto-Plastic Response of Idealized Multistory Structures Subjected to Strong Motion Earthquake." Proceedings of the Second World Conference in Earthquake Engineering, Vol. II, Japan, 1960.

58. Clough, R. W., K. L. Benuska, and E. L. Wilson, "Inelastic Earthquake Response of Tall Buildings," Proceedings of the Third World Conference on Earthquake Engineering. Vol. II, New Zealand, January, 1965.

59. Aoyama, H., and T. Sugano. "A Generalized Inelastic Analysis of Reinforced Concrete Structures based on the Tests of Members." Recent Researches of Structural Mechanics - Contributions in Honour of the 60th Birthday of Prof. Y. Tsuboi, Uno Shoten, Tokyo, Japan, 1968.

60. Gilberson, M. F. "Two Nonlinear Beams with Definitions of Ductility." ASCE Journal of the Structural Division. Vol. 95, No. ST2, (Feb. 1969): 137-157.

61. Chen, W. F., and E. M. Lui. Stability Design of Steel Frames. CRC Press, Boca Raton, Florida, 1991.

62. Kunnath, S. K., and A. M. Reinhorn. "Inelastic Three Dimensional Response Analysis of Reinforced Concrete Building Structures (IDARC-3D)." Technical Report NCEER-89-0011. State University of New York at Buffalo. Buffalo, New York. April 1989.

63. American Concrete Institute. Building Code Requirements for Reinforced Concrete (ACI 318-89). Detroit: ACI, 1989.

64. Clough, R. W., and J. Penzien. Dynamics of Structures. Second Edition. McGraw-Hill, Inc.. 1993.

65. Weaver Jr., W., and P. R. Johnston. Structural Dynamics by Finite Elements. Englewood Cliffs, New Jersey. Prentice-Hall, Inc. 1987.

66. Otani, S. "Inelastic Analysis of R/C Frame Structures." ASCE Journal of the Structural Division. Vol. 100, ST7, (July 1974): 1433-1449.

67. Takayanagi, T., and Schnobrich, W. C., "Computed Behavior of Reinforced Concrete Coupled Shear Walls." Civil Engineering Studies, Structural Research Series, University of Illinois, Urbana, December, 1976.

68. Roufaiel, M. S. L., and Meyer, C. "Analytical Modeling of Hysteretic Behavior of R/C Frames." ASCE Journal of Structural Engineering. Vol. 113, No. 3, (March 1987): 429-444.

69. Blume, J. A., R. L. Sharpe, and E. Elsesser. "A structural dynamic investigation of fifteen school buildings subjected to simulated earthquake motion." Division of Agriculture, Sacramento, Cal., 1961.

70. Jain, S. K., and P. C. Jennings. "Continuous Models for Frame and Shear-Wall Buildings with Flexible Floors." Proc. of the Eight World Conference in Earthquake Engineering. Vol. IV, San Francisco, Cal., 1984.

71. Nakashima, M., T. Huang, and L. Lu. "Effect of Diaphragm Flexibility on Seismic Response of Building Structures." Proc. of the Eigth World Conference on Earthquake Engineering. Vol. IV, San Francisco, Cal., 1984.

72. Button, M. R., T. E. Kelly, and L. R. Jones. "The Influence of Diaphragm Fexibility on the Seismic Response of Buildings." Proc. of the Eigth World Conference on Earthquake Engineering. Vol. IV, San Francisco, Cal., 1984.

73. Hart, G. C., R. E. Englekirk, M. Srinivasan, S. C. Huang, and D. J. Drag. "Seismic Performance Study DPC Gymnasium Elastic Time History Analysis Using SAP90." Report No. 2.1-8, Ewing/Kariotis/Englekirk & Hart, Feb., 1992.

74. Hart, G. C., R. E. Englekirk, M. Srinivasan, S. C. Huang, and D. J. Drag. "Seismic Performance Study TMS Shopping Center Elastic Time History Analysis Using SAP90." Report No. 2.1-8, Ewing/Karlotis/Englekirk & Hart, Feb., 1992.

75. Applied Technology Council. Seismic Resistance of Reinforced Concrete Shear Walls and Frame Joints: Implications of Recent Research for Design Engineers. ATC-11, National Science Foundation. 1983.

76. Prins, M. D. "elemental tests for the seismic resistance of composite floor diaphragms." M.S. Thesis, Iowa State University, Ames, Iowa, 1985.

77. Council on Tall Buildings and Urban Habitat. Cold-Formed Steel in Tall Buildings. Committee S37, McGeaw-Hill, Inc. 1993.

78. Porter, M. L., and L. F. Greimann. "Seismic Resistance of Composite Floor Diaphragms." Final Report, Engineering Research Institute, Iowa State University, May, 1980.

79. Friberg, B. F. "Combined Form and Reinforcement for Concrete Slabs." Proceedings, American Concrete Institute Journal. Vol. 25, (1954): 697:716.

80. Porter, M. L., and Ekberg, C. E., Jr. "Compendium of ISU Research Conducted on Cold-Formed Steel-Deck-Reinforced Slab Systems." Bulletin 200, ISU-ERI-AMES-78263. Engineering Research Institute, Iowa State University,Ames, Iowa, Dec., 1978.

81. Porter, M. L., and C. E. Ekberg, Jr. "Behavior of Steel Deck Reinforced Slabs." ASCE Journal of the Structural Division. Vol. 103, (1977): 663-677.

82. Porter, M. L., Ekberg, C. E., Jr.,Greimann, L. F., and H. A. Elleby. "Shear-Bond Analysis of Steel-Deck-Reinforced Slabs." ASCE Journal of the Structural Division. Vol. 102, (1976): 2225-2268.

83. Prasannan, S., and L. D. Luttrell. "Flexural Strength Formulations for Steel-Deck Composite Slabs." Civil Engineering Studies, Department of Civil Engineering, West Virginia University, Morgantown, West Virginia, Ja., 1984.

84. Lutrell, L. D. "Methods for Predicting Strength in Composite Slabs." Proceedings of the 8th International Specialty Conference on Cold-Formed Steel Structures. University of Missouri-Rolla, Nov., 1986.

85. Easterling, W. S, and M. L. Porter. "Composite Diaphragm Behavior and Strength. "Proceedings of the 9th International Specialty Conference on Cold-Formed Steel Structures. University of Missouri-Rolla, Nov., (1988): 387-404.

86. Departments of the Army, the Navy and the Air Force. Seismic Design for Buildings. Army TM 5-809-10. Washington, D. C. : U. S. Government Printing Office, December, 1982.

87. Lutrell, L. D., "Shear Diaphragms with Lightweight Concrete Fill." The First Speciality Conference on Cold-Formed Steel Structures. ed. Wei-Wen Yu. Rolla: Civil Engineering Dept., University of Missouri-Rolla, 1971, 111-117.

88. Davies, J. M. and Fisher, J. "The diaphragm Action of Composite Slabs." Proceedings of the Institution of Civil Engineeros, Part 2. 67 (1979): 891-906.

89. Porter, M. L., and W. S. Easterling. "Behavior, Analysis, and Design of Steel-Deck-Reinforced Concrete Diaphragms." Final Report, College of Engineering, Iowa State University, March 1988.

90. Umemura, H., and H. takizawa. Dynamic Response of Reinforced Concrete Buildings. Structural Engineering Documents, IABSE-AIPC-IVBH, Switzerland, 1982.

91. McCuen R. H. Statistical Methods for Engineers. Prentice-Hall Inc., Englewood Cliffs, New Jersey, 1985.

92. Draper, N. R. Applied Regression Analysis. Second edition, John Wiley & Sons Inc., 1966.

93. StatSoft, Inc. CSS: STATISTICA User's Manual Tulsa, Ok., 1991

94. Mendenhall, W., and T. Sincich. Statistics for the Engineering and Computer Sciences. Dellen Publishing Company, Santa Clara, Cal., 1984.

95. Ratkowsky, D. A. Handbook of Nonlinear Regression Models. Marcel Dekker, Inc., New York and Basel, 1990.

96. SAS Institute Inc., SAS System for Regression. Secon Edition, Cary, NC: SAS Institue Inc., 1991.

97. Microsoft Corporation. Microsoft Excel, User's Guide. Microsoft Corporation, 1992.

98. Park, Y.J. "Seismic Damage Analysis and Damage-Limiting Design for R/C Structures", Dissertation, University of Illinois, Urbana, Illinois, 1985.

99. Collins, M. P. "Towards a Rational Theory for RC Members in Shear." ASCE Journal of the Structural Division. Vol. 104, (1978): 649-666.

100. Vecchio, J. F., and M. P. Collins. "Predictiong the Response of Reinforced Concrete Beams Subjected to Shear Using the Modified Compression Field Theory." ACI Structural Journal. Vol. 85, No. 3, (1988): 258-268

101. Paulay, T., and M. J. N. Priestley. Seismic Design of Reinforced Concrete and Masonry Buildings. John Wiley & Sons, Inc., 1992.

102. Hsu, T. T. C. Unified Theory of Reinforced Concrete. CRC Press Inc., Boca Raton, Florida (1993).

103. Beedle, L. S. Plastic Design of Steel Frames. John Wiley and Sons, Inc. New York, N. Y., 1958.

104. AISC. Commentary on the Load and Resistance Factor Design Specification for Structural Steel Buildings (September 1, 1986). Chicago, IL: American Institute of Steel Construction, 1986.

105. Ollgaard, J. G., Slutter, R. G., and Fisher, J. W. "Shear Strength of Stud Connectors in Lightweight and Normal Weight Concrete." AISC Engineering Journal 8 (1971): 55-64.

106. Newmark, N. M., "A Method of Computation for Structural Dynamics." ASCE, Journal of Engineering Mechanics Division. Vol. 85, EM3, (1959): 69-86.

107. Bathe, K., and E., Wilson. Numerical Methods in Finite Element Analysis. Prentice-Hall, Inc., Englewood Cliffs, New Jersey, 1976.

108. Adeli, H., Gere, J. M., and W. Weaver. "Algorithms for Nonlinear Structural Dynamics." ASCE, Journal of the Structural Division. Vol. 104, ST2, (1978): 263-280.

109. Cardenas, A. E., and D., Magura. "Stength of High-Rise Shear Walls Rectangular Cross Section," Response of Multistory Concrete Structures to Lateral Forces, SP-36, American Concrete Institute, Detroit, (1973): 119-150.

110. Smith, K., and S. Fereig. "Effect of Loading and Supporting Conditions on the Shear Strength of Deep Beams," Shear in Reinforced Concrete, SP-42-20, American Concrete Institute, Detroit, (1974): 441-460.

111. American Institute of Steel Construction. Manual of Steel Construction. 9th Edition. Chicago: AISC, 1989.

112. American Institute of Steel Construction. Load and Resistance Factor Design Manual of Steel Construction. 1st Edition. Chicago: AISC, 1986.

113. American Iron and Steel Institute. Specification for the Design of Cold-Formed Steel Structural Members. Washington, D.C. : AISI, 1986.

114. Davies, J. M., and E. R. Bryan. Manual of Stressed Skin Diaphragm Design. John Wiley & Sons, New York , 1982.

115. Lutrell, L. D. Steel Deck Institute Diaphragm Design Manual, 2nd Edition. St. Louis: Steel Deck Institute. 1987.

116. Porter, M. L. "Sequential Phased Displacement (SPD) Procedue for TCCMAR Testing." Third Meeting of the Joint Technical Coordinating Committee on Masonry Research. U.S.-Japan Coordinating Earthquake Research Program. Sapporo, Japan, October, 1987.

117. ABK, A Joint Venture, (Ewing, R. D., Johnson, A. W., and Kariotis, J. C.). "Methodology for Mitigation of Seismic Hazards in Existing Unreinforced Masonry Buildings: Interpretation of Diaphragm Tests", ABK-TR-05. South Pasadena, CA

118. Barnes, S. B. and Associates. "Report of Test Program on Mahon Steel Decks to Demonstrate Adequacy When Used as Horizontal Diaphragms." S. B. Barnes and Associates, Los Angeles, April, 1957.

119. Barnes, S. B. and Associates. "Report on use of H. H. Robertson Steel Roof and Floor Decks as Horizontal Diaphragms." S. B. Barnes and Associates, Los Angeles, July, 1963.

120. Biggs, J. M. Introduction to Structural Dynamics McGraw-Hill, Inc. 1964.

121. Paz, M. Structural Dynamics, Theory and Computation, 3rd Edition Van Nostrand Reinhold, New York, 1991.

122. International Conference of Building Officials. Uniform Building Code, Edition 1991 Whittier, California.

123. Kariotis, J. C., Waqfi, O. M., and Ewing, R. D. "A computer Program Using Beam Elements for the Nonlinear, Dynamic Analysis of Lumped Parameter Models." Report No. 2.3-5, U.S.-Japan Coordinated Program for Masonry Building Research, National Science Foundation. February 1992.

124. Mohraz, B. and F. Elghadamsi "Earthquake Ground Motion and Response Spectra." Chapter 2 on The Seismic Design Handbook edited by F. Naeim. Van Nostrand Reinhold. New York 1989.

ACKNOWLEDGEMENTS

This study was conducted as part of a research project sponsored by the National Science Foundation through the Engineering Research Institute at Iowa State University. Additionally, full support was provided for the author's doctorate years of study by the following mexican institutions: Consejo Nacional de Ciencia y Tecnologia (CONACYT), and Instituto Tecnologico y de Estudios Superiores de Monterrey (ITESM).

The author would like to thank his major professors Dr. Max L. Porter and Dr. Terry J. Wipf , for their guidance, encouragement and patience, as well as, for providing the author with many opprtunities to learn and grow professionally. The author also wishes to thank the members of his graduate committee for their time and encouragement. Committee members included Drs. Mardith A. Baenziger, Loren W. Zachary and Thomas R. Rogge. The author would like to express sincere sympathy over the sudden death of one of his committee members, Dr. Frederick Graham. His words and actions of guidance are held in the highest regard.

The author is greatly in debt to his parents. Their constant support and encouragment has been a great source of motivation. The author is deeply grateful to his sons Santiago and Ricardo, whose patience, understanding, and love enabled him to sustain this effort.

The final and most enduring thanks goes to Delma, the author's wife and classmate for her encouragment, friendship and patience during the long hours of the research and preparation of this dissertation. The author is forever grateful and looks forward to repaying the debt over many years to come.

APPENDIX A. PREVIOUS SDRC RESEARCH AT IOWA STATE UNIVERSITY

A1. *Introduction*

Extensive research on behavioral and strength characteristics of diaphragms has been done at Iowa State University. Before ISU started the SDRC research, the quantity of published investigation on the subject had been minimal. Most of it was proprietary testing usually sponsored by steel deck manufacturers, and was used as a source to formulate the design approach in the Seismic Design for Buildings (86).

The majority of the proprietary testing was performed by S. B. Barnes and Associates (118,119). Discussions of the test results indicate that the predominant modes of failure were deck tearing around welds at the edge framing member, shearing of welds, shear failure of the concrete above the flutes of deck, localized cracking and concrete separation from the deck. Diaphragms with a minimum of 1-1/2 inches of concrete or vermiculite fill above the top flange of the deck were tested. Steel deck sections were typically welded to the framing members.

Nine diaphragm tests with lightweight insulating fill were performed at WVU and reported by Luttrell (87). Results showed that the diaphragm stiffness was increased due to the insulated fill. Additionally, the insulated fill provided of warping restraint, forcing the diaphragm failure to occur at the welds as opposed to sheet instability, which had occurred in similar unfilled diaphragm tests. Expressions were presented that correlate diaphragm strength to the number of welds along the edges of the diaphragm.

Davies and Fisher (88) reported four composite diaphragm tests. Trapezoidal and re-entrant steel-deck profiles with concrete cover of approximately two inches were used and attached to the perimeter framing members. In each case the controlling failure mode was reported as a fastener failure, with one specimen failing by a combination of fastener

failure and profile collapse. The fastener spacing ranged from approximately 12 to 28 in. Equations were presented to determine the strength of the diaphragm based only on a fastener failure.

A series of nine diaphragm tests (Phase I) was performed at ISU by Porter and Greimann (78). Numerous SDRC diaphragm parameters were varied and tested. These parameters included steel deck type, fastener type and number, and concrete thickness. Equations were developed to predict stiffness and strength of SDRC diaphragms. These equations were based on an edge zone concept, which considered the force to be transferred from the load frame into the diaphragm within a relatively narrow region adjacent to the framing members. A key component of this edge zone was considered to be the interface between the steel deck and concrete. Edge force distributions that were used to derive predictive equations were based on a linear elastic finite element analysis. Additionally, force distribution at ultimate load levels was assumed.

An additional twenty-three diaphragm tests (Phase II) were performed at ISU by Porter and Easterling (89). Key parameters included steel deck type, fastener type and number, concrete thickness, depth-to-span ratio, loading and framing member size. A major component of the analytical portion of the study was verifying the previously assumed force distributions at ultimate. The principal focus of the analyses was to verify and define the components of the predictive equations, such that the equations might be incorporated into a design methodology.

Results from the two-phase SDRC studies at ISU, are the experimental data source for the development of the hysteretic model described in this work. The following sections describe the test setup, diaphragm configuration, displacement history, elemental testing, as well as results obtained through the test. A more detailed description of the

experimental program is presented in the following references: Porter and Greimman (78), Easterling (29), Neilsen (17), Dodd (18), Prins (76), and Porter et al. (1)

A2. Test Setup and Diaphragm Parameters

A series of 32 full-scale SDRC diaphragms was tested at ISU as part of a two-phase research. The first phase included Tests 1-9 and the second phase included Tests 10-32. Numerous SDRC diaphragm parameters were varied and tested. Variables included deck type, deck thickness, fastener type, number of fasteners, concrete thickness, depth-to-span ratio, load combinations of in-plane and gravity loads and edge member size. Each of these parameters was investigated with regard to their influence on behavior and strength of SDRC diaphragms.

Diaphragms 1-21 were 15 ft. x 15 ft. in plan while Diaphragms 22-32 were 15 ft. x 12 ft. in plan. All diaphragms except Diaphragm 26 were constructed with normal weight concrete, with 26 being constructed with structural lightweight concrete. Eleven different deck types were used (see Table A1). Sketches of deck types are shown in Figures A1-A3. Deck sections were classified as different if the profile, deck thickness or embossment configuration is unlike any other.

A horizontal cantilever test frame was designed in the first phase of the research and is shown schematically in Figure A4. The North-to-South dimension of the span of the diaphragm was the 12-ft. dimension for Tests 22-32. Test frame for Diaphragms 1-31 was constructed with W24x76 steel sections; Diaphragm 32 was tested on a frame with W14x22 steel sections. The south edge of the test frame was constructed using three reinforced concrete blocks. These blocks served as the reaction edges and were anchored to the structural test floor by post-tensioning 2-in. diameter high strength steel rods. A steel plate was embedded in the top of the concrete blocks near the interior edge

Table A1. Diaphragm parameter summary (29)

Slab	Concrete Parameters		Steel Deck Parameters				
Number	Thickness (in.)	f'c (psi)	Deck Type	Thickness (in.)	Yield Strength (ksi)	Ultimate Strength (ksi)	Connections per side
1	5.38	5634	1	0.034	41.7	53.4	30 s
2	5.50	5250	1	0.034	41.7	53.4	30 s
3	5.65	4068	1	0.034	41.7	53.4	60 w
4	5.28	3849	1	0.034	41.7	53.4	60 w
5	3.53	2966	2	0.062	48.2	60.7	30 w
6	7.44	4549	2	0.062	48.2	60.7	60 w
7	5.40	5435	3	0.058	49.7	61.1	4 s N-S, 6 s E-W
8	5.47	3345	1	0.035	41.7	53.4	60 w
9	5.48	5412	4	0.058	51.8	63.2	60 w
10	5.53	3311	5	0.062	40.4	53.2	60 w
11	5.72	3533	6	0.047	89.7	93.7	60 w
12	5.59	3412	5	0.062	40.4	53.2	60 w
13	5.53	6187	4	0.058	51.8	63.2	60 w
14	8.20	3699	5	0.062	40.4	53.4	60 w

Table A1. (Continued)

Slab Number	Concrete Parameters		Steel Deck Parameters				
	Thickness (in.)	f'c (psi)	Deck Type	Thickness (in.)	Yield Strength (ksi)	Ultimate Strength (ksi)	Connections per side
15	4.21	2844	7	0.047	89.7	93.6	60 w
16	4.18	2952	7	0.047	89.7	93.6	60 w
17	7.44	4261	2	0.062	46.0	54.4	60 w
18	5.55	3052	5	0.062	40.4	53.4	60 w
19	5.75	2681	8	0.062	49.4	55.5	60 w
20	5.55	3973	9	0.037	48.6	56.2	40 w
21	5.67	3638	5	0.062	40.4	53.4	15 w
22	5.68	3301	5	0.062	40.4	53.4	60 w N-S, 48 w E-W
23	5.75	3496	9	0.037	48.6	56.2	40 w N-S, 34 w E-W
24	5.63	4047	8	0.062	49.4	55.5	48 w
25	5.69	4672	5	0.062	40.4	53.4	16 s N-S, 8 s E-W
26	4.72	3462	10	0.036	92.8	93.6	8 s+15 w N-S, 11 s E, 7 w W
27	5.66	2883	9	0.037	48.6	56.2	15 w N-S, 8 s+9 w E-W
28	5.60	3611	9	0.037	48.6	56.2	8 s+15 w N-S, 6 s E-W

Table A1. (Continued)

Slab Number	Concrete Parameters		Steel Deck Parameters				Connections per side
	Thickness (in.)	f'c (psi)	Deck Type	Thickness (in.)	Yield Strength (ksi)	Ultimate Strength (ksi)	
29	5.55	2887	11	0.035	86.9	89.8	16 s N-S,11 s E-W
30	5.68	3565	11	0.035	86.9	89.8	12 s+ 4 w N-S, 7 s E-W
31	5.75	3336	11	0.035	86.9	89.8	23 w N-S, 13 w E-W
32	5.66	2452	11	0.035	86.9	89.8	30 w N-S, 23 w E-W

s Stud
w Weld
N, S, E, W North, South, East, West

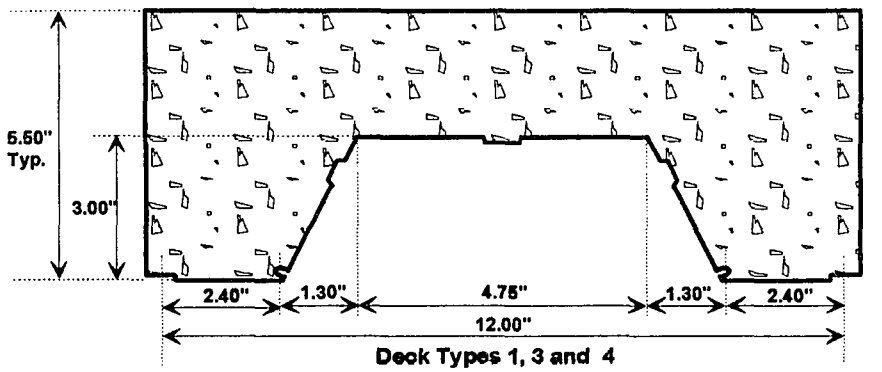

Deck Types 1, 3 and 4

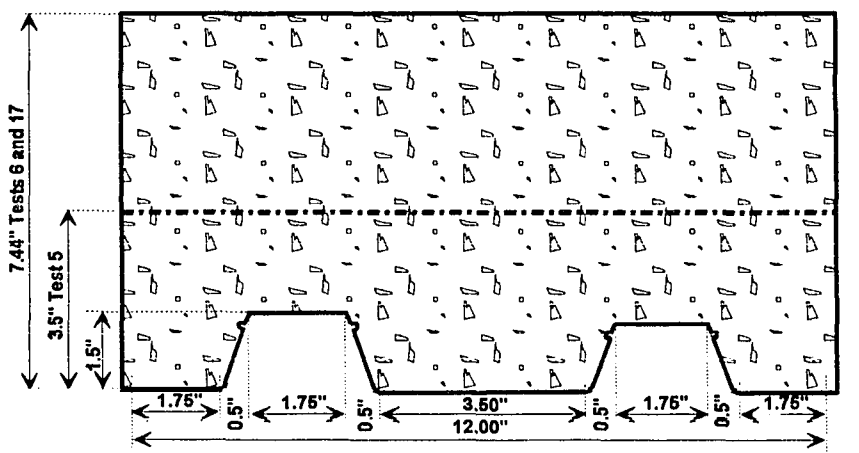

Deck Type 2

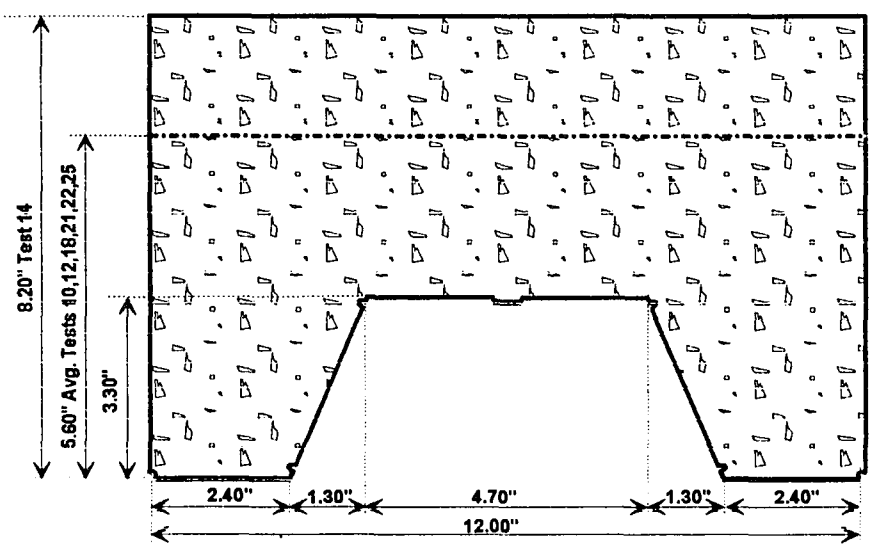

Deck Type 5

Figure A1. Deck types 1-5 (modified from reference 29)

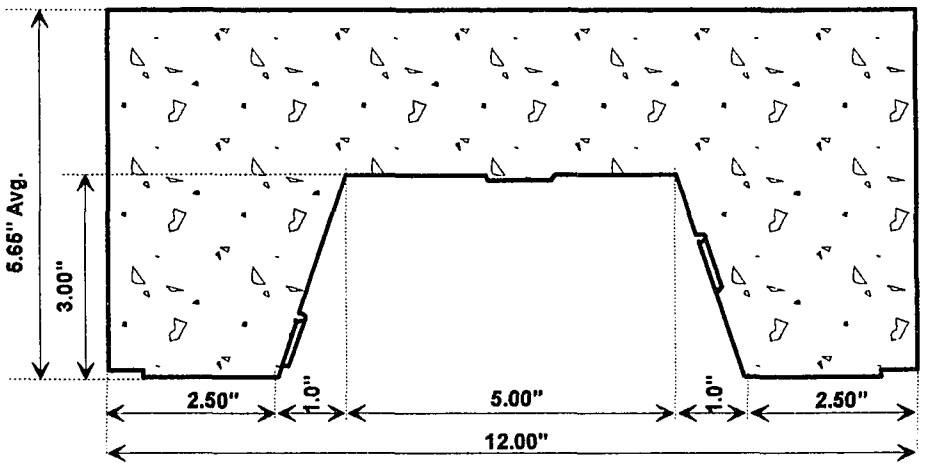

Deck Types 6 and 11

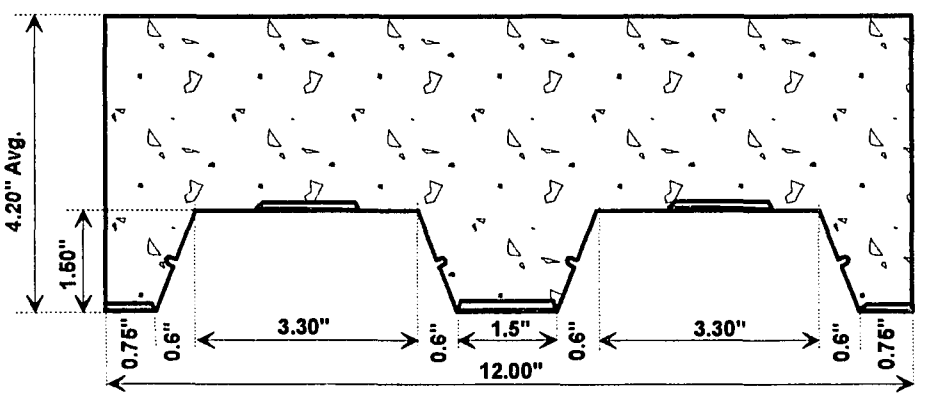

Deck Type 7

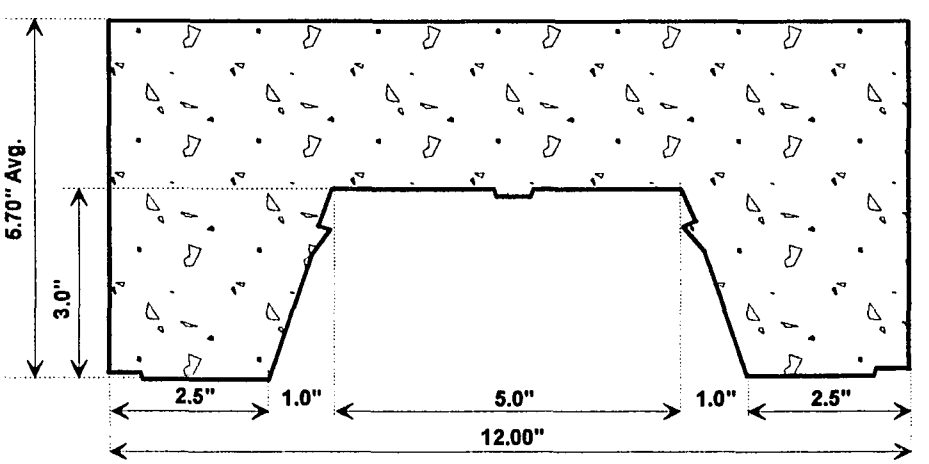

Deck Type 8

Figure A2. Deck types 6,7,8, and 11 (modified from reference 29)

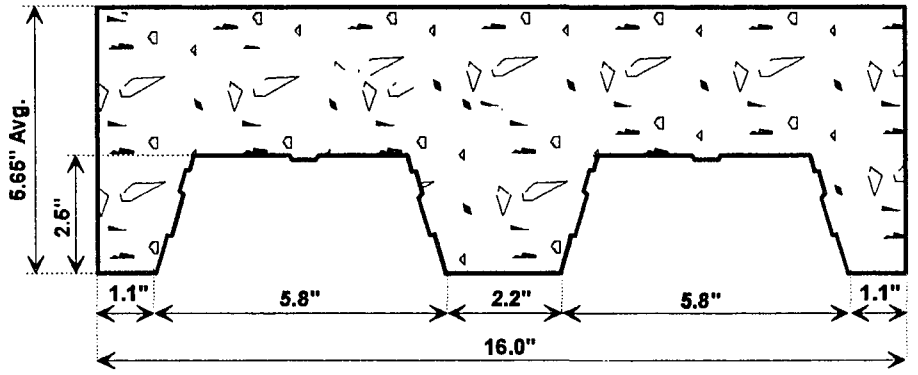

Deck Type 9

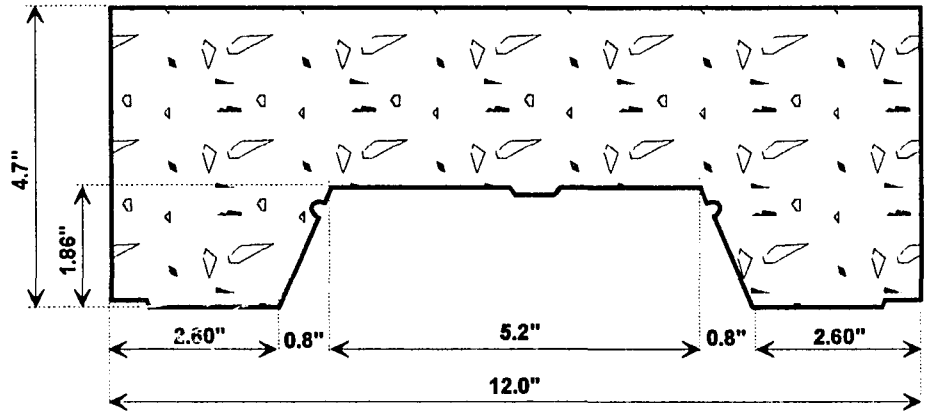

Deck type 10

Figure A3. Deck types 9 and 10 (modified from reference 29)

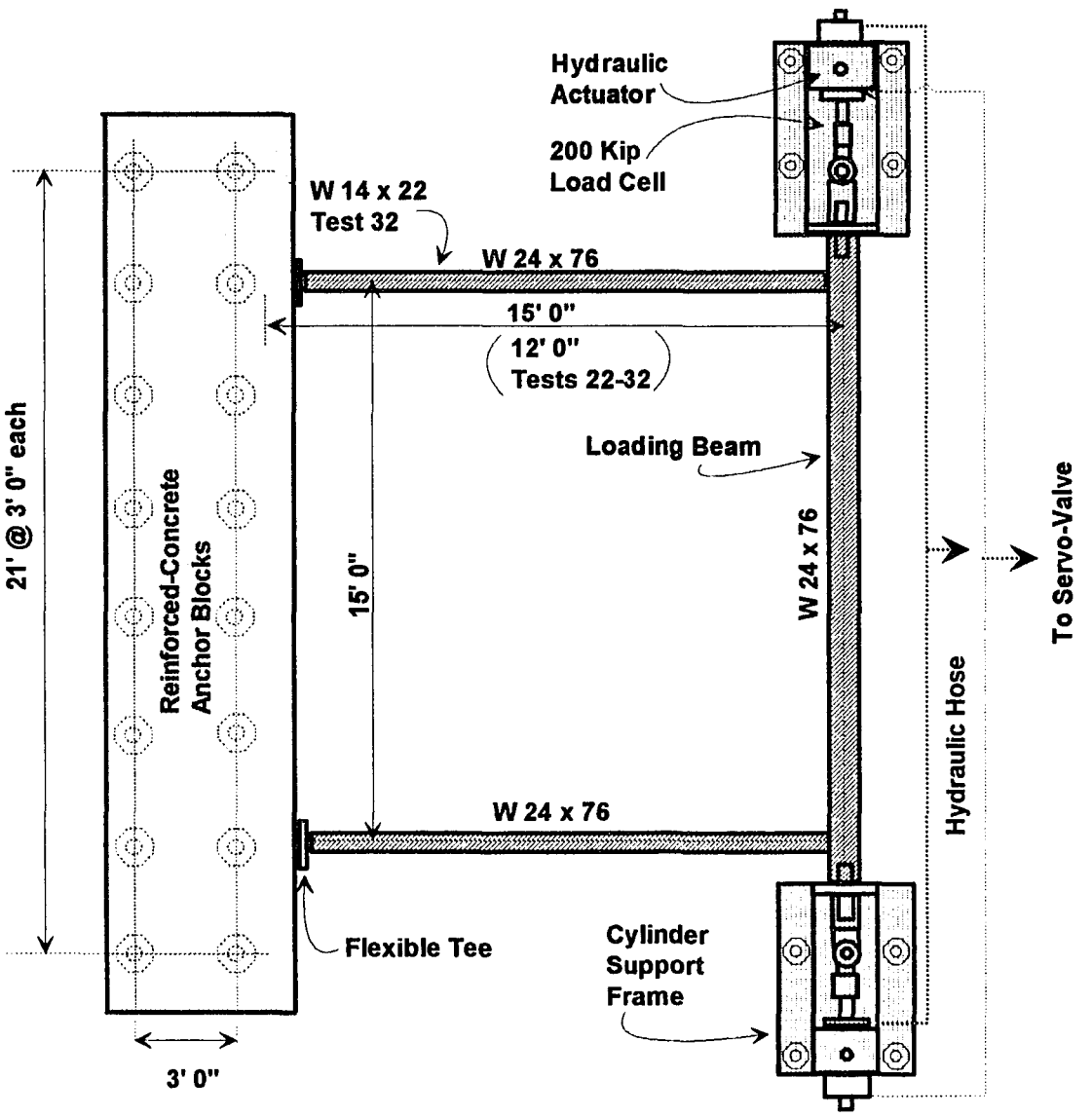

Figure A4. Test frame schematic (modified from reference 78)

of the frame to fasten the steel-deck section to the south edge. Connection of the framing members to each other and to the south edge was made using flexible tee sections.

Load was applied by two reversible hydraulic actuators as shown in Figure A4. The actuators (200 kips capacity each) were driven with a closed loop servo-valve controlled system. Six diaphragms were loaded with both in-plane and vertical load (17). Twenty neoprene pads were used to distribute the vertical load on the surface of the specimen. The amount of vertical load applied was selected to simulate an equivalent distributed load based on equivalent shear area in the one-way direction (parallel to the corrugations).

Collection of data was obtained using the following instrumentation: mechanical dial gages, electrical resistance strain gages, electronic displacement transducers (DCDT), and load cells. Instrumentation was used to measure in-plane loads, in-plane and out-of-plane displacements, strains in the concrete, strains in the steel elements, and relative displacements between different components of the diaphragm. The recorded data were collected using a 150-channel data acquisition system (DAS). Components of the system are micro-computer, digital plotter and printer and a 150-channel digital voltmeter with five independent power supplies. A schematic of the experimental testing arrangement is shown in Figure A5.

A3. Load-Displacement Program

Reversed cyclic loading with displacement control was used for all test specimens, except Test 1 that was monothonically loaded. For the displacement control, a DCDT was used in the northeast corner in line with the push beam as the feedback to the closed loop system. A minimum of three complete cycles was made at each level of displacement in

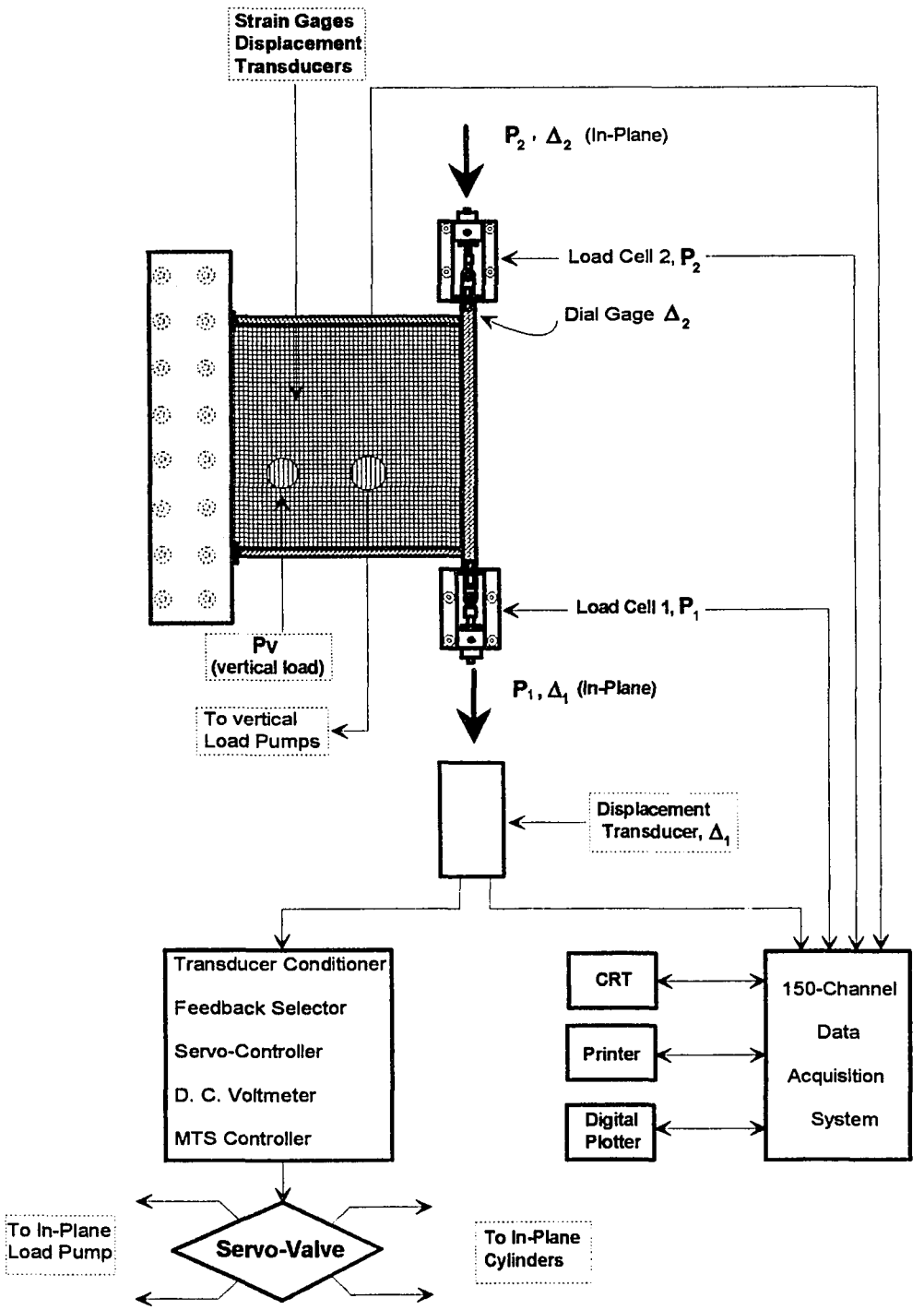

Figure A5. Schematic of servo-hydraulic testing system (modified from reference 78)

the displacement history. The criterion for increasing to the next level was that the load had to stabilize within a certain margin. This margin was defined as being less than a five percent change in load from the previous cycle at the same displacement.

An initial displacement level of 0.025 in. was selected for the experimental program. This displacement was thought to be within the elastic range of behavior for the SDRC diaphragms. The general cycling displacement pattern was: ±0.025 in., ±0.050 in., ±0.100 in., ±0.200 in., ±0.400 in., ±1.000 in., ±2.500 in., and ±5.000, in.

Diaphragm elastic stiffness was determined. These values were evaluated based on the first nominal displacement to 0.025 in. The total load for both actuators was divided by the displacement of the controlling DCDT to obtain the initial stiffness. No adjustments to the experimental stiffness values for test frame stiffness were made, since pre-test frame calibrations without an attached diaphragm, showed the frame to be relatively flexible. Load and displacement were monitored at intervals of approximately one second during the displacement histories. No adjustment was made to strength values based on test frame strength, since frame calibration indicated that the load carried by the base frame alone was approximately 1 kip.

A4. Failure Modes

One of the most significant characteristics of steel-deck-reinforced concrete diaphragms is the mechanical-chemical bond interface existing between steel deck and concrete. Another characteristic is given by the edge connection. Results from an extensive experimental testing at Iowa State University (78, 29, 17,18,76) had established that these characteristics are two of the most important effects triggering failure in SDRC diaphragms.

Diaphragms have as basic function, the transfer of horizontal forces from and to the vertical force resisting system. This transfer is made through the connection between diaphragm and the supporting resisting system. When stud connectors are used, the horizontal forces are directly transferred from the resisting system to the floor slab. When other of fastener types are used, such as arc spot welds, the force is transferred from the resisting system to the steel deck by the fasteners, and into the concrete slab by interfacial shear. According to the path described, the composite diaphragm failure may be described by composite slab, deck-concrete shear transfer mechanism and diaphragm-edge member connections (see Figure A6).

Composite slab failure may occur by several means: first, localized failure, this failure mode can be triggered by localized stress concentrations due to holes in diaphragms, or concentrated forces. Second, stability failure, this failure is recognized as a possible but remote type of failure, since general dimensions of SDRC diaphragms are typically such that avoid a general out-of-plane stability failure. Third, concrete shear failure,this failure may produce with parallel or diagonal cracks on the concrete diaphragm. Diagonal tension crack occurs at approximately 45 degree angle to the side and extends over most of the diaphragm surface. This failure is triggered when the principal tensile strength exceeds the ultimate tensile strength of the concrete. Concrete shear failure parallel to corrugations shows cracking above and parallel to the top flange of a deck flute, and is usually a result of an inadequate concrete cover over the deck (see Figure A7).

Diaphragms without positive shear transfer devices such as studs, have to transfer forces from the steel deck to the concrete through their interface. The interface is made by a combination of chemical component produced by the reaction of cement paste with steel deck surface, and by frictional and mechanical component produced through embossments, holes, or transverse wires. When this interface breaks down, a failure of

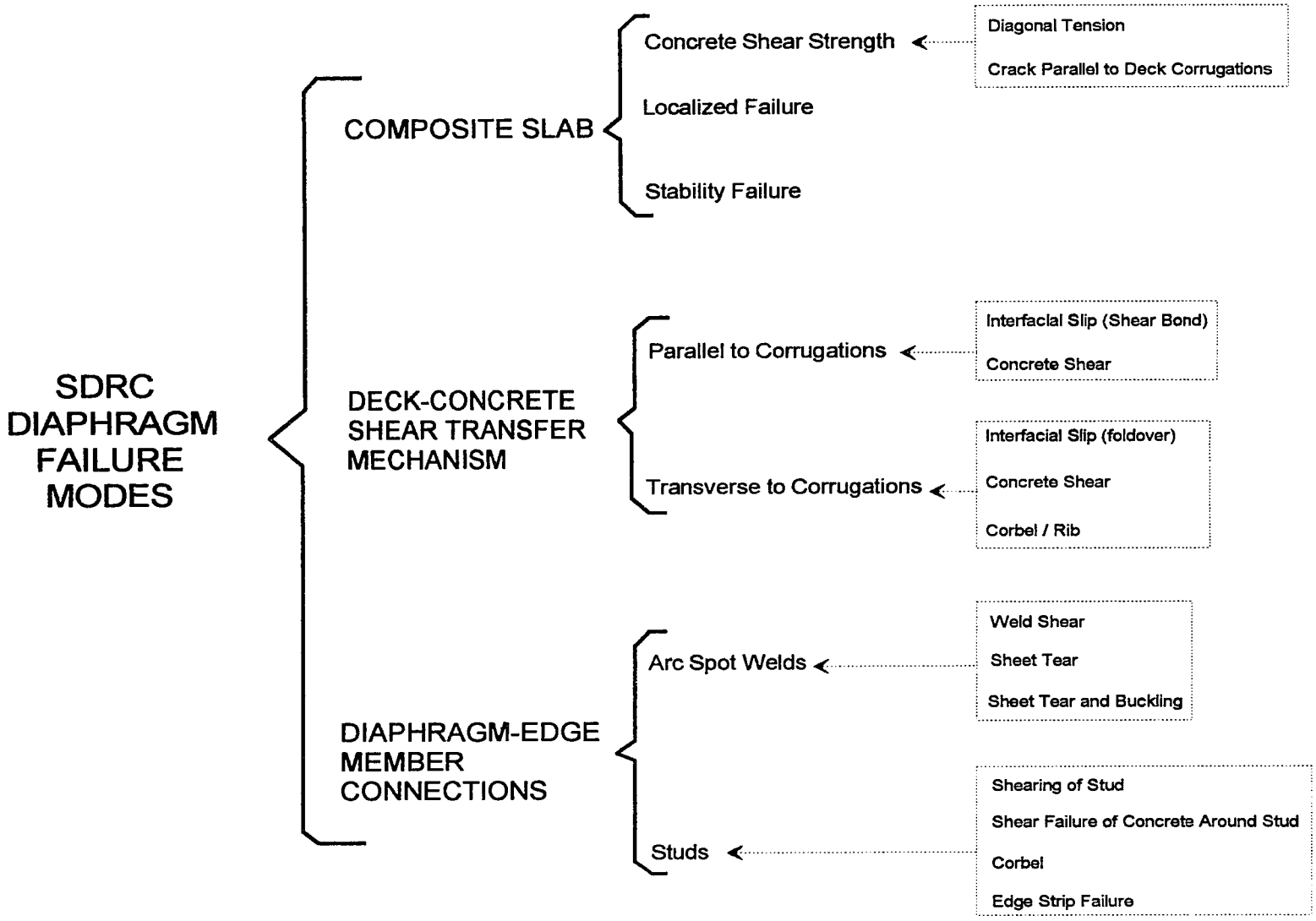

Figure A6. Failure modes for composite diaphragms

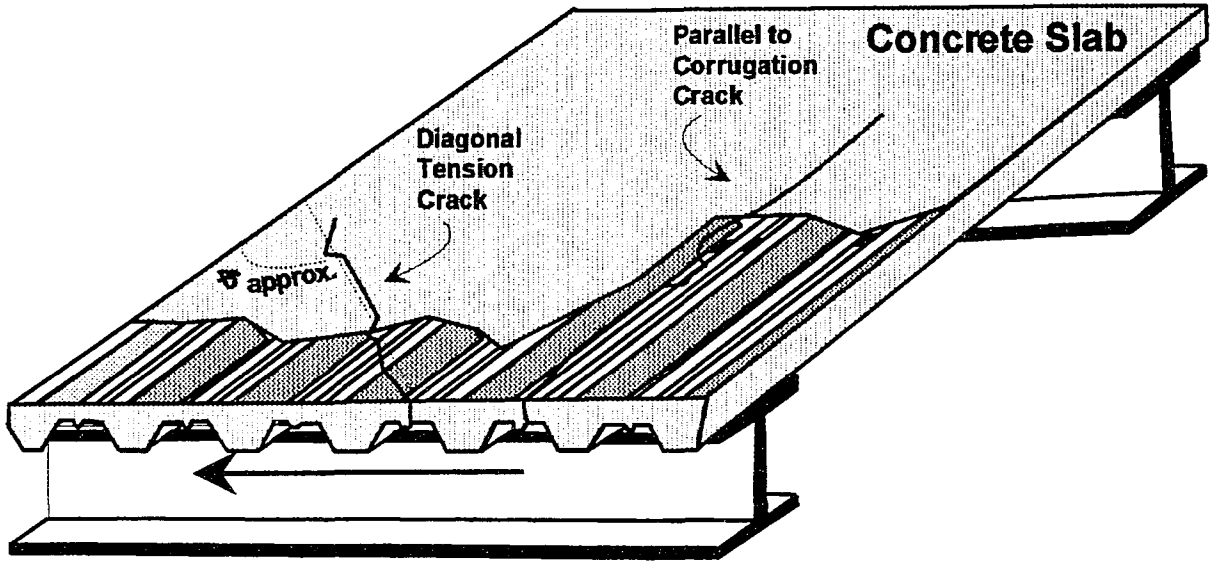

Figure A7. Composite slab failures (modified from reference 78)

the shear transfer mechanism is said to have happen. Shear transfer mechanism failure is divided into failure parallel and transverse to the corrugations. Shear transfer parallel to corrugation may be produced by interfacial slip characterized by a bond loss and large relative displacement between concrete and deck. Other possibility is concrete shear in the down corrugation produced when the embossments are really effective in transferring shear forces. Shear transfer transverse to the corrugations may be described by three failure modes: First, interfacial slip characterized by large relative displacement between concrete and deck as well as deck foldover. Second, concrete shear product of very effective embossments or very stiff deck cell geometry. Third, corbel or concrete rib failure described as a plane failure across the top of the rib and is generally produced by relatively narrow corrugations (see Figure A8).

Diaphragm-edge member connection failure may be classified in weld and stud failure types. Three sub-categories determine the capacity of arc spot welds in shear: weld tear, sheet tear, and sheet tear and buckling. Four failure modes control the capacity of stud connectors: direct shearing of the stud base metal, localized concrete failure around the stud, corbel or edge strip failure of concrete surrounding the studs, and edge strip failure. Corbel failure is similar to concrete rib failure, and is produced when the stud length is less or equal to the deck rib height. Edge strip failure describes the formation of concrete cracks above the deck top flange nearest the slab edge.

A5. Elemental Tests

A series of elemental specimens were tested to evaluate the strength and stiffness of the shear transfer mechanism. The elemental tests consisted of sections of SDRC of approximately 3 ft. by 3 ft. constructed for each deck type and fastener arrangement used

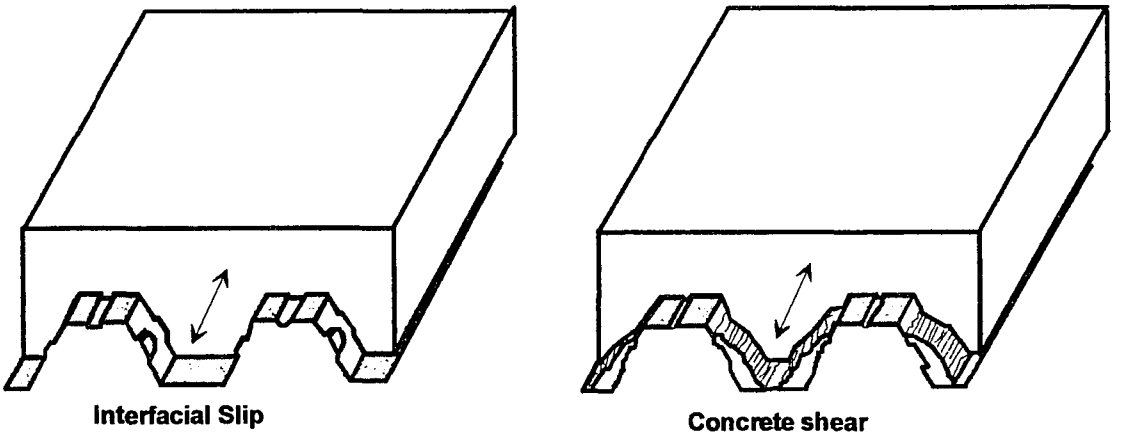

Figure A8. Shear transfer mechanism failures (modified from reference 76)

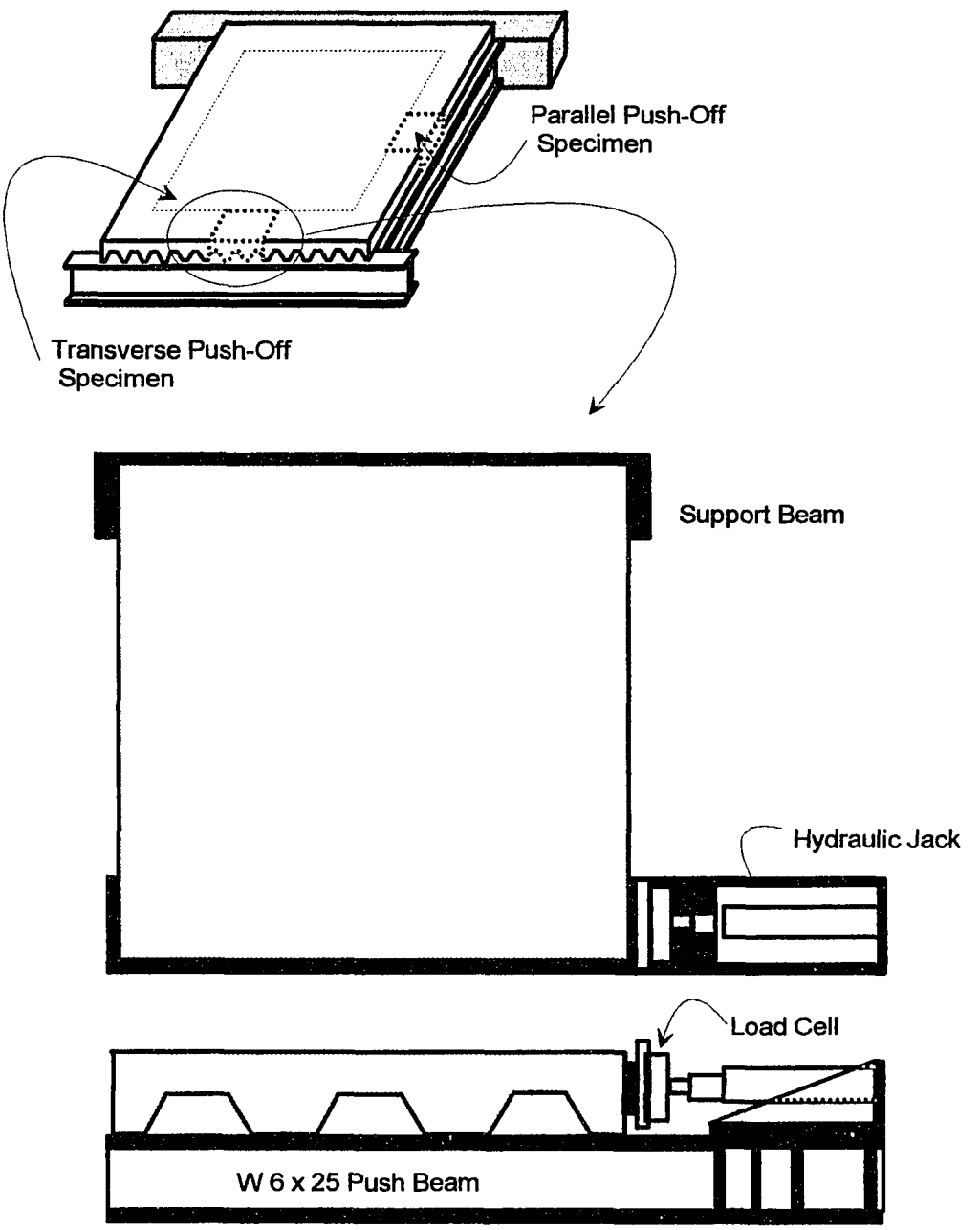

Figure A9. Elemental test set-up (modified from reference 76)

in the full-size tests. In testing the elemental specimens, two directions were considered, parallel and transverse to corrugations. Dodd (18) concluded that the tests were only applicable to modelling diaphragms fastened with welds. Some details of elemental testing are shown in Figure A9.

A6. Measured Results

A6.1 General failure behavior

Three basic failure modes had been identified for SDRC diaphragms as shown in Figure A6. Composite slab failure mode has three sub-modes: concrete shear, localized failure, and stability failure. Only concrete shear failure was experimentally observed as a controlling mode. Under the concrete shear sub-mode, diagonal tension failure was observed to be an upper bound to the diaphragm capacity, because all other failure modes have to be prevented to achieve diagonal tension failure. This mode is characterized by the formation of a diagonal crack approximately at 45 degrees from the side. Once the crack forms, a significant drop in load carrying capacity and a reduction in stiffness was observed. A measurable end slip between concrete and deck was observed before the crack formation, but the interface does not degrade significantly until the crack was formed.

Edge connection failure may be the limiting mode of failure in SDRC diaphragms. Diaphragms attached to the loading frame with welds and had their strength bounded by weld failure, showed measurable end slip and a visible separation at the edge, between deck and concrete. When studs were used, the slip between concrete and deck, was considerable less than that of similar diaphragms fastened with welds. Moreover, the slip was negligible in all cases where studs were used to fasten all diaphragm sides.

Distinction between edge connection and shear transfer mechanism failure was not made for those diaphragms fastened with arc-spot welds, because slip was characteristic of both types of failure. After test completion, concrete was removed and welds were observed. If there were no failed welds, then shear transfer mechanism was the failure mode, otherwise a combination of shear transfer and edge connection failure was assumed because large deflections were imposed to diaphragms which may have caused the welds to fail after a shear transfer mechanism occurred.

Shear transfer mechanism failure was obtained only for those diaphragms fastened to the loading frame with arc-spot welds. Use of shear studs provide an additional restriction at the edge, which does not allow the interface to degrade. Behavior for this type of mechanism was similar to that from edge connection failure mode.

A6.2 Edge zone Concept

The edge zone concept was developed by Porter and Greimman (78), in the first phase of the SDRC research. The edge zone is the narrow region of the interface between concrete and deck where takes place the transfer of load between the framing members and the composite diaphragm.

With the objective of experimentally evaluate the length of the interface (width of edge zone), a series of bonded electrical resistance strain gages were located at the top and bottom of the diaphragm. An evaluation of how much the diaphragm was fully effective was obtained by measuring the strains at top (concrete) and bottom (steel deck) at the same locations . As long as the strains were similar in magnitude, the diaphragm at that section was considered fully effective, therefore, the interface was effective in transferring force. After the bond in the interface failed, a sharp increase in the steel strain was exhibited (load was transferred through frame-deck-concrete path).

Diaphragms fastened with headed shear studs did not show separation of concrete and steel deck at the interface as long as the diagonal tension crack had not formed. Once the diagonal crack formed, a separation of the interface was measured.

A6.3 Diaphragm strength and stiffness

Elastic stiffness values were determined for each diaphragm, based on the first nominal displacement of 0.025 in. Table A2 gives results for each diaphragm. Since the test frame was relative flexible, no adjustments to the experimental stiffness were made. The ultimate load as well as failure mode is shown in Table A2. No adjustment was made to the strength values, since frame calibration indicated 1 kip of shear carrying capacity for the bare frame.

A6.4 Elemental test results

Results of the elemental tests are shown in Table A3. Ultimate strength (Qppo and Qtpo) and energy input (area of the force-displacement curve) are presented in parallel and transverse directions based upon a per inch of specimen basis.

Table A2. Summary of experimental results (modified from reference 29)

Diaphragm Number	Initial Stiffness (Kips/in.)	Ultimate Strength (Kips)	Failure Mode
1	1800	168	DT
2	2000	189	DT
3	1600	91	STM
4	1400	83	STM
5	1800	116	DT
6	2400	147	STM
7	1700	129	STM
8	1000	52	EC
9	1900	214	DT
10	1800	161	DT
11	1700	95	STM
12	1800	180	DT
13	1900	250	DT
14	2000	208	STM
15	1300	103	STM/DT
16	1400	124	DT
17	1700	146	STM
18	1700	161	DT
19	1300	147	DT
20	1400	95	STM/EC
21	1200	122	STM/EC
22	2300	169	DT

Table A2. (Continued)

Diaphragm Number	Initial Stiffness (Kips/in.)	Ultimate Strength (Kips)	Failure Mode
23	1700	106	STM/EC
24	2100	168	DT
25	2000	180	DT
26	1700	87	DT
27	2000	91	EC
28	2000	119	EC
29	2300	137	DT
30	1900	115	EC
31	1500	65	STM/EC
32	1000	60	STM/EC

DT Diagonal Tension
STM Shear Transfer Mechanism
EC Edge Connection

Table A3. Elemental test results (29)

Deck type	Ultimate Strength (lbs./in.)		Energy input @ 0.003 in. (lb.-in./in.)	
	Qppo parallel	Qtpo transverse	parallel	transverse
1	$\left(\frac{f'c}{2950}\right)468$	$\left(\frac{f'c}{6250}\right)454$	0.66	0.39
2	493	933	0.73	1.35
3	__[a]	__[a]	__[a]	__[a]
4	$\left(\frac{f'c}{2583}\right)499$	$\left(\frac{f'c}{2583}\right)520$	0.96	0.87
5	625	627	1.01	0.93
5B	211	326	0.58	0.63
6	293	521	0.67	0.93
7	563	$\left(\frac{f'c}{4019}\right)531$	0.87	0.76
8	554	786	0.57	0.66
9	404	437	0.50	0.78
10	296	__[a]	0.18	__[a]
11	308	361	0.68	0.83

[a]No elemental test performed.

APPENDIX B. STATISTICAL RESULTS FOR THE HYSTERETIC MODEL

B1. General

This appendix presents tables and figures associated with results of the statistical analyses applied on the experimental data. First, tables showing numerical results of the analyses are presented. Next, a series of figures representing graphically the statistical results are shown.

Table B1. MAE mean values and confidence intervals

Model	Estimate	VIRGIN ENVELOPE				STABILIZED ENVELOPE			
		Virgin +[a]	Virgin -[a]	Virgin +[b]	Virgin -[b]	Stab. +[a]	Stab. -[a]	Stab. +[b]	Stab. -[b]
1	Mean	0.126	0.129	0.091	0.100	0.144	0.149	0.119	0.116
1	Lower	0.112	0.116	0.071	0.077	0.132	0.136	0.094	0.093
1	Upper	0.141	0.142	0.110	0.123	0.156	0.162	0.144	0.139
2	Mean	0.158	0.161	0.068	0.079	0.171	0.173	0.093	0.082
2	Lower	0.147	0.151	0.053	0.058	0.159	0.161	0.071	0.062
2	Upper	0.168	0.171	0.082	0.099	0.182	0.185	0.116	0.103
3	Mean	0.222	0.218	0.113	0.129	0.216	0.214	0.129	0.114
3	Lower	0.205	0.200	0.032	0.062	0.196	0.198	0.027	0.065
3	Upper	0.239	0.235	0.194	0.197	0.237	0.230	0.230	0.164
4	Mean	0.067	0.062	0.088	0.083	0.061	0.059	0.083	0.076
4	Lower	0.054	0.049	0.071	0.064	0.052	0.048	0.060	0.059
4	Upper	0.080	0.075	0.106	0.102	0.071	0.070	0.107	0.094
5	Mean	0.032	0.034	1.683	0.440	0.031	0.039	0.759	0.381
5	Lower	0.025	0.024	-0.778	0.257	0.024	0.029	0.210	0.257
5	Upper	0.039	0.045	4.144	0.623	0.038	0.049	1.308	0.506
6	Mean	0.066	0.068	0.092	0.105	0.070	0.071	0.122	0.115
6	Lower	0.058	0.059	0.076	0.084	0.059	0.058	0.097	0.093
6	Upper	0.073	0.077	0.108	0.126	0.081	0.083	0.148	0.136
7	Mean	0.030	0.026	0.061	0.067	0.028	0.032	0.072	0.065
7	Lower	0.024	0.019	0.049	0.054	0.020	0.024	0.054	0.048
7	Upper	0.035	0.034	0.073	0.081	0.035	0.041	0.091	0.082
8	Mean	0.034	0.035	0.075	0.075	0.036	0.039	0.070	0.068
8	Lower	0.026	0.029	0.059	0.057	0.028	0.031	0.048	0.053
8	Upper	0.041	0.042	0.091	0.094	0.043	0.048	0.092	0.083
9	Mean	0.055	0.055	0.072	0.080	0.059	0.064	0.094	0.090
9	Lower	0.044	0.046	0.057	0.061	0.048	0.054	0.072	0.068
9	Upper	0.065	0.063	0.087	0.099	0.069	0.074	0.117	0.111
10	Mean	0.210	0.216	0.077	0.086	0.235	0.240	0.103	0.097
10	Lower	0.194	0.202	0.061	0.066	0.223	0.226	0.081	0.076
10	Upper	0.225	0.230	0.093	0.107	0.247	0.254	0.126	0.118
11	Mean	0.044	0.040	0.126	0.120	0.041	0.043	0.123	0.121
11	Lower	0.035	0.030	0.099	0.093	0.034	0.034	0.092	0.098
11	Upper	0.052	0.051	0.153	0.147	0.048	0.051	0.154	0.144

[a]Pre-peak region
[b]Post-peak region

Table B2. Pvalues from positive/negative envelope force difference tests

	VIRGIN ENVELOPE			STABILIZED ENVELOPE		
test	t	Pvalue	tcr	t	Pvalue	tcr
2	0.19	0.85	2.31	2.30	0.05	2.36
3	1.90	0.09	2.26	1.38	0.20	2.26
4	-0.74	0.48	2.26	-1.29	0.23	2.26
5	1.74	0.12	2.36	-1.43	0.19	2.36
6	2.40	0.04*	2.31	-1.27	0.25	2.36
7	1.55	0.16	2.31	-0.42	0.69	2.31
8	1.65	0.14	2.31	0.00	1.00	2.36
9	0.80	0.45	2.26	-1.06	0.32	2.31
10	2.21	0.06	2.31	0.59	0.57	2.31
11	2.69	0.02*	2.26	-1.95	0.09	2.31
12	2.29	0.06	2.36	-0.33	0.75	2.45
13	0.73	0.48	2.26	-0.73	0.48	2.31
14	1.93	0.09	2.26	0.54	0.61	2.31
15	1.67	0.14	2.36	1.66	0.13	2.31
16	2.09	0.07	2.31	-1.89	0.10	2.36
17	3.88	0.01*	2.26	3.56	0.01*	2.45
18	4.77	0.00**	2.36	2.43	0.05	2.45
19	2.33	0.05	2.36	1.33	0.23	2.36
20	-2.89	0.02*	2.31	-3.94	0.01*	2.36
21	-0.64	0.54	2.36	-1.13	0.30	2.36
22	1.99	0.09	2.36	-1.05	0.34	2.45
23	1.64	0.14	2.31	0.40	0.71	2.45

Table B2. Continue

	VIRGIN ENVELOPE			STABILIZED ENVELOPE		
test	t	Pvalue	tcr	t	Pvalue	tcr
24	2.45	0.05	2.45	1.12	0.30	2.45
25	0.91	0.38	2.23	-0.36	0.73	2.45
26	1.14	0.29	2.36	-0.52	0.62	2.45
27	2.65	0.03*	2.31	-0.04	0.97	2.45
28	2.06	0.07	2.23	-3.73	0.01*	2.45
29	1.48	0.18	2.31	0.76	0.48	2.45
30	0.89	0.40	2.31	-3.81	0.01*	2.45
31	3.46	0.01*	2.45	1.55	0.16	2.36
32	4.31	0.01*	2.45	4.88	0.00**	2.45

*Significant difference at 0.05 level.
**Significant difference at 0.01 level.

Table B3. Regression analysis and ANOVA for post-peak positive envelope(test 3)

Obs.	x	y	ln(x)	y	y-pred	residual
1	1.00	1.00	0.00	1.00	0.97	0.03
2	2.00	0.87	0.69	0.87	0.87	0.00
3	4.02	0.75	1.39	0.75	0.77	-0.02
4	7.01	0.70	1.95	0.70	0.69	0.01
5	9.58	0.64	2.26	0.64	0.65	-0.01
6	20.00	0.48	3.00	0.48	0.54	-0.06
7	30.00	0.47	3.40	0.47	0.48	-0.01
8	40.00	0.47	3.69	0.47	0.44	0.03
9	50.00	0.44	3.91	0.44	0.41	0.03

Regression Statistics

R	0.989
R^2	0.978
Standard Error	0.032
Observations	9

Analysis of Variance (ANOVA)

	df	Sum of Squares	Mean Squares	F	Sign. F
Regression	1	0.3105	0.313	313.57	5E-07
Residual	7	0.0069	0.001		
Total	8	0.3175			

Parameter Estimates

	Coeffs.	Std Error	t Statistic	P-value	Lower 95%	Upper 95%
Intercept	0.9712	0.0211	46.043	5E-11	0.9213	1.0211
ln(x)	-0.144	0.0081	-17.71	1E-07	-0.163	-0.125

Table B4. Log-x regression model results for pre-peak virgin envelope data

	R values			F values		Coefficients		Std. error		P values		95% Confidence Intervals			
test	R	R^2	STD error	F	Sig F	Int.	Slope	Stder int.	Stder slope	Pvalue int.	Pvalue slope	Lower int.	Upper int.	Lower slope	Upper slope
2	0.98	0.96	0.037	46.3	0.0209	0.96	0.37	0.026	0.054	4E-05	0.0065	0.85	1.08	0.14	0.60
3	1.00	1.00	0.006	897.6	0.0011	1.00	0.28	0.005	0.009	2E-07	8E-05	0.98	1.02	0.24	0.32
4	0.99	0.97	0.051	148.6	0.0003	1.03	0.41	0.033	0.034	6E-07	7E-05	0.94	1.12	0.32	0.50
5	0.94	0.88	0.112	52.2	0.0002	0.89	0.25	0.060	0.034	4E-07	9E-05	0.75	1.03	0.17	0.33
6	0.99	0.99	0.029	361.3	5E-05	0.99	0.40	0.019	0.021	5E-08	7E-06	0.94	1.05	0.34	0.46
7	0.97	0.95	0.072	103.2	5E-05	1.07	0.33	0.043	0.033	4E-08	2E-05	0.96	1.17	0.25	0.42
8	0.95	0.91	0.076	48.3	0.0009	1.03	0.28	0.046	0.040	5E-07	0.0004	0.91	1.15	0.18	0.38
9	0.98	0.96	0.068	150.4	2E-05	1.01	0.38	0.040	0.031	4E-08	5E-06	0.91	1.11	0.31	0.46
10	0.99	0.98	0.041	378.0	5E-08	1.03	0.26	0.022	0.013	5E-12	1E-08	0.98	1.09	0.23	0.29
11	0.98	0.97	0.039	248.2	3E-07	1.01	0.20	0.021	0.013	4E-12	7E-08	0.96	1.06	0.17	0.23
12	1.00	1.00	0.017	2362.3	4E-11	1.01	0.27	0.009	0.006	2E-15	3E-12	0.98	1.03	0.26	0.28
13	0.99	0.98	0.050	281.3	3E-06	0.96	0.39	0.029	0.023	7E-09	7E-07	0.89	1.03	0.33	0.45
14	1.00	1.00	0.009	9079.7	2E-13	1.00	0.27	0.005	0.003	6E-18	8E-15	0.99	1.01	0.26	0.27

Table B4. (Continued)

test	R values		STD error	F values		Coefficients		Std. error		P values		95% Confidence Intervals			
	R	R^2		F	Sig F	Int.	Slope	Stder int.	Stder slope	Pvalue int.	Pvalue slope	Lower int.	Upper int.	Lower slope	Upper slope
15	0.97	0.94	0.059	118.6	4E-06	0.94	0.21	0.033	0.020	4E-10	2E-06	0.87	1.02	0.17	0.26
16	0.97	0.95	0.062	152.7	2E-06	0.96	0.25	0.034	0.020	4E-10	6E-07	0.88	1.04	0.20	0.29
17	0.99	0.98	0.035	426.9	3E-08	1.00	0.24	0.019	0.012	2E-12	7E-09	0.95	1.04	0.21	0.27
18	0.98	0.97	0.053	243.3	3E-07	1.05	0.27	0.029	0.017	4E-11	8E-08	0.98	1.12	0.23	0.31
19	1.00	0.99	0.027	895.2	1E-08	1.01	0.29	0.015	0.010	3E-12	2E-09	0.97	1.04	0.27	0.32
20	0.98	0.96	0.053	170.7	1E-06	1.02	0.23	0.029	0.017	6E-11	4E-07	0.95	1.08	0.19	0.27
21	0.99	0.98	0.044	348.4	7E-08	0.95	0.27	0.024	0.014	2E-11	2E-08	0.89	1.01	0.24	0.30
22	1.00	0.99	0.020	1354.9	3E-10	1.01	0.25	0.011	0.007	1E-14	4E-11	0.98	1.03	0.24	0.27
23	0.97	0.95	0.057	122.4	1E-05	0.97	0.24	0.032	0.021	1E-09	4E-06	0.90	1.05	0.18	0.29
24	0.99	0.99	0.031	620.3	7E-09	1.02	0.25	0.017	0.010	5E-13	1E-09	0.98	1.06	0.23	0.28
25	1.00	0.99	0.031	1158.2	2E-12	0.98	0.38	0.017	0.011	5E-16	3E-13	0.94	1.02	0.35	0.40
26	0.92	0.85	0.088	28.7	0.003	0.98	0.26	0.052	0.048	1E-06	0.0017	0.85	1.11	0.13	0.38
27	1.00	0.99	0.014	831.8	9E-07	1.00	0.23	0.009	0.008	3E-11	1E-07	0.98	1.02	0.21	0.25

Table B4. (Continued)

test	R values		STD error	F values		Coefficients		Std. error		P values		95% Confidence Intervals			
	R	R^2		F	Sig F	Int.	Slope	Stder int.	Stder slope	Pvalue int.	Pvalue slope	Lower int.	Upper int.	Lower slope	Upper slope
28	0.96	0.93	0.067	78.9	0.0001	1.01	0.28	0.039	0.032	3E-08	5E-05	0.92	1.11	0.20	0.36
29	0.98	0.97	0.046	178.2	1E-05	1.00	0.32	0.025	0.024	2E-09	3E-06	0.94	1.07	0.26	0.38
30	0.96	0.92	0.074	44.1	0.0027	1.01	0.28	0.045	0.042	3E-06	0.0012	0.88	1.14	0.16	0.40
31	0.94	0.89	0.057	41.5	0.0013	1.01	0.19	0.035	0.030	1E-07	0.0007	0.93	1.10	0.12	0.27
32	1.00	1.00	0.018	807.9	9E-06	1.01	0.39	0.012	0.014	4E-09	1E-06	0.98	1.04	0.35	0.43

Table B5. Log-x regression model results for post-peak virgin envelope data

test	R values		STD error	F values		Coefficients		Std. error		P values		95% Confidence Intervals			
	R	R^2		F	Sig F	Int.	Slope	Stder int.	Stder slope	Pvalue int.	Pvalue slope	Lower int.	Upper int.	Lower slope	Upper slope
2	0.87	0.76	0.086	34.6	0.0001	1.04	-0.17	0.042	0.029	1E-11	7E-05	0.95	1.13	-0.24	-0.11
3	0.97	0.95	0.048	283.5	4E-11	0.99	-0.15	0.023	0.009	6E-18	1E-11	0.95	1.04	-0.17	-0.13
4	0.97	0.95	0.068	218.2	5E-09	1.05	-0.20	0.033	0.013	1E-13	2E-09	0.98	1.12	-0.22	-0.17
5	0.95	0.91	0.091	60.7	0.0002	1.08	-0.30	0.053	0.038	2E-07	0.0001	0.95	1.21	-0.39	-0.20
6	0.95	0.91	0.086	103.2	1E-06	1.03	-0.18	0.042	0.018	7E-11	6E-07	0.94	1.13	-0.22	-0.14
7	0.99	0.98	0.060	378.2	1E-08	1.07	-0.29	0.032	0.015	1E-11	3E-09	1.00	1.15	-0.33	-0.26
8	0.97	0.94	0.073	141.8	8E-07	1.05	-0.20	0.037	0.017	8E-11	3E-07	0.96	1.13	-0.24	-0.16
9	0.98	0.96	0.074	217.9	4E-08	0.96	-0.29	0.038	0.020	4E-11	1E-08	0.87	1.04	-0.34	-0.25
10	0.95	0.90	0.116	53.1	0.0003	1.02	-0.32	0.069	0.044	2E-06	0.0002	0.85	1.19	-0.43	-0.22
11	0.97	0.94	0.088	133.7	1E-06	1.04	-0.36	0.047	0.031	7E-10	4E-07	0.94	1.15	-0.43	-0.29
12	0.97	0.95	0.046	112.5	4E-05	1.02	-0.32	0.029	0.030	4E-09	1E-05	0.95	1.09	-0.40	-0.25
13	0.95	0.90	0.123	111.7	2E-07	0.96	-0.30	0.061	0.029	8E-10	9E-08	0.83	1.09	-0.37	-0.24
14	0.94	0.89	0.117	105.7	1E-07	0.95	-0.34	0.053	0.033	4E-11	7E-08	0.84	1.07	-0.41	-0.27

Table B5. (Continued)

test	R values		STD error	F values		Coefficients		Std. error		P values		95% Confidence Intervals			
	R	R^2		F	Sig F	Int.	Slope	Stder int.	Stder slope	Pvalue int.	Pvalue slope	Lower int.	Upper int.	Lower slope	Upper slope
15	0.88	0.78	0.172	34.9	0.0001	0.93	-0.34	0.090	0.057	5E-07	0.0001	0.73	1.13	-0.46	-0.21
16	0.95	0.90	0.112	91.8	2E-06	1.01	-0.36	0.065	0.037	8E-09	1E-06	0.87	1.16	-0.44	-0.28
17	0.92	0.85	0.156	45.7	0.0001	1.12	-0.58	0.092	0.086	7E-07	8E-05	0.91	1.34	-0.78	-0.38
18	0.94	0.88	0.048	43.9	0.0006	0.99	-0.32	0.032	0.049	1E-08	0.0003	0.91	1.07	-0.44	-0.20
19	0.97	0.94	0.081	164.2	6E-08	1.01	-0.34	0.041	0.027	1E-11	2E-08	0.92	1.10	-0.40	-0.28
20	0.91	0.82	0.172	37.0	0.0003	0.86	-0.32	0.076	0.053	1E-06	0.0002	0.69	1.04	-0.44	-0.20
21	0.91	0.83	0.162	24.1	0.0045	0.84	-0.30	0.091	0.062	9E-05	0.0027	0.61	1.08	-0.46	-0.14
22	0.91	0.83	0.044	30.4	0.0015	1.00	-0.20	0.027	0.036	2E-09	0.0009	0.94	1.07	-0.28	-0.11
23	0.89	0.79	0.127	29.6	0.0006	1.06	-0.44	0.070	0.081	1E-07	0.0004	0.90	1.23	-0.63	-0.25
24	0.88	0.77	0.048	20.5	0.004	1.00	-0.22	0.032	0.049	9E-09	0.0027	0.92	1.07	-0.34	-0.10
25	0.93	0.86	0.067	50.8	1E-04	1.05	-0.25	0.040	0.035	8E-10	5E-05	0.96	1.15	-0.33	-0.17
26	0.92	0.85	0.097	52.7	5E-05	1.06	-0.29	0.057	0.040	4E-09	3E-05	0.93	1.19	-0.38	-0.20
27	0.92	0.85	0.095	68.1	3E-06	0.91	-0.38	0.052	0.046	2E-10	2E-06	0.79	1.02	-0.48	-0.28

Table B5. (Continued)

test	R values		STD error	F values		Coefficients		Std. error		P values		95% Confidence Intervals			
	R	R^2		F	Sig F	Int.	Slope	Stder int.	Stder slope	Pvalue int.	Pvalue slope	Lower int.	Upper int.	Lower slope	Upper slope
28	0.93	0.87	0.107	86.5	4E-07	1.00	-0.44	0.053	0.047	2E-11	2E-07	0.89	1.12	-0.54	-0.34
29	0.87	0.76	0.088	34.5	0.0001	0.86	-0.21	0.043	0.036	1E-10	8E-05	0.77	0.96	-0.29	-0.13
30	0.92	0.86	0.079	88.6	1E-07	0.91	-0.26	0.034	0.027	9E-15	6E-08	0.84	0.98	-0.31	-0.20
31	0.92	0.85	0.131	52.9	5E-05	0.96	-0.39	0.071	0.054	1E-07	3E-05	0.80	1.12	-0.52	-0.27
32	0.98	0.95	0.078	178.8	3E-07	0.96	-0.37	0.041	0.028	5E-10	1E-07	0.87	1.05	-0.44	-0.31

Table B6. Log-x regression model results for pre-peak stabilized envelope data

test	R values			F values		Coefficients		Std. error		P values		95% Confidence Intervals			
	R	R^2	STD error	F	Sig F	Int.	Slope	Stder int.	Stder slope	Pvalue int.	Pvalue slope	Lower int.	Upper int.	Lower slope	Upper slope
2	0.97	0.95	0.054	36.4	0.0264	1.00	0.47	0.038	0.077	0.0001	0.0091	0.84	1.16	0.13	0.80
3	1.00	1.00	0.006	869.6	0.0011	1.00	0.25	0.004	0.008	2E-07	9E-05	0.98	1.02	0.21	0.28
4	0.97	0.95	0.067	71.4	0.0011	1.04	0.37	0.042	0.044	2E-06	0.0004	0.92	1.16	0.25	0.49
5	0.99	0.98	0.042	322.6	2E-06	1.01	0.24	0.023	0.013	8E-10	4E-07	0.95	1.06	0.21	0.27
6	0.89	0.79	0.092	11.2	0.0444	1.03	0.26	0.060	0.079	7E-05	0.0288	0.84	1.22	0.01	0.52
7	0.92	0.85	0.116	28.8	0.003	1.00	0.33	0.070	0.061	7E-06	0.0017	0.82	1.18	0.17	0.49
8	0.99	0.97	0.034	148.4	0.0003	1.01	0.29	0.022	0.024	9E-08	7E-05	0.95	1.07	0.23	0.36
9	0.95	0.90	0.110	43.8	0.0012	0.97	0.38	0.066	0.058	6E-06	0.0006	0.80	1.14	0.23	0.53
10	0.98	0.96	0.056	182.0	9E-07	1.06	0.24	0.031	0.018	7E-11	3E-07	0.99	1.13	0.20	0.28
11	0.99	0.98	0.027	393.8	4E-08	1.01	0.17	0.015	0.009	1E-13	1E-08	0.98	1.05	0.15	0.19
12	1.00	1.00	0.019	1243.9	3E-08	1.00	0.31	0.011	0.009	6E-12	4E-09	0.97	1.03	0.29	0.33
13	0.99	0.99	0.034	589.8	3E-07	1.00	0.38	0.020	0.016	3E-10	5E-08	0.95	1.05	0.34	0.42
14	1.00	1.00	0.019	1871.2	9E-11	1.00	0.26	0.010	0.006	6E-15	9E-12	0.98	1.03	0.25	0.27

Table B6. (Continued)

test	R values		STD error	F values		Coefficients		Std. error		P values		95% Confidence Intervals			
	R	R^2		F	Sig F	Int.	Slope	Stder int.	Stder slope	Pvalue int.	Pvalue slope	Lower int.	Upper int.	Lower slope	Upper slope
15	0.99	0.98	0.030	508.9	2E-08	1.00	0.22	0.016	0.010	4E-13	3E-09	0.96	1.04	0.20	0.24
16	0.99	0.98	0.036	305.2	2E-06	0.97	0.29	0.022	0.017	7E-10	5E-07	0.92	1.03	0.25	0.33
17	0.99	0.98	0.032	471.8	2E-08	0.99	0.23	0.018	0.010	9E-13	4E-09	0.95	1.03	0.20	0.25
18	0.99	0.98	0.041	254.9	4E-06	1.00	0.30	0.024	0.019	1E-09	9E-07	0.94	1.06	0.25	0.35
19	0.99	0.99	0.037	554.7	1E-08	1.03	0.28	0.020	0.012	2E-12	2E-09	0.98	1.08	0.25	0.31
20	0.95	0.90	0.076	56.6	0.0003	0.95	0.26	0.045	0.035	1E-07	0.0001	0.83	1.06	0.18	0.35
21	0.99	0.99	0.029	756.9	3E-09	1.01	0.26	0.016	0.010	3E-13	5E-10	0.97	1.05	0.24	0.28
22	0.99	0.98	0.031	498.6	2E-08	1.03	0.23	0.017	0.010	5E-13	3E-09	0.99	1.07	0.20	0.25
23	0.96	0.91	0.078	75.0	5E-05	1.00	0.25	0.044	0.029	1E-08	2E-05	0.90	1.11	0.18	0.32
24	1.00	0.99	0.020	1160.4	4E-08	1.00	0.31	0.012	0.009	8E-12	5E-09	0.97	1.03	0.29	0.33
25	0.98	0.96	0.061	139.0	2E-05	1.05	0.33	0.036	0.028	2E-08	7E-06	0.96	1.14	0.26	0.40
26	0.96	0.92	0.068	45.1	0.0026	1.02	0.34	0.044	0.051	3E-06	0.0011	0.90	1.14	0.20	0.49
27	0.99	0.99	0.021	266.1	8E-05	0.99	0.24	0.013	0.015	9E-09	2E-05	0.95	1.03	0.20	0.29

Table B6. (Continued)

test	R values		STD error	F values		Coefficients		Std. error		P values		95% Confidence Intervals			
	R	R^2		F	Sig F	Int.	Slope	Stder int.	Stder slope	Pvalue int.	Pvalue slope	Lower int.	Upper int.	Lower slope	Upper slope
28	0.98	0.95	0.049	122.8	3E-05	1.04	0.25	0.029	0.022	4E-09	1E-05	0.96	1.11	0.19	0.30
29	0.98	0.96	0.048	92.9	0.0006	0.97	0.33	0.031	0.034	6E-07	0.0002	0.89	1.06	0.23	0.42
30	1.00	0.99	0.022	492.4	2E-05	1.00	0.36	0.015	0.016	1E-08	3E-06	0.96	1.04	0.31	0.40
31	0.92	0.84	0.060	21.7	0.0096	1.01	0.20	0.038	0.042	1E-06	0.0055	0.91	1.11	0.08	0.31
32	0.90	0.81	0.082	16.8	0.0149	1.05	0.25	0.053	0.061	6E-06	0.0094	0.90	1.19	0.08	0.42

Table B7. Log-x regression model for post-peak stabilized envelope data

test	R values			F values		Coefficients		Std. error		P values		95% Confidence Intervals			
	R	R^2	STD error	F	Sig F	Int.	Slope	Stder int.	Stder slope	Pvalue int.	Pvalue slope	Lower int.	Upper int.	Lower slope	Upper slope
2	0.97	0.94	0.047	155.9	2E-07	1.04	-0.22	0.026	0.017	3E-13	8E-08	0.98	1.09	-0.25	-0.18
3	0.98	0.96	0.047	364.9	2E-11	1.01	-0.18	0.023	0.009	2E-17	6E-12	0.96	1.06	-0.20	-0.16
4	0.99	0.97	0.051	438.3	8E-11	1.04	-0.21	0.025	0.010	3E-15	2E-11	0.98	1.09	-0.23	-0.19
5	0.96	0.92	0.110	68.0	0.0002	1.09	-0.38	0.064	0.046	6E-07	8E-05	0.94	1.25	-0.49	-0.27
6	0.86	0.75	0.161	32.2	0.0001	1.14	-0.17	0.077	0.030	5E-09	0.0001	0.97	1.31	-0.24	-0.10
7	0.93	0.87	0.152	58.4	3E-05	1.04	-0.27	0.077	0.035	1E-07	2E-05	0.86	1.21	-0.35	-0.19
8	0.97	0.94	0.080	124.2	4E-06	1.05	-0.21	0.040	0.019	8E-10	1E-06	0.96	1.14	-0.25	-0.16
9	0.89	0.80	0.191	35.3	0.0002	0.93	-0.26	0.098	0.044	3E-06	0.0001	0.71	1.15	-0.37	-0.16
10	0.96	0.91	0.107	62.3	0.0002	0.91	-0.32	0.064	0.041	2E-06	1E-04	0.75	1.06	-0.42	-0.22
11	0.99	0.99	0.043	472.6	6E-07	0.97	-0.36	0.026	0.017	2E-09	1E-07	0.91	1.03	-0.40	-0.32
12	0.91	0.83	0.104	19.4	0.0116	1.07	-0.29	0.065	0.065	2E-05	0.007	0.89	1.25	-0.47	-0.11
13	0.91	0.83	0.148	42.4	0.0001	0.81	-0.28	0.082	0.043	2E-06	7E-05	0.62	0.99	-0.38	-0.18
14	0.96	0.91	0.111	64.5	0.0002	0.90	-0.33	0.067	0.040	3E-06	9E-05	0.74	1.07	-0.42	-0.23

Table B7. (Continued)

test	R values		STD error	F values		Coefficients		Std. error		P values		95% Confidence Intervals			
	R	R^2		F	Sig F	Int.	Slope	Stder int.	Stder slope	Pvalue int.	Pvalue slope	Lower int.	Upper int.	Lower slope	Upper slope
15	0.78	0.61	0.207	12.5	0.0077	0.76	-0.26	0.109	0.073	7E-05	0.0064	0.51	1.01	-0.42	-0.09
16	0.94	0.89	0.124	61.7	5E-05	1.03	-0.29	0.065	0.037	7E-08	3E-05	0.88	1.18	-0.37	-0.20
17	1.00	1.00	0.011	2966.1	0.0003	1.00	-0.67	0.008	0.012	1E-06	1E-05	0.97	1.03	-0.72	-0.61
18	0.99	0.98	0.024	168.3	0.0002	1.01	-0.19	0.015	0.015	1E-08	5E-05	0.97	1.05	-0.23	-0.15
19	0.99	0.98	0.054	177.3	0.0002	0.97	-0.39	0.034	0.029	1E-06	4E-05	0.88	1.07	-0.47	-0.31
20	0.83	0.68	0.228	15.2	0.0059	0.86	-0.26	0.120	0.067	1E-04	0.0046	0.57	1.14	-0.42	-0.10
21	0.89	0.80	0.202	16.0	0.016	0.85	-0.31	0.123	0.078	0.0009	0.0103	0.51	1.19	-0.53	-0.10
22	0.99	0.98	0.033	126.6	0.0078	1.00	-0.40	0.023	0.036	3E-05	0.0015	0.90	1.10	-0.55	-0.25
23	0.95	0.90	0.127	28.3	0.013	0.99	-0.51	0.083	0.096	0.0003	0.006	0.72	1.25	-0.81	-0.20
24	0.87	0.75	0.097	12.3	0.0248	1.06	-0.21	0.060	0.060	1E-05	0.0172	0.89	1.23	-0.38	-0.04
25	1.00	1.00	0.012	2480.9	1E-06	1.01	-0.37	0.008	0.008	5E-10	6E-08	0.98	1.03	-0.39	-0.35
26	0.98	0.95	0.057	119.0	4E-05	1.01	-0.26	0.033	0.024	1E-08	1E-05	0.93	1.09	-0.32	-0.20
27	0.95	0.91	0.090	60.9	0.0002	0.99	-0.30	0.052	0.038	3E-07	0.0001	0.86	1.11	-0.39	-0.20

Table B7. (Continued)

test	R values		STD error	F values		Coefficients		Std. error		P values		95% Confidence Intervals			
	R	R^2		F	Sig F	Int.	Slope	Stder int.	Stder slope	Pvalue int.	Pvalue slope	Lower int.	Upper int.	Lower slope	Upper slope
28	0.94	0.89	0.125	32.9	0.0046	0.92	-0.45	0.079	0.079	8E-05	0.0023	0.70	1.14	-0.67	-0.23
29	0.98	0.97	0.048	177.7	1E-05	0.96	-0.26	0.027	0.020	4E-09	3E-06	0.89	1.03	-0.31	-0.22
30	0.99	0.99	0.033	456.2	7E-07	0.99	-0.30	0.019	0.014	3E-10	1E-07	0.94	1.03	-0.33	-0.26
31	0.97	0.94	0.094	124.3	4E-06	1.01	-0.38	0.054	0.034	2E-08	1E-06	0.88	1.13	-0.46	-0.30
32	0.96	0.91	0.101	73.9	6E-05	0.89	-0.34	0.058	0.039	3E-07	3E-05	0.76	1.03	-0.43	-0.24

Table B8. Correlation matrix for the effects of key experimental parameters

	V^1 slope	V^2 slope	S^1 slope	S^2 slope	Ki	Deck t	Fy	Con.h	Con. top h	f'c	L1/L2
V^1 slope	1.00										
V^2 slope	0.45	1.00									
S^1 slope	0.67	0.48	1.00								
S^2 slope	0.33	0.78	0.44	1.00							
Ki	0.15	0.22	0.18	0.00	1.00						
Deck t	0.05	-0.08	-0.09	-0.16	0.28	1.00					
Fy	-0.20	-0.17	-0.12	0.02	-0.17	-0.42	1.00				
Con. h	0.15	-0.15	-0.12	-0.22	0.31	0.23	-0.33	1.00			
Con. top h	-0.01	-0.34	-0.26	-0.33	0.28	0.17	-0.09	0.77	1.00		
f'c	0.53	0.22	0.55	0.14	0.34	0.21	-0.31	0.23	0.13	1.00	
L1/L2	0.10	0.07	0.07	0.24	-0.28	0.36	-0.32	0.03	0.10	0.27	1.00

[1]Pre-peak envelope
[2]Post-peak envelope

Table B9. Correlation coefficients related to the force ratio parameter

Force Ratio	Virgin Envelope		Stabilized Envelope	
and	Pre-peak	Post-peak	Pre-peak	Post-peak
x	0.93	-.081	0.93	-0.80
q	0.21	0.01	0.15	0.04
L1L2	-0.07	-0.09	-0.11	-0.08
CT	-0.04	-0.11	-0.09	-0.08
GL	-0.09	-0.10	-0.14	-0.02
D1	0.05	-0.02	0.02	-0.06
D2	-0.06	0.05	0.01	0.12
D3	-0.15	0.10	-0.09	0.04
D4	0.14	-0.05	0.14	-0.07
D5	-0.05	-0.13	-0.04	-0.07
D6	-0.02	0.05	-0.07	0.10
D7	0.07	-0.04	0.02	-0.03
Qx	0.83	-0.67	0.85	-0.66
L1L2x	0.92	-0.78	0.92	-0.77
CTx	0.54	-0.54	0.60	-0.51
GLx	0.36	-0.37	0.41	-0.28
D1x	0.25	-0.30	0.30	-0.36
D2x	0.24	-0.11	0.20	-0.05
D3x	0.46	-0.17	0.41	-0.23
D4x	0.08	-0.25	0.07	-0.28
D5x	0.18	-0.25	0.18	-0.19
D6x	0.18	-0.10	0.24	-0.03
D7X	0.13	-0.23	0.18	-0.21

Table B10. Forward stepwise regression envelope results

Envelope region	Parameters included	Coefficient	Std. error of Coefficient	t statistic	Pvalue
Pre	Qx	0.012	0.002	5.74	---[a]
Peak	D1x	0.242	0.021	11.76	---[a]
Virgin	D2x	0.198	0.019	10.64	---[a]
Region	D3x	0.217	0.013	16.22	---[a]
	D4x	0.122	0.021	5.83	---[a]
	D5x	0.184	0.017	10.59	---[a]
	D6x	0.188	0.017	10.92	---[a]
	D7x	0.119	0.022	5.47	---[a]
	GLx	-0.035	0.010	-3.47	---[a]
Post	GL	-0.098	0.014	-7.03	---[a]
Peak	D1x	-0.187	0.009	-21.70	---[a]
Virgin	D2x	-0.195	0.016	-12.21	---[a]
Region	D3x	-0.250	0.018	-14.31	---[a]
	D4x	-0.330	0.016	-21.08	---[a]
	D5x	-0.288	0.020	-14.21	---[a]
	D6x	-0.303	0.026	-11.81	---[a]
	D7x	-0.391	0.020	-19.62	---[a]

Table B10. (Continued)

Envelope region	Parameters included	Coefficient	Std. error of Coefficient	t statistic	Pvalue
Pre	Qx	0.011	0.002	5.43	---[a]
Peak	D1x	0.255	0.021	11.92	---[a]
Stabilized	D2x	0.143	0.019	7.44	---[a]
Region	D3x	0.181	0.014	12.81	---[a]
	D4x	0.111	0.021	5.38	---[a]
	D5x	0.171	0.018	9.31	---[a]
	D6x	0.216	0.017	12.83	---[a]
	D7x	0.144	0.022	6.55	---[a]
Post	GLx	-0.050	0.021	-2.40	0.017
Peak	D1x	-0.201	0.011	-18.65	---[a]
Stabilized	D2x	-0.143	0.018	-7.92	---[a]
Region	D3x	-0.294	0.024	-12.45	---[a]
	D4x	-0.323	0.020	-16.23	---[a]
	D5x	-0.264	0.027	-9.64	---[a]
	D6x	-0.267	0.047	-5.70	---[a]
	D7x	-0.322	0.025	-12.81	---[a]

[a]No significant

Table B11. Results from the nonlinear regression analysis for envelope force

	Pre-peak Region			Post-peak Region	
Coefficient	Virgin	Stabilized	Coefficient	Virgin	Stabilized
a_1	-0.036	na	b_1	-0.100	-0.052
a_2	0.013	0.012	b_2	-0.201	-0.222
a_3	0.248	0.259	b_3	-0.212	-0.164
a_4	0.201	0.145	b_4	-0.274	-0.325
a_5	0.222	0.184	b_5	-0.354	-0.353
a_6	0.126	0.114	b_6	-0.307	-0.290
a_7	0.188	0.173	b_7	-0.327	-0.306
a_8	0.193	0.219	b_8	-0.418	-0.351
a_9	0.121	0.147	-	-	-

Table B12. Mean values and 95% CI for strength degradation factor

number of cycles		2			3		
		95% Confidence Interval			95% Confidence Interval		
eep		Lower	Upper	Mean	Lower	Upper	Mean
>0	<.10	0.87	0.92	0.90	0.86	0.90	0.88
>.10	<.20	0.88	0.92	0.90	0.85	0.89	0.87
>.20	<.30	0.87	0.90	0.88	0.85	0.89	0.87
>.30	<.50	0.88	0.94	0.91	0.83	0.89	0.86
>.50	<.70	0.87	0.91	0.89	0.83	0.88	0.86
>.70	<1.0	0.83	0.87	0.85	0.78	0.82	0.80
>1.05	<2.0	0.82	0.89	0.85	0.71	0.85	0.78
>2.0	<5.0	0.64	0.70	0.67	0.56	0.62	0.59
>5.0	<10.0	0.59	0.67	0.63	0.52	0.60	0.56
>10.0	<25.0	0.59	0.72	0.65	0.47	0.59	0.53

Table 13. Strength degradation factor regression analysis for pre-peak region

coefficient of	Estimate	Std. error	t statistic	P value
D1x	-0.046	0.009	-5.22	<1E-05
D2x	-0.120	0.012	-10.48	<1E-05
D3x	-0.101	0.006	-16.09	<1E-05
D4x	-0.137	0.007	-19.07	<1E-05
D5x	-0.143	0.008	-17.67	<1E-05
D6x	-0.132	0.010	-12.76	<1E-05
D7x	-0.102	0.007	-14.38	<1E-05
(e/ep)x	-0.085	0.007	-11.92	<1E-05

Table B14. Strength degradation factor regression analysis for post-peak region

coefficient of	Estimate	Std. error	t statistic	P value
D1x	-0.209	0.016	-13.32	<1E-05
D2x	-0.258	0.024	-10.88	<1E-05
D3x	-0.266	0.015	-18.13	<1E-05
D4x	-0.319	0.012	-26.03	<1E-05
D5x	-0.365	0.019	-19.69	<1E-05
D6x	-0.388	0.020	-19.10	<1E-05
D7x	-0.302	0.013	-23.25	<1E-05
(e/ep)x	-0.008	0.001	-7.52	<1E-05
GLx	-0.062	0.014	-4.35	<1E-05

Table B15. MAE average values and 95% CI for pinch force data

Regression Model	Virgin Data						Stabilized Data					
	Pre-peak Region			Post-peak Region			Pre-peak Region			Post-peak Region		
	Mean	Lower	Upper	Mean	Lower	Upper	Mean	Lower	Upper	Mean	Lower	Upper
1	0.008	0.006	0.010	0.027	0.022	0.033	0.006	0.004	0.008	0.018	0.014	0.022
2	0.015	0.012	0.018	0.027	0.021	0.033	0.010	0.007	0.014	0.019	0.014	0.024
3	0.197	-0.006	0.399	0.033	0.026	0.039	0.040	0.027	0.053	0.024	0.016	0.033
4	0.029	0.023	0.034	0.034	0.027	0.041	0.019	0.015	0.023	0.020	0.016	0.024
5	0.030	0.019	0.042	0.045	0.035	0.055	0.022	0.011	0.034	0.029	0.022	0.036
6	0.014	0.011	0.016	0.027	0.021	0.033	0.010	0.007	0.012	0.019	0.014	0.023
7	0.018	0.015	0.021	0.030	0.023	0.037	0.012	0.009	0.014	0.019	0.014	0.023
8	0.008	0.006	0.010	0.032	0.025	0.039	0.006	0.004	0.008	0.022	0.017	0.027
9	0.017	0.014	0.019	0.028	0.022	0.034	0.012	0.009	0.014	0.018	0.014	0.022
10	0.013	0.010	0.016	0.027	0.021	0.033	0.008	0.006	0.011	0.018	0.014	0.023
11	0.021	0.017	0.024	0.036	0.029	0.043	0.013	0.010	0.016	0.021	0.017	0.026

Table B16. Regression Coefficients and 95% CI for pinch force virgin data

	Pre-peak Virgin Data			Post-peak Virgin Data					
test	Slope	L95%	U95%	Inter.	L95%	U95%	Slope	L95%	U95%
2	0.074	0.038	0.267	0.213	--[a]	--[a]	-0.008	--[a]	--[a]
3	0.135	0.086	0.183	0.237	0.208	0.267	-0.002	-0.004	-0.001
4	0.126	0.070	0.181	0.284	0.123	0.444	-0.008	-0.034	0.018
5	0.069	0.017	0.121	0.207	0.151	0.263	-0.007	-0.016	0.002
6	0.094	0.040	0.148	0.298	0.058	0.538	-0.003	-0.011	0.004
7	0.163	0.149	0.177	0.239	0.048	0.430	-0.009	-0.023	0.005
8	0.171	0.097	0.245	0.184	0.107	0.260	-0.005	-0.010	0.001
9	0.124	0.084	0.165	0.194	0.044	0.344	-0.007	-0.018	0.003
10	0.170	0.161	0.179	0.274	-0.237	0.786	-0.015	-0.080	0.051
11	0.181	0.120	0.241	0.166	-0.266	0.597	-0.007	-0.061	0.048
12	0.157	0.137	0.176	0.401	--[a]	--[a]	-0.046	--[a]	--[a]
13	0.108	0.087	0.130	0.257	0.030	0.483	-0.016	-0.039	0.008
14	0.167	0.155	0.179	0.331	0.144	0.518	-0.020	-0.042	0.001
15	0.156	0.129	0.183	0.192	--[a]	--[a]	-0.009	--[a]	--[a]
16	0.195	0.175	0.214	0.332	--[a]	--[a]	-0.018	--[a]	--[a]
17	0.259	0.185	0.333	0.494	--[a]	--[a]	-0.071	--[a]	--[a]
18	0.227	0.214	0.240	--[a]	--[a]	--[a]	--[a]	--[a]	--[a]
19	0.202	0.187	0.216	0.320	0.031	0.609	-0.020	-0.055	0.016
20	0.219	0.205	0.233	0.152	--[a]	--[a]	-0.007	--[a]	--[a]
21	0.197	0.176	0.218	0.177	--[a]	--[a]	-0.008	--[a]	--[a]
22	0.174	0.163	0.185	--[a]	--[a]	--[a]	--[a]	--[a]	--[a]
23	0.177	0.163	0.191	--[a]	--[a]	--[a]	--[a]	--[a]	--[a]

Table B16. (Continued)

	Pre-peak Virgin Data			Post-peak Virgin Data					
test	Slope	L95%	U95%	Inter.	L95%	U95%	Slope	L95%	U95%
24	0.220	0.206	0.234	--[a]	--[a]	--[a]	--[a]	--[a]	--[a]
25	0.103	0.087	0.119	0.219	0.030	0.407	-0.018	-0.071	0.034
26	0.070	0.034	0.105	0.148	0.106	0.191	-0.003	-0.010	0.003
27	0.237	0.183	0.291	0.248	--[a]	--[a]	-0.035	--[a]	--[a]
28	0.135	0.104	0.166	0.224	--[a]	--[a]	-0.026	--[a]	--[a]
29	0.115	0.058	0.173	0.202	0.051	0.352	-0.018	-0.052	0.016
30	0.094	0.084	0.105	0.139	0.036	0.243	-0.005	-0.023	0.013
31	0.184	0.145	0.223	0.180	--[a]	--[a]	-0.025	--[a]	--[a]
32	0.081	0.051	0.110	0.207	-0.529	0.944	-0.017	-0.132	0.098
Avge.	0.15	0.14	0.17	0.24	0.21	0.27	-0.02	-0.02	-0.01

[a] Insufficient data

Table B17. Regression Coefficients and 95% CI for pinch force stabilized data

	Pre-peak Stabilized Data			Post-peak Stabilized Data					
test	Slope	L95%	U95%	Inter.	L95%	U95%	Slope	L95%	U95%
2	0.025	0.015	0.036	0.138	0.106	0.170	-0.008	-0.013	-0.003
3	0.063	0.042	0.083	0.214	0.184	0.243	-0.002	-0.003	-0.001
4	0.042	0.034	0.049	0.240	0.144	0.336	-0.014	-0.030	0.001
5	0.040	0.026	0.054	0.122	-0.062	0.305	-0.006	-0.035	0.023
6	0.028	0.024	0.032	0.256	0.131	0.381	-0.002	-0.004	0.001
7	0.098	0.089	0.107	0.125	0.063	0.187	-0.004	-0.008	0.000
8	0.125	0.046	0.204	0.138	0.098	0.178	-0.002	-0.003	0.000
9	0.095	0.063	0.128	0.099	-0.011	0.208	-0.003	-0.011	0.004
10	0.131	0.123	0.139	0.209	-0.150	0.568	-0.012	-0.058	0.034
11	0.135	0.084	0.186	0.101	-0.354	0.556	-0.006	-0.064	0.052
12	0.070	0.049	0.091	0.235	--[a]	--[a]	-0.028	--[a]	--[a]
13	0.112	0.082	0.143	0.135	0.063	0.206	-0.007	-0.014	0.000
14	0.136	0.112	0.161	0.197	-0.175	0.570	-0.011	-0.055	0.034
15	0.130	0.098	0.162	0.136	--[a]	--[a]	-0.008	--[a]	--[a]
16	0.114	0.092	0.136	0.202	-0.100	0.504	-0.005	-0.026	0.015
17	0.242	0.184	0.300	--[a]	--[a]	--[a]	--[a]	--[a]	--[a]
18	0.117	0.109	0.125	0.321	--[a]	--[a]	-0.035	--[a]	--[a]
19	0.159	0.146	0.171	0.203	--[a]	--[a]	-0.013	--[a]	--[a]
20	0.075	0.065	0.086	0.099	-0.276	0.475	-0.003	-0.028	0.023
21	0.138	0.128	0.148	0.102	--[a]	--[a]	-0.003	--[a]	--[a]
22	0.143	0.130	0.156	--[a]	--[a]	--[a]	--[a]	--[a]	--[a]
23	0.067	0.048	0.086	0.175	--[a]	--[a]	-0.022	--[a]	--[a]

Table B17. (Continued)

	Pre-peak Stabilized Data			Post-peak Stabilized Data					
test	Slope	L95%	U95%	Inter.	L95%	U95%	Slope	L95%	U95%
24	0.077	0.071	0.084	0.255	--[a]	--[a]	-0.017	--[a]	--[a]
25	0.066	0.056	0.077	0.155	--[a]	--[a]	-0.020	--[a]	--[a]
26	0.069	0.035	0.104	0.096	0.002	0.190	-0.005	-0.020	0.010
27	0.077	0.037	0.117	0.106	-0.297	0.509	-0.009	-0.075	0.057
28	0.090	0.068	0.112	0.078	--[a]	--[a]	-0.006	--[a]	--[a]
29	0.048	0.021	0.075	0.082	-0.165	0.330	-0.004	-0.044	0.035
30	0.046	0.031	0.062	0.080	-0.008	0.167	-0.005	-0.020	0.010
31	0.065	0.041	0.090	0.117	-0.357	0.591	-0.007	-0.080	0.065
32	0.094	0.077	0.111	0.109	-0.046	0.264	-0.007	-0.031	0.018
Avge.	0.09	0.08	0.11	0.16	0.13	0.18	-0.01	-0.01	-0.01

[a] Insufficient data

Table B18. Pinch force regression coefficients

	Pre-peak Region					Post-peak Region			
Source	Virgin Data		Stabilized Data		Source	Virgin Data		Stabilized Data	
Parameter	Coefficient	Stderr Coef	Coefficient	Stderr Coef	Parameter	Coefficient	Stderr Coef	Coefficient	Stderr Coef
D1x	0.120	0.014	0.063	0.012	x	-0.023	0.003	-0.016	0.002
D2x	0.176	0.021	0.142	0.018	D1	0.219	0.011	0.138	0.009
D3x	0.162	0.013	0.103	0.011	D2	0.267	0.019	0.198	0.016
D4x	0.149	0.015	0.087	0.013	D3	0.249	0.014	0.170	0.011
D5x	0.169	0.025	0.146	0.021	D4	0.151	0.013	0.085	0.011
D6x	0.198	0.025	0.123	0.021	D5	0.246	0.025	0.183	0.020
D7x	0.184	0.017	0.068	0.015	D6	0.292	0.025	0.203	0.021
D8x	0.089	0.034	0.086	0.029	D7	0.151	0.018	0.091	0.013
					D8	0.156	0.028	0.079	0.023
					Qx	0.002	2.5E-4	0.001	2.0E-4

Table B19. Mae values and 95% CI for virgin characteristic slopes

	K0			K1			K2		
Model	Mean	L95%	U95%	Mean	L95%	U95%	Mean	L95%	U95%
1	0.11	0.08	0.13	0.09	0.07	0.11	0.35	0.28	0.43
2	0.30	0.24	0.35	0.45	0.35	0.55	0.56	0.47	0.65
3	0.38	0.33	0.44	0.35	0.27	0.43	1.37	0.66	2.08
4	0.21	0.18	0.25	0.23	0.19	0.26	0.32	0.27	0.38
5	0.54	0.34	0.74	0.36	0.30	0.41	1.05	0.53	1.57
6	0.35	0.30	0.40	0.33	0.27	0.38	1.02	0.89	1.15
7	0.11	0.09	0.13	0.12	0.10	0.14	0.20	0.16	0.25
8	0.16	0.12	0.19	0.23	0.18	0.28	0.40	0.31	0.48
9	0.07	0.06	0.08	0.06	0.05	0.07	0.27	0.21	0.34
10	0.14	0.12	0.16	0.13	0.11	0.16	0.40	0.33	0.48
11	0.14	0.12	0.17	0.16	0.12	0.19	0.24	0.19	0.28

Table B20. Mae values and 95% CI for stabilized characteristic slopes

	K0			K1			K2		
Model	Mean	L95%	U95%	Mean	L95%	U95%	Mean	L95%	U95%
1	0.07	0.05	0.10	0.12	0.09	0.14	0.30	0.24	0.36
2	0.29	0.23	0.34	0.36	0.30	0.43	0.52	0.44	0.59
3	0.31	0.26	0.35	0.38	0.33	0.42	2.22	0.56	3.88
4	0.22	0.19	0.25	0.21	0.19	0.24	0.31	0.26	0.37
5	0.82	0.29	1.35	0.82	0.37	1.27	1.92	0.75	3.10
6	0.30	0.25	0.35	0.37	0.31	0.42	0.88	0.75	1.00
7	0.12	0.10	0.14	0.09	0.08	0.11	0.19	0.16	0.22
8	0.13	0.08	0.17	0.22	0.16	0.29	0.35	0.28	0.42
9	0.06	0.05	0.07	0.07	0.05	0.09	0.22	0.17	0.27
10	0.11	0.09	0.14	0.16	0.13	0.19	0.35	0.29	0.41
11	0.15	0.13	0.17	0.13	0.11	0.15	0.23	0.18	0.27

Table B21. Mean and 95% confidence interval values for K0 slope coefficient

	Virgin K0			Stabilized K0		
Test	Coeff	L95%	U95%	Coeff	L95%	U95%
2	0.71	0.61	0.81	0.62	0.50	0.75
3	0.72	0.59	0.85	0.61	0.49	0.74
4	0.68	0.58	0.78	0.70	0.54	0.86
5	0.70	0.63	0.76	0.81	0.72	0.90
6	0.64	0.56	0.72	0.70	0.59	0.81
7	0.62	0.54	0.70	0.62	0.53	0.70
8	0.70	0.62	0.78	0.67	0.57	0.78
9	0.59	0.50	0.68	0.60	0.51	0.69
10	0.58	0.52	0.63	0.60	0.54	0.67
11	0.63	0.54	0.73	0.59	0.48	0.69
12	0.52	0.47	0.57	0.55	0.48	0.63
13	0.48	0.41	0.55	0.51	0.43	0.59
14	0.43	0.37	0.48	0.44	0.38	0.50
15	0.43	0.36	0.49	0.49	0.41	0.57
16	0.38	0.35	0.42	0.46	0.40	0.51
17	0.39	0.32	0.45	0.42	0.34	0.49
18	0.52	0.45	0.59	0.58	0.50	0.66
19	0.43	0.37	0.49	0.43	0.36	0.51
20	0.46	0.37	0.56	0.53	0.39	0.67
21	0.37	0.35	0.40	0.41	0.36	0.46
22	0.48	0.42	0.54	0.49	0.39	0.58
23	0.37	0.31	0.44	0.34	0.25	0.42

Table B21. (Continued)

	Virgin K0			Stabilized K0		
Test	Coeff	L95%	U95%	Coeff	L95%	U95%
24	0.40	0.34	0.45	0.36	0.32	0.40
25	0.38	0.34	0.42	0.41	0.36	0.47
26	0.44	0.40	0.49	0.46	0.38	0.54
27	0.65	0.48	0.82	0.48	0.38	0.58
28	0.45	0.38	0.51	0.49	0.42	0.56
29	0.39	0.32	0.46	0.42	0.31	0.52
30	0.57	0.46	0.68	0.44	0.35	0.54
31	0.52	0.44	0.61	0.46	0.36	0.55
32	0.61	0.49	0.74	0.58	0.46	0.70
Average	0.52	0.48	0.57	0.52	0.49	0.56

Table B22. Mean and 95% confidence interval values for K1 slope coefficient

	Virgin K1			Stabilized K1		
Test	Coeff	L95%	U95%	Coeff	L95%	U95%
2	0.58	0.43	0.74	0.62	0.49	0.75
3	0.48	0.34	0.62	0.58	0.46	0.69
4	0.56	0.45	0.66	0.62	0.50	0.75
5	0.73	0.63	0.83	0.71	0.64	0.77
6	0.55	0.46	0.64	0.62	0.52	0.72
7	0.54	0.46	0.63	0.58	0.51	0.64
8	0.57	0.47	0.66	0.65	0.56	0.74
9	0.47	0.39	0.54	0.54	0.45	0.62
10	0.53	0.47	0.59	0.58	0.52	0.63
11	0.44	0.35	0.53	0.58	0.52	0.65
12	0.46	0.39	0.54	0.61	0.55	0.67
13	0.47	0.41	0.53	0.52	0.44	0.60
14	0.47	0.39	0.54	0.54	0.48	0.59
15	0.44	0.38	0.50	0.58	0.51	0.64
16	0.39	0.36	0.43	0.53	0.48	0.58
17	0.46	0.39	0.53	0.53	0.48	0.58
18	0.51	0.44	0.59	0.61	0.55	0.67
19	0.43	0.37	0.49	0.52	0.45	0.60
20	0.45	0.38	0.53	0.59	0.52	0.67
21	0.35	0.31	0.38	0.51	0.44	0.58
22	0.48	0.41	0.55	0.65	0.58	0.72
23	0.38	0.30	0.46	0.59	0.53	0.65

Table B22. (Continued)

	Virgin K1			Stabilized K1		
Test	Coeff	L95%	U95%	Coeff	L95%	U95%
24	0.38	0.33	0.43	0.55	0.49	0.61
25	0.52	0.43	0.61	0.65	0.55	0.75
26	0.50	0.41	0.59	0.63	0.55	0.72
27	0.37	0.25	0.48	0.64	0.55	0.73
28	0.55	0.46	0.64	0.66	0.57	0.74
29	0.51	0.43	0.59	0.67	0.58	0.76
30	0.50	0.43	0.58	0.69	0.58	0.80
31	0.41	0.31	0.50	0.71	0.56	0.85
32	0.52	0.39	0.64	0.67	0.53	0.81
Average	0.48	0.46	0.51	0.60	0.58	0.62

Table B23. Mean and 95% confidence interval values for K2 slope coefficient

	Virgin K2			Stabilized K2		
Test	Coeff	L95%	U95%	Coeff	L95%	U95%
2	1.12	0.93	1.31	0.83	0.71	0.95
3	1.12	0.98	1.25	0.89	0.77	1.01
4	0.83	0.71	0.94	0.79	0.69	0.90
5	0.93	0.84	1.02	1.00	0.92	1.08
6	0.80	0.72	0.89	0.86	0.79	0.92
7	0.79	0.70	0.87	0.77	0.70	0.84
8	0.94	0.84	1.05	0.92	0.82	1.02
9	0.69	0.60	0.79	0.72	0.63	0.81
10	0.72	0.58	0.87	0.70	0.56	0.84
11	1.55	1.20	1.89	1.47	1.19	1.75
12	1.52	1.18	1.87	1.63	1.36	1.90
13	1.06	0.81	1.30	1.12	0.86	1.38
14	1.40	1.20	1.60	1.40	1.20	1.61
15	1.51	1.22	1.79	1.41	1.16	1.66
16	1.22	0.97	1.47	1.55	1.13	1.96
17	1.28	1.18	1.38	1.38	1.24	1.52
18	1.74	1.49	1.98	1.48	1.28	1.68
19	1.29	0.94	1.65	1.20	0.91	1.48
20	1.28	0.96	1.60	1.28	0.98	1.58
21	1.27	0.88	1.67	1.34	1.02	1.66
22	1.27	1.10	1.44	1.44	1.25	1.63
23	1.23	0.92	1.53	1.15	0.90	1.41

Table B23. (Continued)

	Virgin K2			Stabilized K2		
Test	Coeff	L95%	U95%	Coeff	L95%	U95%
24	1.65	1.42	1.88	0.72	0.39	1.05
25	1.41	1.12	1.69	1.66	1.35	1.97
26	1.58	1.30	1.87	1.35	0.96	1.73
27	2.37	2.06	2.68	2.00	1.59	2.40
28	1.84	1.42	2.27	1.85	1.46	2.23
29	1.79	1.53	2.04	1.77	1.62	1.92
30	1.62	1.23	2.00	1.67	1.30	2.03
31	1.37	1.16	1.58	1.28	1.10	1.45
32	1.34	1.04	1.65	1.51	1.20	1.83
Average	1.31	1.18	1.44	1.26	1.13	1.39

Table B24. Mean values and 95% CI for Coefficients of characteristic slope equation

		Virgin Values				Stabilized Values			
SLOPE	Var.	COEFF	Std err	L95%	U95%	COEFF	Std err	L95%	U95%
K0	XD1	0.63	0.02	0.60	0.66	0.62	0.02	0.58	0.65
	XD2	0.64	0.02	0.60	0.68	0.62	0.02	0.58	0.66
	XD3	0.50	0.02	0.47	0.54	0.53	0.02	0.50	0.57
	XD4	0.54	0.02	0.50	0.59	0.49	0.02	0.45	0.54
	XD5	0.45	0.03	0.39	0.51	0.52	0.04	0.45	0.59
	XD6	0.42	0.03	0.37	0.47	0.40	0.03	0.35	0.46
	XD7	0.47	0.02	0.43	0.52	0.45	0.03	0.40	0.50
	XD8	0.44	0.05	0.34	0.54	0.46	0.06	0.35	0.57
	XGL	-0.09	0.02	-0.12	-0.05	-0.09	0.02	-0.13	-0.05
K1	XD1	0.52	0.02	0.49	0.56	0.58	0.02	0.55	0.61
	XD2	0.65	0.02	0.62	0.69	0.67	0.02	0.63	0.70
	XD3	0.49	0.02	0.46	0.53	0.61	0.02	0.58	0.64
	XD4	0.48	0.02	0.44	0.52	0.66	0.02	0.62	0.70
	XD5	0.44	0.03	0.38	0.50	0.58	0.03	0.52	0.64
	XD6	0.41	0.03	0.36	0.46	0.54	0.02	0.49	0.58
	XD7	0.44	0.02	0.40	0.49	0.62	0.02	0.57	0.66
	XD8	0.50	0.05	0.40	0.60	0.63	0.05	0.54	0.73
	XGL	-0.05	0.02	-0.09	-0.02	-0.06	0.02	-0.09	-0.02
K2	XD1	1.06	0.11	0.84	1.28	1.12	0.11	0.91	1.33
	XD2	1.28	0.14	1.00	1.56	1.38	0.14	1.11	1.65
	XD3	1.34	0.05	1.24	1.44	1.37	0.05	1.27	1.47

Table B24. (Continued)

		Virgin Values				Stabilized Values			
SLOPE	Var.	COEFF	Std err	L95%	U95%	COEFF	Std err	L95%	U95%
	XD4	1.55	0.08	1.40	1.71	1.56	0.08	1.41	1.71
	XD5	1.35	0.10	1.15	1.56	1.48	0.11	1.26	1.69
	XD6	1.44	0.10	1.25	1.62	0.93	0.08	0.77	1.09
	XD7	1.63	0.09	1.46	1.79	1.54	0.09	1.38	1.71
	XD8	1.58	0.19	1.22	1.95	1.35	0.19	0.98	1.71

Table B25. Polynomial order suggested for cyclic force-displacement path

Maximum displacement (inches)	Quarter cycle regression	Half cycle regression	Coefficient of Determination R^2	Standard error of estimate S_e
0.025	2nd		0.996	0.033
0.025	2nd		0.997	0.034
0.025		3rd	0.998	0.044
0.025		3rd	0.999	0.030
0.050	2nd		0.999	0.011
0.050		3rd	0.999	0.031
0.050		3rd	0.999	0.010
0.050		3rd	0.999	0.010
0.100	2nd		0.999	0.010
0.100	2nd		0.999	0.016
0.100	2nd		0.998	0.017
0.100		3rd	0.999	0.010
0.100		3rd	0.998	0.070
0.100		3rd	0.999	0.021
0.100		3rd	0.998	0.014
0.200	2nd		0.994	0.049
0.200	4th		0.999	0.010
0.200	2nd		0.988	0.066
0.200	2nd		0.981	0.075
0.200		4th	0.995	0.060
0.200		3rd	0.996	0.050
0.200		3rd	0.999	0.062
0.400	2nd		0.997	0.038

Table B25. (Continued)

Maximum displacement (inches)	Quarter cycle regression	Half cycle regression	Coefficient of Determination R^2	Standard error of estimate S_e
0.400	3rd		0.977	0.070
0.400	2nd		0.998	0.029
0.400	2nd		0.907	0.163
0.400		3rd	0.997	0.048
0.400		4th	0.994	0.057
0.400		3rd	0.999	0.029
0.400		3rd	0.985	0.129
1.000	2nd		0.942	0.165
1.000	2nd		0.956	0.132
1.000		2nd	0.998	0.057
1.000		3rd	0.992	0.102
1.000		3rd	0.989	0.129
1.000		2nd	0.950	0.219
2.000		3rd	0.970	0.173
5.000		2nd	0.965	0.191

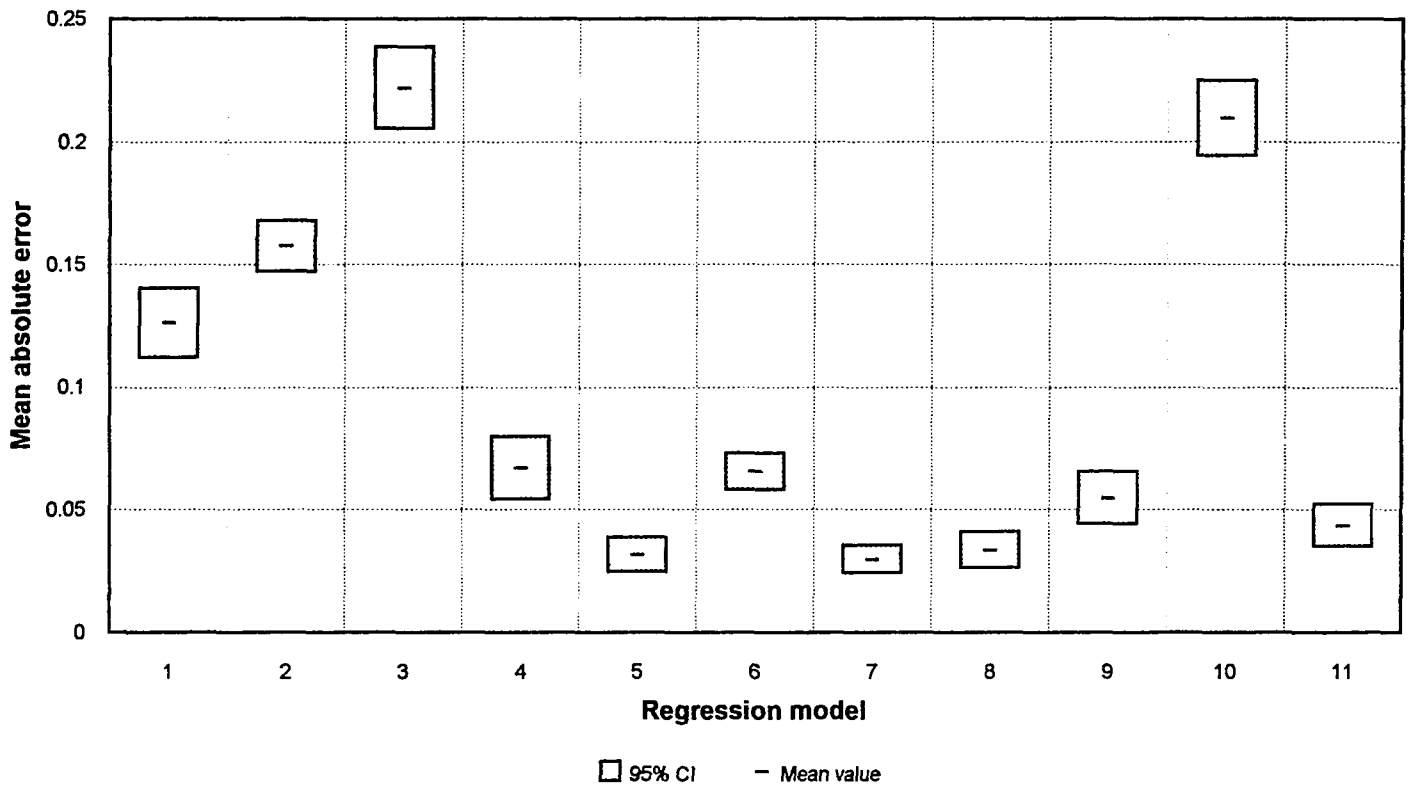

Figure B1. MAE mean value and 95% CI for virgin positive pre-peak region envelope data

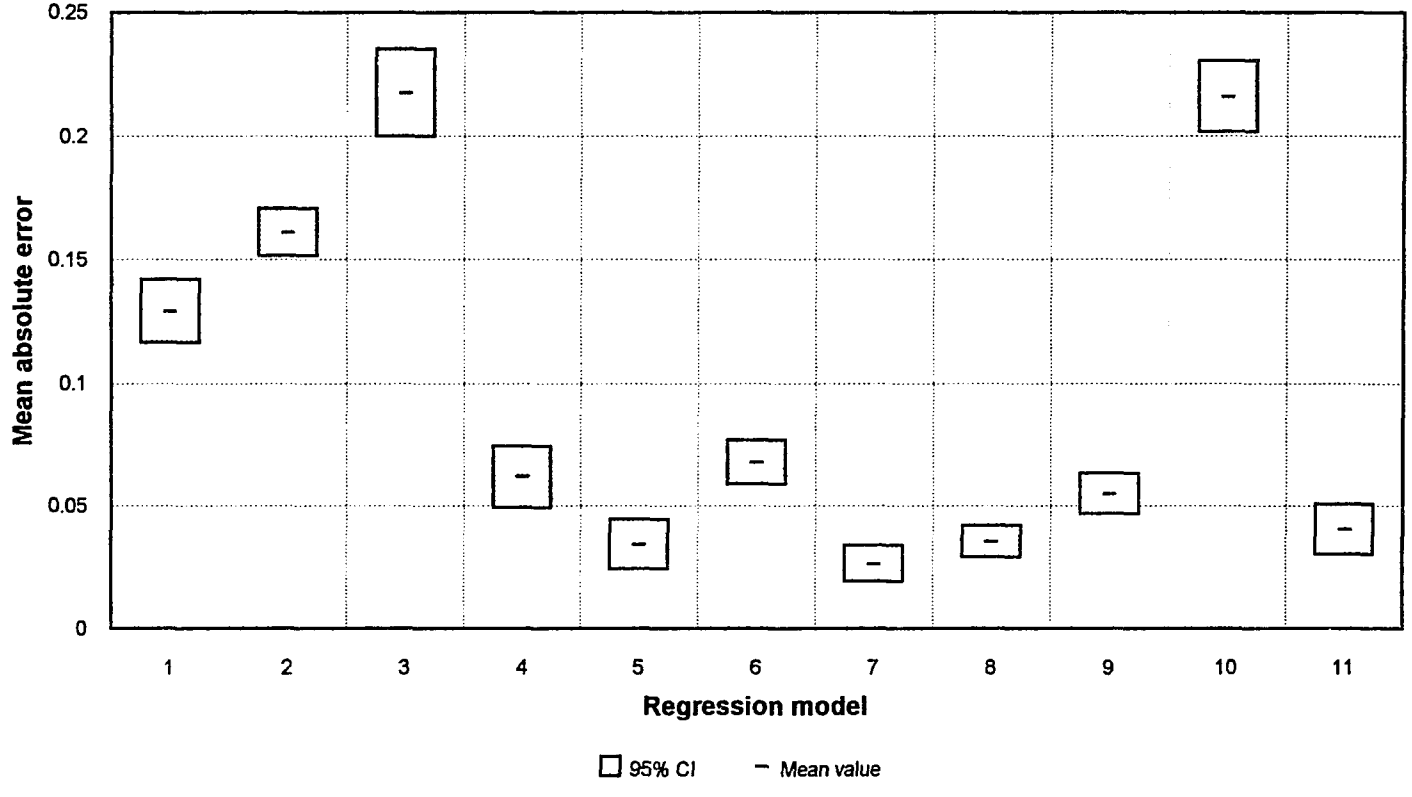

Figure B2. MAE mean value and 95% CI for virgin negative pre-peak region envelope data

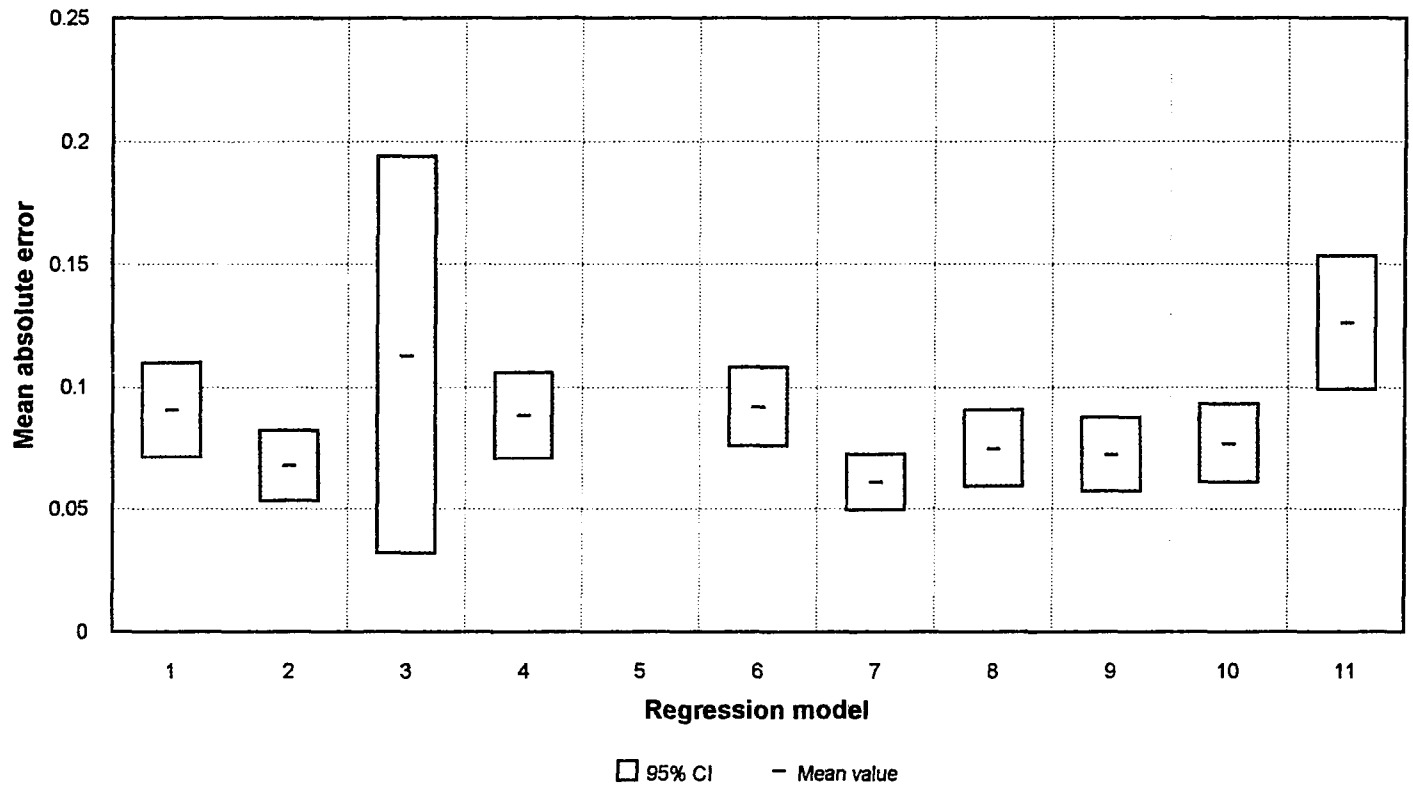

Figure B3. MAE mean value and 95% CI for virgin positive post-peak region envelope data

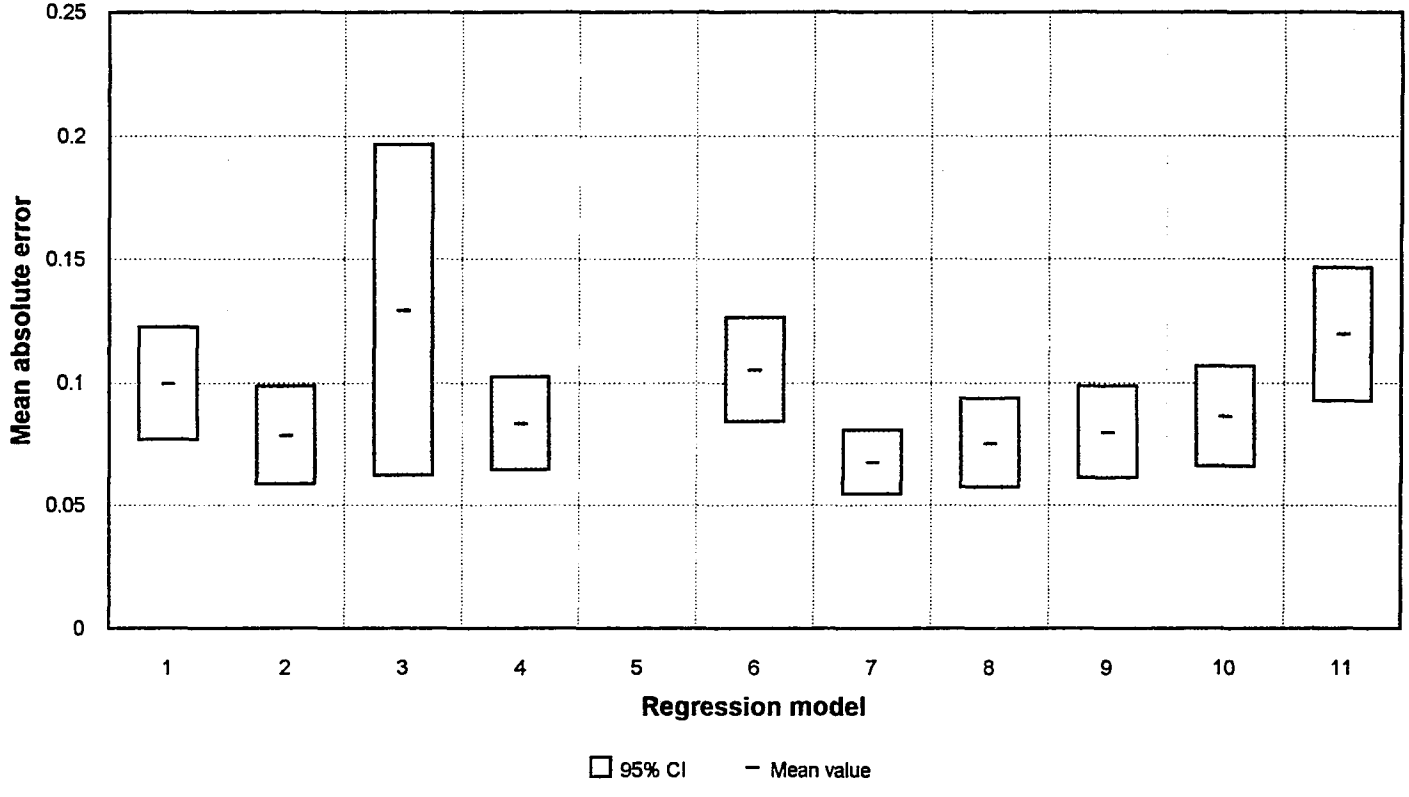

Figure B4. MAE mean value and 95% CI for virgin negative post-peak region envelope data

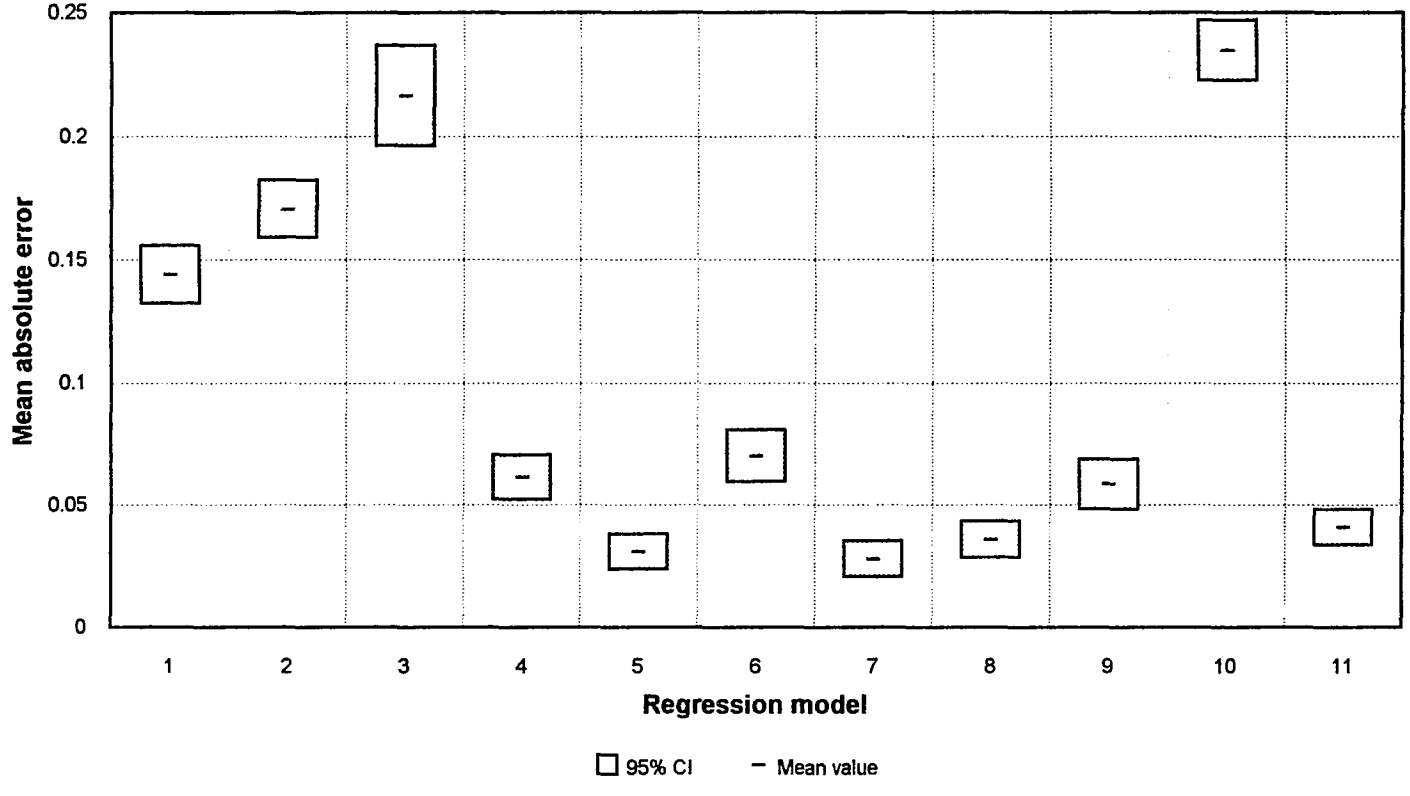

Figure B5. MAE mean value and 95% CI for stabilized positive pre-peak region envelope data

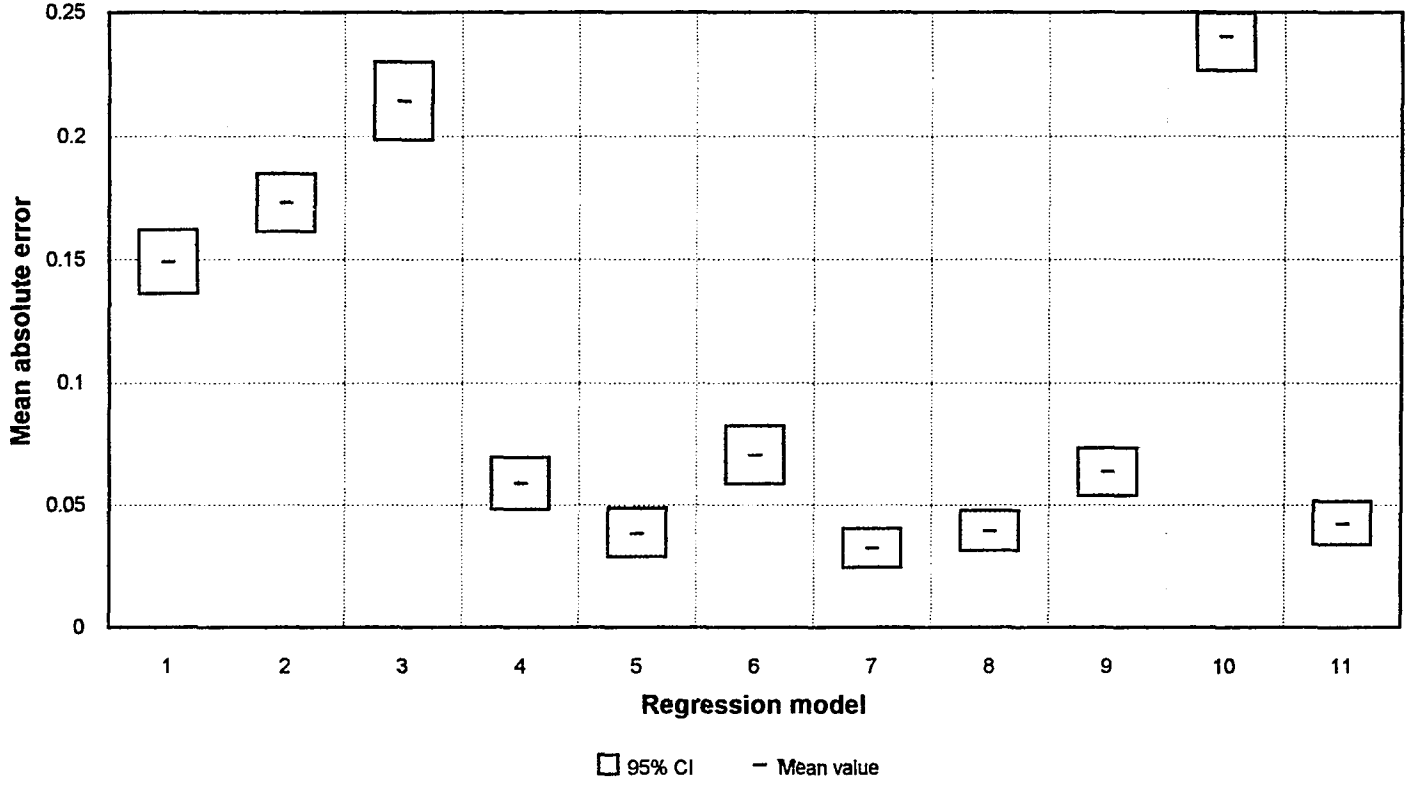

Figure B6. MAE mean value and 95% CI for stabilized negative pre-peak region envelope data

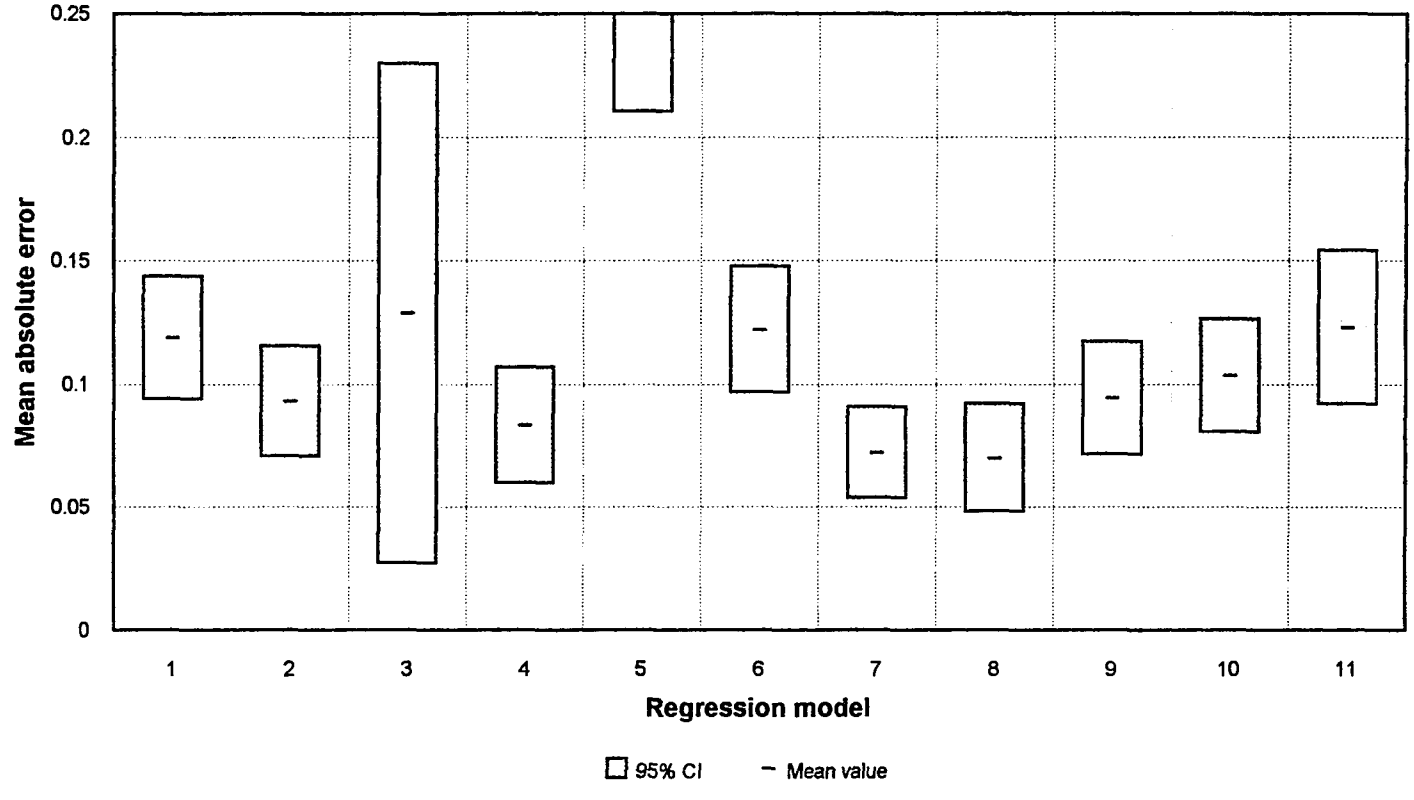

Figure B7. MAE mean value and 95% CI for stabilized positive post-peak region envelope data

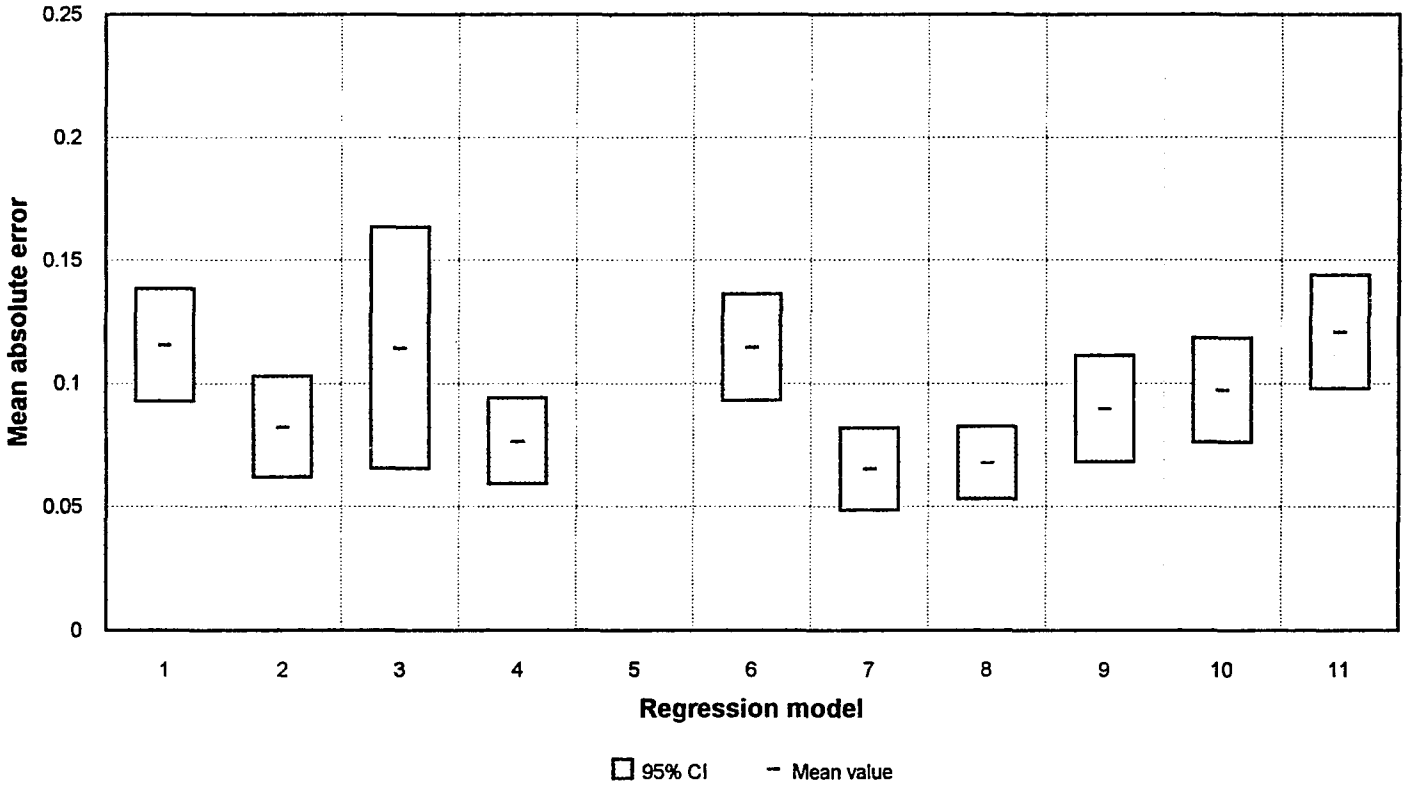

Figure B8. MAE mean value and 95% CI for stabilized negative post-peak region envelope data

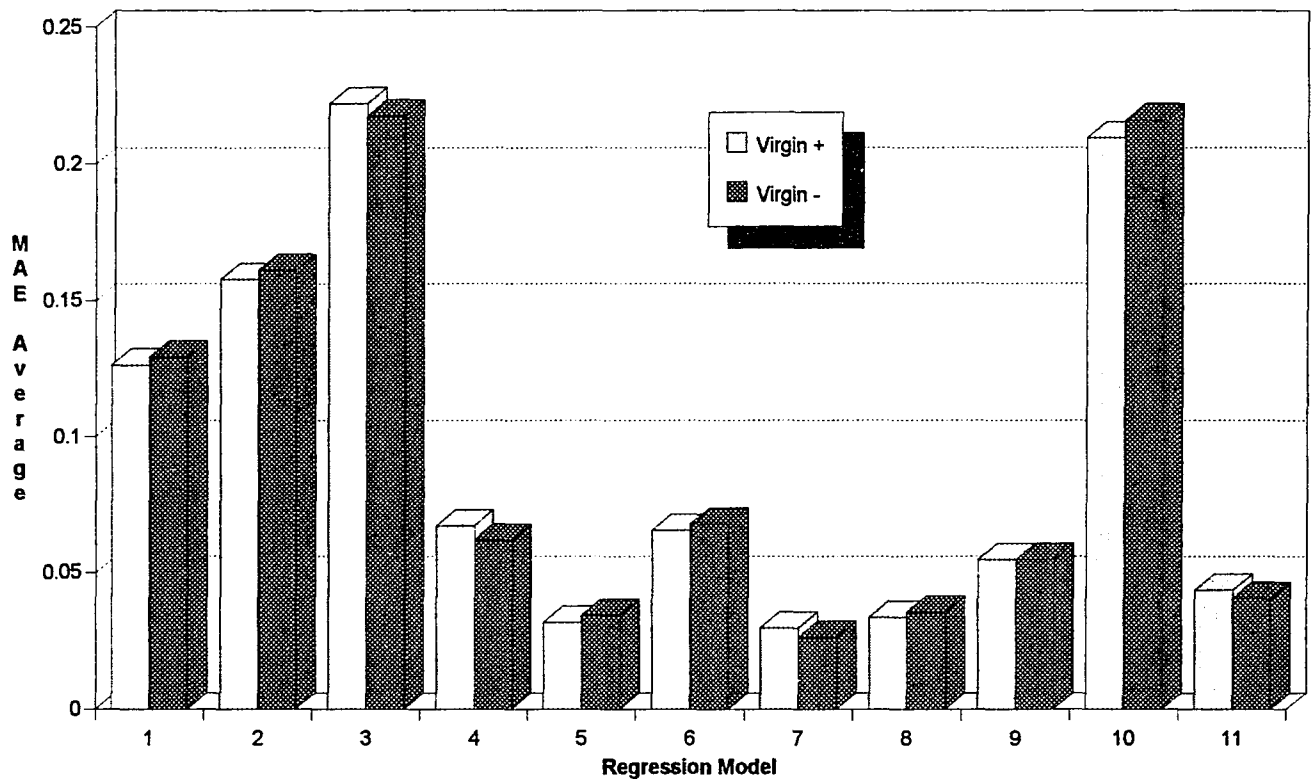

Figure B9. MAE comparison for virgin positive and negative pre-peak envelope data

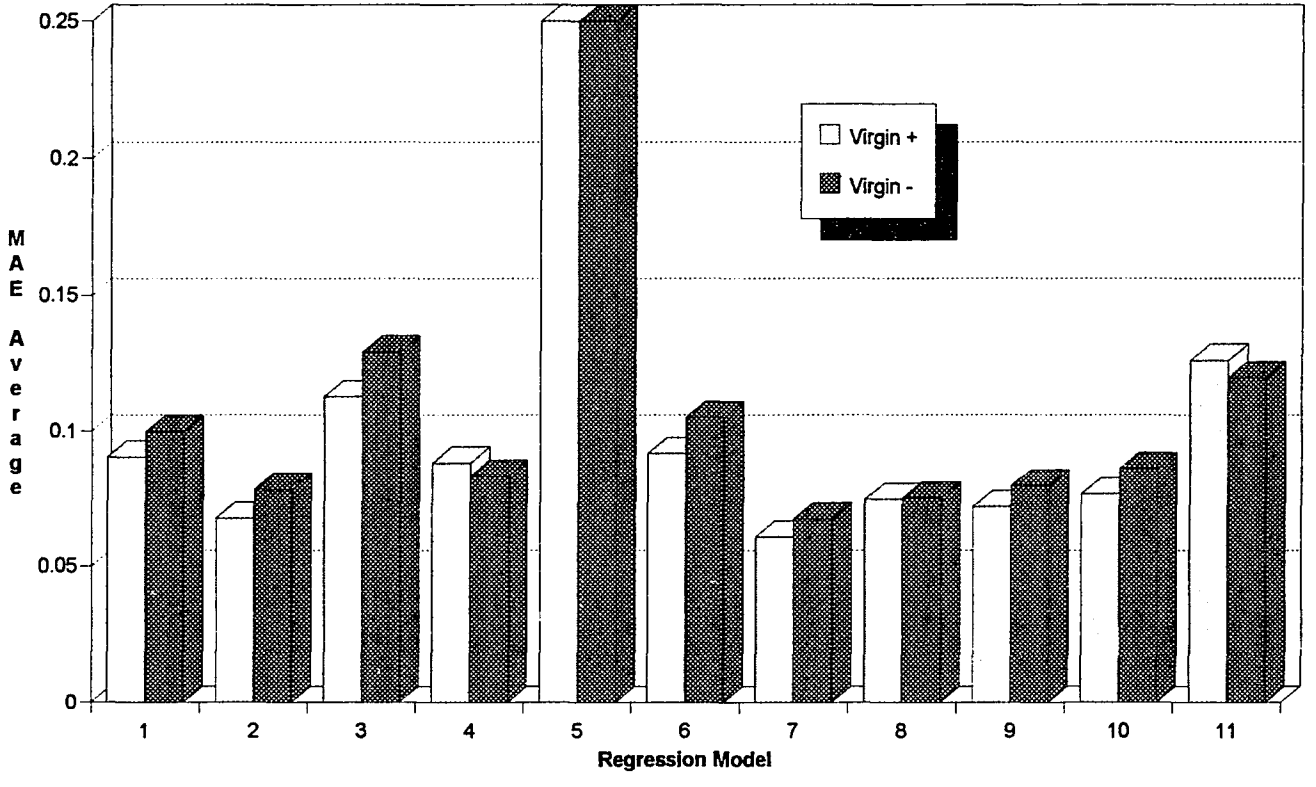

Figure B10. MAE comparison for virgin positive and negative post-peak envelope data

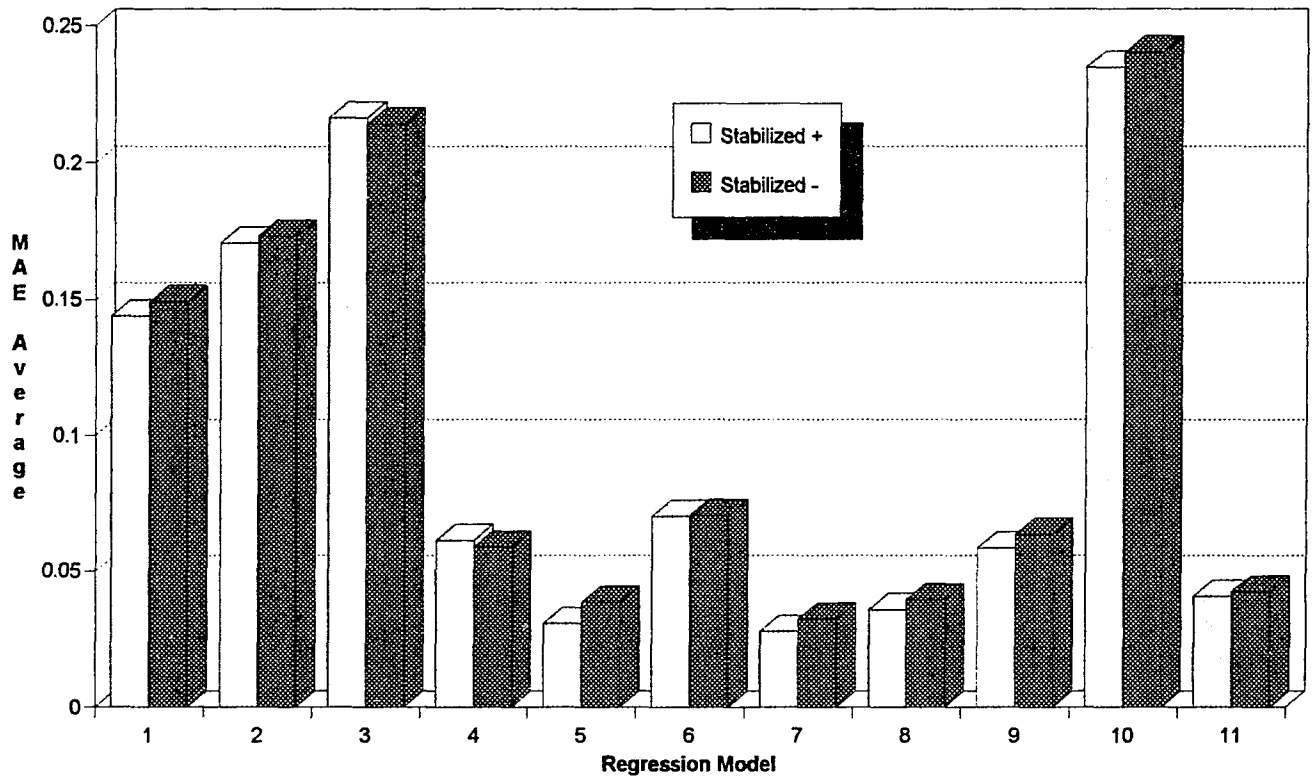

Figure B11. MAE comparison for stabilized positive and negative pre-peak envelope data

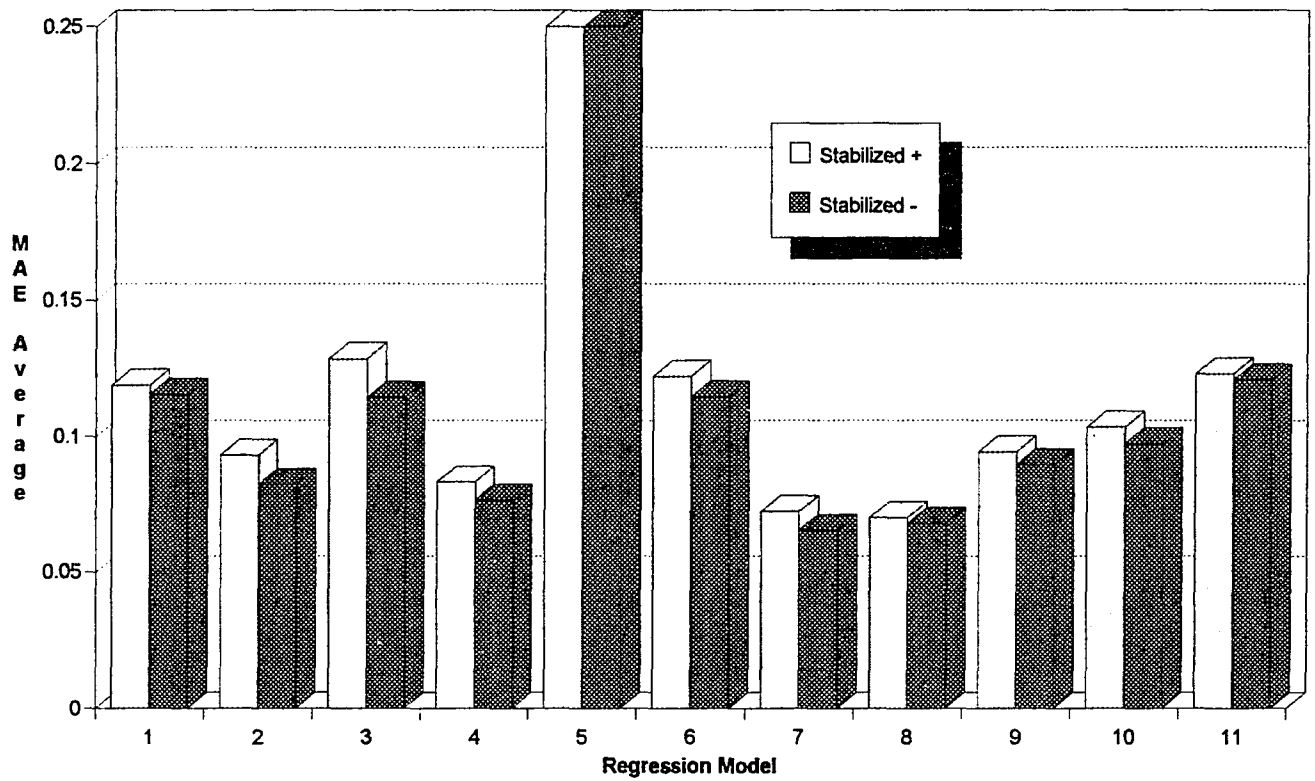

Figure B12. MAE comparison for stabilized positive and negative post-peak envelope data

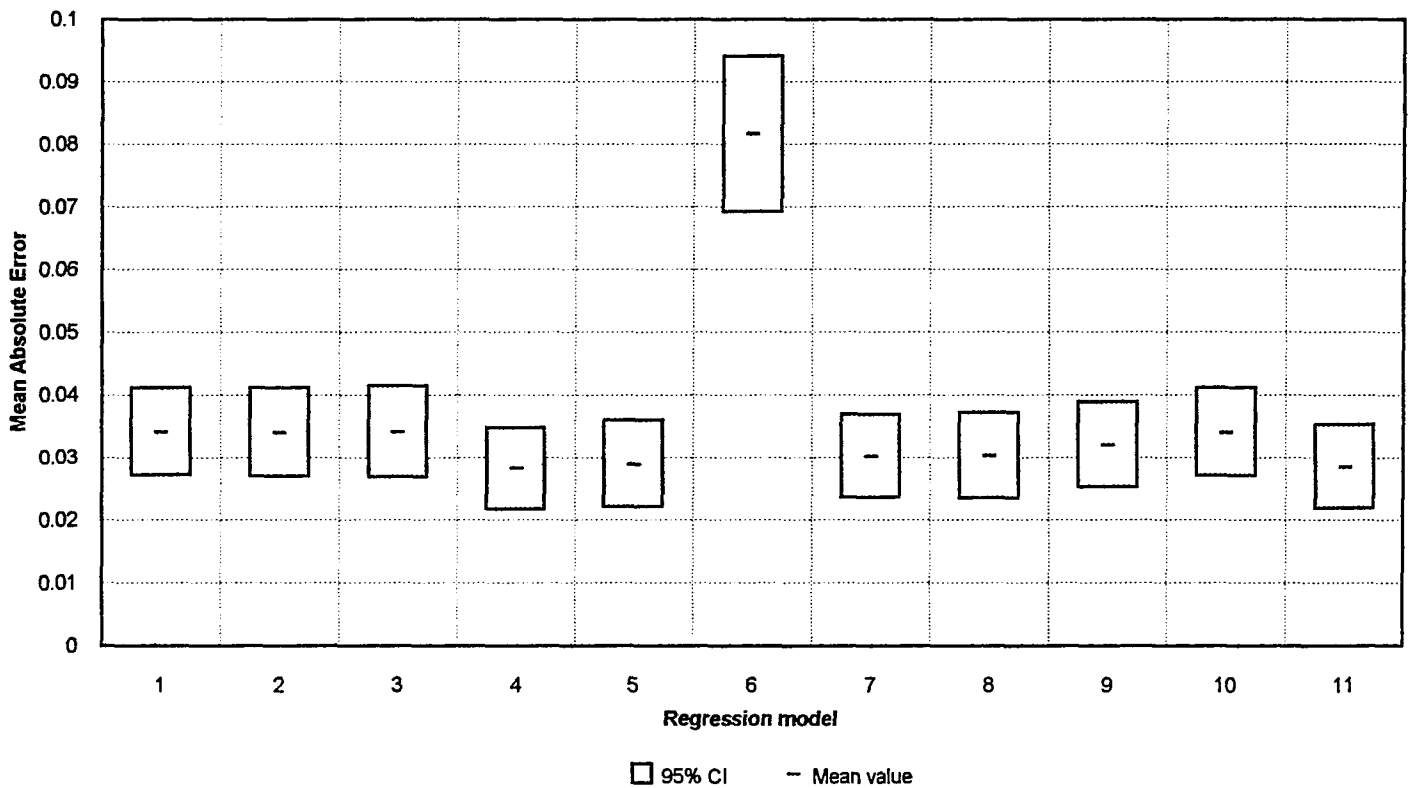

Figure B13. MAE values and 95% confidence intervals for degradation factor vs n at pre-peak region

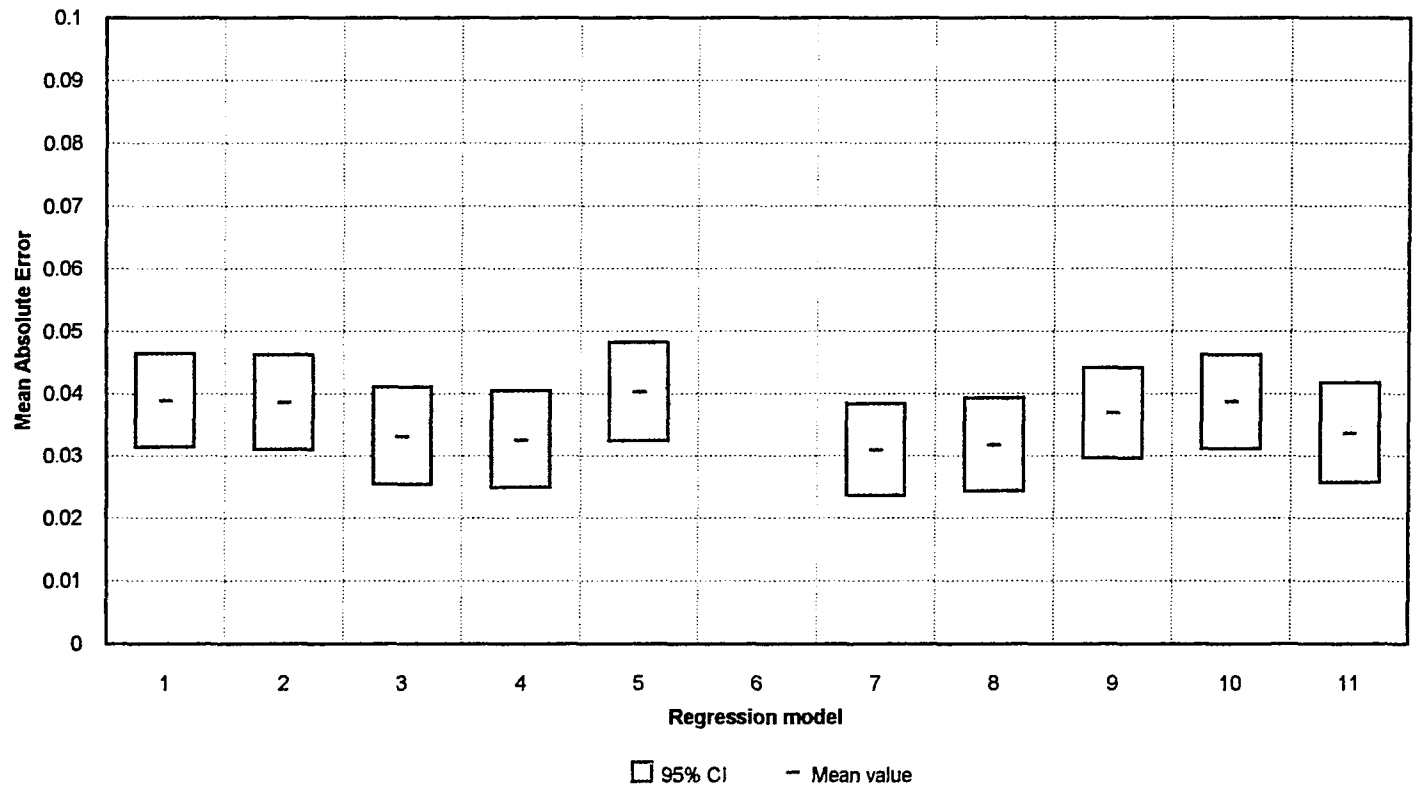

Figure B14. MAE values and 95% confidence intervals for degradation factor vs n at peak region

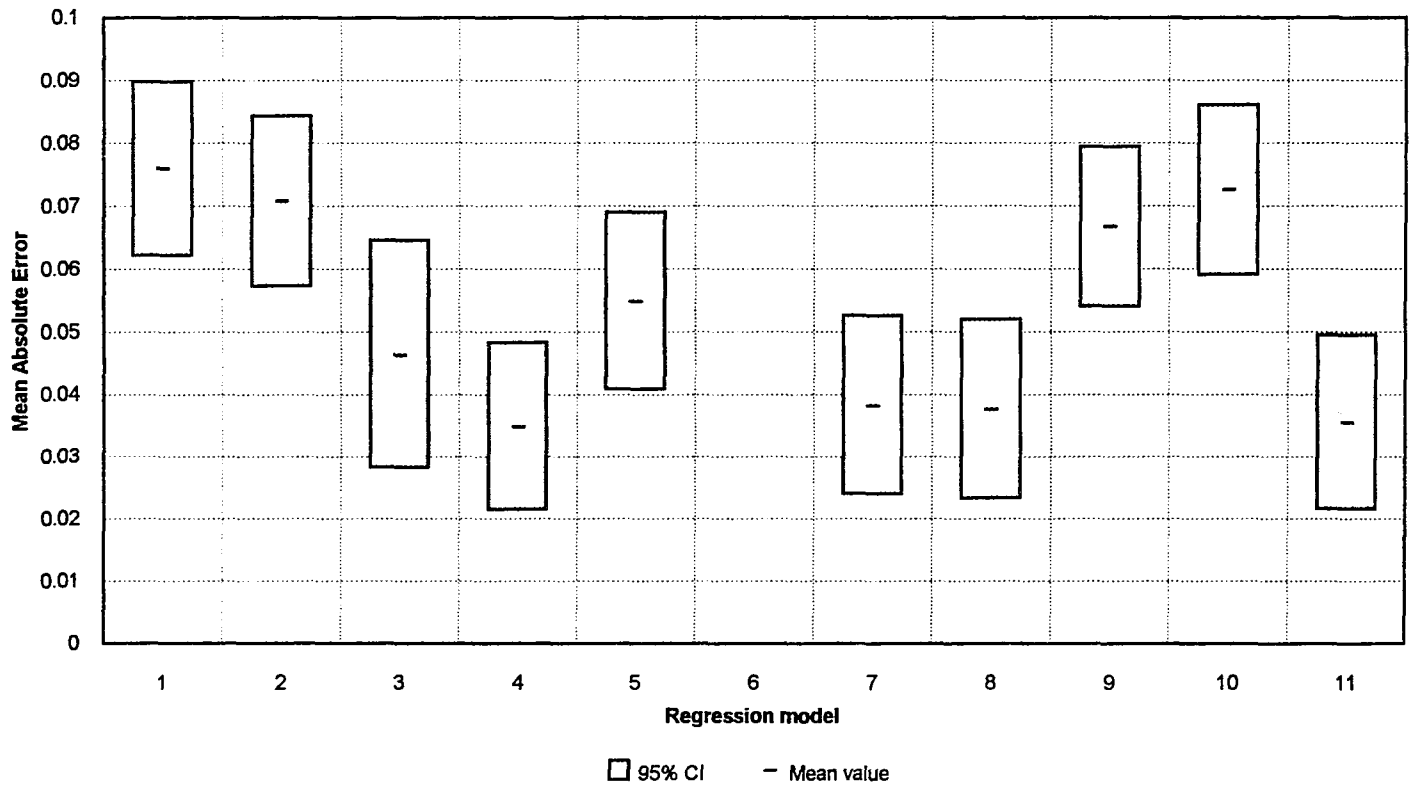

Figure B15. MAE values and 95% confidence intervals for degradation factor vs n at post-peak region

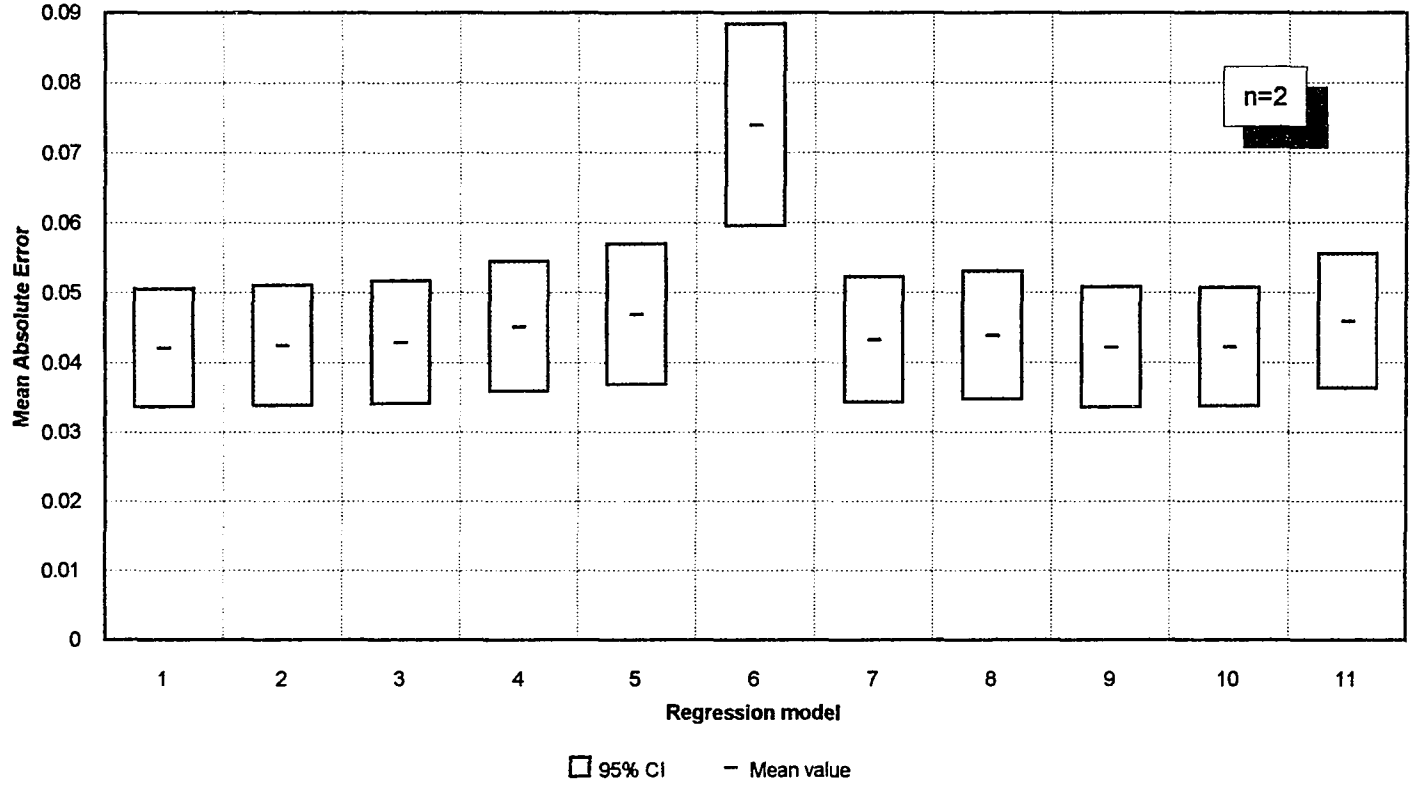

Figure B16. MAE values and 95% confidence intervals for degradation factor vs e/ep at pre-peak region (n=2)

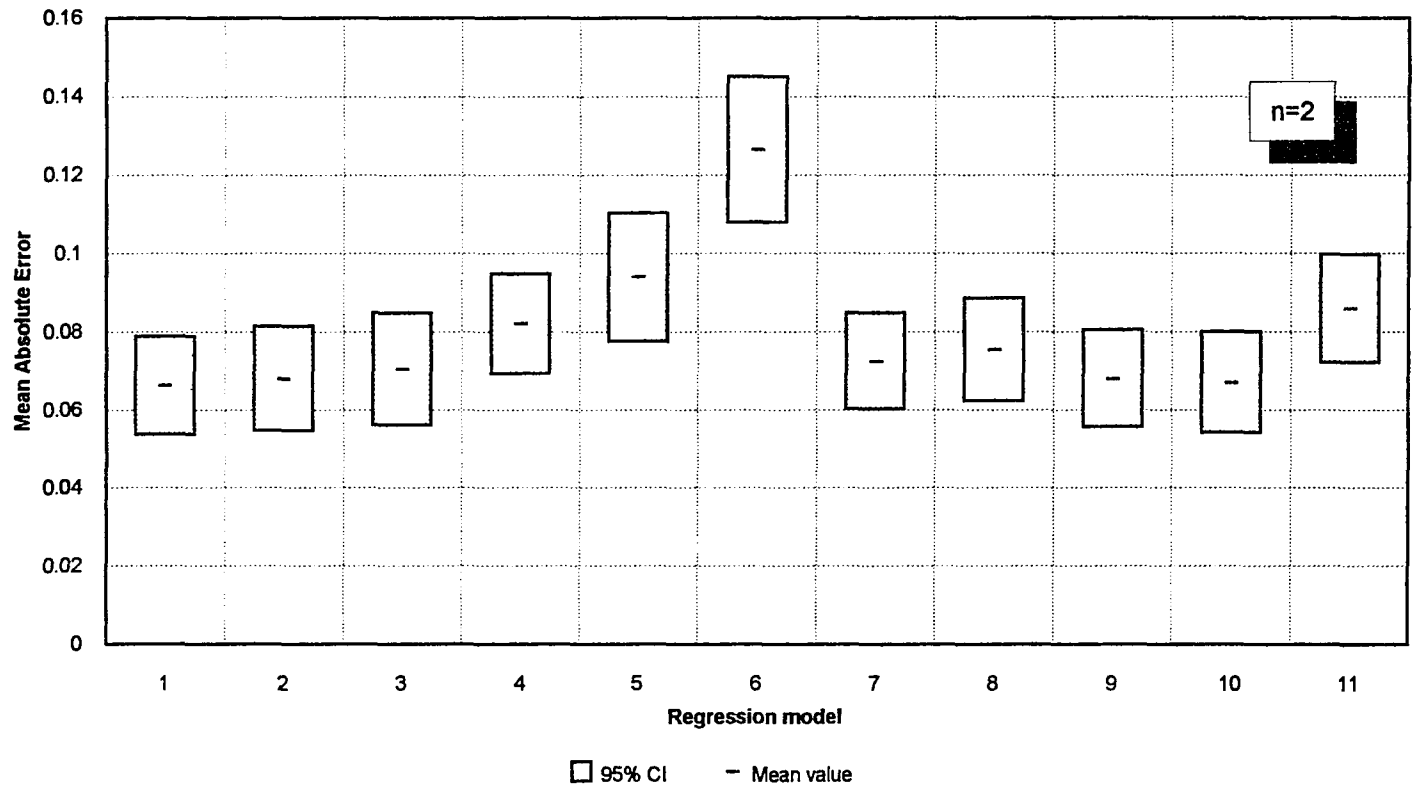

Figure B17. MAE values and 95% confidence intervals for degradation factor vs e/ep at post-peak region (n=2)

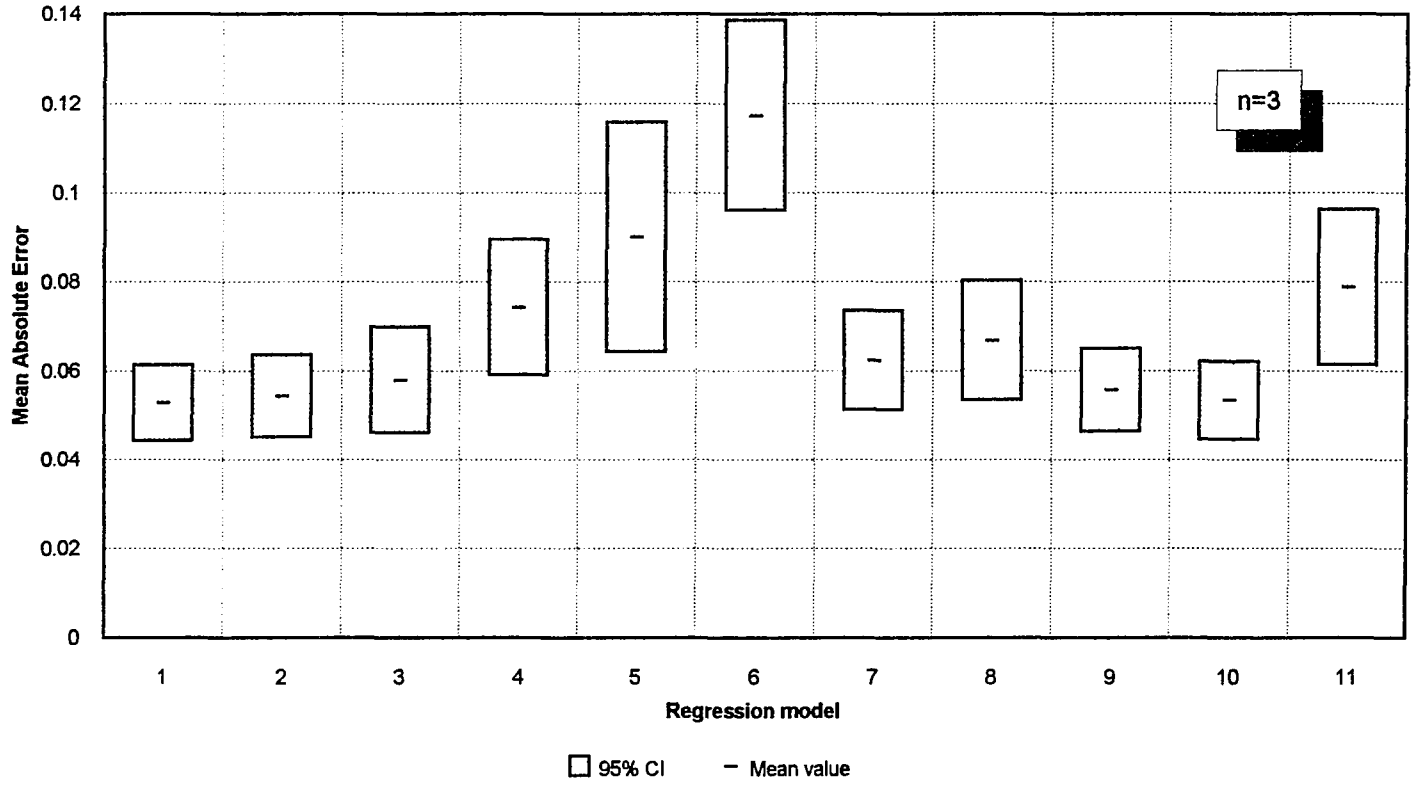

Figure B18. MAE values and 95% confidence intervals for degradation factor vs e/ep at pre-peak region (n=3)

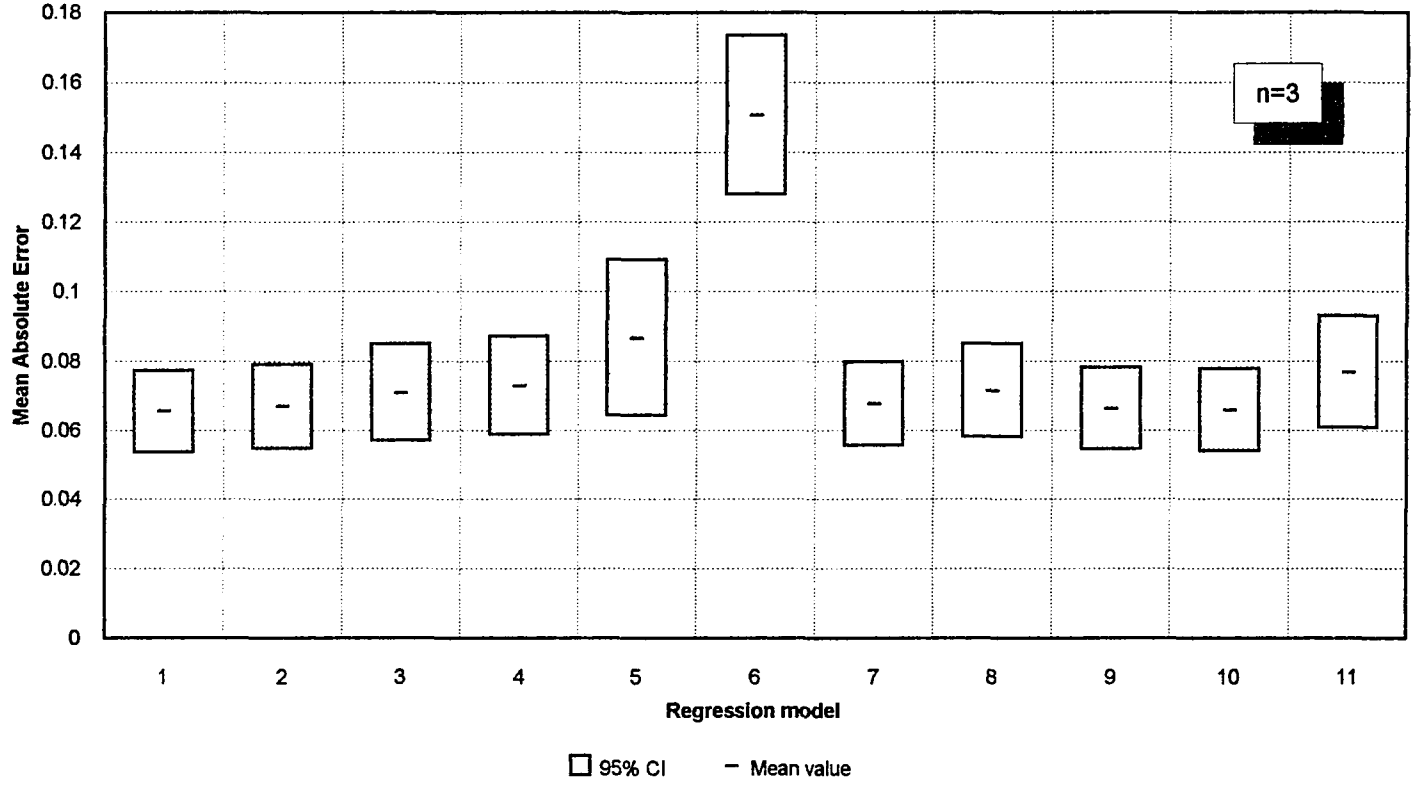

Figure B19. MAE values and 95% confidence intervals for degradation factor vs e/ep at post-peak region (n=3)

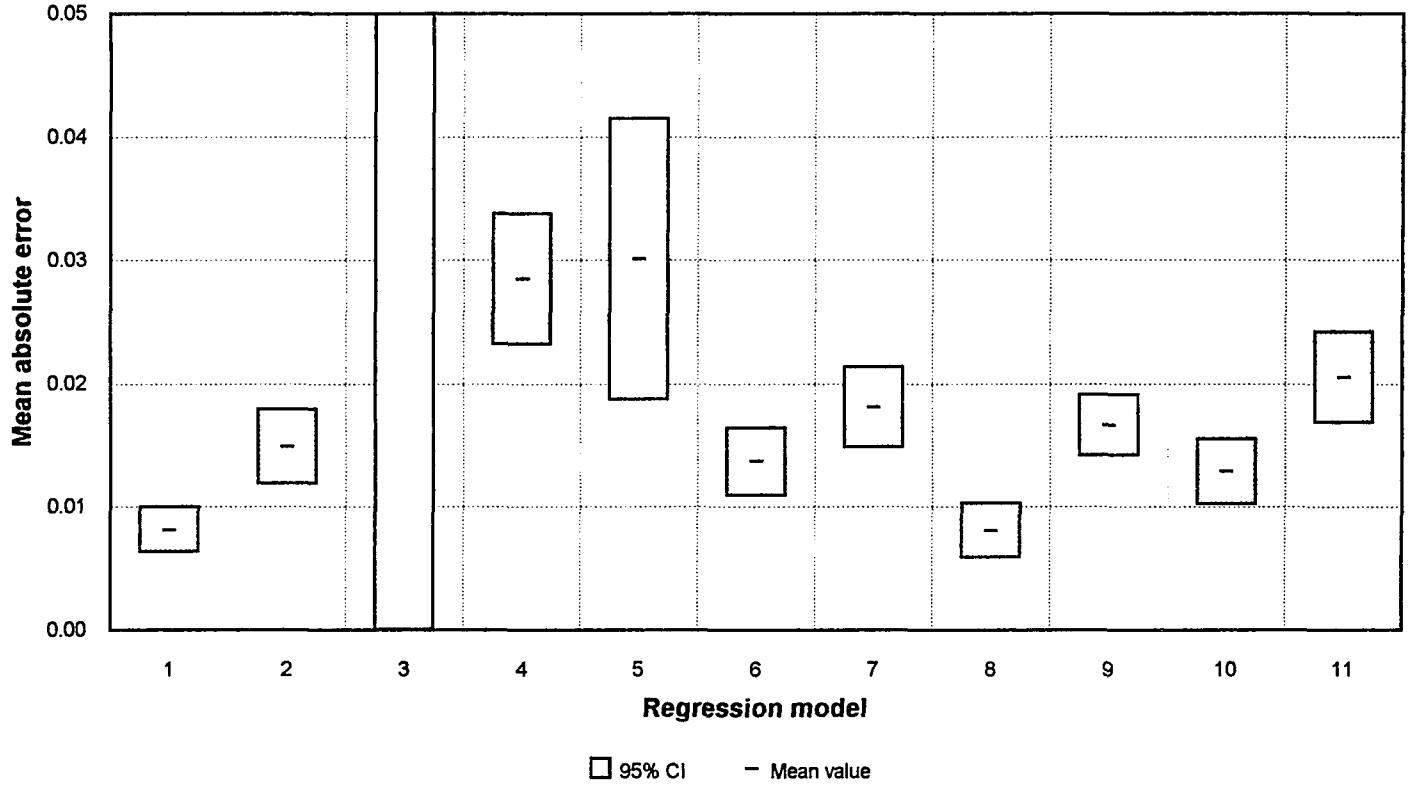

Figure B20. MAE values and 95% confidence intervals for pinch force pre-peak virgin data

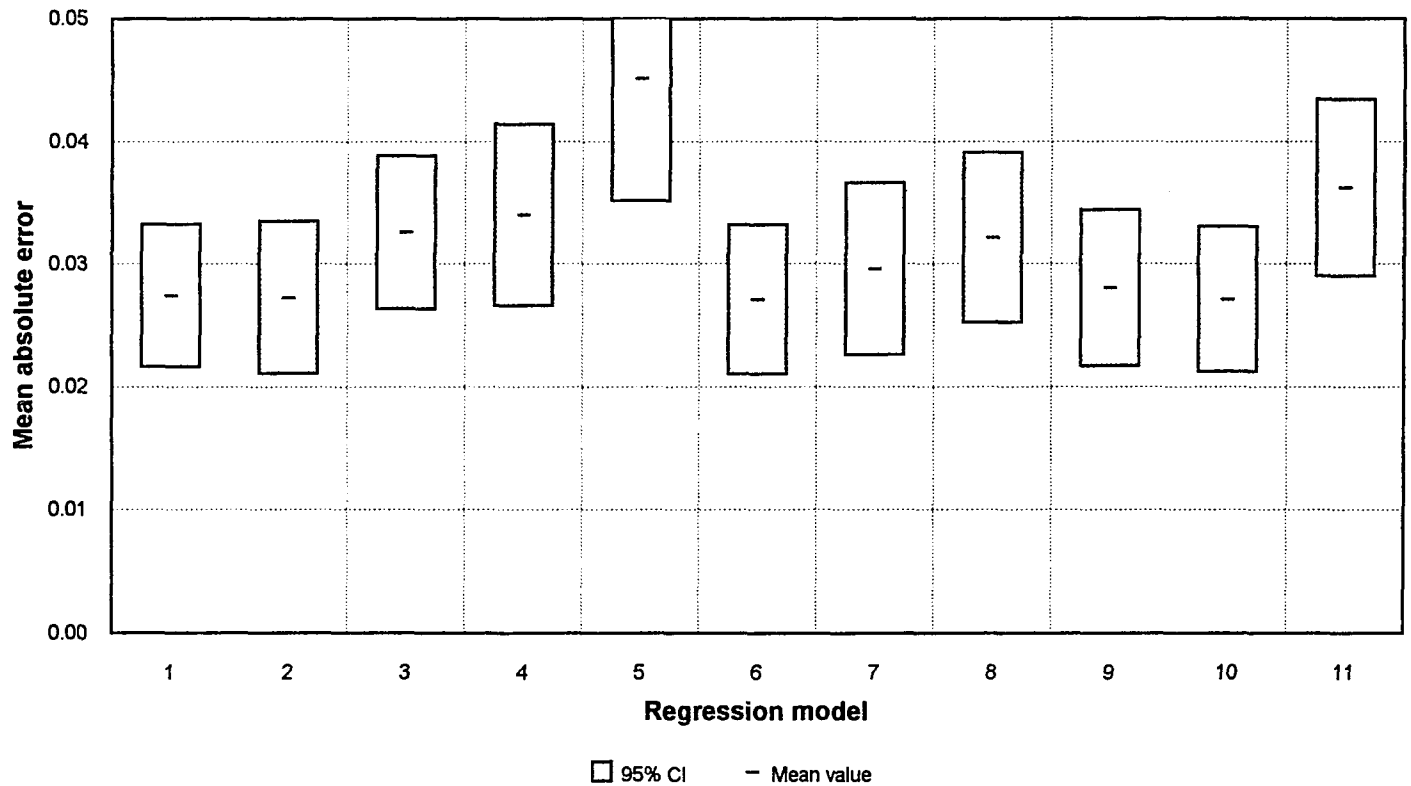

Figure B21. MAE values and 95% confidence intervals for pinch force post-peak virgin data

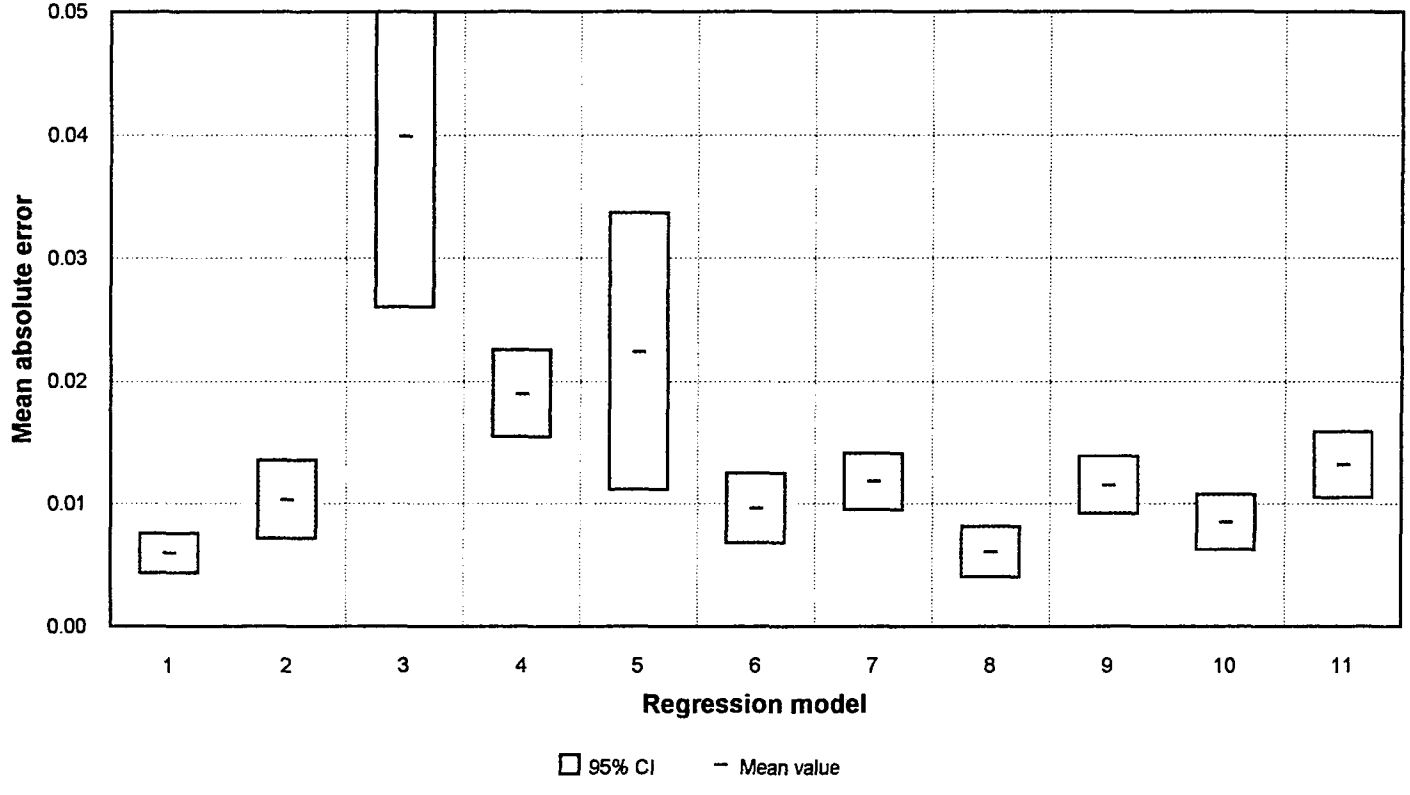

Figure B22. MAE values and 95% confidence intervals for pinch force pre-peak stabilized data

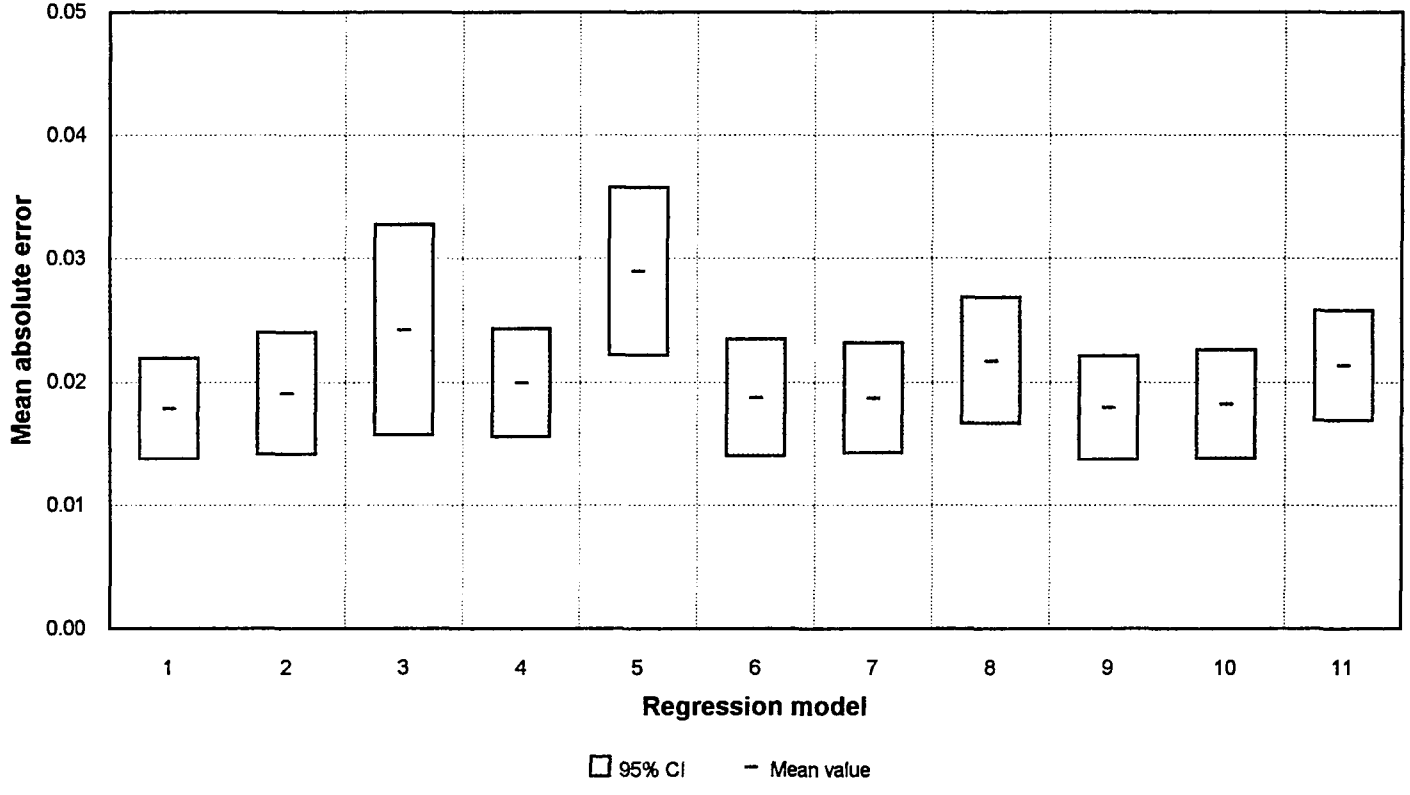

Figure B23. MAE values and 95% confidence intervals for pinch force post-peak stabilized data

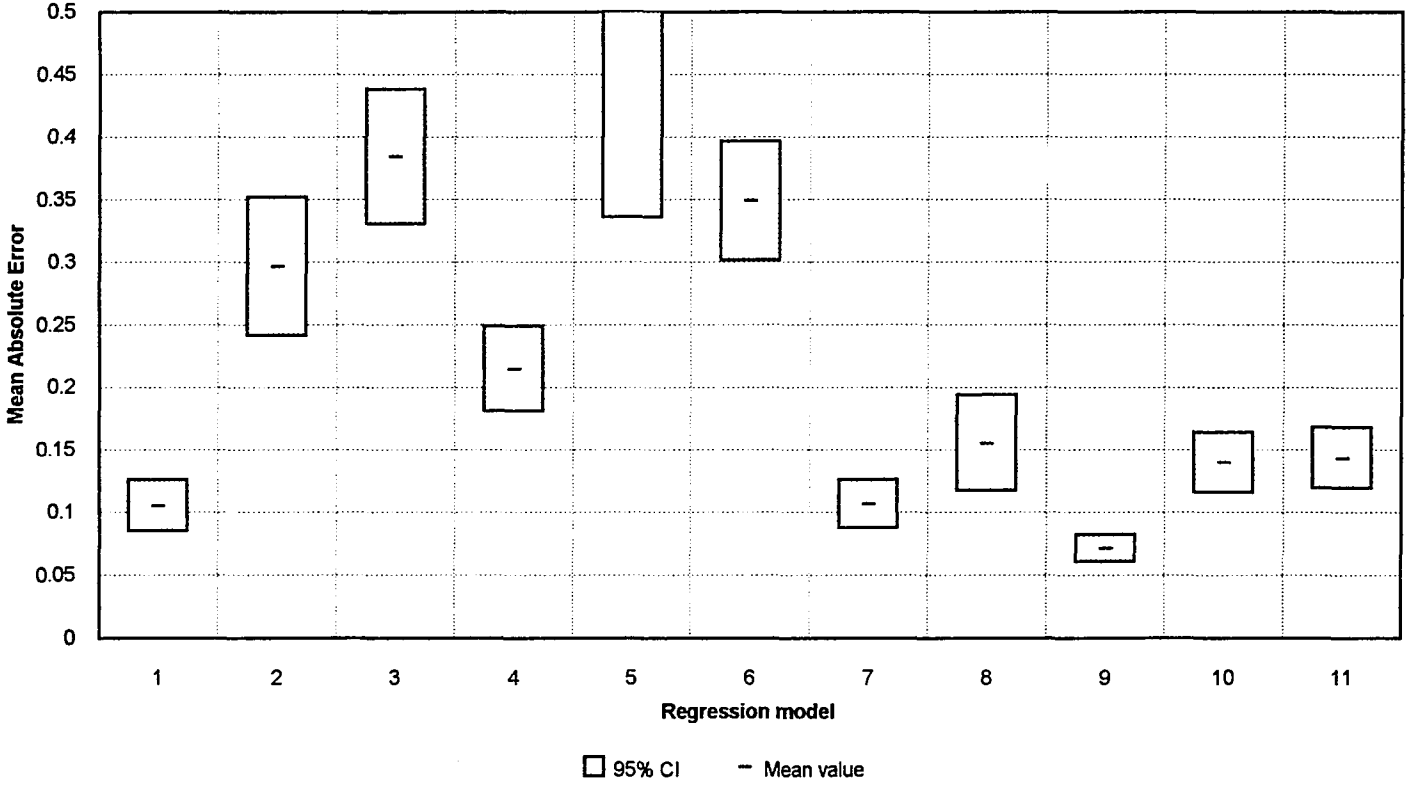

Figure B24. MAE values and 95% confidence intervals for virgin Ko characteristic slope

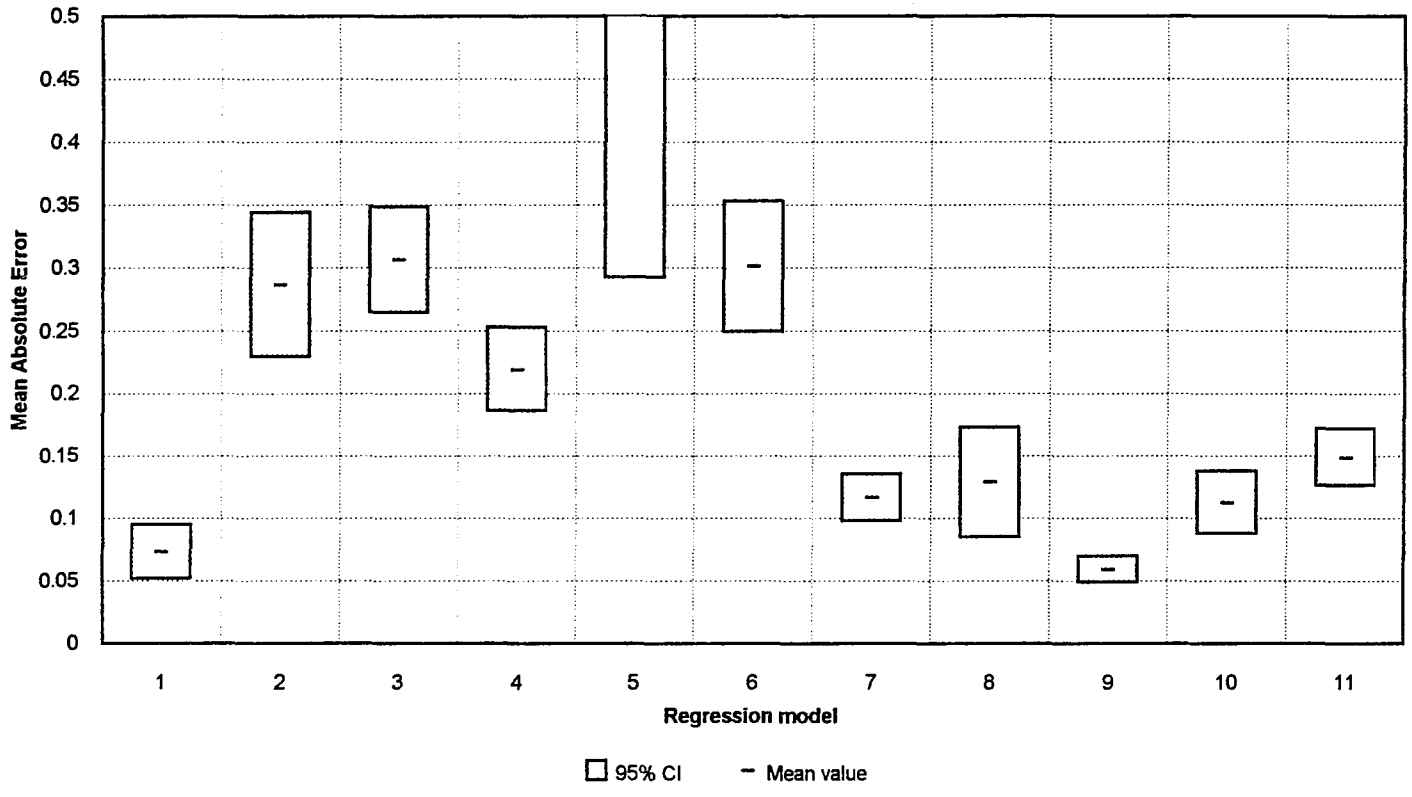

Figure B25. MAE values and 95% confidence intervals for stabilized Ko characteristic slope

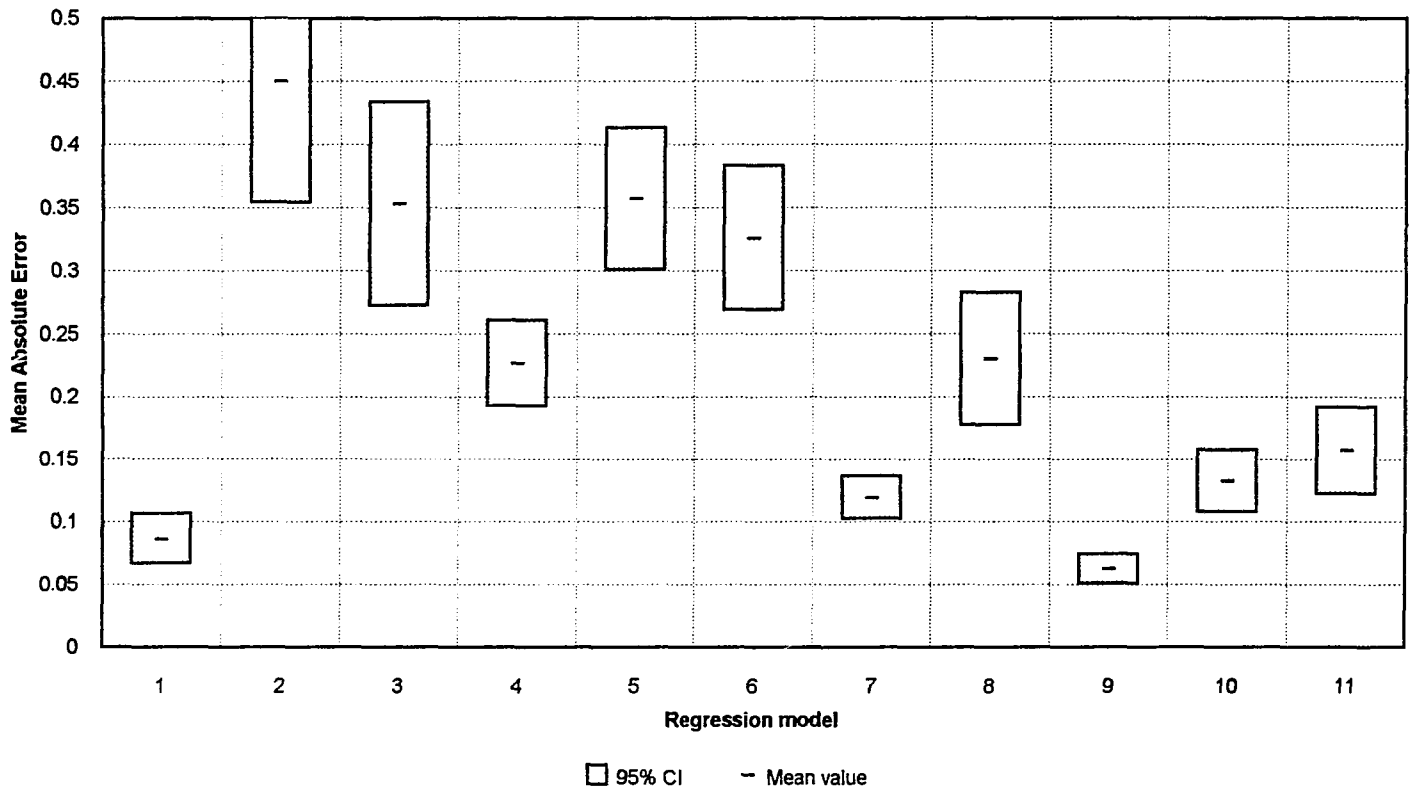

Figure B26. MAE values and 95% confidence intervals for virgin K1 characteristic slope

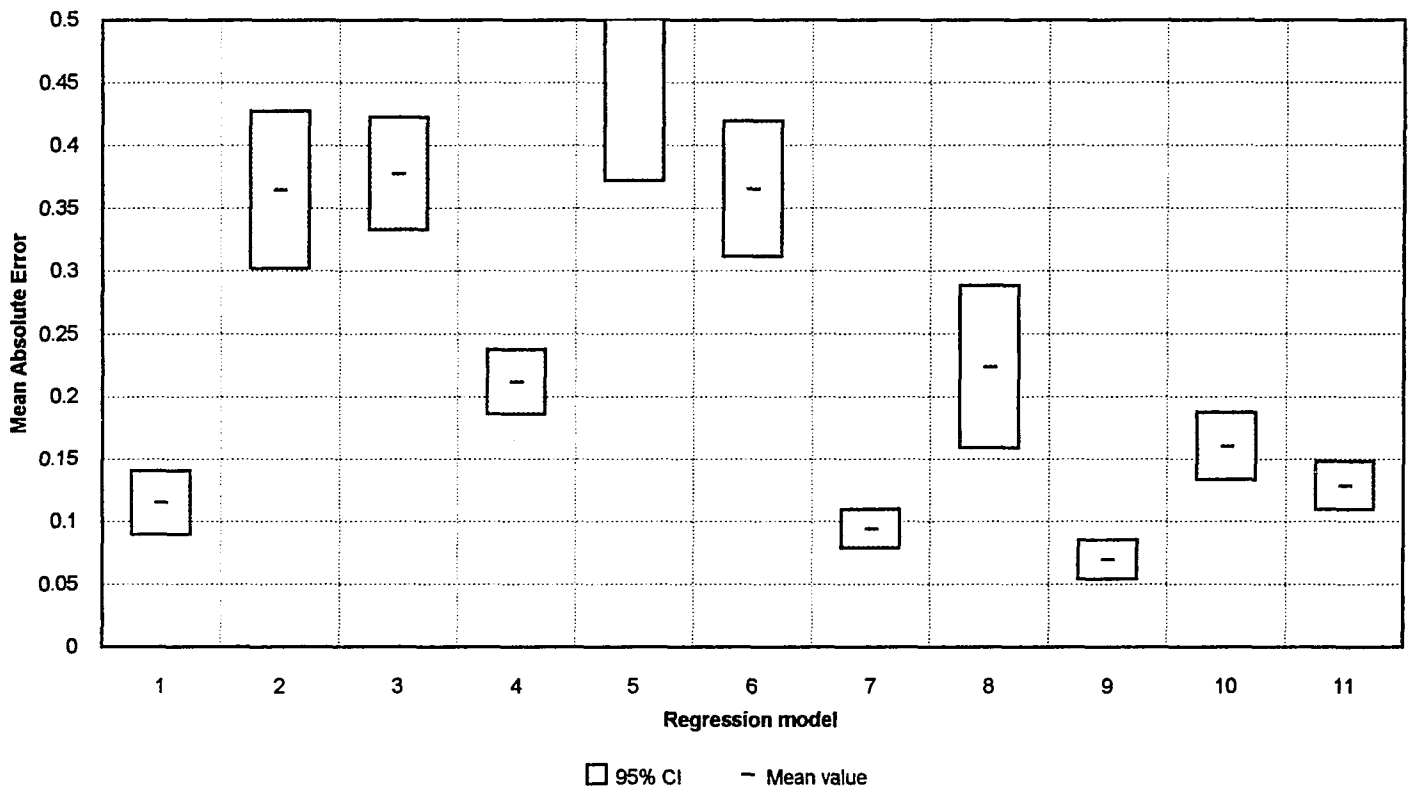

Figure B27. MAE values and 95% confidence intervals for stabilized K1 characteristic slope

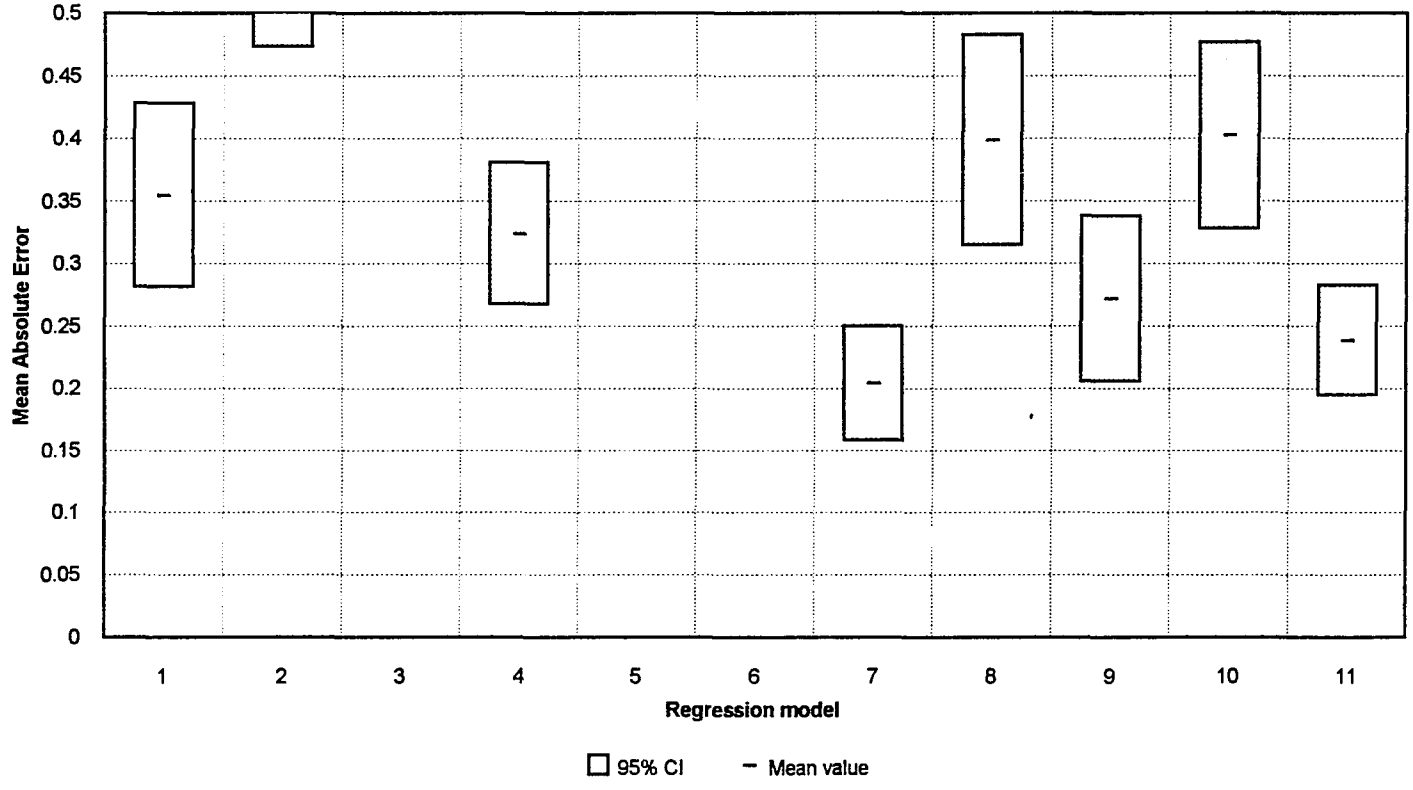

Figure B28. MAE values and 95% confidence intervals for virgin K2 characteristic slope

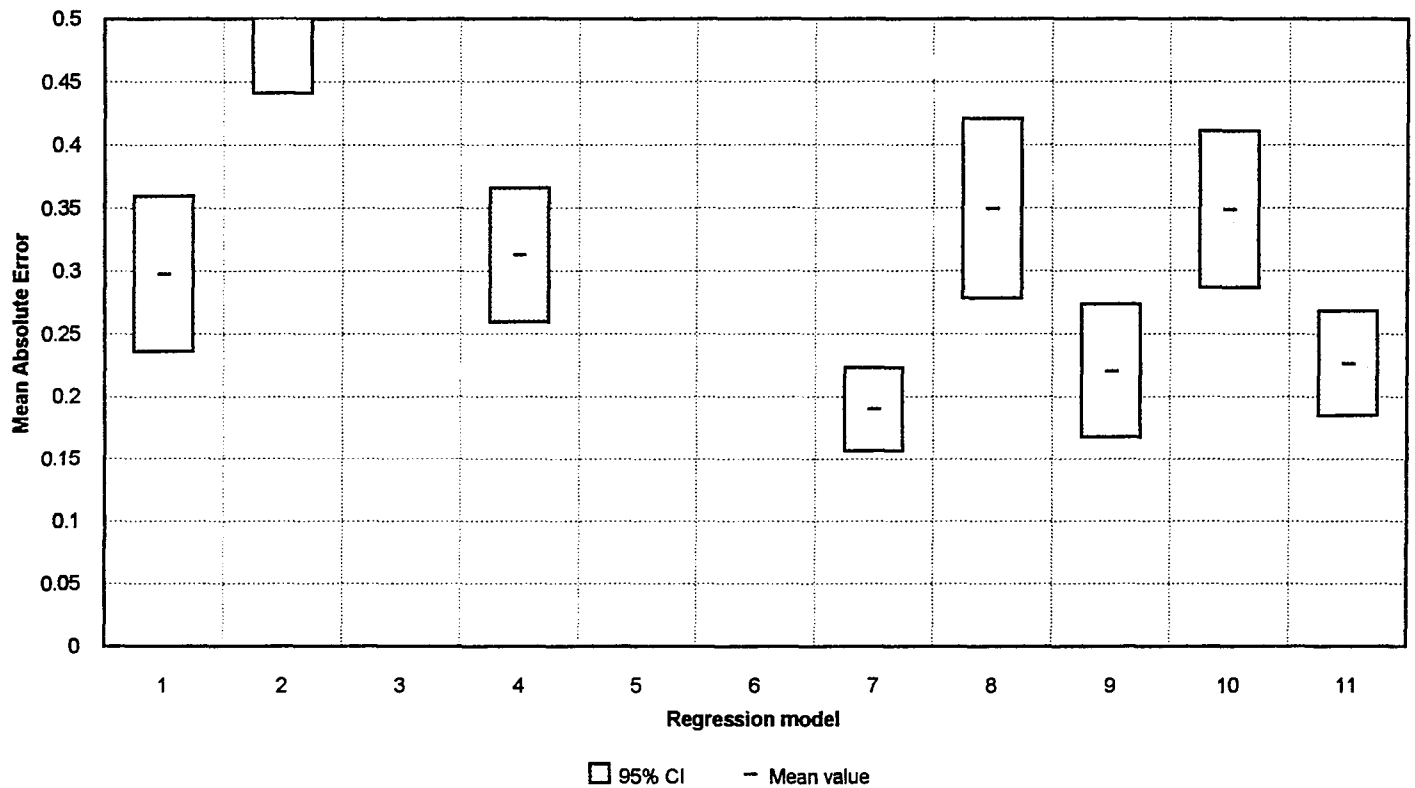

Figure B29. MAE values and 95% confidence intervals for stabilized K2 characteristic slope